

**Adipose Stromal Cell-Based Elastogenesis Therapy
for Adult and Pediatric Aortic Defects**

by

Aneesh Krishna Ramaswamy

Bachelor of Science in Biomedical Engineering, Purdue University, 2011

Master of Science in Biomedical Engineering, Purdue University, 2013

Submitted to the Graduate Faculty of
The Swanson School of Engineering in partial fulfillment
of the requirements for the degree of
Doctor of Philosophy

University of Pittsburgh

2019

UNIVERSITY OF PITTSBURGH
SWANSON SCHOOL OF ENGINEERING

This dissertation was presented

by

Aneesh Krishna Ramaswamy

It was defended on

March 25, 2019

and approved by

Marie Billaud, Ph.D., Research Assistant Professor, Departments of Cardiothoracic Surgery and
Bioengineering

Thomas G. Gleason, M.D., Professor, Departments of Cardiothoracic Surgery and
Bioengineering

Zsolt Urban, Ph.D., Associate Professor, Department of Human Genetics

Jonathan P. Vande Geest, Ph.D., Professor, Department of Bioengineering

Dissertation Co-Director: David A. Vorp, Ph.D., Professor, Departments of Bioengineering,
Surgery, Cardiothoracic Surgery, and Chemical and Petroleum Engineering

Dissertation Co-Director: Justin S. Weinbaum, Ph.D., Research Assistant Professor, Departments
of Bioengineering and Pathology

Copyright © by Aneesh Krishna Ramaswamy

2019

Adipose Stromal Cell-Based Elastogenesis Therapy for Adult and Pediatric Aortic Defects

Aneesh K. Ramaswamy, Ph.D.

University of Pittsburgh, 2019

Aortic aneurysm (AA) is a balloon-like enlargement of the aorta exceeding 1.5-times original diameter and possessing a life-threatening risk of rupture if left untreated, representing the 15th leading cause of death in the United States. Currently, surgical intervention is governed by aortic diameter measurements, recommended after adult AA enlarge beyond a “critical diameter” of 5.5cm and pediatric AA exceed a 0.5cm/year growth rate. AA diameter growth is mediated by inflammatory damage to extracellular matrix protein elastin, responsible for aortic recoil during pulsatile blood flow. Therapeutic options for sub-critical AA are limited to “watchful waiting” imaging every 6-to-12 months to monitor diameter growth, or broad-targeted therapeutics (beta blockers, ACE inhibitors) that do not work to rebuild the aortic wall.

Recent work by our lab has shown that delivery of adipose-derived stromal cells (ASCs) can slow AA dilation and preserve elastic fibers, by either suppressing inflammatory elastin breakdown or stimulating new elastin deposition. This dissertation work utilized a versatile, fibrin-based 3D SMC aortic culture platform to test whether paracrine signaling using ASC secreted factors (ASC-SF) could induce new human elastin deposition by three different classes of aortic smooth muscle cells (SMCs): healthy adult SMCs, aneurysmal adult SMCs, and aneurysmal pediatric SMCs.

Elastin deposition was evaluated at four different points of interest on the elastogenesis cascade: elastin organizational protein transcription (generating tropoelastin, fibulin-4, and

fibulin-5 coacervates/globules) [1-3], elastic fiber organization (through LTBP-4, fibulin-4, and fibulin-5 mediated deposition onto fibrillin-1 microfibrils), cross-linked elastin chemical maturity (mediated by lysyl oxidase or LOX, and lysyl oxidase-like 1 or LOXL-1), and mechanical functionality of the deposited extracellular matrix. Additionally, two methods were explored to maximize clinical translation of ASC-SF therapeutic delivery: potency of ASC-SF-derived exosomes, and a magnetic-guided periadventitial *in vivo* delivery system.

Table of Contents

Preface.....	xxiii
1.0 Introduction.....	1
1.1 Aorta and Aortic Aneurysm	1
1.1.1 Aorta Anatomy.....	1
1.1.2 Aortic Aneurysms and Their Incidence.....	2
1.1.3 Genetic Disorders that Lead to Aortic Elastin Disruption and Aortic Aneurysm	3
1.2 Elastin	5
1.2.1 Elastogenesis and Elastin Chaperone Matricellular Proteins	5
1.2.2 Elastin Chaperone Matricellular Proteins in Regenerative Medicine.....	8
1.2.3 Elastin and Matricellular Proteins in Aortic Disease	9
1.2.4 Elastin in Regenerative Medicine and Vascular Tissue Engineering	10
1.3 Aortic SMCs.....	12
1.3.1 SMC Differentiation in Diseased Aortic Tissue	12
1.3.2 Local Matricellular Proteins and Microenvironment Can Act To Regulate Aortic SMCs.....	14
1.3.3 Aortic SMC ECM Secretion and Neointimal Hyperplasia	18
1.3.4 <i>In Vitro</i> SMC Cultures.....	20
1.4 Treatment for Aortic Aneurysm	22
1.4.1 Surgical Diameter Criterion for Aortic Aneurysm.....	22
1.4.2 Treatment for Sub-Critical Aortic Aneurysm	23

1.5 Previous Work in the Advisor’s Laboratory: Stem Cell-Based Therapies for AA	24
1.6 Hypothesis and Specific Aims.....	26
2.0 Specific Aim 1: Development of <i>In Vitro</i> 3D Fibrin Construct Platform & Elastogenesis Impact of Adipose-Derived Stromal Cell Secreted Factors on Healthy Adult Smooth Muscle Cells	29
2.1 Introduction	29
2.2 Methods	33
2.2.1 RFL-6 Cell Culture Conditions	33
2.2.2 SMC Cell Culture Conditions.....	33
2.2.3 3D Fibrin Gel SMC Constructs on Stiff and Soft Substrates	33
2.2.4 ASC Culture Conditions and Conditioned Media Collection.....	36
2.2.5 Exogenous Media Treatment Conditions	37
2.2.6 SMC scratch assay to analyze migration.....	37
2.2.7 qRT-PCR analysis of tropoelastin and elastin chaperone proteins	38
2.2.8 Elastic fiber imaging via immunostaining and multiphoton microscopy, and elastic fiber quantification	40
2.2.9 Ninhydrin (Insoluble Elastin) and Hydroxyproline (Collagen) Assay.....	41
2.2.10 Tensile Testing of Soft Substrate Fibrin Gel Constructs	42
2.2.11 Statistical Analysis	43
2.3 Results.....	45
2.3.1 2D culture elastin deposition by RFL-6 cells with no exogenous stimulation and adaptation of fiber analysis code	45

2.3.2 Fibrinolysis inhibitor aminocaproic acid is required for fibrin construct maintenance and modulates RFL-6 elastin deposition	48
2.3.3 TGF-β1 stimulation induces insoluble elastin deposition in 3D fibrin gel constructs	51
2.3.4 RFL-6 elastic fiber networking quantification following TGF-β1 stimulation using modified fiber analysis code	53
2.3.5 RFL-6 insoluble elastin fraction is increased after TGF-β1 stimulation and decreased after ASC-SF stimulation within fibrin gel constructs	55
2.3.6 RFL-6 deposition of fibulin-5 and elastic fiber networking analysis following ASC-SF stimulation.....	57
2.3.7 Cyclic uniaxial loading of soft substrate constructs induces RFL-6 total elastin deposition and multiphoton imaging of deposited elastin	59
2.3.8 ACA to prevent SMC construct fibrinolysis, and TGF-β1 stimulation of SMCs induces no significant insoluble elastin deposition on soft substrates.....	61
2.3.9 ASC-SF and NCM increase early migration of SMCs on 2D substrates.....	64
2.3.10 ASC-SF increases SMC myosin heavy chain expression.....	66
2.3.11 ASC-SF induce SMC transcription of tropoelastin and elastin chaperone proteins fibrillin-1, fibulin-5, LOX, and LOXL-1	68
2.3.12 Elastic fiber networking quantifiably increases with ASC-SF treatment under all stiffness and loading conditions.	70
2.3.13 Insoluble elastin increases with ASC-SF treatment after 20 and 30 constrained culture days regardless of substrate stiffness, and after 30 days under soft substrate cyclic loading.....	76

2.3.14 Collagen fraction increases with ASC-SF treatment after 30 days cultured on stiff substrate constructs, and after both 20 and 30 days on constrained and dynamic soft substrate constructs.	76
2.3.15 High modulus is increased in ASC-SF stimulated soft substrate SMC constrained constructs after 30 days.	80
2.4 Discussion	82
2.5 Conclusion	85
2.6 Future Work	85
3.0 Specific Aim 2, Part 1: Elastogenesis Impact of Adipose-Derived Stromal Cell Secreted Factors on Adult Aneurysmal Smooth Muscle Cells	89
3.1 Introduction	89
3.2 Methods	92
3.2.1 Adult SMC cell culture conditions and patient information	92
3.2.2 Fibrin gel construct formation and exogenous stimulation conditions.....	93
3.2.3 qPCR transcription analysis of SMC-deposited tropoelastin and elastin chaperone proteins	95
3.2.4 Ninhydrin protein assay for insoluble elastin and hydroxyproline protein assay for total collagen	95
3.2.5 Statistical Analysis	96
3.3 Results.....	96
3.3.1 Elastogenesis is muted in MFS 05-07 SMCs after 30 days of TGF- β 1 stimulation, while collagen deposition is slightly increased.....	96

3.3.2 MFS 05-04 SMC elastogenesis is muted after 20 days of ASC-SF stimulation but statistically increased after 30 days of NCM stimulation, while collagen deposition is statistically unchanged with ASC-SF and NCM stimulation..	99
3.3.3 TAV-TAA SMC elastogenesis is increased after TGF- β 1 stimulation, but collagen is reduced.....	101
3.3.4 BAV-NA fibrillin-1 transcription is significantly increased after 30 days of ASC-SF stimulation, while both LOX and LTBP-4 are muted with ASC-SF.	103
3.3.5 BAV-TAA transcription of fibrillin-1 is increased after 30 days of ASC-SF, while NCM increases LTBP-4 deposition.	105
3.3.6 BAV SMCs from both non-aneurysmal (NA) and aneurysmal (TAA) aortas produce increased insoluble elastin when stimulated with ASC-SF and NCM, but only non-aneurysmal SMC collagen fraction is increased.	107
3.4 Discussion	109
3.5 Conclusion.....	111
3.6 Future Work	112
4.0 Specific Aim 2, Part 2: Elastogenesis Impact of Adipose-Derived Stromal Cell	
Secreted Factors on Pediatric Aneurysmal Smooth Muscle Cells.....	114
4.1 Introduction	115
4.2 Methods	118
4.2.1 Inclusion criteria for explanted pediatric dilated aortic tissue.....	118
4.2.2 Isolation, culture, and storage of medial SMCs and adventitial fibroblasts from explanted pediatric aortic tissue	122

4.2.3 Fibrin gel construct formation and exogenous stimulation conditions.....	124
4.2.4 qPCR analysis of elastin chaperone protein transcription	124
4.2.5 Ninhydrin and hydroxyproline protein analysis of insoluble protein and total collagen.....	125
4.2.6 Statistical Analysis	125
4.3 Results.....	126
4.3.1 MOR 1-01 SMCs treated with ASC-SF increased transcription of tropoelastin, fibrillin-1, and LOX, and decreased transcription of fibulin-5, LOXL-1, and LTBP-4.	126
4.3.2 MOR 1-01 SMCs saw increased insoluble elastin and muted collagen deposition after ASC-SF stimulation.	128
4.3.3 MOR 1-04 qPCR.....	130
4.3.4 MOR 1-04 SMCs produce increased insoluble elastin and total collagen percentage after 30 days of ASC-SF stimulation, and increased total collagen percentage after 30 days of NCM stimulation.	132
4.3.5 MOR 1-07 deposition of fibulin-5, LOX, and LOXL-1 was significantly increased with either ASC-SF or NCM stimulation, with no changes to tropoelastin deposition observed.....	134
4.3.6 MOR 1-07 insoluble elastin deposition is induced after ASC-SF or NCM stimulation for 30 days, but total collagen is unchanged.	136
4.4 Discussion	138
4.5 Conclusion	140
4.6 Future Work	141

5.0 Specific Aim 3, Part 1: Periadventitial Magnetic Localization of Mesenchymal Stem Cells to a Murine Abdominal Aortic Aneurysm	144
5.1 Introduction	144
5.2 Methods	146
5.2.1 Iron nanoparticle delivery optimization through fibrin gels	146
5.2.2 Tri-Syringe Delivery Device for FeMSC-loaded fibrin gels.....	147
5.2.3 Iron nanoparticle-loaded MSC localization optimization following fibrin gel delivery to rat peritoneal cavity	148
5.2.4 Optimization of Tri-Syringe fibrin gel delivery and iron nanoparticle-loaded MSC localization using explanted chicken wing radial artery.....	149
5.2.5 Tri-Syringe periadventitial delivery and magnet-guided localization of iron nanoparticle-loaded MSCs in an elastase-induced AAA mouse model.....	150
5.3 Results.....	154
5.3.1 Fabrication of “Tri-Syringe” mixing chamber to deliver cell-seeded fibrin gel constructs	154
5.3.2 <i>In vitro</i> magnet-guided migration of iron nanoparticle-loaded MSCs within fibrin gels.....	158
5.3.3 FeMSCs localize to the aortic surface when delivered via Tri-Syringe to a rat peritoneal cavity within a fibrin gel in the presence of an external magnet	160
5.3.4 Agar-embedded chicken brachial artery <i>in vitro</i> model of catheter-delivered Fe-MSC fibrin gel constructs to a surgical sponge shows distance bounds of magnet-guided migration.....	162

5.3.5 Delivery of Fe-MSC seeded fibrin gels to growing elastase-induced mouse aneurysm shows external magnet guidance and cell retention both 1 hour and 3 days after delivery.....	165
5.4 Discussion	167
5.5 Conclusion.....	168
5.6 Future Work	169
6.0 Specific Aim 3, Part 2: Elastogenesis Impact of Adipose-Derived Stromal Cell Secreted Extracellular Vesicles on Healthy Adult Smooth Muscle Cells	171
6.1 Introduction	171
6.2 Methods	173
6.2.1 ASC isolation and culture	173
6.2.2 Isolation of ASC secreted exosomes	174
6.2.3 Transmission electron microscopy to visualize ASC secreted exosome morphology	175
6.2.4 Dynamic light scattering of ASC secreted exosomes	175
6.2.5 Determination of total protein concentration contained within ASC secreted exosomes	176
6.2.6 Healthy adult SMC culture.....	176
6.2.7 Fibrin gel construct formation and culture	177
6.2.8 Exogenous stimulation treatment groups	177
6.2.9 SMC proliferation analysis	178
6.2.10 SMC scratch assay migration analysis.....	178
6.2.11 qPCR analysis of tropoelastin and elastin chaperone transcription.....	180

6.2.12 Ninhydrin and hydroxyproline protein analysis of insoluble elastin and total collagen.....	180
6.2.13 Mechanical testing of soft substrate SMC fibrin gel constructs.....	181
6.2.14 Statistical Analysis	182
6.3 Results.....	182
6.3.1 Visual characterization of ASC secreted EVs	182
6.3.2 Dynamic light scattering size characterization and BCA protein analysis of ASC-EVs.....	184
6.3.3 1x EV causes an increase in SMC proliferation, but significantly less than supplemented ASC culture media, full conditioned media, EV-depleted conditioned media, or non-conditioned media.....	186
6.3.4 While all treatment groups slightly accelerate SMC migration only non-conditioned ASC media induces full scratch wound closure.....	188
6.3.5 ASC secreted EVs induce an SMC transcriptional increase in organizational proteins fibulin-4 and fibulin-5, and crosslinking protein LOX.	190
6.3.6 ASC secreted factors and EVs increase insoluble elastin deposition in stiff substrate SMC constructs.....	193
6.3.7 ASC secreted factors and EVs increase collagen protein deposition in stiff substrate SMC constructs.....	193
6.3.8 Mechanical activity of SMC ECM following ASC secreted exosome stimulation.....	195

6.3.9 ASC-SF and 1x EV treatments induce increased SMC insoluble elastin deposition, and increased total collagen is induced after ASC-SF, 1x EV, and 3x EV treatment on soft substrate tensile tested fibrin gel constructs	197
6.4 Discussion	199
6.5 Conclusion	201
6.6 Future Work	201
7.0 Project Summary	203
7.1 Summary of Results	203
7.1.1 Specific Aim 1	203
7.1.2 Specific Aim 2	204
7.1.3 Specific Aim 3	205
7.2 Summary of Accomplishments	206
7.3 Future Work	210
Bibliography	211

List of Tables

Table 1: List of frequently-used abbreviaions	xxiv
Table 2: RT-qPCR Primers.....	39
Table 3: Database of the newly established pediatric aortic cell bank stored at the Vascular Bioengineering Laboratory/Vascular ECM Dynamics Laboratory, sourced from UPMC Children’s Hospital of Pittsburgh	120

List of Figures

Figure 1: SMC elastogenesis cascade.....	7
Figure 2: Three-dimensional fibrin gel culture constructs and ASC-SF collection.....	35
Figure 3: Soft substrate fibrin gel preparation for tensile testing.	44
Figure 4: Immunostaining for RFL-6 and WI-38 elastin on 2D cultures (glass coverslips).	46
Figure 5: MATLAB elastin network identification on 2D RFL-6 immunostained elastin images.	47
Figure 6: RFL-6 elastogenesis is dependent on fibrinolysis inhibitor concentration.	49
Figure 7: SMC fibrin gel construct stability under a concentration panel of fibrinolysis inhibitor ACA.....	50
Figure 8: TGF- β 1 stimulation induces RFL-6 insoluble elastin deposition within fibrin gel constructs.....	52
Figure 9: RFL-6 elastic fiber network quantification within 3D fibrin gel constructs after TGF- β 1 stimulation (1ng/mL).	54
Figure 10: RFL-6 total elastin increase after TGF- β 1 stimulation and insoluble elastin fraction decrease after ASC-SF stimulation.....	56
Figure 11: RFL-6 elastic fiber network quantification within 3D fibrin gel constructs after TGF- β 1 stimulation (1ng/mL).	58
Figure 12: RFL-6 deposited elastin multiphoton imaging and total elastin content increases after ASC-SF stimulation.....	60
Figure 13: ACA concentration panel of SMC seeded fibrin gel constructs.	62

Figure 14: SMC insoluble elastin deposition within soft substrate fibrin constructs, when stimulated with 1ug/mL TGF-β1 for 20 or 30 days and subjected to Constrained or Dynamic loading.....	63
Figure 15: 2D SMC migration is enhanced when treated with ASC-SF and NCM.	65
Figure 16: SMC phenotype marker transcription in response to 30 days of ASC-SF stimulation.	67
Figure 17: Transcriptional changes in tropoelastin and elastin chaperone matricellular proteins after 30 days of ASC-SF stimulation of SMCs.....	69
Figure 18: Multiphoton composite image (1x5) of control NT-stimulated SMC autofluorescence signal.....	71
Figure 19: Multiphoton composite image (2x5) of ASC-SF stimulated SMC elastic fiber deposition.....	72
Figure 20: Multiphoton composite image (3x5) of ASC-SF stimulated SMC elastic fiber deposition.....	73
Figure 21: Elastic fiber imaging and fiber network quantification on stiff substrates.....	74
Figure 22: Elastic fiber imaging and fiber network quantification on soft substrates, with constrained and dynamic culture conditions.....	75
Figure 23: Insoluble elastin and collagen are enhanced by ASC-SF stimulation of SMC constructs plated on stiff substrates.	78
Figure 24: Insoluble elastin and collagen are enhanced by ASC-SF stimulation of soft substrate SMC constructs, under Constrained and Dynamic loading conditions.	79
Figure 25: Mechanical properties of constrained, soft substrate ASC-SF stimulated SMC constructs.....	81

Figure 26: Insoluble elastin and total collagen deposition of TGF- β 1 stimulated CTRL 01-25 and MFS 05-07 constructs, after 20 and 30 days.....	98
Figure 27: Insoluble elastin and total collagen deposition of CTRL 01-25 and MFS 05-07 constructs, after 20 and 30 days of TGF- β 1 or ASC-SF exogenous stimulation.....	100
Figure 28: Tricuspid aortic valve (TAV) non-aneurysmal (NA) and ascending thoracic aortic aneurysmal (TAA) SMC insoluble elastin and total collagen deposition after 30 days of TGF- β 1 stimulation.....	102
Figure 29: Preliminary data on BAV-NA transcriptional changes in tropoelastin and elastin chaperone matricellular proteins after 30 days of ASC-SF stimulation.	104
Figure 30: Preliminary data on BAV-TAA transcriptional changes in tropoelastin and elastin chaperone matricellular proteins after 30 days of ASC-SF stimulation.	106
Figure 31: Bicuspid aortic valve (BAV) non-aneurysmal (NA) and ascending thoracic aortic aneurysmal (TAA) SMC insoluble elastin and total collagen deposition after 30 days of ASC-SF and NCM stimulation.....	108
Figure 32: Cellular isolation technique from medial and adventitial layers of explanted pediatric aneurysmal tissue.....	123
Figure 33: MOR1-01 SMC transcriptional analysis reveals an ASC-SF induced increase in tropoelastin, microfibril protein fibrillin-1, and crosslinking protein LOX, with a decrease in fibulin-5, LOXL-1, and LTBP-4.....	127
Figure 34: MOR 1-01 SMCs, from the medial layer of a 2-year-old dilated aortic root explanted following a Ross Procedure, deposit significantly increased insoluble elastin and decreased total collagen after 30 days of ASC-SF stimulation.	129

Figure 35: MOR1-04 SMC transcriptional analysis reveals ASC-SF and NCM induced increases in tropoelastin, elastin organizational protein fibulin-5, and crosslinking protein LOX, with a decrease in LTBP-4 and an NCM-only increase in microfibril protein fibrillin-1. 131

Figure 36: MOR 1-04 SMCs, from the aortic medial layer SMCs from an 11-year-old patient with ascending TAA, deposit significantly increased insoluble elastin after 30 days of ASC-SF stimulation, and significantly increased total collagen after 30 days of both ASC-SF and NCM stimulation..... 133

Figure 37: MOR1-07 SMC transcriptional analysis reveals 30 days of ASC-SF and NCM stimulation induced increased in fibulin-5, LOX, and LOXL-1, with NCM inducing a decrease in LTBP-4. 135

Figure 38: MOR 1-07 SMCs, from the aortic root medial layer of a 15-year-old patient following a valve-sparing root replacement and root dilation, deposit significantly increased insoluble elastin after 30 days of ASC-SF and NCM stimulation, but no change in total collagen. 137

Figure 39: Surgical stage for FeMSC periadventitial delivery and localization during mouse surgeries, designed and printed for surgeries performed by Dr. John Curci’s group at Vanderbilt University..... 153

Figure 40: “Tri-Syringe” mixing device iterations to form and deliver cell-rich fibrin gel constructs. 155

Figure 41: Additional views of the Tri-Syringe fibrin gel injection delivery device. 156

Figure 42: Tri-Syringe fibrin gel injection device in use during *in vitro* FeMSC localization studies, with syringes for fibrinogen (clear solution, right), FeMSCs (brown solution, middle), and thrombin (pink solution, left) being combined and injected through an 18-gauge needle into the port/catheter/sponge device designed by Dr. John Curci’s group at Vanderbilt University. 157

Figure 43: Quantitative analysis of cell location via MTT assay, with and without the presence of a magnetic field and at different distances.....	159
Figure 44: Magnet-driven localization and quantification of FeMSC-rich fibrin gel constructs within a rat peritoneal cavity.....	161
Figure 45: Agarose-embedded chicken wing brachial artery <i>in vitro</i> model for FeMSC delivery through port/catheter/sponge device, within a 10cm petri dish.	163
Figure 46: Light microscopy of delivered FeMSCs within agarose and artery setup.	164
Figure 47: Periadventitial delivery and magnet-driven localization of FeMSCs (red) to an elastase-induced murine abdominal aortic aneurysm (autofluorescence in green).	166
Figure 48: TEM images of ASC secreted EVs.	183
Figure 49: Dynamic light scattering (DLS) characterization of ASC-EVs, and BCA protein analysis of encapsulated protein.	185
Figure 50: SMC proliferation, via Alamar Blue assay, when treated with ASC-sereted exosomes or full conditioned media.....	187
Figure 51: SMC migration, via scratch assay, when treated with ASC-sereted exosomes or full conditioned media.....	189
Figure 52: EV-induced SMC transcription analysis of elastin chaperone proteins reveals in increase in organizational proteins fibulin-4 and fibulin-5 and crosslinking protein LOX after treatment with 3x EV concentration.	192
Figure 53: SMC insoluble elastin and collagen deposition is increased after both ASC secreted factor and ASC secreted EV treatment.	194
Figure 54: Low and high modulus of ASC secreted exosome-treated SMC fibrin gel constructs.	196

Figure 55: SMC insoluble elastin and collagen deposition on tensile-tested soft substrates are increased after 30 days of EV-containing treatment groups..... 198

Preface

The completion of this dissertation would not be possible without the support of my family and friends, beginning with Samantha, (Dr.) Nandini, Ashok, and Keshav Ramaswamy.

The mentorship of Dr. David Vorp and Dr. Justin Weinbaum invaluabley guided my progress both as a scientist and as a professional. Colleagues within the Vascular Bioengineering Lab and Vascular Extracellular Matrix Dynamics Lab who helped complete this dissertation work include Rachel Sides, Katherine Lorentz, Dr. Eoghan Cunnane, Dr. Kory Blose, Dr. Jeff Krawiec, Trevor Kickliter, Leila Reines, Dr. Tim Chung, Dr. Darren Haskett, Joseph Pichamuthu, Abby Snyder, Prerak Gupta, Yogev Baruch, Kamiel Saleh, Deborah Cleary, and Melissa Penkrot.

Thanks to Pitt's Thoracic Aortic Disease Research Laboratory – Tom Gleason MD, Dr. Julie Phillippi, Dr. Marie Billaud, Jennifer Hill, Tara Richards, and Leonid Emerel MD.

Thanks to our collaborators at the UPMC Children's Hospital of Pittsburgh – Victor Morell MD, Melita Viegas MD, Tamara Maihle, Lori Schmitt, Lindsay Hogue, and everyone involved within the Divisions of Pediatric Cardiothoracic Surgery and Pediatric Pathology.

Thanks to collaborators at Vanderbilt University – John Curci MD and Jamie Adcock.

Thanks to everyone at sciVelo for my development as a scientific professional, including Dr. Don Taylor, Dr. Andrew Brown, Dr. Danielle Minter, Peter Kant, Dr. Megan Waldman (née Breski), Dr. James Eles, Dr. Alyssa Lypson, Dr. Bradley Campbell, Dr. Chelsea Stillman, Dr. Julie Cramer, all the associates, architects, and teams I've had the privilege of working with. Extended thanks to everyone at the Clinical and Translational Science Institute – Dr. Mike Flock, Prachi Joshi, Phil Cicco, Dana Farrell, John Maier MD, and Steve Reis MD.

In addition to the grants and fellowships summarized in **Section 7.2**, this work was supported by the National Institute of Health grants R21 HL129066 and R21 HL130784 (to Dr. David Vorp), the University of Pittsburgh Competitive Medical Research Fund (to Dr. Justin Weinbaum), and the Department of Bioengineering at the University of Pittsburgh.

Table 1: List of frequently-used abbreviaions

VBL	Vascular Bioengineering Laboratory
VEDL	Vascular Extracellular Dynamics Laboratory
ECM	extracellular matrix
SMC	aortic smooth muscle cell
EC	aortic endothelial cell
AA	aortic aneurysm
AAA	abdominal aortic aneurysm
(A)TAA & ATAA	(ascending) thoracic aortic aneurysm
MFS	Marfan syndrome
BAV	Bicuspid Aortic Valve Disease
TGF- β	transforming growth factor β
LTBP	latent TGF- β binding protein
LOX	lysyl oxidase
LOXL-1	LOX like 1
ASC	adipose-derived stromal cell
ASC-CM	ASC conditioned media
ASC-SF	ASC secreted factor therapy
ASC-EV	ASC secreted extracellular vesicles

1.0 Introduction

1.1 Aorta and Aortic Aneurysm

1.1.1 Aorta Anatomy

The aorta is the large blood vessel that carries oxygenated blood from the left heart throughout the body. The aortic root, the closest section of the aorta to the heart, is part of the left ventricular outflow tract and supports the leaflets of the tricuspid aortic valve [4]. The ascending thoracic aorta follows, typically under 2.1cm/m^2 in diameter for healthy adults [5]. The subsequent aortic arch includes the branching brachiocephalic trunk, the left common carotid artery, and the left subclavian artery. Distal to the left subclavian artery is the descending thoracic aorta, diameter typically under 1.6cm/m^2 in healthy adults, continuing until the diaphragm. The abdominal aorta, typically 3cm in diameter for healthy adults, extends from the diaphragm to the iliac bifurcation [5].

The aorta wall is comprised of three distinct layers, each providing functionality towards the overall stability of the dynamic blood vessel. The outer layer, or the tunica adventitia, is rich in fibroblasts and consists of basement membrane extracellular matrix (**ECM**) proteins collagen (types I and III), fibronectin, and laminin to maintain vascular strength and structure [6]. The aorta's central layer, the tunica media, is the thickest and consists of alternating layers of smooth muscle cells (**SMCs**) and lamellar sheets of ECM rich in elastin. Elastic lamellar sheets in the medial layer are typically solid and uninterrupted layers, clearly visible as dark purple or black on Verhoeff-Van Gieson staining of histological tissue as elastin binds with the iron-hematoxylin

complex in the staining reagent. Additionally, the tunica media consists of collagen I and III, fibronectin, proteoglycans, and glycosaminoglycans that fortify aortic stiffness and integrity, while elastic layers provide vascular elastic recoil properties necessary to pump oxygen-rich blood to branching arteries during systole and diastole (known as the Windkessel effect) [7]. The media is flanked on both its inner and outer sides by elastic layers, the external elastic lamina separating the media and adventitia and the internal elastic lamina separating the media and the aorta's inner-most intima layer. The intima consists of a single uninterrupted layer of endothelial cells (**ECs**) designed as a hemocompatible anti-inflammatory surface for blood flow, and a subendothelial layer consisting of SMC-like pericytes (thickness of the subendothelial layer is age-dependent) [8] and basement membrane ECM deposited primarily by ECs. EC-secreted basement membrane is rich in collagens I, III, and IV alongside fibronectin, laminin, thrombospondin, and proteoglycans heparan sulfate, dermatan sulfate, and chondroitin sulfate to prevent cellular or particulate infiltration within the aortic wall [9].

1.1.2 Aortic Aneurysms and Their Incidence

Aortic aneurysm (**AA**) is a balloon-like enlargement of the aorta defined as aortic dilation to 1.5-times its original diameter, possessing a life-threatening risk of rupture. AA are most prominent in both aging populations (primarily smokers) and pediatric or young adult patients with connective tissue genetic disorders [10].

AA is typically characterized by a breakdown in elastin within the tunica media layer of the aortic wall. Elastin fragmentation within the ascending thoracic aorta (ascending thoracic aortic aneurysm, **ATAA**) or complete elastic fiber destruction within the infrarenal abdominal aorta (abdominal aortic aneurysm, **AAA**) leads to a decrease in aneurysmal wall compliance,

resulting in wall shape irregularities, turbulent blood flow, and irregularities in ECM regeneration causing concentrated regions of stiff tissue prone to rupture [11].

Approximately 5 million Americans over the age of 50 are living with AAA or ATAA [12, 13], with over 200,000 new AAs diagnosed annually [14]. Actively dilating AAs, if left untreated, can weaken and ultimately rupture or dissect, with over 15,000 annual AA ruptures/dissections [15, 16] and an 80-90% AA mortality rate contributing to AAs being the 15th leading cause of death in the United States in 2018 [17-19].

1.1.3 Genetic Disorders that Lead to Aortic Elastin Disruption and Aortic Aneurysm

Marfan Syndrome (**MFS**) is the result of mutations within the gene coding for the ECM protein fibrillin-1 (*FBNI*), which serves as the main template for proper elastin formation and cross-linking. To date, over 1,000 different *FBNI* mutations have been identified in MFS patients [20]. The Ghent nosology, a set of defined clinical criteria to identify MFS, is reliant on presence of aortic dilation (particularly within the aortic root section) as a result of systemic elastin disruption. The Ghent nosology also includes on family history, aortic root dilation, fibrillin-1 mutation, ectopia lentis (or a dislocation of the eye's lens), and a number of visible systemic features (such as chest asymmetry, hindfoot deformity, and joint extension) for accurate detection and diagnosis of MFS [21]. Early diagnosis and aortic treatment, both surgical and non-surgical, has been critical to increasing life expectancy of MFS patients (mean death age 32±16 years in 1972, 45±17 years in 1998) [22, 23]. MFS diagnosis incidence reports range between 6.5 [24] to 10.2 [25] out of 100,000 individuals, with a mean diagnosis age of 19 years old.

Loeys-Dietz syndrome (**LDS**) is an autosomal dominant genetic disorder with mutations linked to transforming growth factor beta (**TGF- β**) receptor disruptions; features of the disease include increasing aortic tortuosity and, like MFS, severe aortic dilation and aneurysm formation [26]. LDS is difficult to diagnose, and often presents with the most aggressive and rapid cardiovascular complication rates in patients as young as 6 months old [27, 28]. Aortic dilation is present among 80% of children diagnosed with MFS [29], and the mean age of death for LDS patients is 26.1 years old (with sudden aortic rupture as the primary cause of death [26]).

Bicuspid Aortic Valve (**BAV**) Disease is among the most commonly diagnosed congenital cardiovascular disorders, with studies placing prevalence anywhere from 0.6% to 1.5% of the general population [30-32]. A healthy aortic valve, located at the proximal end of the aortic root, has three leaflets that open and close to allow only forward blood flow from the left ventricle through the aorta. BAV patients typically have only two separate leaflets, unequal in size, formed during valvulogenesis within the first eight weeks of fetal development [33]. BAV is commonly diagnosed among patients over 40 years old, with only ~2% diagnosed during childhood [34]. While survival rate among BAV patients is statistically similar to the general population, incidence of adverse cardiovascular events were increased, such as aortic root dilation and ATAA [35], ascending thoracic aorta dissection [36], calcification-related complications leading to leaflet or aortic stenosis [31], aortic incompetence due to myoxid degeneration of the valves [37], and coarctation of the aorta.

Williams Syndrome (**WS**) is a genetic disorder diagnosed in ~10 per 100,000 individuals [38], involving the mutation or heterozygous deletion of the elastin-encoding ELN gene on chromosome 7 [39]. Cardiovascular implications of WS include supraaortic stenosis and narrowing of the ascending aorta [40].

Non-surgical treatments are limited for pediatric patients with these genetic diseases, and typically require actively disrupting normal growth of the aorta during adolescence. A therapeutic approach that targets disrupted elastic fibers, particularly within pediatric and young adult populations vulnerable to aortic aneurysm, has the end goal of fortifying aortic vasculature and reducing repeated surgeries following aortic dilation.

1.2 Elastin

1.2.1 Elastogenesis and Elastin Chaperone Matricellular Proteins

Mature aortic elastin is formed during early childhood stages of human development, and while multiple matricellular chaperone proteins are essential to the formation of mature elastic fibers, the process must begin by expression of the 64 kilodalton protein tropoelastin [41]. A single tropoelastin-promoting gene, *ELN*, is present in the mammalian genome, and mutation or heterozygosity of the gene is linked to several human diseases including WS [42], cutis laxa [43], and supraaortic stenosis [44]. Tropoelastin's amino acid sequence has alternating hydrophobic (primarily glycine, valine, and proline) and hydrophilic (primarily lysine, alanine, and proline) domains. Elasticity is driven by the shape and entropic spring-like properties of conjoined tropoelastin monomers, forming a "condensed coil" responsible for elasticity. The C-terminal region, exposed after proper coiling, is responsible for cell binding [45].

Tropoelastin can be upregulated by TGF- β signaling, occurring post-transcriptionally through stabilization of the messenger RNA [46]. One component of the elastic fiber, the matricellular protein microfibril-associated glycoprotein-1 (**MAGP-1**), activates latent TGF- β

signaling directly [47], potentially presenting an opportunity for molecular engineers looking to encourage elastogenesis. MAGP-1, a matricellular protein that helps modulate SMC homeostasis during spreading [48], inhibits binding of latent TGF- β binding protein (**LTBP**)-1 to fibrillin-1, and could fine tune concentration and deposition of the large latent TGF- β complex (**LLC**) [49].

An additional potential regulator of TGF- β activity upstream of elastin transcription is the matricellular protein emilin-1, which associates with elastic fiber components and inhibits all three pro-TGF- β molecules [50] as a regulatory mechanism for blood pressure [51].

After transcription and translation, elastin is trafficked to the surface of the cell, where it is chaperoned to fibrillin microfibrils and assembled (**Figure 1**). Tropoelastin and chaperone proteins assemble outside of the cell, creating elastin “coacervates” or “globules” with two major classes of interactions [1-3]. One is mediated by fibulin-4, which binds to tropoelastin and facilitates cross-linking by lysyl oxidase (**LOX**). The other is mediated by fibulin-5, which binds tropoelastin together with lysyl oxidase-like 1 (**LOXL-1**). Tropoelastin coacervates are deposited along the fibrillin-1 microfibril complex, with initial interaction mediated by LTBP-4 [52-55]. Subsequent tropoelastin cross-linking involves the chemical modification of lysine residues, followed by condensation reactions to form desmosine and isodesmosine cross-links. Note that many important steps of microfibril assembly prior to elastin deposition, including the involvement of fibronectin and other members of the LTBP family, are excluded here for clarity.

Deposited tropoelastin coacervates are integrated within the fibrillin-1 microfibril complex, creating the structure for mature functional elastic fibers. Intra and inter-molecular crosslinking of deposited tropoelastin coacervates is performed by LOX and LOXL-1 within lysine-rich hydrophilic tropoelastin domains [56, 57], opening the coacervate structure and to form a mature, mechanically-active resilient elastic macrostructure.

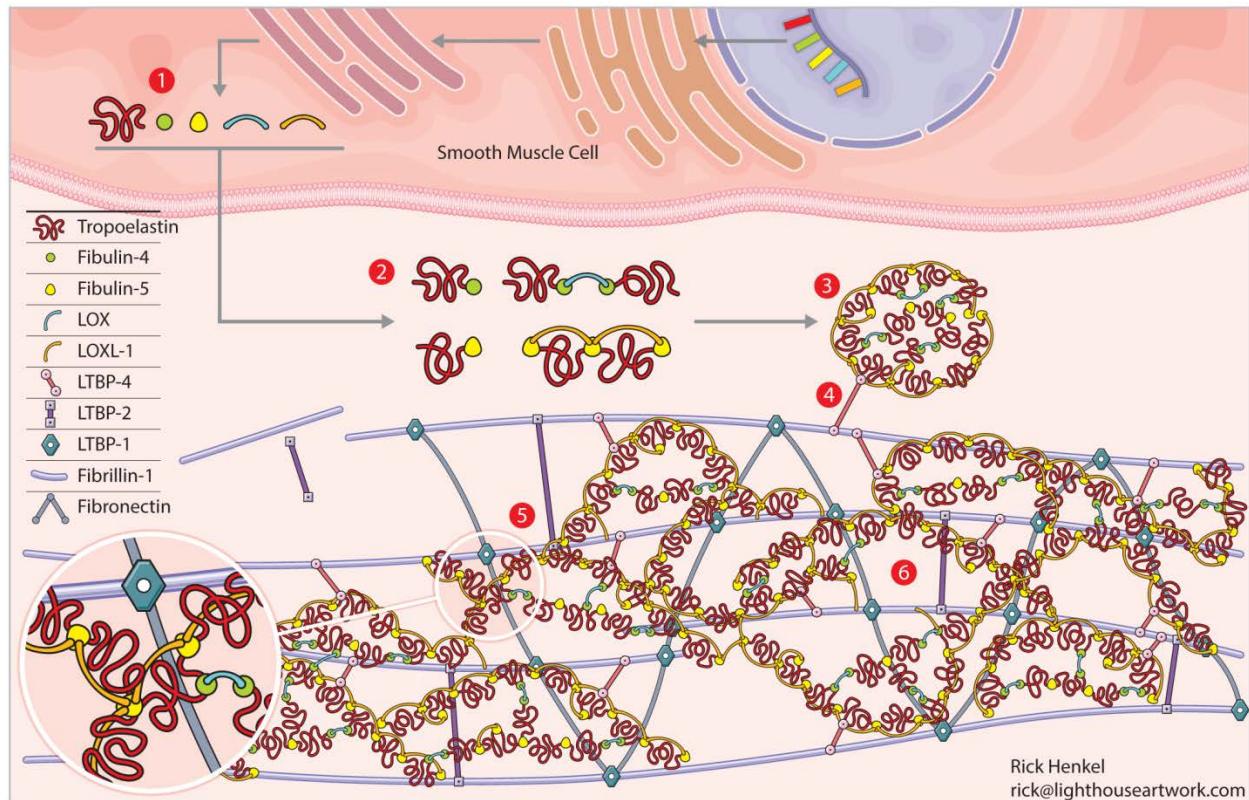


Figure 1: SMC elastogenesis cascade.

(1) Transcription of tropoelastin and its chaperone organizational matricellular proteins. (2) Tropoelastin and chaperone proteins assemble outside of the cell, with two major classes of interactions. One is mediated by fibulin-4, which binds to tropoelastin and facilitates cross-linking by lysyl oxidase (LOX). The other is mediated by fibulin-5, which binds tropoelastin together with lysyl oxidase-like 1 (LOXL-1). (3) Tropoelastin coacervates, or globules of tropoelastin and chaperone proteins, are formed. (4) Tropoelastin coacervates are deposited along the fibrillin-1 microfibril complex, with initial interaction mediated by LTBP-4. Note that many important steps of microfibril assembly prior to elastin deposition, including the involvement of fibronectin, are excluded here for clarity. (5) Deposited tropoelastin coacervates integrate within the fibrillin-1/LTBP-1/LTBP-2/fibronectin microfibril complex. (6) Cross-linking, via LOX and LOXL-1, occurs between deposited tropoelastin coacervates within the microfibril complex, opening the coacervate structure and forming mature, mechanically-active elastic fibers. Original illustration, made in coordination with Rick Henkel at Light House Artwork (rick@lighthouseartwork.com).

(Published in Publication #3 from Section 7.2)

1.2.2 Elastin Chaperone Matricellular Proteins in Regenerative Medicine

Aforementioned elastin organizational matricellular proteins (members of the fibrillin, fibulin, LOX, and LTBP families) are downregulated during adulthood within healthy aortic walls [58, 59]. The interplay of elastin chaperone proteins is crucial for mature, functional elastin deposition. Current regenerative analysis methods often limit their scope to molecular analysis of tropoelastin, omitting the milieu of chaperone proteins involved within aortic elastogenesis.

Fibrillin-1 and fibrillin-2 are both important for elastic fiber development and maintenance of a healthy vasculature. Fibrillin-2 displays preferential accumulation in elastin rich areas [60] while fibrillin-1 is more widely expressed, making it unsurprising that MFS patients have a wide spectrum of pathologies [61]. Fibrillin-1 [62] and fibrillin-2 [63] deficient mice both die soon after birth due to aortic rupture, although qualitative differences were observed in the medial wall between the two forms of fibrillin deficiency. One theory for the different modes of action of the fibrillin isoforms is that initial fibrillin-2 involvement aids aortic matrix stability, but continued fibrillin-1 expression is essential for maturation and post-neonatal vascular function [63].

Fibulin-2, a protein that binds extracellular ligands, is thought to provide redundancy with fibulin-1 (which interacts with elastin precursor tropoelastin), since fibulin-1 knockout mice produce vessels with viable elastic fibers [64]. Fibulin-2 interacts with virtually all elastin precursors (though it is not associated with tropoelastin deposition by fibroblasts [65]) and expressed in basement membrane of heart, with an enhanced role during development [66]. Fibulin-2 has the highest binding affinity to elastin of the fibulins, and interacts with fibulin-5 to form the elastic lamina by directing elastic fiber microassembly during development and after

injury [67]. Fibulin-5 is itself an elastin binding protein involved in primary organization and assembly of elastic fibers [68].

Dr. Hiromi Yanagisawa's group has shown that fibulin-5 is essential for mature elastin deposition both *in vivo* and *in vitro* [69]. Though groups have identified basic fibulin-5 biochemical interactions, particularly its proteolytic cleavage in diseased tissue and impact on desmosine formation [70], few have targeted fibulin-5 as a cardiovascular regenerative medicine tool to help organize newly deposited aortic tropoelastin. In a mouse fibrosis model, loss of fibulin-5 resulted in a reduction in aortic stiffness, possibly halting the stiffness-induced local inflammatory response and deposition of ECM [71]. Mutation to fibulin-5 alone causes a cutis laxa phenotype highly susceptible to arterial tortuosity, but without presenting with aneurysm [72]. Other members of the fibulin family have key role in the elastogenesis and ECM deposition cascade as well. As reviewed in [73], mutations in the matricellular protein fibulin-4 have been linked to cutis laxa, causing both high arterial tortuosity and ATAA formation [74].

1.2.3 Elastin and Matricellular Proteins in Aortic Disease

Elastin degradation is the most common feature within AA walls, with other features including mechanical wall stress [75-77], inflammatory response and proteolytic degradation [78-80], and exogenous circulating growth factors (primarily activating the TGF- β pathway) [81] disrupting local AA SMCs and elastic fibers [82], leading to increased risk of rupture.

MFS is a systemic mutation of the microfibrillar protein fibrillin-1, impacting the elastin coacervate deposition stage of the elastogenesis cascade and resulting in a lack of mature insoluble elastin [83]. Deficiency of fibrillin-1 commonly results in a dilation of the aorta for MFS patients, though fibrillin-1 may be more vital to aortic tissue homeostasis rather than elastic

fiber assembly [62] pointing to the inability of MFS aortic walls to adapt to high hemodynamic stress as the primary driver of dilation and aneurysm.

LDS is caused by a mutation in TGF- β 1 or TGF- β 2 receptor genes (*TGFBR1* and *TGFBR2*) [73, 84], leading to the overproduction of collagen I/III and disorganization of elastic fibers with loss of mature insoluble elastin protein within aortic walls [85]. Additional LDS-related mutations have been found in TGF- β 2 [86] and Smad3 [87], a downstream signaling molecule within the TGF- β pathway.

ATAA in BAV patients is often attributed to adverse hemodynamic flow conditions, smooth muscle cell death and subsequent synthetic phenotypic changes, and an imbalance of collagen I/III to elastin production within the affected aortic region [77]. Elastin destruction is more localized within the concave region of BAV-ATAA [88], with an accompanied production of tenascin and fibronectin observed at these sites of severe elastic fiber fragmentation. Similar to MFS, a subset of BAV patients exhibit mutations in the fibrillin-1 gene [89], as well as abnormalities in the NOTCH1 [90] and actin alpha 2 smooth muscle aorta (ACTA2) [91] genes seen in BAV-ATAA patients highly prone to aneurysm and dissection.

1.2.4 Elastin in Regenerative Medicine and Vascular Tissue Engineering

Pro-elastogenic regeneration strategies typically focus on one of three major mechanisms of elastin breakdown within diseased aortic tissue: (1) suppression of inflammatory degradation of elastin (elastolysis), (2) SMC dysfunction and modulation of SMC phenotype to regulate elastolysis, and (3) induction of new mature elastin deposition.

Strategies to inhibit elastolysis include clinical evaluations of matrix metalloproteinase (MMP)-inhibitors to halt AA dilation and broad-targeted antihypertensives to reduce vascular wall stresses and slow pediatric AA growth, further discussed in **Section 1.4.2** .

Regeneration strategies working to both regulate SMC phenotype and induce new elastin deposition include exogenous stimulation using soluble factors. A combination of TGF- β and oligomers of the glycosaminoglycan hyaluronan induced elastin deposition *in vitro* on murine SMCs isolated from early- and late-stage AAA [92].

Additionally, bioreactor cultures within SMC-seeded vascular grafts have been used to leverage induction of elastin deposition into a functional vascular scaffold. Human SMCs have been seeded within an electrospun poly(ethylene glycol) dimethacrylate/poly(L-lactide) (or, PEGdma/PLA) scaffold, with a laminar shear stress bioreactor inducing elastin protein transcription and elastin chaperone protein upregulation (fibrillin-1, fibrillin-2, fibulin-4, fibulin-5, and LOX) [1]. Similarly, induced pluripotent stem cell-derived SMCs seeded within PEGdma/PLA scaffolds showed the same pattern of elastin and elastin chaperone protein deposition [93]. Elastin deposition was also induced by adult baboon SMCs seeded within a poly(glycerol sebacate) scaffold using unsupplemented culture media within a pulsatile flow bioreactor [94], with smaller pore sizes as a mechanism to increase SMC seeding density and ECM deposition density. Acellular fibrin gel pulmonary artery grafts, seeded with ovine dermal fibroblasts, were repopulated by SMCs and saw significant elastin and collagen deposition after 42 weeks of implantation within a growing lamb model [95].

Elastin has also been used as an essential biomaterial integrated within tissue engineered vascular grafts and other related aortic biomaterials. Incorporation of insoluble elastin within an electrochemically-aligned collagen fiber graft mimicked the mechanical properties of native

vasculature and increased SMC recruitment and phenotype modulation within the graft [96]. A stabilized elastin tubular scaffold was created by decellularizing and digesting collagen from porcine carotid arteries via alkaline extraction, and treating the remaining ECM with penta-galloyl glucose [97]. However, proteomic analysis comparing three different human adipose extracellular matrix decellularization techniques (enzymatic, detergent, and solvent-based methods) showed minimal evidence of elastin preservation alongside significant maintenance of collagen, fibrillin, laminin, and vimentin, signaling even the most sophisticated decellularization techniques require a stabilizing agent to preserve elastic fibers [98]. An elastin-based polymer was synthesized using the main polypeptide elastin sequence glycine-valine-glycine-valine-proline (GVGVP), as a potential alternative solution for elastin within tissue engineered vascular biomaterials [99].

1.3 Aortic SMCs

1.3.1 SMC Differentiation in Diseased Aortic Tissue

SMC response to the local microenvironment (via ECM stiffness, exogenous factor signaling, or other external stimuli) plays a significant role in aortic wall maintenance, regulating ECM secretion, MMP activity, inflammatory response, and atherosclerosis. SMCs are responsible for the synthesis, alignment, and maintenance of elastin during development to provide effective passive recoil in response to hemodynamics and local tissue deformation. Pro-inflammatory cytokines play a key role in SMC regulation within the aortic wall, with monocyte chemoattractant protein 1 (**MCP-1**), involved in the recruitment of monocytes and accelerate

macrophage differentiation [100], induced following leukocyte adhesion to EC-expressed adhesion proteins VCAM-1 and E/P-selectin [101]. Differentiated macrophages internalize lipoproteins and form foam cells [102], which also work to modulate local aortic SMC microenvironment regulation.

Medial SMCs undergo phenotypic switching along a “spectrum” of differentiation status [103], moving from a contractile or quiescent phenotype towards a hyper-proliferative synthetic (or hyperplastic) phenotype [104, 105]. Foam cell-induced phenotype modulation is induced through inflammatory cytokine and circulating factor signaling [106], including platelet-derived growth factor and the TGF- β family, foam cell lipid byproducts [107], or paracrine signaling by neighboring cells [105]. Mechanical stimulation has also been shown to modulate SMC phenotype, both *in vitro* and *in vivo* [108, 109].

Atherogenesis, or the formation of atherosclerotic plaques, starts as synthetic SMCs absorb surrounding foam cell-secreted lipid byproducts to form a thick collagen-rich fibrous cap below the intimal aortic EC monolayer [110, 111]. The underlying SMC and ECM layers undergo necrosis as macrophages secrete MMPs, with MMP-2 and MMP-9 acting as primary drivers for ECM degradation below the plaque surface [102]. Local secretion of tumor necrosis factor alpha (**TNF- α**) and interleukin-1 by macrophages and SMCs help drive SMCs further towards a synthetic phenotype [112]. Interferon gamma (**IFN- γ**), Interleukin-1 beta (**IL-1 β**), and TNF- α all have the ability to induce the local expression of nitric oxide synthase (**NOS**) [113], resulting in an upregulation of EC and SMC apoptosis [114]. Macrophage-derived serine and cysteine proteases also modulate degradation of collagen and elastin within the fibroatheroma plaque, causing platelet aggregation and increased risk of downstream deep vein thrombosis.

Angiotensin II (**AngII**) helps to promote atherosclerosis by inducing the adhesion and migration of SMCs, and is mediated by osteopontin [115].

Similar SMC phenotype modulation can change local protease activity and pro-inflammatory cytokine production, increasing extracellular matrix breakdown within AA. MMP-2 activity and MMP-9 expression correlates strongly with human AAA elastolysis in explanted tissue [116], with effects augmented by macrophage infiltration [117] Upregulation of local MMP-2 and MMP-9 in a murine AAA by SMCs with decreased expression of α -smooth muscle actin and SM22 α occurs early in AA progression, resulting in detectible fragmented elastin even before ‘aneurysmal’ dilation threshold of 150% is crossed [118]. AAA has a similarly high level of MCP-1-mediated macrophage infiltration to atherosclerotic models, with additional upregulation in oxidative stress markers mitochondrial superoxide dismutase and peroxiredoxin-1, potentially driving AAA elastin fragmentation [119]. Recruitment and phenotypic modulation of T cells [120] and inhibition of key pro-inflammatory cytokines (IL-1 β inhibition, for example) has been targeted as key targets for small abdominal AA therapeutics [121]. Though significantly less characterized than atherosclerosis, SMC phenotypic modulation has shown to be a key target for small aneurysm therapies, serving as a key mediator to potentially reduce MMP expression, slow ECM breakdown, and stabilize AA.

1.3.2 Local Matricellular Proteins and Microenvironment Can Act To Regulate Aortic SMCs

Aortic SMCs are essential for maintenance of structure and integrity of vascular walls and are highly influenced by locally-deposited extracellular matrix and matricellular proteins, making aortic SMCs key targets for aneurysmal therapeutics.

SMCs also can potentially synthesize new elastin in response to damage; however, current strategies have been limited in their ability to generate mature elastin deposition from adult SMCs at the transcriptional level. Instead, SMC adhesion and migration have been vascular engineering targets, and elastogenesis stimulation can be targeted by a combination of SMC recruitment and phenotype regulation to produce organizational elastin chaperone proteins.

Fibulin-5, in addition to its well-documented role on elastogenesis, is the primary mediator of urokinase-type plasminogen activator (**uPA**)-driven migration of SMCs [122]. The mechanism for this appears to be that fibulin-5 binding facilitates activation of uPA, which then activates plasmin to cleave the portion of fibulin-5 that binds β_1 integrin, driving cell migration. This action increases SMC remodeling and vascularization after injury and antagonizes angiogenesis by inducing thrombospondin-1 (**TSP-1**) and antagonizing FN receptors [122, 123]. Galectin-1, a glycan-binding protein primarily involved within anti-inflammatory cardiac tissue response to acute myocardial infarction, has shown to restrict SMC motility and modulates focal adhesion turnover on fibronectin, via *in vitro* assays using galectin-1 knockout mouse SMCs [124].

Vitronectin, an adhesive matricellular protein active within tissue remodeling conditions, significantly mediates differentiation of Flk-1+ cardiac progenitor cells seeded within a vitronectin-coated electrospun polycaprolactone/gelatin scaffold [125]. The scaffold guided pluripotent embryonic stem cells into cardiomyocytes, SMCs, and ECs and promoted cell spreading and high proliferation rates among the differentiated cells [126]. A novel α_v integrin antagonist was developed to prevent vitronectin-tenascin integrin interactions locally and suppresses angiogenesis in both cardiac and tumor models [127]. Taken together, vitronectin

presents with an advantageous coating substrate for 3D vascular scaffolds [128], and inhibition of vitronectin binding is a novel target for anti-angiogenic tumor therapeutics.

In post-injury vasculature, galectin-1 is upregulated within proliferating SMCs, and reciprocally an engineered galectin-1 fusion protein is able to drive SMC proliferation [129]. Galectin-1 was upregulated in both murine experimental acute myocardial infarction cardiac tissue and by human cardiac fibroblasts from end-stage heart failure patients [130]. Galectin-1-deficient mice displaying increased cardiac macrophages and killer T cells and impaired cardiac function 7 days after infarction induction, which was reversed by treatment with recombinant galectin-1. Taken with its effects on increasing SMC proliferation and restricting SMC motility, galectin-1 presents as a potential supplement for cardiac therapeutics post-myocardial infarction and a serum biomarker for cardiac stress [131] with a well-characterized mouse model for *in vivo* evaluations.

The CCN family of matricellular proteins have significant, yet indirect, effects aiding vascularization and angiogenesis that might be considered in engineering microenvironment applications. Full length CCN2 (or CTGF, connective tissue growth factor) utilizes integrin $\alpha_6\beta_1$ to promote adhesion and spreading of SMCs [132]. CCN5 (or WISP2, WNT1-inducible signaling pathway protein-2) also inhibits SMC proliferation and motility without affecting apoptosis and adhesion [133, 134], and has potential to be used as a delivered therapeutic CCN2 antagonist to control SMC migration, adhesion, and phenotype [135]. CCN5's effects are modulated in a dose-dependent fashion by platelet derived growth factor (**PDGF**) and TGF- β , with some possible quiescence-related SMC properties [133]. A reduction in CCN2 expression was observed in Notch1 haploinsufficiency murine abdominal aortic aneurysm models, leading

to a maintenance of contractile SMC phenotype and a reduction in aortic dilation [136]. CCN2 presents with a key target for SMC phenotype maintenance in vasculopathy.

CCN4 (or WISP1, WNT1-inducible signaling pathway protein-1), is upregulated in migrating SMC in a Wnt2-dependent manner; loss of CCN4 leads to inhibited SMC integrin mediated migration [137]. Wnt5a, which induces b-catenin signaling in mouse via SMCs, saw CCN4 rescue SMCs from H₂O₂ induced apoptosis within atherosclerotic plaque [138, 139]. CCN4 was expressed within advanced human coronary artery lesions [137] but absent in Wnt5a positive intimal SMCs, indicating that CCN4 deficiency may provoke SMC apoptosis in coronary plaques, ultimately resulting in instability. Loss of CCN4 leads to reduced intimal thickening, related to CCN4's aforementioned positive effect on SMC migration [137].

SMC also cooperate with EC to regulate vascular tone. EC receive signals from the circulation that stimulate production of the second messenger nitric oxide (**NO**), inducing SMC relaxation and vessel dilation. In contrast, agents such as angiotensin II act directly on SMC, causing the cell to contract and the vessel to constrict.

Tenascin-C (**TNC**) overexpression can result in pulmonary hypertension, and is expressed in adventitia and media of saphenous vein grafts under above average arterial stress pressure [140]. TNC within the context of atherosclerotic plaques promotes SMC proliferation and migration via PDGF signaling [141]. Areas of human AAA with high TNC expression by medial SMCs correlate strongly with inflammation and tissue ECM destruction [142] and acts as a murine hemodynamic stress dampening mechanism to preserve aortic integrity [143]. Taken together, TNC presents with a SMC-linked biomarker target to assess atherosclerosis or aneurysm pathological state.

Substrate stiffness has also shown an effect to modulate both SMC and EC phenotype, and as a mechanosensor that governs secretion of cytokines and deposition of extracellular matrix proteins. While effects of exogenous delivery of TGF- β -family molecules *in vivo* has produced both a pro-remodeling cardioprotective response and induced aberrant ECM deposition by hyperplastic cells, TGF- β 1 has been consistently upregulated in SMCs and ECs seeded onto stiff substrates, acting as a possible chemokine mechanosensor of the local ECM microenvironment [144].

In vitro influence of substrate stiffness is also clear, favoring further vascular SMC and EC studies within 3D constructs and seeded on a substrate with adventitial stiffness. ECM protein fibronectin, for example, is essential for SMC durotaxis migration across substrates of varying stiffness [145], and mediates EC shear stress-induced responses via fiber alignment and availability of heparin-binding regions [146]. Fibronectin to modulate substrate stiffness is also essential for EC internalization of vascular endothelial growth factor (VEGF), through EC surface receptor CD29 interactions with fibronectin in the 3D construct. DNA methyltransferase 1, an enzyme that catalyzes methyl-group transfer to DNA, directly alters SMC phenotype in response to *in vitro* matrix stiffness of embedding construct substrates, and acts *in vivo* to negatively regulate arterial stiffening by maintaining SMC contractile phenotype [147].

1.3.3 Aortic SMC ECM Secretion and Neointimal Hyperplasia

Neointimal hyperplasia, a thickening of the aortic intimal layer due to overproliferation of SMCs and deposition of proteoglycan-rich ECM, is a common complication of vascular disease intervention [148]. The main target for anti-neointimal formation is SMC phenotype, given the predisposition of unregulated hyperplastic SMC proliferation to accelerate neointimal

formation. Many extracellular matrix proteins have shown efficacy in controlling SMC phenotype and adhesion, and therapeutics often target at upregulation of these factors. TSP-1 targets NO-mediated SMC relaxation to increase tissue survival and facilitate tissue perfusion to preserve tissues under ischemic stress [149]. SMC are also induced to proliferate by TSP-1 [150]. Fibromodulin adenovirus-mediated gene transfer inhibits restenosis in an organ culture saphenous vein graft disease model of neointimal hyperplasia, at a much greater level than decorin or beta-galactosidase gene transfer [151]. Fibromodulin could be a key member of the small leucine-rich proteoglycan family for study within ECM-based vein grafts.

Another ECM-related inducer of neointimal formation is fibulin-1, whose expression is closely overlapped with fibrinogen. Fibulin-1 and fibrinogen bind tightly within atherosclerotic lesions, but this does not hold true in ECM associated with SMC surrounding the identified lesion. Fibulin-1 is associated with atherogenesis in diabetic patients, and at high levels fibulin-1 becomes an accurate indicator of cardiovascular risk in patients prior to acute cardiovascular events, obesity, or diabetes risk markers [152]. SMCs display increased SMC contractile differentiation markers with fibulin-5 overexpression [68], and SMC phenotype has also been regulated through fibulin-4 expression in murine models [153]. Overexpression of fibulin-5 has been shown post-injury to increase SMC motility in a step to aid in vascular remodeling [122].

CCN3 (or NOV, nephroblastoma overexpressed) exhibited a protective role within the progression of murine abdominal aortic aneurysm model [154], and inhibited neointimal hyperplasia by inhibiting SMC migration and proliferation [155]. Novel CCN3-based peptides have recently been developed, aiding in the modulation of pro-fibrotic factors CCN-2, plasminogen activator inhibitor (PAI)-1, and post-translational fibrotic collagen modification [156].

Osteopontin (**OPN**, also known as bone sialoprotein I or BSP-1), a matricellular protein first identified within osteoblasts, is expressed by SMC derived foam cells after immune response, and plays a large role in the calcification of atherosclerotic lesions [157]. Increased OPN expression during neointimal hyperplasia formation was seen as a major microenvironment component of human atherosclerotic plaque progression. OPN downregulates SMC differentiation markers α -smooth muscle actin and calponin, transitioning from quiescent status into an unregulated proliferative phenotype [158]. Galectin-1 binds to lipoprotein(a) (**LPA**), which binds tightly to low density lipoprotein (**LDL**) and are both co-implicated in atherogenesis. LPA binds poorly to tissue with galectin-1 inhibition, suggesting that LPA accumulation changes have an effect on atherogenesis, possibly mediated through t-antigens on LPA and LDL [159]. A novel engineering approach modulating OPN protein expression or galectin-1 binding within atherogenic arterial walls could present as a key mediating factor for downstream neointimal hyperplasia.

1.3.4 *In Vitro* SMC Cultures

Coculturing of aortic SMCs with ECs or stem cells in 2D or 3D cultures, or mimicking cellular communication via exogenous factors, have been the primary *in vitro* methods to mimic aortic wall biology. Vascularization as a function of oxygen diffusion [160], angiogenic microRNA expression of cocultures under shear stress conditions [161], and VEGF-induced manipulation of SMC proliferation and EC quiescence [162] have all been key evaluation targets for *in vitro* SMC-EC coculture studies. Proliferator-Activated Receptor α , induced by shear stress on ECs, is a key factor driving SMCs towards quiescence in coculture platforms [163]. Shear stress induced miRNAs within EC-SMC cocultures contain atheroprotective signals, with

delivery possibly mediated by secreted extracellular vesicles [164]. Substrate stiffness, even within SMC cocultures [165] and SMC-EC 3D constructs [166], has shown a significant impact on cellular drug uptake and effectiveness in SMC phenotype modulation and ECM secretion.

Aortic SMC/EC coculture with mesenchymal stem cells has a synergistic modulating effect, with MSCs guided towards cardiomyocyte or SMC differentiation when cocultured with SMCs [167] or ECs [168], and MSC mRNA guiding SMC actin filament organization [169]. Tunneling nanotubes have shown to be one mechanism for SMC-MSC communication, with mitochondrial exchange guiding both SMC phenotype and MSC differentiation [170]. Intercellular communication extends to matrix components, as EC-deposited ECM help guide MSC vascular differentiation independent from cell-cell contact [171]. EC and embryonic stem cell pericyte coculture can be engineered to form microchannel-sized vascular tubes, an essential tool for high-throughput studies of vascular abnormalities and cardiovascular intercellular interactions within organ-on-a-chip cultures [172]. Direct coculture of adipose-derived stem cells with a murine AAA wall as the culture substrate induced a phenotype change within the AAA wall SMCs, reducing overall MMP-2 and MMP-9 expression and inducing fresh deposition of elastin [173] and highlighting another mechanism for quasi-representative *in vitro* culture conditions to evaluate cardiovascular therapeutics.

1.4 Treatment for Aortic Aneurysm

1.4.1 Surgical Diameter Criterion for Aortic Aneurysm

Adults are diagnosed with AA once the aortic diameter exceeds ~1.5-times its normal value [174], and surgical intervention of repair is generally recommended after the AA exceeds a “critical diameter” of ~5.5cm and 1cm/year growth rate [17, 175]. For young adult patients, this dilation threshold is typically closer to 4.5cm [176, 177]; for pediatric patients, the critical threshold is a constant growth rate of 1cm/year [26]. Currently, endovascular aortic repair (**EVAR**) is the standard intervention for abdominal AA, with aortic diameter measurements determining the threshold for surgical intervention. Standard non-surgical options for patients with small AA (classified as an AA with a diameter above the aneurysmal classification threshold but below the “critical” threshold) are limited to semi-annual ultrasound or CT imaging surveillance, with current pharmacological agents providing minimal evidence of AA-targeted effects [178, 179].

Around 20% of WS patients will need surgical intervention before 15 years of age, primarily consisting of a Y-shaped Brom patch [180]. Though repeated WS interventions are rare, the underlying deficiency in functional vascular elastin remains [39]. Endovascular aneurysm repair is the primary surgical interventional method for most MFS and LDS aneurysm patients at high risk of aneurysm rupture [181], delivering a synthetic graft via catheterization. While early screening has reduced rupture rates over the last two decades [182], there is no standard intervention for patients with aortic diameter below the aforementioned critical threshold of 5.5cm in adults and 4-5cm in pediatric patients to prevent further, possibly lethal, ECM degradation without surgical intervention. Studies have shown that graft placement

performed on sub-critical dilated aneurysms provide no further benefit to long-term survival, highlighting the need for a non-surgical treatment [174].

Non-surgical aortic treatment alternatives for MFS, LDS, and WS patients under 20 years old would delay surgical intervention. MFS patients undergoing elective care (surgical or otherwise) after 25 years old have lower morbidity & mortality rates than patients without intervention, but mortality rates dramatically increase in cases where insufficient (or nonexistent) sub-critical diameter treatment has led to emergency aortic replacement [183]. Recurring aneurysm in LDS patients, in particular, is another major area of need for studies to maximize time between repeated surgical interventions [26], as 33% of patients require additional surgeries.

MFS and WS are genetic diseases that manifest with severe aortic complications (primarily within the thoracic aorta and aortic arch). Surgical outcomes for sub-4.5cm aortic dilations often improve as patients age, underscoring the need for a non-surgical intervention to enhance the underlying disrupted elastin deposition.

1.4.2 Treatment for Sub-Critical Aortic Aneurysm

The primary treatment for adult small AAA is prescription of a standard monitoring and surveillance regime, or “watchful waiting”, which involves a CT scan or MRI every 6, 12, or 24 months as tailored to each patient. The balance for both patients and clinicians as the small aneurysm continues to grow is weighing risk of rupture versus risk of repair. Mortality rates for the roughly 27,000 annual surgical repairs, both open and EVAR, are ~2%. However, 23.4% of sub-critical adult AAs ranging between 4.1 and 5.5cm rupture [184], and the cost of passive

surveillance (\$40,592 on average, per patient for four years of standard surveillance) is significantly higher than the potential cost of early endovascular repair (\$15,197 on average, per patient for four years post-surgery) [185]. The current small aneurysm standard-of-care of passive monitoring must be improved, as it both leaves the patient at a high risk for sub-critical rupture and incurs a high cost for both patient and payer.

A targeted, non-surgical therapeutic option for dilating AAs is needed as a supplement to imaging and monitoring regimens. Broad-targeted therapies, such as beta blockers or angiotensin-converting-enzyme (ACE) inhibitors are prescribed to slow aneurysmal growth [179, 186-188], particularly within pediatric patients. Pre-clinical aneurysmal therapies, including MMP inhibitors doxycycline [189, 190] and several modified tetracyclines [191], are currently being evaluated as non-surgical options to prevent elastin degradation.

Low elastin content in ascending thoracic aortic aneurysms and lowered elastin concentration in infrarenal abdominal aortic aneurysms [80] have pointed to the secretion, coacervation and cross-linking of elastin as a worthwhile aneurysmal therapeutic target. A targeted regenerative treatment, wherein functional elastic fibers are restored, could offer a non-surgical therapeutic option for adults with small AA, and an AA maintenance therapy for children with connective tissue disorders.

1.5 Previous Work in the Advisor's Laboratory: Stem Cell-Based Therapies for AA

It is hypothesized that ASCs help maintain existing elastic fibers by modulating SMC phenotype to repress immune inflammatory response in local AA tissue [192], suppress elastin breakdown [193], or stimulate new elastin deposition [194]. Other groups have shown that

human ASCs suppress inflammatory response within elastase-induced murine abdominal AA, with paracrine signaling decreasing T cells (CD8+ and CD4+), neutrophils, and activated monocytes, while increasing Tregs and CD206+ M2 macrophages [195]. Subdermal implantation of ASC-seeded scaffolds within diabetic rat models helped suppress inflammatory cell recruitment (CD8+ T-cells and CD68+ pan-macrophages) when compared to cell-free scaffolds, suggesting that immunomodulatory effects of autologous adipose-derived stem cells still plays a significant role [196]. Previous work by the Vascular Bioengineering Laboratory (VBL, Director: Dr. David Vorp, Associate Director: Dr. Justin Weinbaum) at the University of Pittsburgh has shown that seeding tissue engineered murine AAA grafts with adipose stromal cells isolated from both elderly and diabetic patients resulted in a loss of this inflammatory response suppression and decreased fibrinolysis, highlighting the need for healthy adipose stromal cell therapeutic signaling within aneurysmal walls [197].

The VBL has also induced elastin regeneration via delivery of non-diabetic non-smoking adipose-derived stromal cells (ASCs) within the AA context. Periadventitial ASC delivery to a growing elastase-induced mouse abdominal AA halts aneurysmal growth, prevents further elastin degradation, and possibly stimulates new elastin synthesis, as evidenced by maintenance of elastic lamellae [198]. The VBL has produced a small-diameter tissue engineered vascular graft, our group has demonstrated that ASCs and pericytes are required for patency and ECM remodeling of an elastomeric tubular scaffold within interpositional abdominal aortic implants [199, 200]. These studies also show evidence of extracellular matrix deposition (elastin and collagen) eight weeks post-implantation within a murine model [201, 202].

1.6 Hypothesis and Specific Aims

The work of this dissertation at the VBL and Vascular Extracellular Dynamics Laboratory (VEDL, Director: Dr. Justin Weinbaum) addresses the need for a non-surgical therapy for sub-critical aortic aneurysm in both adult and pediatric populations. Each chapter emphasizes different stages of clinical translation for this therapeutic approach, including ASC-SF effects on healthy adult aortic SMCs, diseased SMCs provided through our collaborators at UPMC Presbyterian Hospital and the UPMC Children's Hospital of Pittsburgh, and commercialization avenues for scaling ASC-based therapies including a magnetic-guided fibrin gel ASC delivery mechanism and the effects of only ASC-SF extracellular vesicles on SMC elastogenesis.

Specific Aim 1: *Development of In Vitro 3D Fibrin Construct Platform & Elastogenesis Impact of Adipose-Derived Stromal Cell Secreted Factors on Healthy Adult Smooth Muscle Cells.*

Induction of elastin deposition by adult aortic SMCs is central to the development of a non-surgical therapeutic strategy for small aortic aneurysm. Here, we hypothesize that the elastin-preservative effect summarized in **Section 1.4.2** and **Section 1.5** can be replicated using only paracrine signaling factors secreted by ASCs, using an ASC conditioned media-based exogenous culture media. To analyze the elastogenic effects of the ASC secreted factors (ASC-SF), we created a three-dimensional fibrin gel *in vitro* culture platform, and utilized a multi-level analysis of mature elastin deposition that quantifies four levels of the elastogenesis cascade: transcription of tropoelastin and elastin chaperone proteins necessary for mature elastin

deposition, elastic fiber network formation, insoluble elastin protein deposition, and mechanical characterization of deposited ECM (**Chapter 2.0**).

We hypothesized that ASC-SF would increase SMC elastin chaperone protein transcription and increase insoluble elastin deposition when compared to both standard SMC culture media and non-conditioned ASC culture media, providing an initial proof-of-concept for ASC-SF as an elastin-targeted small aortic aneurysm therapeutic.

Specific Aim 2: *Elastogenesis Impact Analysis of Adipose-Derived Stromal Cell Secreted Factors on Patient-Derived Aortic Aneurysmal Cells.*

Integration of aneurysmal SMCs into the established *in vitro* fibrin gel culture system and elastogenesis analysis structure outlined in Specific Aim 1 provided a closer representation of the effects of ASC-SF on at-risk patients. We hypothesized that cells isolated from explanted aneurysmal aortic medial layers would increase elastin chaperone protein transcription and insoluble elastin deposition when stimulated with ASC-SF.

Chapter 3.0 outlines a collaboration with the Thoracic Aortic Disease Research group, under the direction of Thomas Gleason, MD, to integrate SMCs explanted from adult aortic tissue samples within our elastogenesis cascade analysis system. **Chapter 4.0** outlines a collaboration with the Division of Pediatric Cardiothoracic Surgery at the UPMC Children's Hospital of Pittsburgh, under the direction of Victor Morell, MD. Here, we outline a mechanism to explant, culture, and store cells from explanted pediatric aortic samples, and integrate medial layer cells into our elastogenesis cascade analysis system.

Specific Aim 3: *Development of Clinical Translation Approaches for ASC Therapeutic Delivery.*

Ultimately, translation of ASC and ASC-SF as therapeutics for small aneurysm elastin regeneration has two major initial hurdles. First, localization to the aneurysmal site without destabilizing the weakened aortic tissue is vital, with previous work by the VBL targeting a periadventitial delivery modality. **Chapter 5.0** outlines the development of a magnetic-based periadventitial ASC localization system, and a Tri-Syringe device designed to form injectable ASC-rich fibrin gel constructs at the aneurysmal site. We hypothesized that this delivery mechanism would enable formation of an *in vivo* solid fibrin gel within a mouse abdomen, and would combine with an external magnetic field to localize iron nanoparticle-loaded ASCs to the periadventitial surface of an elastase-induced abdominal aortic aneurysm.

The second clinical translational hurdle is the infeasibility of whole-cell ASC therapy as an off-the-shelf solution to regenerate elastic fibers within small aneurysmal walls. **Chapter 6.0** outlines the isolation of ASC-secreted extracellular vesicles (ASC-EVs), and their ability to induce the elastogenesis cascade within the same healthy adult aortic SMC *in vitro* model established in Chapter 2.0. We hypothesized that ASC-EVs would increase elastin chaperone transcription and insoluble elastin deposition by healthy adult aortic SMCs, after 30 days of culture within our fibrin gel construct system.

2.0 Specific Aim 1: Development of *In Vitro* 3D Fibrin Construct Platform & Elastogenesis

Impact of Adipose-Derived Stromal Cell Secreted Factors on Healthy Adult

Smooth Muscle Cells

Prior studies within the Vascular Bioengineering Laboratory at the University of Pittsburgh have established adipose-derived stromal cells (ASCs) as a mechanism to preserve elastic fibers within murine elastase-induced abdominal aortic aneurysms [198]. Here, we attempt to determine whether that pro-elastogenic effect can be replicated by using only ASC secreted factors (ASC-SF), with the goal of producing a cell-free and elastin-targeted therapeutic option for small aortic aneurysm. An *in vitro* three-dimensional fibrin culture system was established for healthy adult aortic smooth muscle cells (SMCs), with a series of elastogenesis cascade analysis tools used to provide a multi-level evaluation of ASC-SF induced elastin deposition. We hypothesized that ASC-SF would increase SMC transcription of elastin chaperone proteins, increase elastic fiber networking, increase insoluble elastin fraction within SMC-seeded fibrin gel constructs, and would produce a mechanically-active extracellular matrix (ECM) microenvironment.

2.1 Introduction

Aortic aneurysms (AA) are balloon-like enlargements of the aorta that possesses a life-threatening risk of rupture. AA are most prominent in both aging populations (primarily smokers) and pediatric or young adult patients with connective tissue genetic disorders [10].

Approximately 5 million Americans over the age of 50 are living with abdominal or thoracic AA [12, 13], with over 200,000 new AAs diagnosed annually [14]. Actively dilating AAs, if left untreated, can weaken and ultimately rupture or dissect, with over 15,000 annual AA ruptures/dissections [15, 16] and an 80-90% AA mortality rate representing the 15th leading cause of death in the United States [17-19].

One feature of AA dilation is the degradation of elastin, the extracellular matrix (ECM) protein within the aortic wall responsible for recoil forces during diastole. SMCs form mature elastin during late fetal and early postnatal stages of human development, and the expression of tropoelastin (elastin core protein) and elastin organizational matrix proteins (such as specific members of the fibrillin, fibulin, lysyl oxidase, and latent transforming growth factor β binding protein, or LTBP, families) are then downregulated during adulthood [58, 59]. Mechanical wall stress [75-77], inflammatory response and proteolytic degradation [78-80], and exogenous circulating growth factors (primarily activating the TGF- β pathway) [81] have been shown to disrupt local AA SMCs and elastic fibers [82], leading to increased risk of rupture.

Currently, endovascular aortic repair is the standard intervention for abdominal AA, with aortic diameter measurements determining the threshold for surgical intervention. Adults are diagnosed with AA once the aortic diameter exceeds ~1.5-times its normal value, and surgical intervention of repair is generally recommended after the AA exceeds a “critical diameter” of ~5.5cm and 1cm/year growth rate [17, 175]. Standard non-surgical options for patients with small AA (classified as an AA with a diameter above the aneurysmal classification threshold but below the “critical” threshold) are limited to semi-annual ultrasound or CT imaging surveillance, with current pharmacological agents providing minimal evidence of AA-targeted effects [178, 179].

However, 23.4% of sub-critical adult AAs ranging between 4.1 and 5.5cm rupture [184], underscoring the need for a targeted, non-surgical therapeutic option for dilating AAs. A targeted regenerative treatment, wherein functional elastic fibers are restored, could offer a non-surgical therapeutic option for adults with small AA, and an AA maintenance therapy for children with connective tissue disorders. Pediatric patients with “rapid aortic expansion” of AA (exceeding 0.5cm/year rate) typically undergo surgical intervention, often with several repeated surgeries and broad-targeted therapies (beta blockers, ACE inhibitors) prescribed [179, 186-188]. No elastin-targeted therapeutic is available for patients with small sub-critical AA, regardless of age.

Previous work by our lab has shown that periadventitial adipose-derived stromal cell (ASC) delivery to a growing elastase-induced mouse abdominal AA halts aneurysmal growth, prevents further elastin degradation, and possibly stimulates new elastin synthesis, as evidenced by maintenance of elastic lamellae [198]. It is hypothesized that ASCs help maintain existing elastic fibers by modulating SMC phenotype to repress immune inflammatory response in local AA tissue [192], suppress elastin breakdown [193], or stimulate new elastin deposition [194]. While it was initially theorized that these ASC subpopulations differentiate into functional vascular cells [203], subsequent studies have suggested that ASC secreted factors (ASC-SF) act in a paracrine manner on neighboring vascular host SMCs and ECs and possess a more potent immunomodulatory capacity than bone marrow-derived stromal cells [204], specifically pointing to the importance of urokinase-type plasminogen activator [205] and monocyte chemoattractant protein-1 [206] in remodeling. ASC-SF are rich in pro-angiogenic [207] and pro-inflammatory growth factors [208] (vascular endothelial growth factor, hepatocyte growth factor, interleukin-1 β , interleukin-6, interleukin-8, tumor necrosis factor- α), which play important roles in SMC ECM deposition [193, 209].

While multiple mechanisms can potentially explain the ASC effect, we hypothesize that paracrine signaling, through ASC-SF, could induce deposition of mature insoluble elastin by healthy adult aortic SMCs after 30 days of three-dimensional (3D) *in vitro* culture, resulting in improved viscoelastic aortic response via SMC-secreted matricellular ECM proteins *in vivo* [210]. The elastogenesis cascade requires a cadre of ECM accessory proteins for proper elastin processing and assembly (**Figure 1**), and these proteins must be monitored in a context that combines cellular biology with regenerative tissue engineering.

Our study utilized a versatile, fibrin-based 3D SMC aortic medial layer-mimicking culture platform (**Figure 2**) [211] and multi-level elastin analysis assays, initially established using a pro-elastogenic cell line (RFL-6, rat fetal lung fibroblasts) and simple exogenous stimulation factors (TGF- β 1) as a proof-of-concept for continued SMC studies. We analyzed ASC-SF induced SMC elastin deposition at four different points of interest on the elastogenesis cascade: elastin organizational mRNA levels (generating tropoelastin, fibulin-4, and fibulin-5 coacervates/globules) [1-3], elastic fiber organization (through LTBP-4, fibulin-4, and fibulin-5 mediated deposition onto fibrillin-1 microfibrils) [52-55], cross-linked elastin chemical maturity (mediated by lysyl oxidase or LOX, and lysyl oxidase-like 1 or LOXL-1) [56, 57], and mechanical functionality. In addition, post-translational modification and mechanical function of the counterpart vascular ECM protein collagen were also studied.

2.2 Methods

2.2.1 RFL-6 Cell Culture Conditions

Rat fetal lung fibroblasts, RFL-6 cells, were purchased from ATCC (Manassas, VA) and plated between passage 6 and 12. RFL-6 cells were grown in standard Dulbecco's modified Eagle's medium/F12 medium, with 100U/mL penicillin, 100U/mL streptomycin (Invitrogen, Carlsbad, CA), and 20% fetal bovine serum (ThermoFisher Scientific, Waltham, MA) added. Supplements to culture media included ϵ -aminocaproic acid (ACA) (Sigma, St. Louis, MO) and recombinant human TGF- β 1 (R&D Systems, Minneapolis, MN). All media changes occurred every 36-48 hours.

2.2.2 SMC Cell Culture Conditions

Human aortic SMCs (ATCC #PCS-100-012, Manassas, Virginia) were cultured at 37°C and 5% CO₂, with growth media (#311K-500, Cell Applications Inc, San Diego, CA) changes every 48-72 hours. Cells used in experimental cultures were between passages 4 and 12.

2.2.3 3D Fibrin Gel SMC Constructs on Stiff and Soft Substrates

SMC-seeded fibrin gel constructs [212, 213] were formed using 3.7mg/mL bovine fibrinogen type I (Sigma-Aldrich #8630), 0.21U/mL bovine thrombin (Sigma-Aldrich #T7513), and 5×10^5 SMCs/mL. 'Stiff substrate' 200 μ L fibrin gel constructs (**Figure 2A**) were seeded

within heat-stamped circular molds made using 7.94mm (5/16") diameter cork borers onto tissue-culture treated plastic. "Soft substrate" 600 μ L fibrin gel constructs (**Figure 2B**) were formed between nylon anchors of FlexCell Linear TissueTrain untreated plates (FlexCell Int'l Corp #T-5001U), with "constrained" constructs cultured without external mechanical stimuli. "Dynamic" soft substrate fibrin gel constructs were subjected to a 10% stretch at 1 Hertz cyclic uniaxial mechanical loading using a FlexCell FX-4000 strain unit, to mimic standard aortic cardiovascular conditions [214]. Aminocaproic acid (ACA) (Sigma-Aldrich #07260), a lysine-mimicking fibrinolysis inhibitor, was added at 12mM to inhibit cell-driven degradation of the fibrin gel constructs. Treatment changes (see: "Media treatment conditions") were made every 48-72 hours, beginning 24 hours after initial gel polymerization and continuing through harvest at 20- or 30-days post-fabrication.

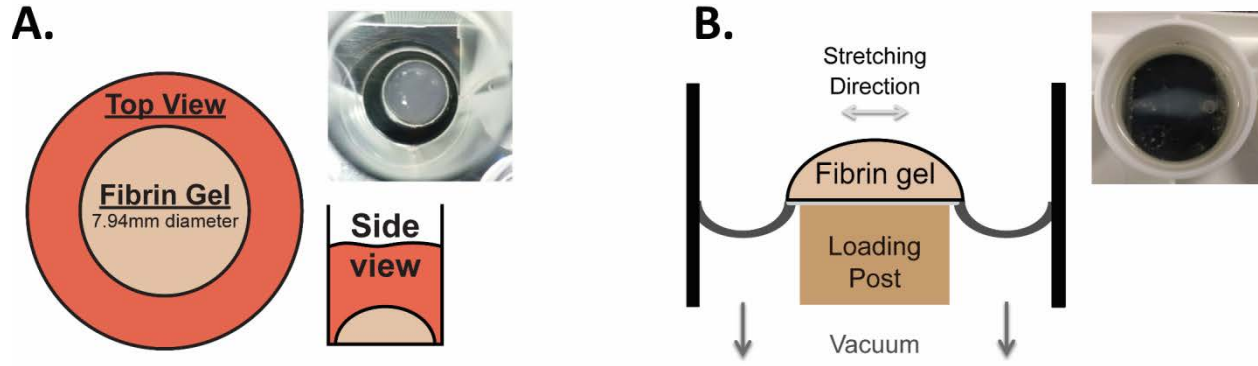


Figure 2: Three-dimensional fibrin gel culture constructs and ASC-SF collection.

(A) “Stiff substrate” fibrin gel SMC constructs (200µL), plated on 24-well tissue culture plates within 7.94mm diameter heat-stamped templates. (B) “Soft substrate” fibrin gel SMC constructs (600µL), plated between nylon tabs of FlexCell Linear TissueTrain untreated plates.

2.2.4 ASC Culture Conditions and Conditioned Media Collection

ASCs were obtained from deidentified waste human adipose tissue collected during body sculpting surgeries of non-smoking, non-diabetic patients under 45 years old at UPMC Presbyterian Hospital, with ASC-SF collected from multiple donors meeting this selection criteria. 100ml of human adipose tissue was mechanically minced and digested in collagenase (1mg/mL) and bovine serum albumin (35 mg/mL) (protease free heat shock, Equitech-Bio Inc #BAH65), followed by filtration and incubation for one hour in a 37°C shaker bath [201, 202]. After secondary filtration (0.5mm gauze, ThermoFisher Scientific #22-415-469) to remove large particles, samples were centrifuged at 1000rpm and 4°C for 10 minutes, with pellets resuspended in 10mL of ACK Lysing Buffer (ThermoFisher Scientific #A10492-01). The suspension was passed through a sieve (500µm, pluriSelect #43-50500-01) and centrifuged again under the same conditions. This ASC pellet was resuspended in “ASC culture media”, consisting of 33% Dulbecco’s Modified Eagle’s Medium (High Glucose, Gibco #12100046), 33% DMEM/F12 Medium (HEPES, Gibco #12400024), 7.5% fetal bovine serum (FBS, Premium Select Atlanta Biologics #S11550), 0.75% fungizone (Lonza BioWhittaker Antibiotics #BW17836E), 0.75% penicillin streptomycin (10,000 U/mL, ThermoFisher Scientific #15140122), 0.075 µM Dexamethasone (Sigma-Aldrich #D4902), and 25% Preadipocyte Growth Medium (PromoCell #C-39425). ASC conditioned media was collected every 24-72 hours between passage 0 and 1 while cells progressed from 40 to 70% confluence, and immediately frozen at -80°C.

2.2.5 Exogenous Media Treatment Conditions

No Treatment (NT) was standard SMC growth media, used to initially culture SMCs. TGF- β 1 (R&D Systems, #240-B-002) dosing concentrations (0.1ng/mL and 1ng/mL) were diluted in each cell type's standard culture media. Non-conditioned media (NCM) was made using a 1:1 ratio of the 'ASC culture media' and SMC growth media. ASC secreted factors (ASC-SF) were prepared by mixing freshly-thawed ASC conditioned media at a 1:1 ratio with SMC growth media. All fibrin gel culture and treatment conditions were supplemented with 12mM ACA for fibrinolysis inhibition to preserve the 3D SMC constructs.

2.2.6 SMC scratch assay to analyze migration

SMCs were seeded within a 24 well tissue culture treated plate, at 5.5×10^4 cells per well, and cultured for 24-36 hours in standard culture media before being used in the scratch assay. Prior to scratch, culture media was removed, and cells were washed once in 0.5mL sterile 1xHBSS. CellTracker Red CMTPX Dye (#C34552, Invitrogen) was diluted to 10mM in DMSO, diluted further to 20 μ M in unsupplemented SMC basal media (#311K-500, Cell Applications Inc), and added to each well after wash (150 μ L per well) for a 20-minute incubation at 37°C and 5% CO₂.

Following incubation, 350 μ L per well of SMC growth supplemented media was added slowly down the walls of each well, without removing CellTracker and disturbing the bed of SMCs. A scratch was created by moving a sterile 1mL plastic pipette tip from the top to the bottom of each 24 well plate, without allowing the pipette tip to skip or scratch the tissue culture plate surface. CellTracker-rich media is then slowly removed via manual pipetting at the

endpoint site of the scratch. Each well then received 250 μ L of unsupplemented SMC basal media, orthogonal to each scratch and slowly down the side of each well's wall. 250 μ L of each treatment group was then added, as summarized below.

Treatment groups included: (1) a No Treatment (NT) positive control of SMC growth supplemented media; (2) ASC-SF, by adding 250 μ L of freshly-thawed ASC conditioned media; (3) NCM; and (4) Unsupplemented SMC basal media.

The lid was placed onto the 24 well plate and taken to the Thoracic Aortic Disease Research Lab (McGowan Institute for Regenerative Medicine, Pittsburgh PA 15219) for imaging on a Nikon TE2000-E Inverted Fluorescence Eclipse Microscope with Intensilight System E, within a Tokai Hit Microscope Stage Top Incubator for Live Cell Imaging (37°C and 5% CO₂). Images were taken every 2 hours for a 36-hour incubation period, with scratch area evaluated using image processing package Fiji (ImageJ, open source). Wound closure percentage was defined as [(initial scratch area – timepoint scratch area) / initial scratch area].

2.2.7 qRT-PCR analysis of tropoelastin and elastin chaperone proteins

Following sonication of frozen fibrin gel constructs, RNA collection (illustra RNAspin Mini Kit, GE Healthcare Life Sciences #25050070) and RNA concentration quantification (BioTek Take3) was performed. After pre-heating template (65°C, 5 minutes), synthesis of first-strand cDNA used SuperScript IV First-Strand Synthesis System (Invitrogen #18091050) (23°C/10 minutes, 55°C/10 minutes, 80°C/10 minutes). RT-qPCR was performed using KicqStart SYBR Green ReadyMix with ROX (Sigma-Aldrich # KCQS02), and forward/reverse primers listed in **Table 2**. Post-amplification melt curves validated proper amplification.

Table 2: RT-qPCR Primers

Gene	Forward Primer	Reverse Primer
Tropoelastin	CCAAGGTGGCTGCCAAAG	GACGCCGACACCAACTCC
Fibrillin-1	AGCGGAGCCGAGCAGTGG	GCTGCTCCCCTTCAGGC
LTBP-4	AGCGTTGCTGTTTGTGCTG	TTGAGGGACACCTGTCTCTTC
Fibulin-4	GCTTCTCCTGCAGTGATATTGAT	CTGACGTTGTTGATTTGCCTAA
Fibulin-5	TTCCTCTGCCAACATGAGTG	TGGTTCCTGTGCTCACATTC
LOX	CATAGACTGCCAGTGGATTGA	ATGTCACAGCGCACAAACATT
LOXL-1	AGCGCTATGCATGCACCTCTCATA	TGCAGAAACGTAGCGACCTGTGTA
GAPDH	CCACCCAGAAGACTGTGGAT	TTCAGCTCAGGGATGACCTT

2.2.8 Elastic fiber imaging via immunostaining and multiphoton microscopy, and elastic fiber quantification

An immunofluorescence assay was conducted at time points between 3 and 15 days post-cellular confluence to detect whether elastin was found within each cell type. All fibrin gels were fixed using a 4% paraformaldehyde incubation for 30 minutes, then washed and stored in 1x PBS. RFL-6 cells were stained for elastin using rabbit conjugated anti-mouse recombinant tropoelastin (α -MRT) (1:1000, a generous donation from Dr. Robert Mecham's lab at Washington University in St Louis), goat anti-rabbit polyclonal AlexaFluor 488 (1:500), and a nuclear Hoechst stain (1:50). Images were obtained using an Olympus FluoView FV1000 confocal microscope, using a UPLSAPO super apochromat Olympus 20x oil objective (NA=0.85). Laser excitation was set to 473nm, with a sampling speed of 4 μ s/pixel.

SMC constructs were successfully fixed using either ice cold methanol or 2% paraformaldehyde. Immunostaining for elastin (primary: rabbit polyclonal anti-human aortic elastin, Elastin Products Company #PR533, 1:1000 dilution; secondary: goat anti-rabbit IgG fluorescein conjugated, Rockland Immunochemicals #611-1202, 1:750 dilution) and DAPI (ThermoFisher Scientific #D1306) to identify cell nuclei was conducted using confocal microscopy (Olympus Fluoview FV1000 with XLPlan N25X water objective, NA = 1.05) and reconstructed using brightest-pixel z-stack composite (FIJI, public domain). Elastic fiber network formation was analyzed using a modified, previously published MATLAB script [215] to quantify elastic fiber length and intersection density. Image background filtration and gain adjustments were held constant as images were collected, and no further contrast enhancement was performed prior to MATLAB quantification. MATLAB code did not include any contrast adjustment step during fiber skeletonization and segmentation.

Multiphoton images in **Figure 12** were collected on an Olympus FV10 multiphoton microscope, using an XLPlan N25x (NA = 1.05) water immersion objective with a 0.17 correction for the glass cover slip. 400 μ L static and dynamic fibrin gels were fixed using 4% paraformaldehyde for 30 minutes, then washed and stored in 1x PBS. Elastin fibers' intrinsic fluorescence was visualized using the RXD2 channel (525 ± 25 nm), using a laser wavelength of 830nm and a sampling speed of 8 μ s/pixel.

Multiphoton images in **Figure 18**, **Figure 19**, and **Figure 20** were performed using the Advanced Intravital Microscope at the Soft Tissue Biomechanics Laboratory, under the direction of Dr. Jonathan Vande Geest. A Zeiss Plan-Apochromat 20x objective (NA = 0.8, WD = 0.55mm) was used with a glass concave microscope slide (ThermoFisher Scientific, #1519006) with samples submerged in PBS. Samples were excited at a wavelength of 780nm, with a constant laser power of 1.35milliwatts and a depth step-size of 2 μ m.

2.2.9 Ninhydrin (Insoluble Elastin) and Hydroxyproline (Collagen) Assay

Fibrin gel constructs, frozen at -80°C following culture without fixation, were thawed immediately before base hydrolysis (0.5mL 0.1M NaOH, 1 hour, 98°C) for fibrin gel digestion and solubilization of non-elastin proteins, which was separated using subsequent centrifugation to separate insoluble elastin protein from solubilized non-elastin protein [216]. Acid hydrolysis (0.5mL 6N HCl, 24 hours, 110°C) solubilized all proteins, and assay quantification on both soluble and insoluble fractions (ninhydrin-based for elastin, hydroxyproline-based for collagen) allow for protein deposition quantification within each 3D construct. Ninhydrin content was detectable using an absorbance reading (at 570nm) after 1-hour incubation with a stannous chloride-based solution within a 56°C water bath. Hydroxyproline content was detectable using

an absorbance reading (570nm) after 15 minute room temperature incubation in a Chloramine-T solution and 30 minute 37°C incubation in a dimethylaminobenzaldehyde solution.

2.2.10 Tensile Testing of Soft Substrate Fibrin Gel Constructs

Constructs were harvested, without fixation, by cutting the pair of nylon tabs within the Linear TissueTrain plates to keep each gel intact. Fibrin constructs were gently peeled away from the top half of the nylon tabs, leaving a section of nylon exposed to grip within pneumatic clamps discussed subsequently (**Figure 3**). Tensile testing was performed on all samples as all sample width-to-length ratios were less than 0.25:1 (Mean = 0.17 ± 0.05 , Range: 0.12-0.23) [217].

A uniaxial tensile testing device (Instron, #5543A, Norwood, MA) was used to assess the tensile mechanical properties of the SMC fibrin gel constructs (**Figure 3**, **Figure 25**). The dried nylon tabs of each sample were secured in compression-based pneumatic clamps lined with sandpaper to improve grip fidelity [218, 219]. Exposed nylon tabs were dried to improve grip within sandpaper-lined pneumatic clamps. The thickness (average: 2.17 ± 0.32 mm NT vs 2.06 ± 0.41 mm ASC-SF), width (average: 2.55 ± 0.47 mm NT vs 2.53 ± 0.54 mm ASC-SF), and gauge length (average: 15.47 ± 1.05 mm NT vs 13.99 ± 1.81 mm ASC-SF) of the samples were measured using photos obtained after 0.01N pre-loading to eliminate sample slack (**Figure 25A**) (FIJI, public domain), as no significant construct deformation was detected before this point. Construct dimensions were not significantly different between treatment groups.

A constant 0.1 mm/second crosshead speed extension was used until failure to characterize the mechanical behavior of the samples under quasi-static loading [220]. Force and displacement values were recorded throughout the test and converted to stress-stretch ratio plots as described in [221], where – Stretch ratio: $\lambda=L/L_0$; Stress $\sigma=F/A_0$. These measurements were

calculated from the sample gauge length in the loaded (L) and unloaded configuration (L_o). Force (F) and original cross-sectional area (A_o) were recorded during each mechanical test [221].

Low and high modulus are defined as the slope of the linear portion of the mechanical response curve in the ‘low’ and ‘high’ stretch regions respectively, defined as follows. The ‘low’ vs ‘high’ stretch transition point is the point of the stress–stretch ratio curve with the maximum normal distance from the global secant (the line between the curve’s initial and final points) [222, 223]. This translated to dividing the curves into three equal parts and treating the initial and final thirds of the curve as the low and high stretch regions respectively. The low stretch region ranged from 1 to 1.13 ± 0.02 for both the ASC-SF the NT groups, and 1 to 1.16 ± 0.04 for the blank gels. The high stretch region ranged from 1.26 ± 0.04 to 1.39 ± 0.06 for the ASC-SF group, 1.26 ± 0.04 to 1.4 ± 0.06 for the NT group and 1.32 ± 0.07 to 1.49 ± 0.11 for the blank gels.

2.2.11 Statistical Analysis

Means comparisons were conducted using individual t-tests or one-way ANOVA with Tukey post-hoc tests, as appropriate. Significance threshold of $\alpha = 0.05$ was set for all presented data, with experimental sample size of tested constructs listed on each figure. IBM SPSS was used for all statistical analysis. All displayed data values written after “ \pm ” are standard deviation values.

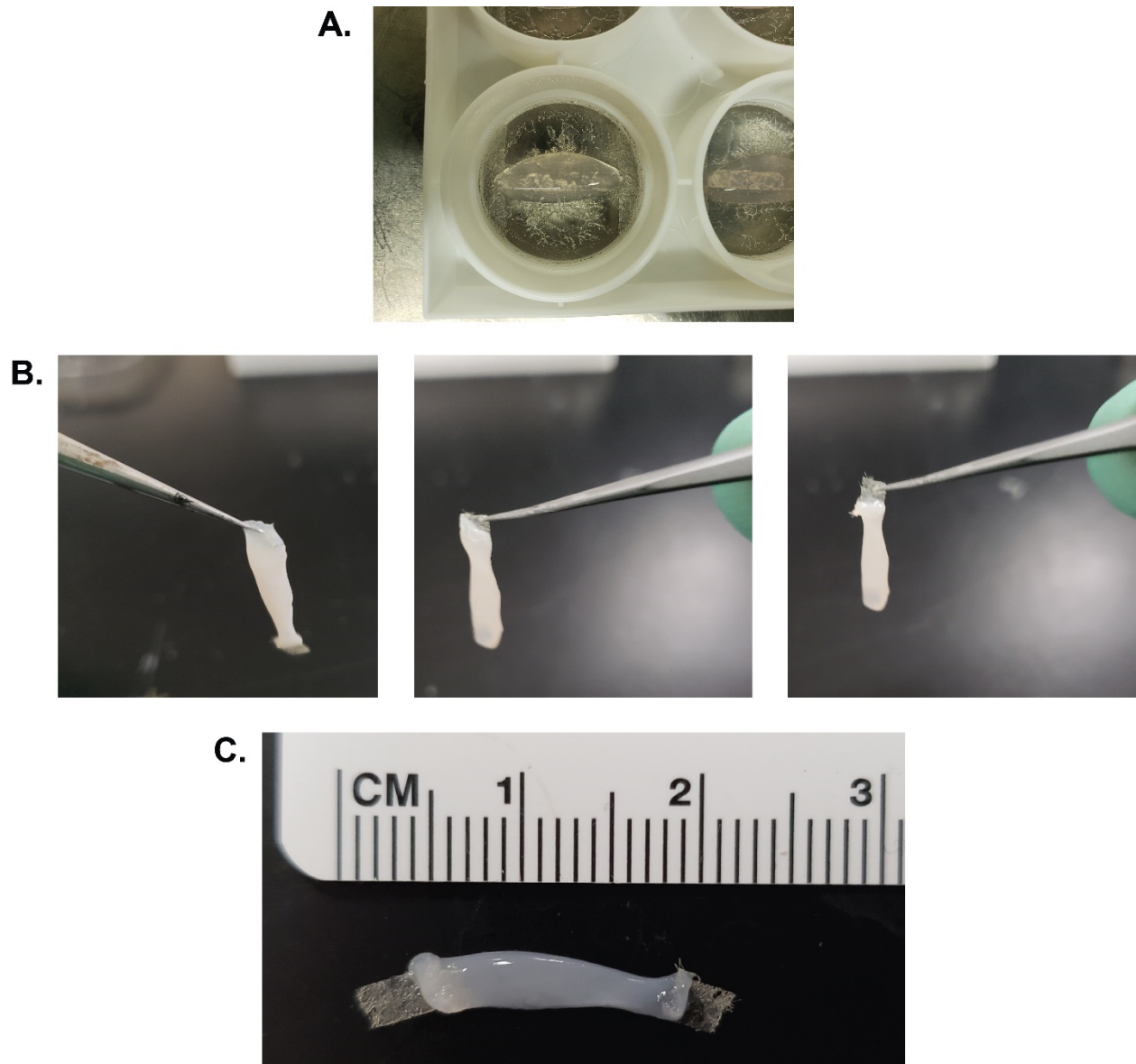


Figure 3: Soft substrate fibrin gel preparation for tensile testing.

- A) Soft substrate fibrin gel construct on FlexCell TissueTrain plates, immediately after gel formation.
- B) Steps taken to peel away fibrin construct from top half of nylon tabs of TissueTrain plates, resulting in an exposed tab that can be dried and clamped by sandpaper-aided pneumatic clamps.
- C) Entire harvested soft substrate fibrin gel construct, with both nylon tabs exposed for clamping during tensile testing.

2.3 Results

2.3.1 2D culture elastin deposition by RFL-6 cells with no exogenous stimulation and adaptation of fiber analysis code

Elastic fiber staining revealed rat fetal lung fibroblast cell line RFL-6 seeded directly onto glass coverslips deposited an expanding elastic fiber matrix within the span of 15 days without any exogenous stimulation, outside of standard growth media (plus 20% serum) conditions. A qualitative elastin network was formed as early as 6 days in culture (**Figure 4**). Comparatively, human fetal lung fibroblast cell line WI-38 revealed no visible elastin deposited after 6 or 15 days in culture and no exogenous stimulation outside standard culture media. A MATLAB network quantification code, previously developed in the VBL for analyzing multiphoton images of ECM [215], was adapted to analyze both 2D single frames and 3D brightest-pixel projections of elastin networks. **Figure 5** shows RFL-6 fiber skeleton identification after 8 culture days.

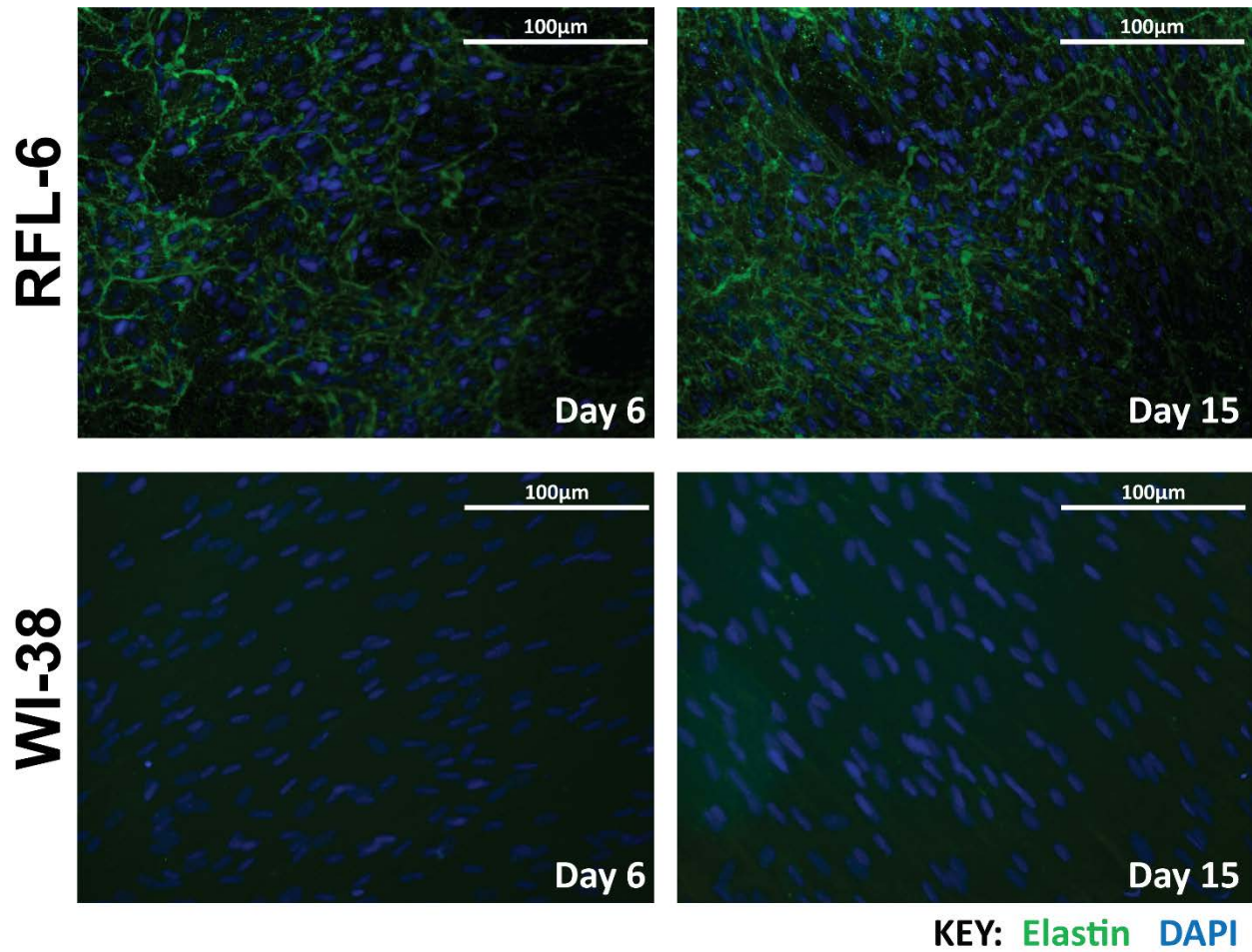


Figure 4: Immunostaining for RFL-6 and WI-38 elastin on 2D cultures (glass coverslips).

Immunostaining for elastin (green) without exogenous stimulation, using a known elastogenic cell line RFL-6 and a control cell line WI-38 that does not produce elastin without exogenous stimulation. Cultures were allowed to continue for 6 days (left) and 15 days (right), with media changes every 48-72 hours.

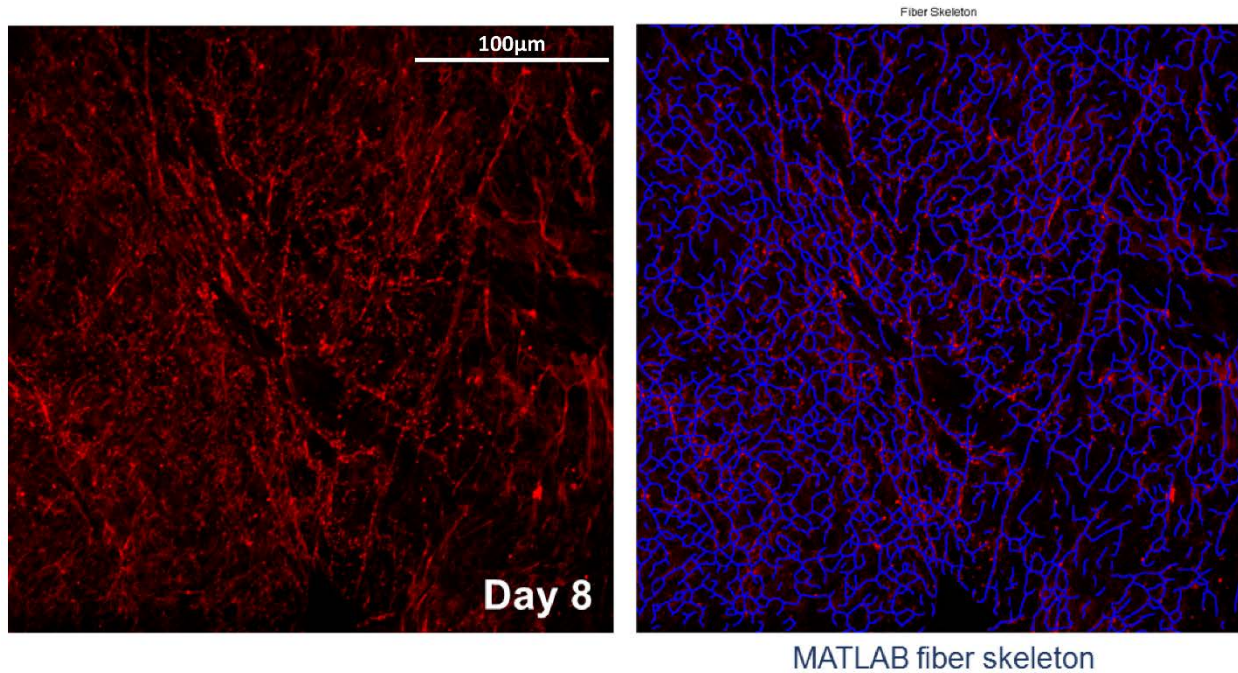


Figure 5: MATLAB elastin network identification on 2D RFL-6 immunostained elastin images.

Adapted MATLAB fiber analysis code run on 2D 8 day RFL-6 elastin (red) networks (left), with the identified fiber skeleton (blue) shown overlaid (right).

2.3.2 Fibrinolysis inhibitor aminocaproic acid is required for fibrin construct maintenance and modulates RFL-6 elastin deposition

Integration of RFL-6 cells within 3.7mg/mL fibrin gels produced domed “constructs” within 24-well tissue culture plates. After 24 hours in standard culture media, RFL-6 cells have induced a fibrinolytic cascade and digested the gels, settling on the bottom surface of the tissue culture plate (**Figure 6A**). Integration of a fibrinolysis inhibitor, ACA, at above 8mM produced constructs that lasted over one week (**Figure 6A**). Maximum fibrinolysis occurs within the first 48 hours of culture, with constructs stabilizing if they remain after that period. Similarly, SMC construct fibrinolysis is stabilized between 8mM and 12mM of ACA present (**Figure 7**).

Insoluble elastin deposition by elastogenic RFL-6 cells increased as concentration of ACA increased, in a dose-dependent manner (**Figure 6B**). While constructs were stable and deposited insoluble elastin in 8mM ACA ($9.43 \pm 3.56\%$ elastin of total protein), elastin increased by 119% when ACA concentration increased to 12mM ($20.6 \pm 6.86\%$), and 175% when increased to 15mM ($25.9 \pm 6.26\%$).

As a positive control to indicate that our insoluble elastin assay was functional, elastin percentage of total protein within an explanted rat abdominal aortic explanted section (stored at -80C) was detected at $17.2 \pm 2.04\%$. This value cannot be directly compared to the RFL-6 seeded constructs, as Total Protein levels are significantly higher in the explanted aortic section when compared to the *in vitro* seeded constructs.

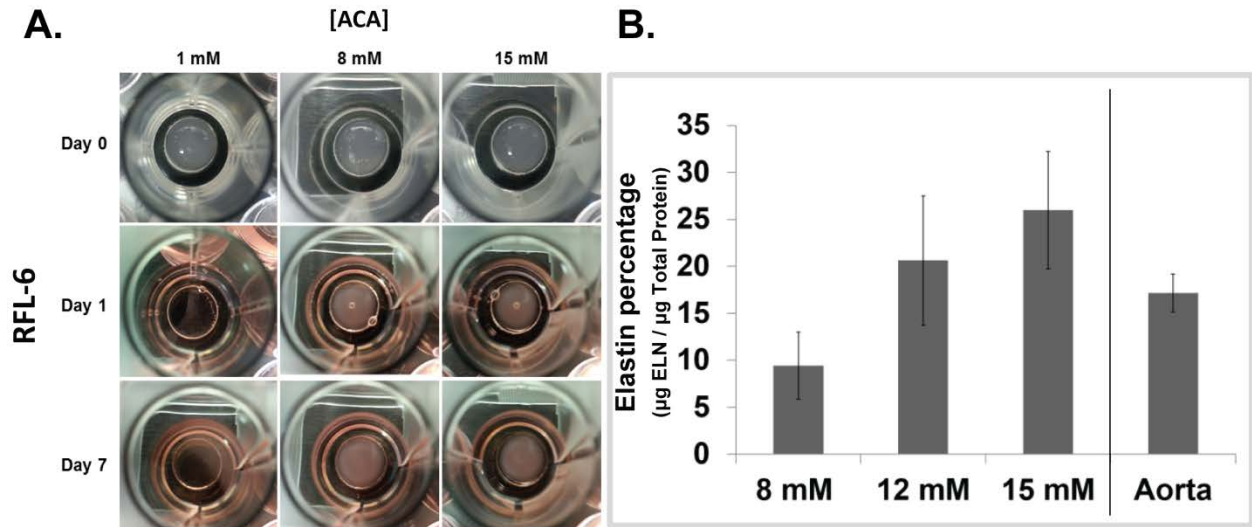


Figure 6: RFL-6 elastogenesis is dependent on fibrinolysis inhibitor concentration.

A) RFL-6 loaded fibrin gel construct images (7.94mm diameter) through 7 days of culture in three different concentrations of fibrinolysis inhibitor ACA (1mM, 8mM, 15mM). Media changes were made every 48-72 hours.

B) Insoluble elastin percentage of total protein deposited by RFL-6 cells in fibrin gel constructs after 7 days in culture, within three different concentrations of ACA (8mM, 12mM, 15mM). Positive control used was an explanted and frozen section (1.5mm) of explanted non-aneurysmal rat aorta (Aorta).

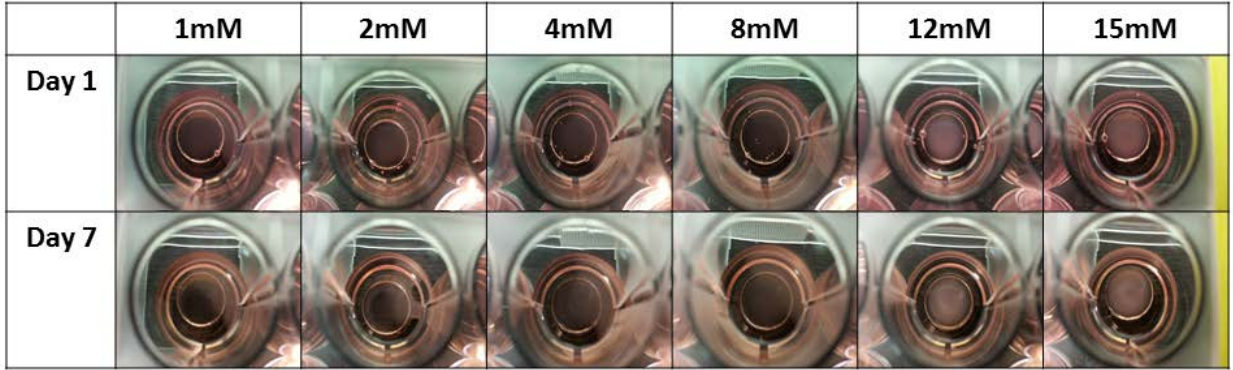


Figure 7: SMC fibrin gel construct stability under a concentration panel of fibrinolysis inhibitor ACA.

SMC loaded fibrin gel construct images (7.94mm diameter) through 7 days of culture in six different concentrations of fibrinolysis inhibitor ACA (1mM, 2mM, 4mM, 8mM, 12mM, 15mM), diluted in SMC growth supplemented media. Media changes were made every 48-72 hours.

2.3.3 TGF- β 1 stimulation induces insoluble elastin deposition in 3D fibrin gel constructs

15mM ACA produced stable, non-degraded RFL-6 embedded fibrin gel constructs after 7 days within all stimulation conditions (standard culture media, low TGF- β 1, high TGF- β 1) (**Figure 8A**). Immunostaining and confocal microscopy revealed a qualitative increase in elastin network formation over time within all treatment conditions (**Figure 8B**), with mature networks seen after 10 days in culture across all conditions. Quantitative analysis was necessary to determine Day 7 and Day 10 differences between network formation.

Without exogenous stimulation, RFL-6 cells within fibrin gel constructs deposited statistically similar amounts of insoluble elastin (**Figure 8C**) after 3 days ($0.32\pm 0.45\%$) and 7 days ($0.12\pm 0.029\%$) in culture, with statistically increased amounts after 10 culture days ($4.33\pm 0.78\%$). Low TGF- β 1 stimulation (0.1ng/mL) produced statistically similar levels of insoluble elastin after 7 days in culture ($1.40\pm 0.22\%$), but dramatically increased insoluble elastin after 10 days ($14.3\pm 1.18\%$). High TGF- β 1 stimulation (1ng/mL) induced significantly increased insoluble elastin deposition after both 7 days ($5.7\pm 1.1\%$) and 10 days ($14.4\pm 1.38\%$) in culture.

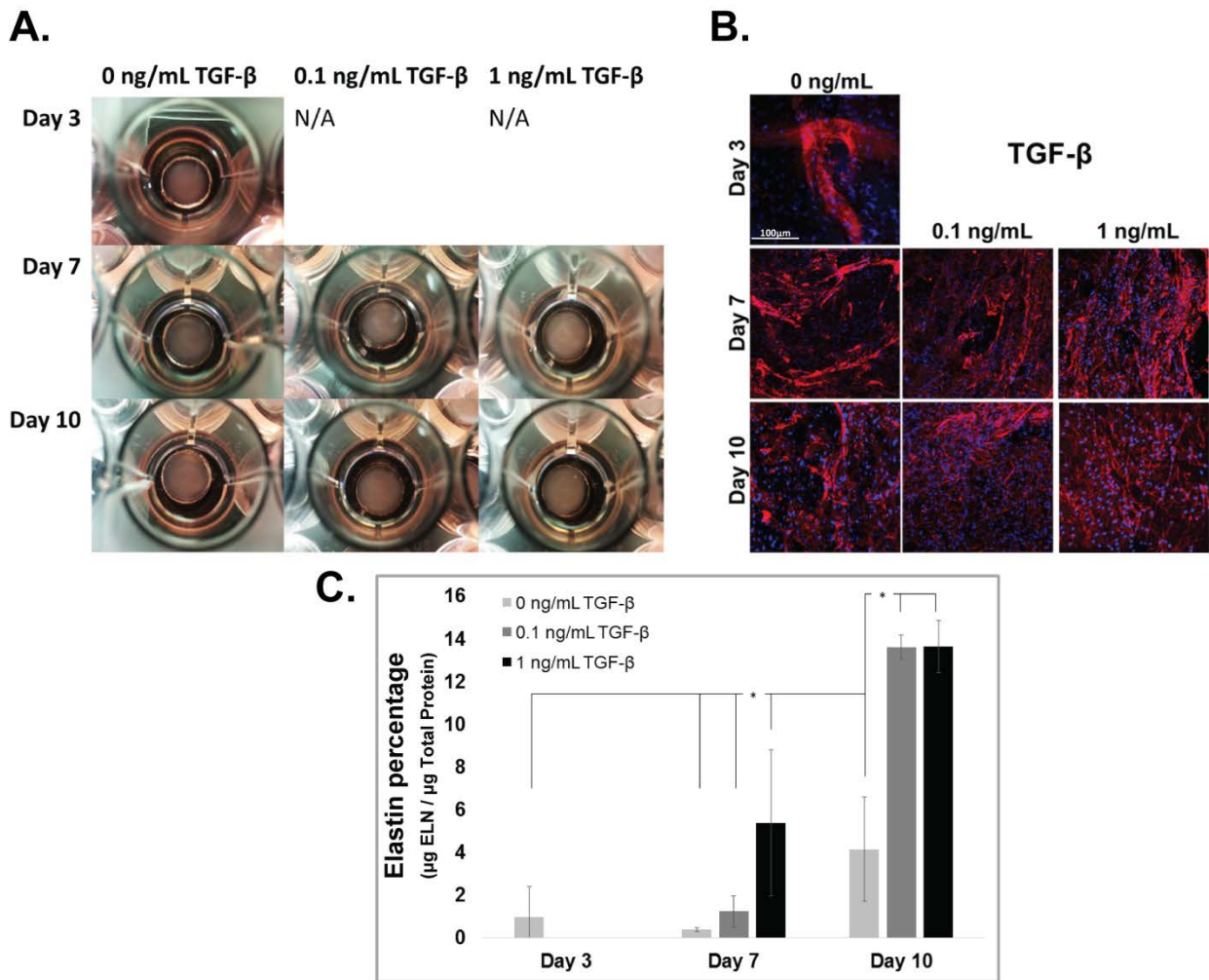


Figure 8: TGF- β 1 stimulation induces RFL-6 insoluble elastin deposition within fibrin gel constructs.

A) Images of RFL-6 loaded fibrin gel constructs (7.94mm diameter), stimulated with three different concentrations of TGF- β 1 (0ng/mL negative control, 0.1ng/mL “Low” concentration, and 1ng/mL “High” concentration) after 7 and 10 days in culture. Treatments were diluted in standard F12 growth supplemented media, with TGF- β 1 addition beginning after 3 days in culture and media changes containing refreshed treatment groups every 48-72 hours.

B) Immunostaining for elastin (red) and DAPI nuclei staining (blue) following cold methanol fixation under each corresponding TGF- β 1 treatment condition from Figure 8A.

C) Insoluble elastin percentage of total protein, under each corresponding TGF- β 1 treatment condition from Figure 8A. $\alpha = 0.05$, $n = 5$ for all.

2.3.4 RFL-6 elastic fiber networking quantification following TGF- β 1 stimulation using modified fiber analysis code

Staining of RFL-6 deposited elastic fibers within 3D fibrin gel constructs after 7 or 10 days of 1ng/mL TGF- β 1 stimulation revealed clear, uninterrupted elastic fiber networks via immunostaining and confocal imaging with brightest-pixel reconstruction (**Figure 9A**). Modified MATLAB analysis revealed the elastic fiber normalized parameters able to be analyzed: average segment length, mean fiber diameter, fiber concentration, fiber tortuosity, and fiber intersection diameter.

Elastic fiber segment length (**Figure 9B**), normalized to the earliest NT timepoint, significantly decreased after both 7 days (0.823 ± 0.048) and 10 days (0.826 ± 0.061) of TGF- β 1 stimulation when compared to Day 3 No Treatment control (1 ± 0.0624). Additionally, mean fiber diameter (**Figure 9C**) decreased after 7 days of TGF- β 1 stimulation (0.898 ± 0.050 vs 1 ± 0.0591 NT control).

Normalized fiber concentration (**Figure 9D**), however, increased after both 7 days (1.774 ± 0.360) and 10 days (2.058 ± 0.299) of TGF- β 1 stimulation when compared to Day 3 NT control (1 ± 0.2864). Tortuosity (**Figure 9E**), a measurement of single fiber curvature, increased after only 10 days of TGF- β 1 stimulation (1.034 ± 0.015) when compared to 10 days of NT control (0.991 ± 0.012). Fiber intersection density (**Figure 9F**) increased after both 7 days (1.394 ± 0.0577) and 10 days (1.790 ± 0.0401) of TGF- β 1 stimulation when compared to Day 3 NT control (1 ± 0.0520).

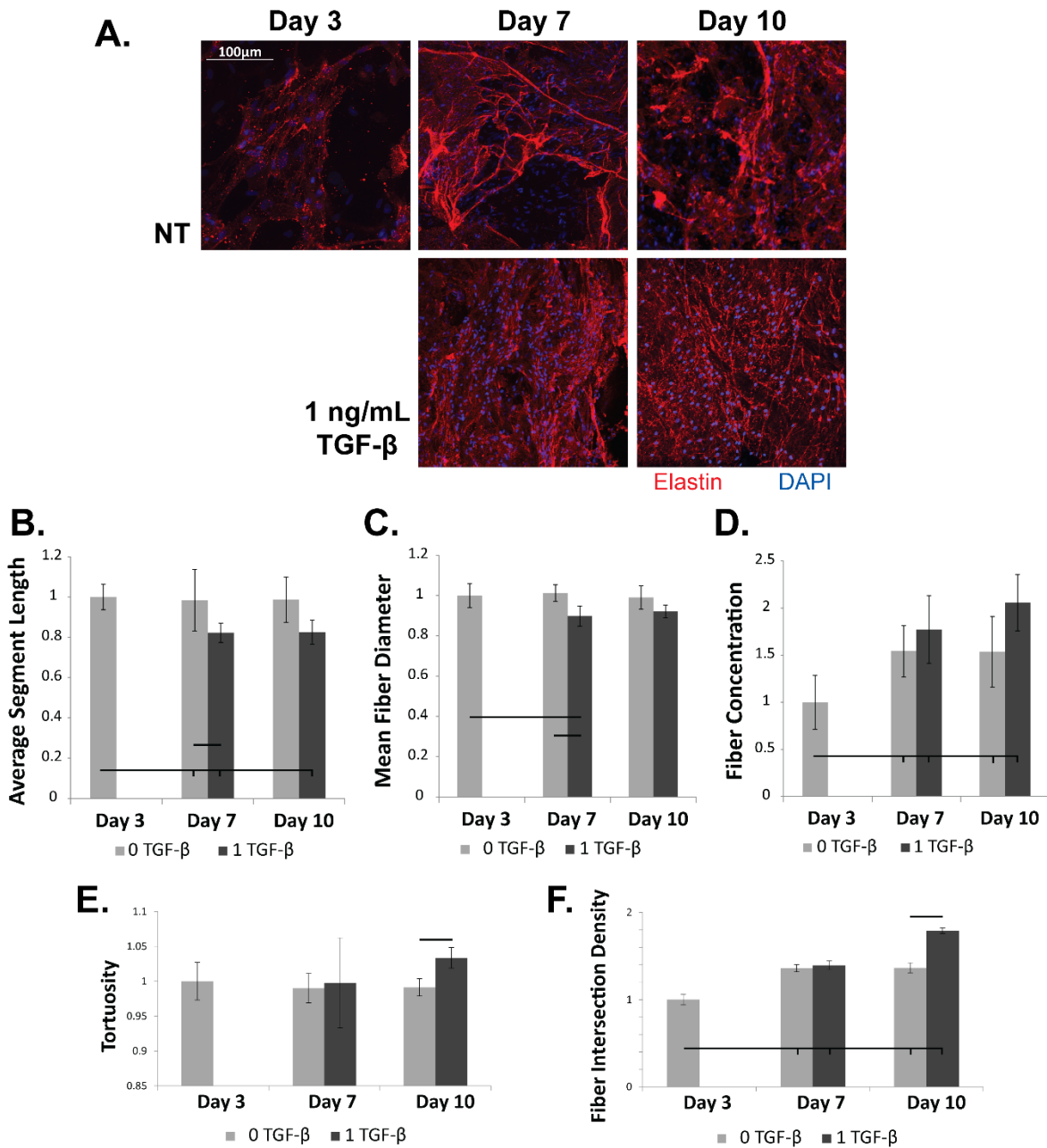


Figure 9: RFL-6 elastic fiber network quantification within 3D fibrin gel constructs after TGF-β1 stimulation (1ng/mL).

A) Immunostaining and confocal imaging for elastin (red) and RFL-6 nuclei (blue) within 3D fibrin gel constructs under “No Treatment” negative control standard F12 culture media (NT) and TGF-β1 stimulation (1ng/mL), after 3, 7, and 10 days of stimulation.

B-E) MATLAB quantification of normalized B) elastic fiber segment length, C) elastic fiber diameter, D) elastic fiber concentration, E) elastic fiber tortuosity, and F) elastic fiber intersection density. $\alpha = 0.05$, $n = 5$ for all.

2.3.5 RFL-6 insoluble elastin fraction is increased after TGF- β 1 stimulation and decreased after ASC-SF stimulation within fibrin gel constructs

After 7 days of TGF- β 1 stimulation (1ng/mL), a Fastin assay revealed a 27.4% increase in total elastin (soluble tropoelastins, lathyrogenic elastins, and insoluble elastin) as normalized to 10mg of wet fibrin gel construct ($2.13\pm 0.19\mu\text{g}$ elastin with TGF- β 1, vs $1.67\pm 0.074\mu\text{g}$ elastin in standard F12 media) (**Figure 10A**). Total elastin after 14 days was statistically similar both with and without TGF- β 1 stimulation, but both were significantly increased compared to Day 7 0ng/mL control ($2.81\pm 0.29\mu\text{g}$ elastin Day 14 standard media, $2.59\pm 0.24\mu\text{g}$ elastin Day 14 with TGF- β 1). Insoluble elastin fraction was not recorded for these TGF- β 1 stimulated constructs.

ASC-SF stimulation resulted an RFL-6 insoluble elastin fraction decrease, as measured by ninhydrin assay, after both 10 days ($0.30\pm 0.0042\%$ F12 control, $0.0095\pm 0.0026\%$ ASC-SF) and 20 days ($0.21\pm 0.0045\%$ F12 control, $0.11\pm 0.0036\%$ ASC-SF) in culture (**Figure 10B**). Notably, ASC-SF stimulated constructs saw a time-dependent significant increase in elastin between 10 days and 20 days of stimulation.

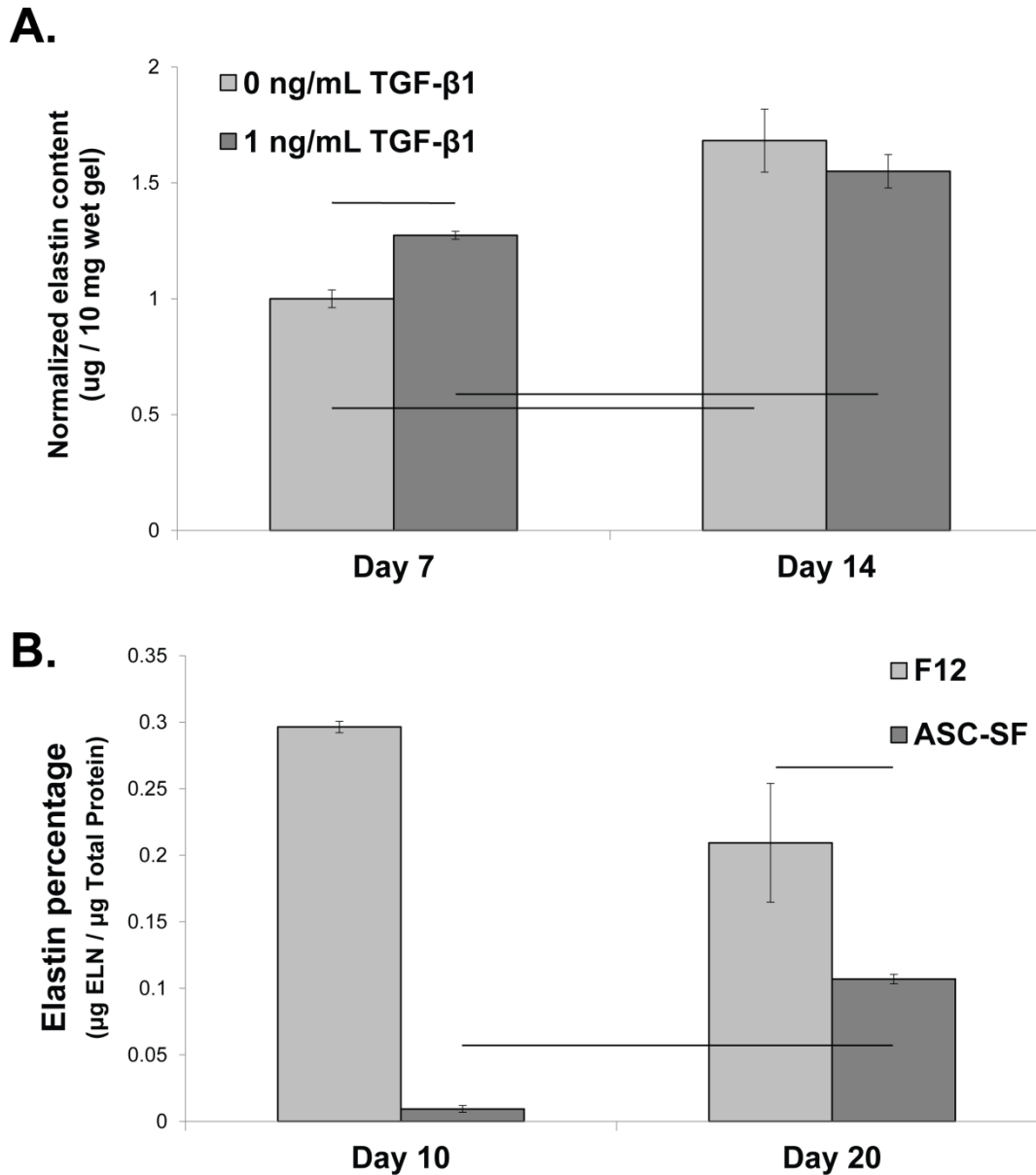


Figure 10: RFL-6 total elastin increase after TGF- β 1 stimulation and insoluble elastin fraction decrease after ASC-SF stimulation.

A) Fastin assay for total elastin (soluble tropoelastins, lathyrogenic elastins, and insoluble elastin) of RFL-6 seeded fibrin gels cultured in standard F12 culture media (0ng/mL TGF- β 1) or 1 ng/mL TGF- β 1, after either 7 days or 14 days in culture. Fresh exogenous treatment media added every 48-72 hours. $\alpha = 0.05$, $n = 4$.

B) Ninhydrin assay for insoluble elastin fraction of RFL-6 seeded fibrin gel constructs, after either 10 days or 20 days of ASC-SF stimulation. Treatments changed every 48-72 hours. $\alpha = 0.05$, $n = 3$.

2.3.6 RFL-6 deposition of fibulin-5 and elastic fiber networking analysis following ASC-SF stimulation

Immunostaining of RFL-6 seeded fibrin gel constructs revealed a colocalization of deposited elastin and fibulin-5 after 20 days of ASC-SF stimulation, while both standard F12 culture media and TGF- β 1 stimulation (1ng/mL) did not induce a elastin/fibulin-5 localization pattern (**Figure 11A**).

MATLAB analysis of deposited elastic fibers showed a significant decrease in normalized fiber concentration after 10 days of ASC-SF stimulation (0.65 ± 0.16 ASC-SF vs 1.0 ± 0.090 F12 control) (**Figure 11B**) and an increase in normalized average segment length after 10 days TGF- β 1 stimulation (1.1 ± 0.079 TGF- β 1 vs 1.0 ± 0.048 F12) (**Figure 11D**), but statistically similar normalized fiber diameters (**Figure 11C**) and fiber intersections (**Figure 11E**). 20 days of stimulation resulted in ASC-SF induced increases in fiber length (1.2 ± 0.044 ASC-SF vs 1.0 ± 0.0085 F12) (**Figure 11D**), as well as time-dependent increases in TGF- β 1 induced fiber concentration (0.83 ± 0.11 Day 10 vs 0.97 ± 0.017 Day 20) (**Figure 11B**) and fiber intersection density (1.1 ± 0.14 Day 10 vs 1.4 ± 0.080 Day 20) (**Figure 11E**).

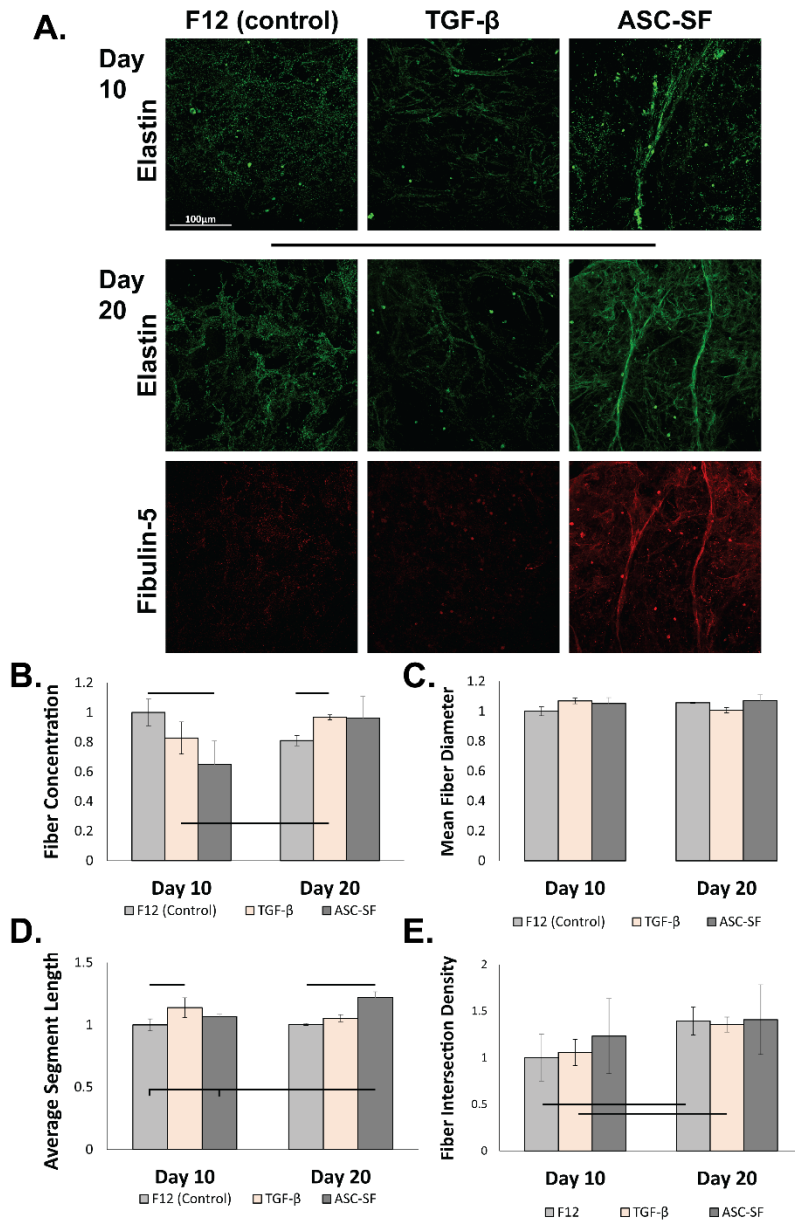


Figure 11: RFL-6 elastic fiber network quantification within 3D fibrin gel constructs after TGF- β 1 stimulation (1ng/mL).

A) Immunostaining and confocal imaging for elastin (green) and elastin chaperone protein fibulin-5 (red) within 3D RFL-6 seeded fibrin gel constructs under negative control standard culture media (F12), TGF- β 1 stimulation (1ng/mL), and ASC-SF after 10 and 20 days of stimulation.

B-E) MATLAB quantification of normalized: B) elastic fiber concentration, C) elastic fiber diameter, D) elastic fiber segment length, and E) elastic fiber intersection density. $\alpha = 0.05$, $n = 5$ for all.

2.3.7 Cyclic uniaxial loading of soft substrate constructs induces RFL-6 total elastin deposition and multiphoton imaging of deposited elastin

RFL-6 seeded fibrin gels were plated on soft substrate FlexCell TissueTrain plates and were cultured for 7 days while subjected to either no external mechanical loading (“Constrained” between the loading posts) or a 1Hz 10% displacement cyclic uniaxial loading condition (“Dynamic”). Multiphoton microscopic images captured RFL-6 deposited elastin autofluorescence in both Constrained and Dynamic constructs after culture in standard culture media (**Figure 12A**). An endpoint digestive elastin assay (Fastin assay) showed a 32.7% increase in total elastin deposition (soluble tropoelastins, lathyrogenic elastins, and insoluble elastin) when unstimulated RFL-6 constructs were subjected to Dynamic loading ($2.22 \pm 0.084 \mu\text{g}$ elastin per 10mg wet Dynamic construct, vs $1.67 \pm 0.074 \mu\text{g}$ elastin per 10mg wet Constrained construct) (**Figure 12B**).

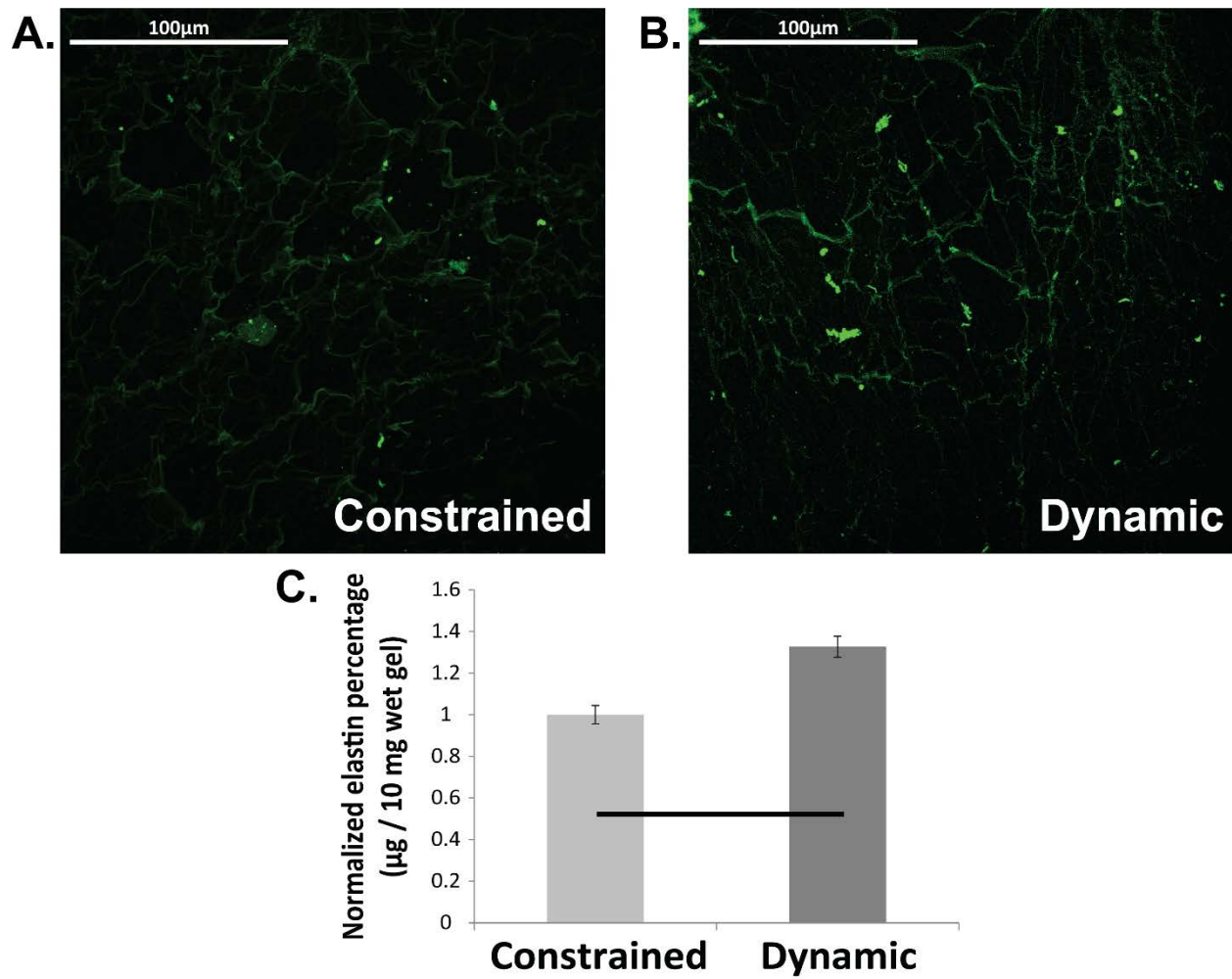


Figure 12: RFL-6 deposited elastin multiphoton imaging and total elastin content increases after ASC-SF stimulation.

A) Multiphoton images of RFL-6 deposited elastin within fibrin gel constructs, after 7 days of culture on soft substrate culture plates. Constrained constructs were not subjected to any external mechanical load, while Dynamic constructs were subjected to a 1Hz, 10% displacement cyclic uniaxial loading condition.

B) Fastin assay for total elastin (soluble tropoelastins, lathyrogenic elastins, and insoluble elastin) on RFL-6 seeded fibrin gel constructs on soft substrates, cultured for 7 days under either Constrained or Dynamic conditions.

$\alpha = 0.05$, $n = 3$.

2.3.8 ACA to prevent SMC construct fibrinolysis, and TGF- β 1 stimulation of SMCs induces no significant insoluble elastin deposition on soft substrates

An ACA concentration panel was performed to gauge the acceptable fibrin construct resiliency following SMC integration and 7 days of culture (**Figure 13**). ACA was diluted in SMC growth supplemented media at concentrations of 1mM, 2mM, 4mM, 8mM, 12mM, and 15mM. SMC constructs cultured within 1mM, 2mM, and 4mM ACA were either entirely digested or reduced by >70% of original thickness, while 8mM, 12mM, and 15mM ACA constructs remained intact. ACA concentrations of 12-15mM were used in all subsequent SMC construct experiments.

After 20 days of culture on soft substrates, SMC fibrin gel constructs did not deposit a significant difference in insoluble elastin when stimulated with 1ng/mL TGF- β 1 when compared to NT control (standard SMC culture media, plus 12mM ACA) in either Constrained ($0.14\pm 0.014\%$ NT vs $0.16\pm 0.11\%$ TGF- β 1) or Dynamic ($0.23\pm 0.098\%$ NT vs $0.22\pm 0.14\%$ TGF- β 1) constructs.

After 30 days, however, a mechanical loading-induced significant difference in insoluble elastin deposition is seen in both NT ($0.098\pm 0.018\%$ Constrained vs $0.294\pm 0.030\%$ Dynamic) and TGF- β 1 ($0.084\pm 0.045\%$ Constrained vs $0.25\pm 0.070\%$ Dynamic) constructs (**Figure 14**). No significant TGF- β 1 induced difference in insoluble elastin deposition was seen within Constrained or Dynamic constructs.

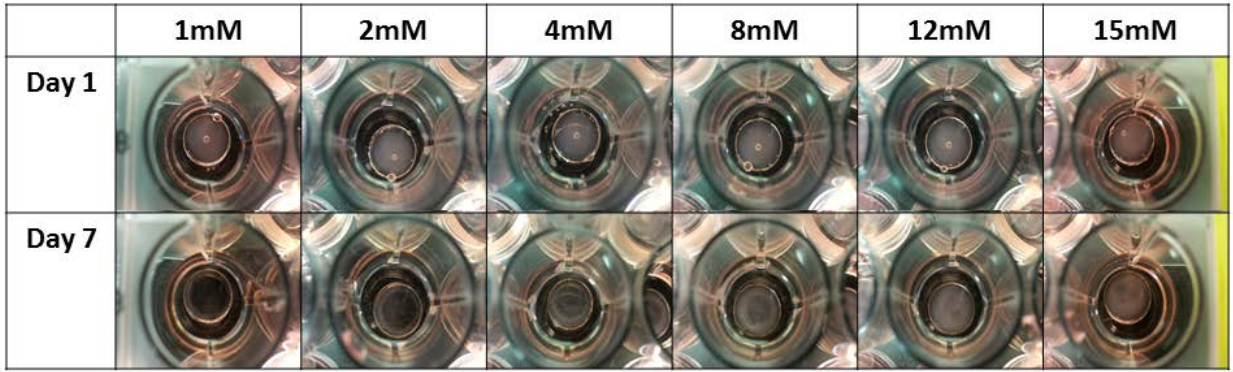


Figure 13: ACA concentration panel of SMC seeded fibrin gel constructs.

Constructs (7.94mm diameter) were seeded with 1×10^5 SMCs per fibrin gel, seeded within 7.94mm heat-stamped templates in tissue-culture treated 24 well plates. ACA concentrations (1mM, 2mM, 4mM, 8mM, 12mM, 15mM) were diluted in SMC growth media and cultured for 7 days, with media changes every 36-48 hours.

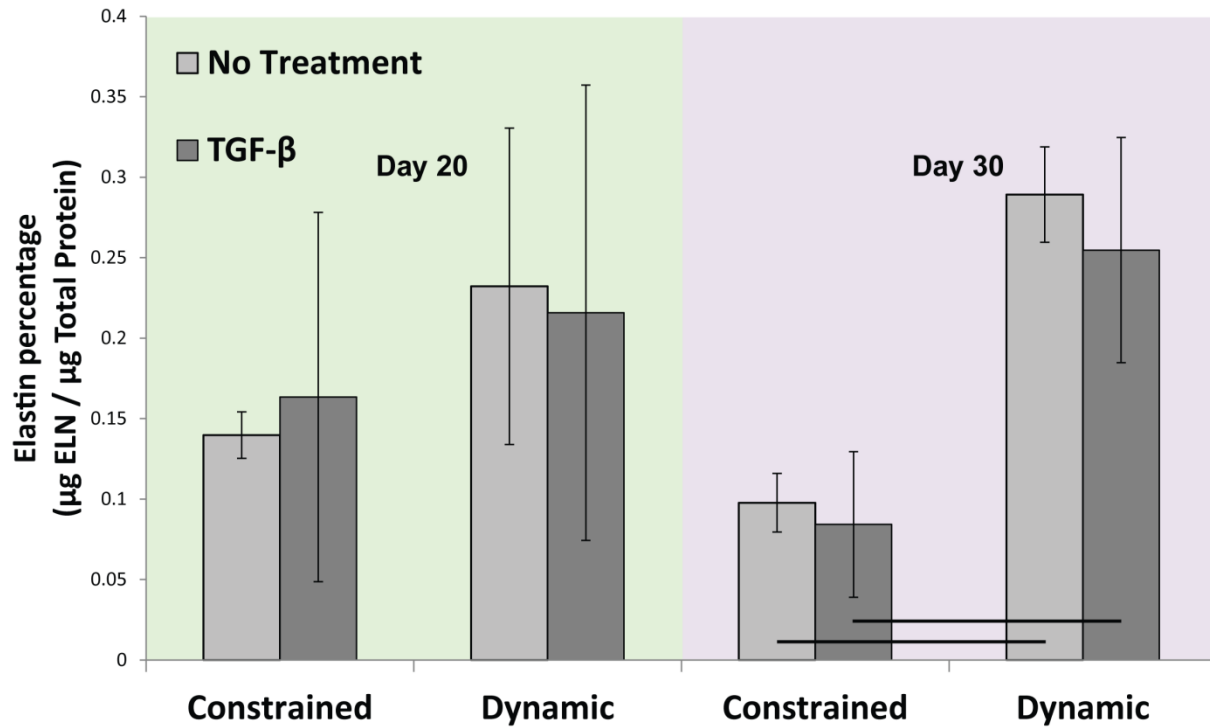


Figure 14: SMC insoluble elastin deposition within soft substrate fibrin constructs, when stimulated with 1µg/mL TGF-β1 for 20 or 30 days and subjected to Constrained or Dynamic loading.

Constructs were cultured within 12mM ACA fibrinolysis inhibitor and either No Treatment (SMC culture media) or 1ng/mL TGF-β1 for 20 or 30 days, with media changes every 48-72 hours. 1Hz, 10% displacement conditions were used for Dynamic cyclic uniaxial loading. $\alpha = 0.05$, $n = 6$.

2.3.9 ASC-SF and NCM increase early migration of SMCs on 2D substrates

After 12 hours of 2D culture, SMC wound closure significantly increased with ASC-SF ($38\pm 4.4\%$) and NCM ($38\pm 6.4\%$) when compared to both NT ($24\pm 5.6\%$) and Unsupplemented media negative control ($23\pm 6.9\%$) (**Figure 15**). That trend holds after 18 hours ($58\pm 13\%$ ASC-SF and $50\pm 4.7\%$ NCM, vs $35\pm 5.7\%$ NT and $29\pm 6.8\%$ Unsupplemented).

After 24 hours, wound closure for NT ($57\pm 11\%$) is not significantly different from ASC-SF ($73\pm 8.5\%$) or NCM ($74\pm 9.0\%$), but is significantly higher than Unsupplemented media ($29\pm 11\%$). NT closure peaked at 36 hours ($80\pm 8.8\%$), while ASC-SF ($80\pm 8.7\%$) and NCM ($77\pm 11\%$) remained statistically similar to 24-hour levels of wound closure. Unsupplemented media remained at significantly lower levels ($35\pm 12\%$) after 36 hours. ASC-SF does not induce any effect on SMC migration significantly different from NCM.

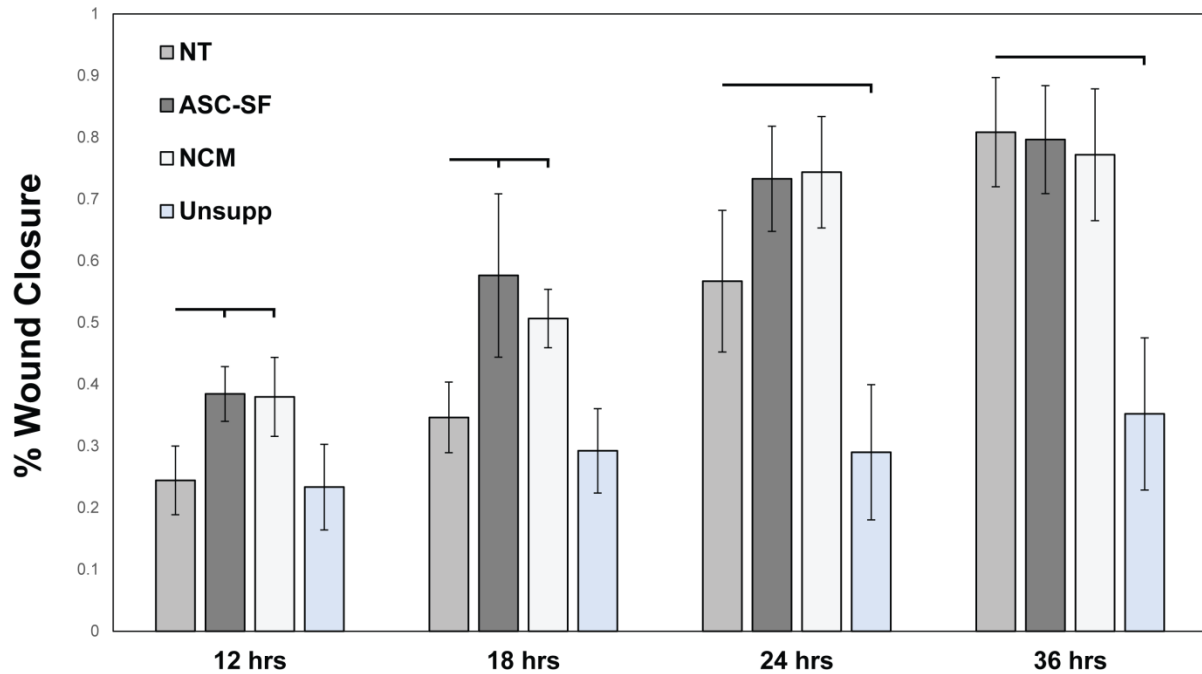


Figure 15: 2D SMC migration is enhanced when treated with ASC-SF and NCM.

SMC migration to close a scratch wound, after plating on a 2D tissue culture-treated 24 well plate at 5.5×10^4 cells/well. Media treatments of NT (No Treatment, SMC growth supplemented media as a positive control), ASC-SF, NCM (Non-Conditioned Media), and Unsupp (Unsupplemented SMC basal media as a negative control) and with CellTracker dye were added after 36 hours, and scratch wounds were imaged every two hours for a 36-hour window. Wound closure percentage was defined as $[(\text{initial scratch area} - \text{timepoint scratch area}) / \text{initial scratch area}]$. $\alpha = 0.05$, $n = 6$.

2.3.10 ASC-SF increases SMC myosin heavy chain expression

qPCR analysis (**Figure 16**) revealed a transcriptional increase in SMC differentiation marker myosin heavy chain (MYH11) after ASC-SF stimulation (3.916 ± 1.952) when compared to both NT control (1 ± 0.0003) and NCM (0.8443 ± 0.6187).

No difference was seen in transcription of α smooth muscle actin (ACTA2) after ASC-SF stimulation (0.5731 ± 0.2137) when compared to both NT control (1 ± 0.1319) and NCM (0.4924 ± 0.2644). No difference was seen in transcription of calponin (CAL) after ASC-SF stimulation (1.303 ± 0.4857) when compared to both NT control (1 ± 0.2543) and NCM (0.9533 ± 0.2896).

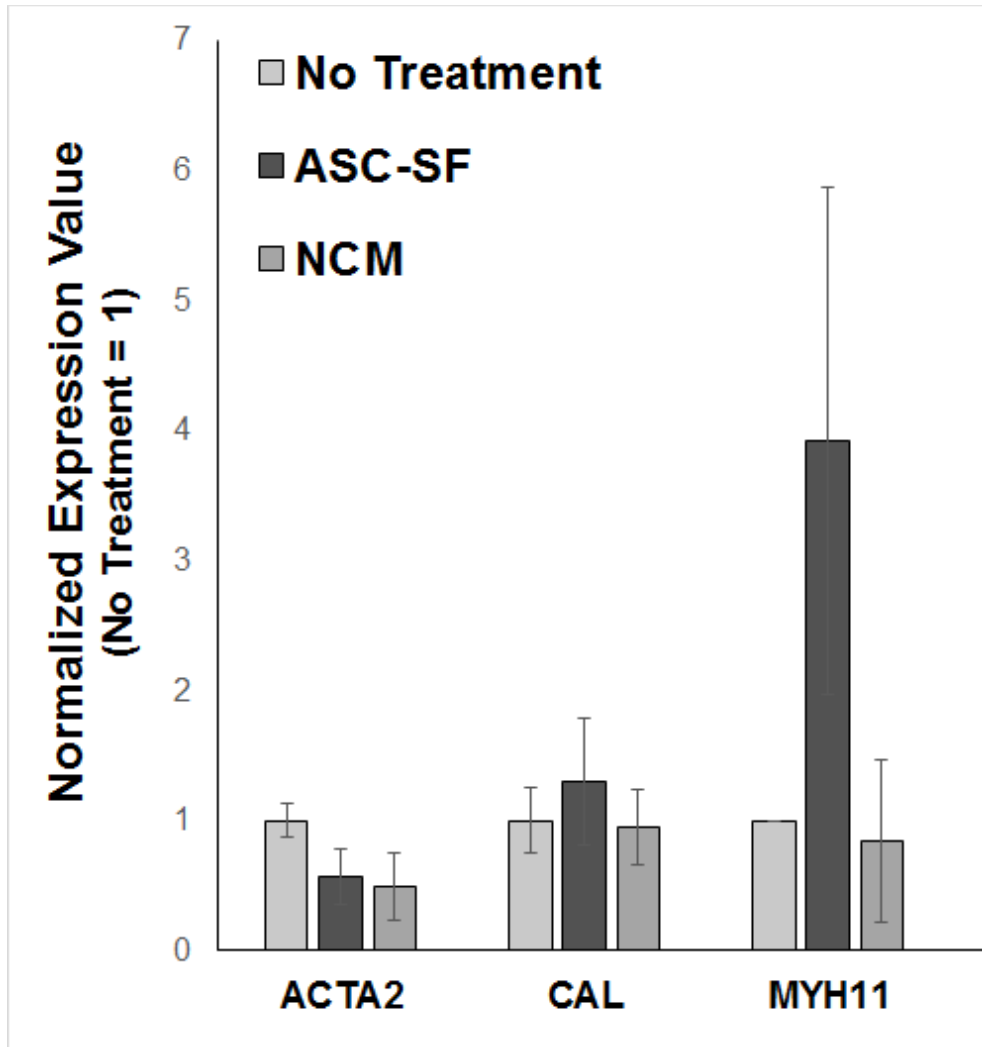


Figure 16: SMC phenotype marker transcription in response to 30 days of ASC-SF stimulation.

RT-qPCR revealed an increase in myosin heavy chain (MYH11) after ASC-SF stimulation, while both α smooth muscle actin (ACTA2) and calponin (CAL) were unchanged. $n = 3$.

2.3.11 ASC-SF induce SMC transcription of tropoelastin and elastin chaperone proteins fibrillin-1, fibulin-5, LOX, and LOXL-1

After 30 days in 3D stiff substrate constructs, qPCR revealed that both ASC-SF (4.94±0.71-fold increase vs NT control, $p < 0.0001$) and NCM (3.09±0.29-fold increase, $p = 0.001$) induced a significant increase in SMC tropoelastin (**Figure 17**). ASC-SF also increased SMC transcription of microfibril protein fibrillin-1 (4.22±1.10-fold increase, $p = 0.00014$), elastin organizational protein fibulin-5 (5.42±0.53-fold increase, $p < 0.0001$), and cross-linking proteins LOX (2.31±0.44-fold increase, $p = 0.00046$) and LOXL-1 (2.22±0.53-fold increase, $p = 0.0052$). Expression of LTBP-4, responsible for elastin coacervate globule deposition onto fibrillin-1 microfibrils, was significantly downregulated with both ASC-SF stimulation (0.98±0.02-fold decrease versus NT control, $p < 0.0001$) and NCM (0.99±0.02-fold decrease, $p < 0.0001$). Expression of elastin organizational matricellular protein fibulin-4 was unchanged with ASC-SF stimulation. NCM did not induce a significant difference in deposition of fibrillin-1, fibulin-4, fibulin-5, LOX, or LOXL-1, when compared to NT control.

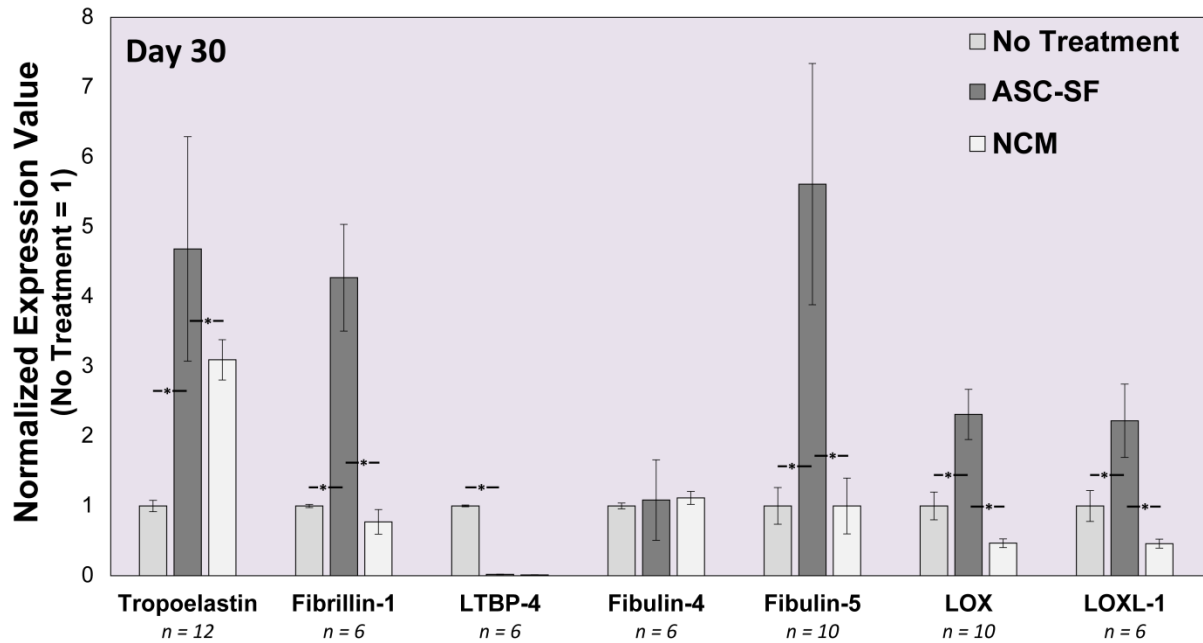


Figure 17: Transcriptional changes in tropoelastin and elastin chaperone matricellular proteins after 30 days of ASC-SF stimulation of SMCs.

RT-qPCR revealed increases in SMC production of tropoelastin induced by both ASC-SF and NCM, as well as ASC-SF induced increases in microfibril protein fibrillin-1, organizational matricellular protein fibulin-5, and cross-linking proteins lysyl oxidase (LOX) and lysyl oxidase-like 1 (LOXL-1). Fibulin-4 production was unchanged with both ASC-SF stimulation and NCM9 when compared to NT, and LTBP-4 production was significantly reduced with both ASC-SF stimulation and NCM.

2.3.12 Elastic fiber networking quantifiably increases with ASC-SF treatment under all stiffness and loading conditions.

Elastic fibers were clearly distinguishable in ASC-SF stimulated SMC constructs, regardless of substrate stiffness, after both 20 days and 30 days (**Figure 21A**). Quantification of elastin immunostaining images revealed an ASC-SF induced increase in elastic fiber length ($+36.2 \pm 7.55\%$, $p = .0064$) within 20-day stiff substrate SMC constructs (**Figure 21B**). ASC-SF stimulated elastic fiber length decreased after 30 days in stiff substrate constructs, with levels statistically similar to both control groups. Fiber intersection density within stiff substrate constructs increased after both 20 days ($+43.6 \pm 8.69\%$, $p = .0028$) and 30 days ($+80.8 \pm 25.1\%$, $p = 0.018$) (**Figure 21C**).

Soft substrate SMC gel constructs saw a decrease in average segment length after 20 days in both constrained ($-33.5 \pm 8.37\%$, $p = 0.0499$) and dynamic ($-21.7 \pm 2.63\%$, $p = 0.0496$) construct conditions, holding constant through 30 days (**Figure 22A**). Fiber intersection density on ASC-SF stimulated soft substrate constrained constructs saw an increase after 20 days ($+79.7 \pm 33.4\%$, $p = 0.0096$), holding constant relative to NT control after 30 days in culture. Dynamic ASC-SF stimulated constructs saw increases in fiber intersection density after both 20 days ($+28.5 \pm 14.0\%$, $p = 0.16$) and 30 days ($+48.2 \pm 9.28\%$, $p = 0.0068$) in culture (**Figure 22B**).

Additionally, multiphoton microscopy qualitatively confirmed the presence of wavy, continuous elastic fibers after ASC-SF stimulation (**Figure 19, Figure 20**) when compared to a lack of visible fibers in NT control constructs (**Figure 18**).

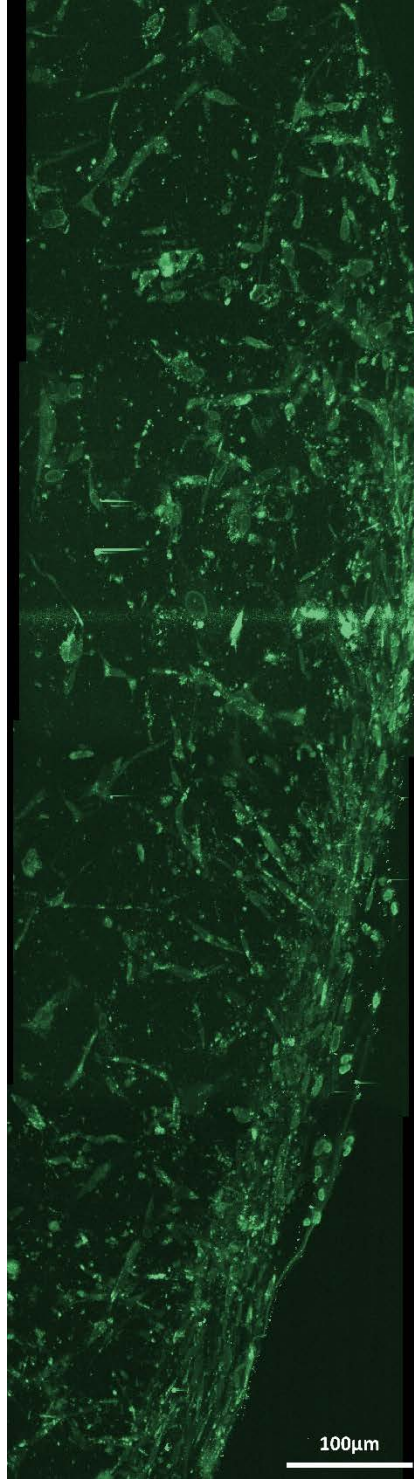


Figure 18: Multiphoton composite image (1x5) of control NT-stimulated SMC autofluorescence signal.
Performed on the Advanced Intravital Microscope at the Soft Tissue Biomechanics Laboratory, as described in Section 2.2.8 .

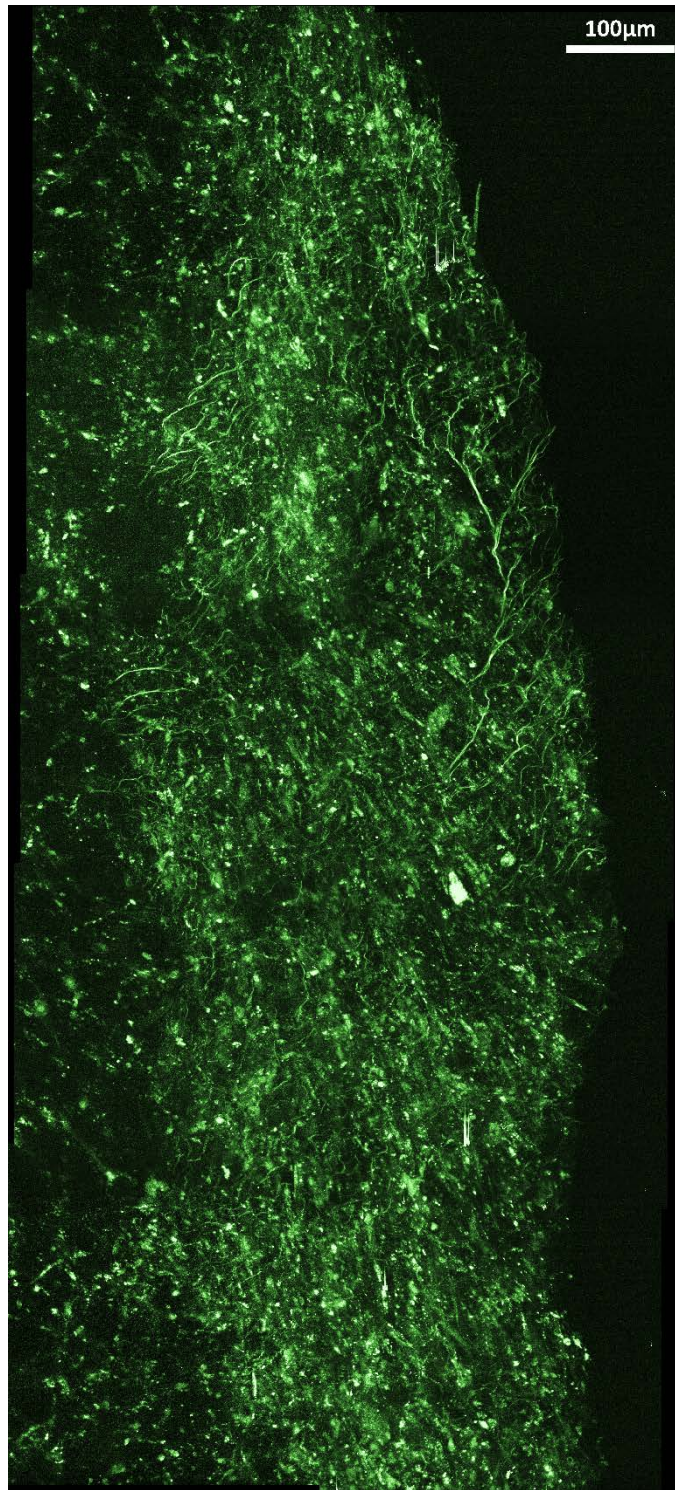


Figure 19: Multiphoton composite image (2x5) of ASC-SF stimulated SMC elastic fiber deposition.

Performed on the Advanced Intravital Microscope at the Soft Tissue Biomechanics Laboratory, as described in Section 2.2.8 .

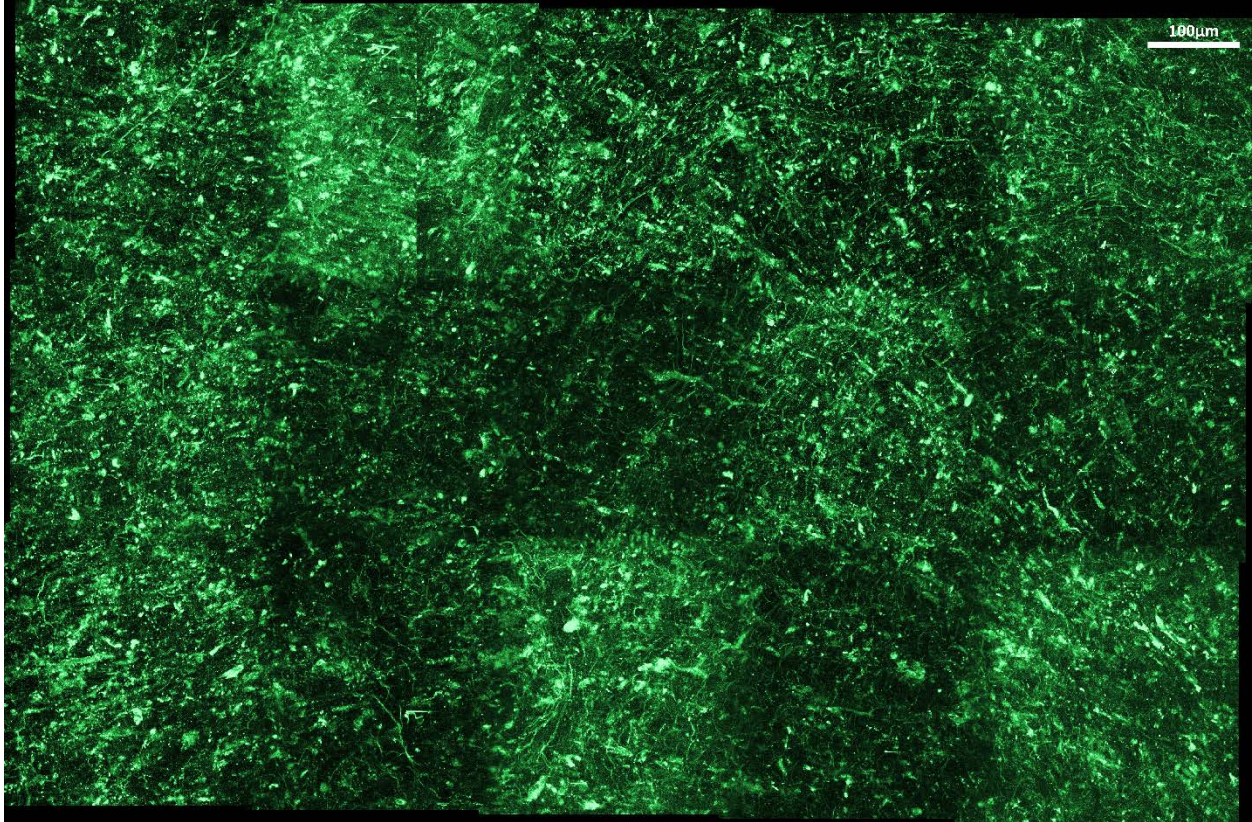
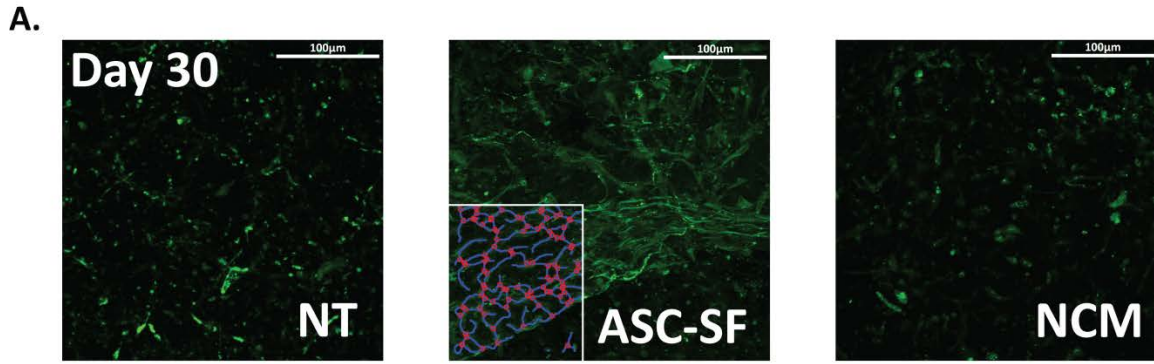


Figure 20: Multiphoton composite image (3x5) of ASC-SF stimulated SMC elastic fiber deposition.

Performed on the Advanced Intravital Microscope at the Soft Tissue Biomechanics Laboratory, as described in Section 2.2.8 .



Stiff Substrate

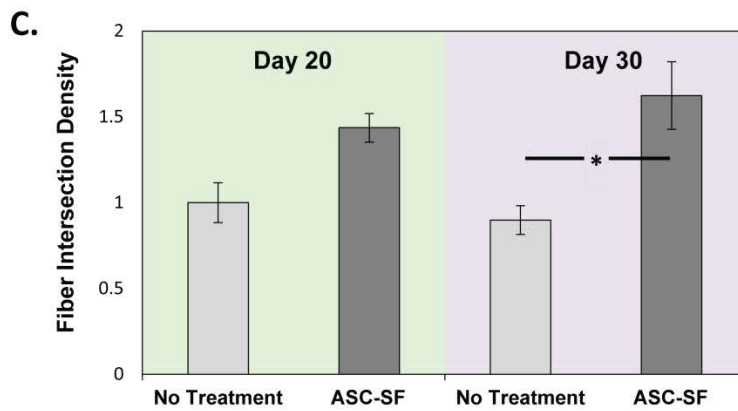
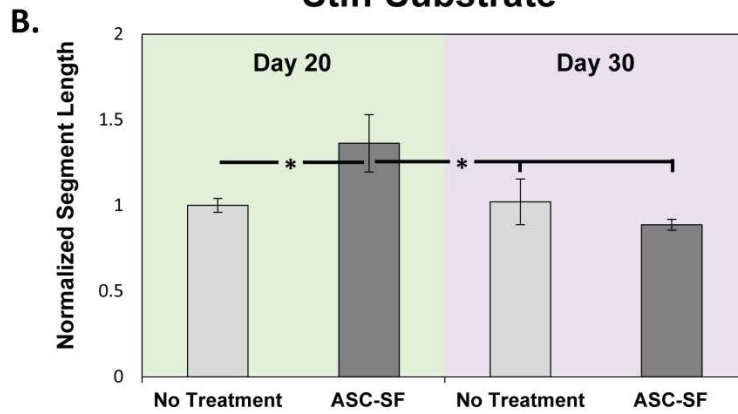
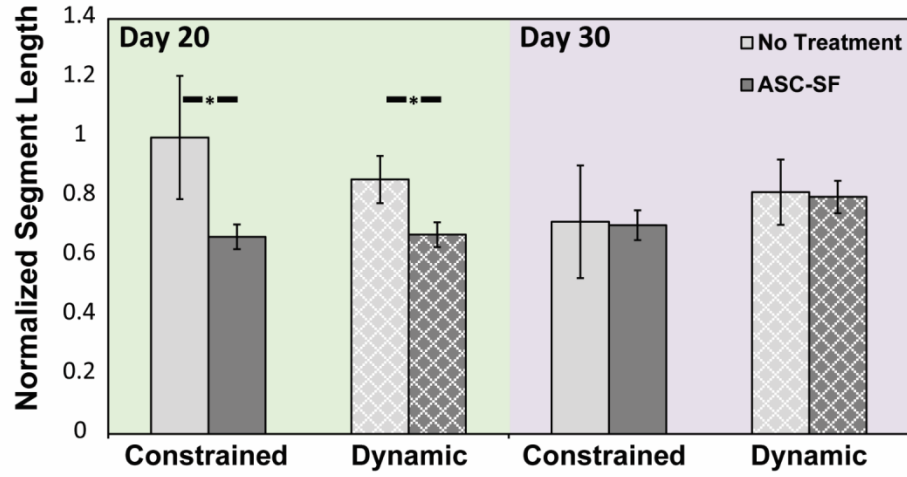


Figure 21: Elastic fiber imaging and fiber network quantification on stiff substrates.

(A) SMC elastic fibers (green) were revealed after ASC-SF stimulation, when compared to both No Treatment (NT) and Non-Conditioned Media (NCM) negative controls, in sample images of z-stacked confocal images of the 30-day stiff substrate fibrin gel constructs. Inset for the ASC-SF image shows an example of the MATLAB image quantification code identifying fibers (blue lines) and fiber intersections (red circles). (B-C) Stiff substrate fibrin gel constructs revealed (B) increased elastic fiber length and (C) intersections after 20 days in culture. After 30 days, length decreases while intersection density increases. $\alpha = 0.05$, $n = 5$.

Soft substrate

A.



B.

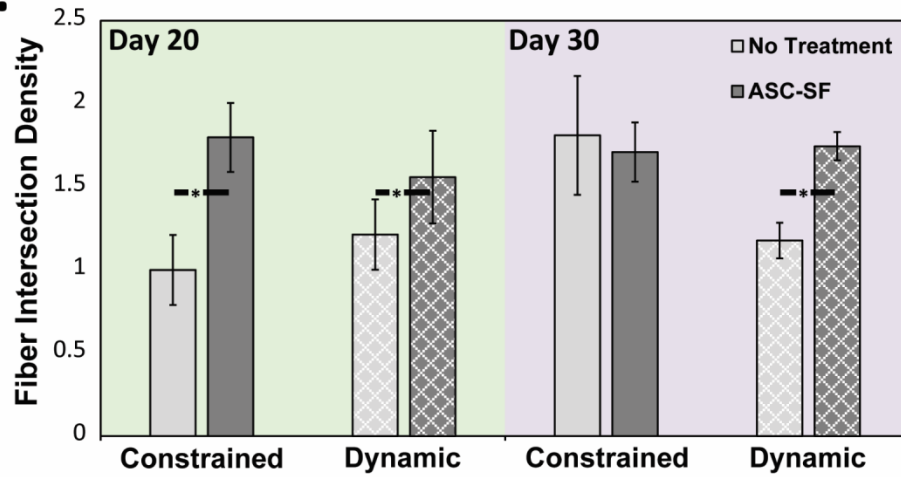


Figure 22: Elastic fiber imaging and fiber network quantification on soft substrates, with constrained and dynamic culture conditions.

Soft substrate ASC-SF stimulated fibrin gel constructs revealed (A) decreased elastin segment length and (B) increased fibril intersection density compared to NT control after 20 culture days in both constrained (solid bars) and dynamic (checked bars) loading conditions, with additionally increased intersection density after 30 days of dynamic culture. $\alpha = 0.05$, $n = 5$.

2.3.13 Insoluble elastin increases with ASC-SF treatment after 20 and 30 constrained culture days regardless of substrate stiffness, and after 30 days under soft substrate cyclic loading.

ASC-SF stiff substrate SMC stimulation induced a 136% increase versus NT control in insoluble elastin percentage of total protein after 20 days ($0.15 \pm 0.023\%$ NT control and $0.15 \pm 0.03\%$ NCM control, vs $0.37 \pm 0.13\%$ ASC-SF, $p = 0.045$), and a 94% increase after 30 days ($0.12 \pm 0.04\%$ NT control & $0.098 \pm 0.038\%$ NCM control, vs $0.25 \pm 0.07\%$ ASC-SF, $p = 0.050$) (**Figure 23A**).

Insoluble elastin deposition on soft substrate constrained constructs saw a similar 154% increase after 20 days ($0.14 \pm 0.015\%$ NT control vs $0.36 \pm 0.12\%$ ASC-SF, $p = 0.013$) and 124% increase after 30 days ($0.13 \pm 0.08\%$ NT control vs $0.30 \pm 0.076\%$ ASC-SF, $p = 0.0031$) (**Figure 24A**). Dynamic SMC constructs, subjected to cyclic uniaxial strain to mimic standard aortic stretching intensity and frequency, produced statistically similar levels of insoluble elastin percentage after 20 days in culture regardless of ASC-SF. After 30 days, however, a 148% increase in elastin percentage was observed ($0.29 \pm 0.030\%$ NT control vs $0.50 \pm 0.069\%$ ASC-SF, $p = 0.016$) (**Figure 24A**).

2.3.14 Collagen fraction increases with ASC-SF treatment after 30 days cultured on stiff substrate constructs, and after both 20 and 30 days on constrained and dynamic soft substrate constructs.

After 20 days of fibrin gel culture on stiff substrates, ASC-SF stimulation resulted in a statistically similar level of collagen (relative to total protein) when compared to both NT and

NCM controls. Extending stiff substrate constructs to 30 days, however, resulted in a 233% collagen increase with ASC-SF stimulation ($0.045\% \pm 0.028\%$ NT vs $0.15 \pm 0.063\%$ ASC-SF, $p = 0.023$). NCM did not result in any detectable collagen after 30 days in culture, despite cellular viability and elastin detection on the same 3D construct set (**Figure 23B**).

Constrained soft substrate SMC constructs saw ASC-SF induced collagen increases after both 20 days ($0.0055 \pm 0.0033\%$ NT control vs $0.047 \pm 0.0060\%$ ASC-SF, $p = 0.00047$) and 30 days ($0.013 \pm 0.0032\%$ NT control vs $0.11 \pm 0.023\%$ ASC-SF, $p = 0.0026$). Additionally, dynamic soft substrate SMC constructs saw collagen increases after both 20 days (below the detectable threshold for the NT control, vs $0.10 \pm 0.026\%$ ASC-SF) and 30 days (NT control below detectable threshold vs $0.19 \pm 0.0079\%$ ASC-SF, $p < 0.0001$) (**Figure 24B**).

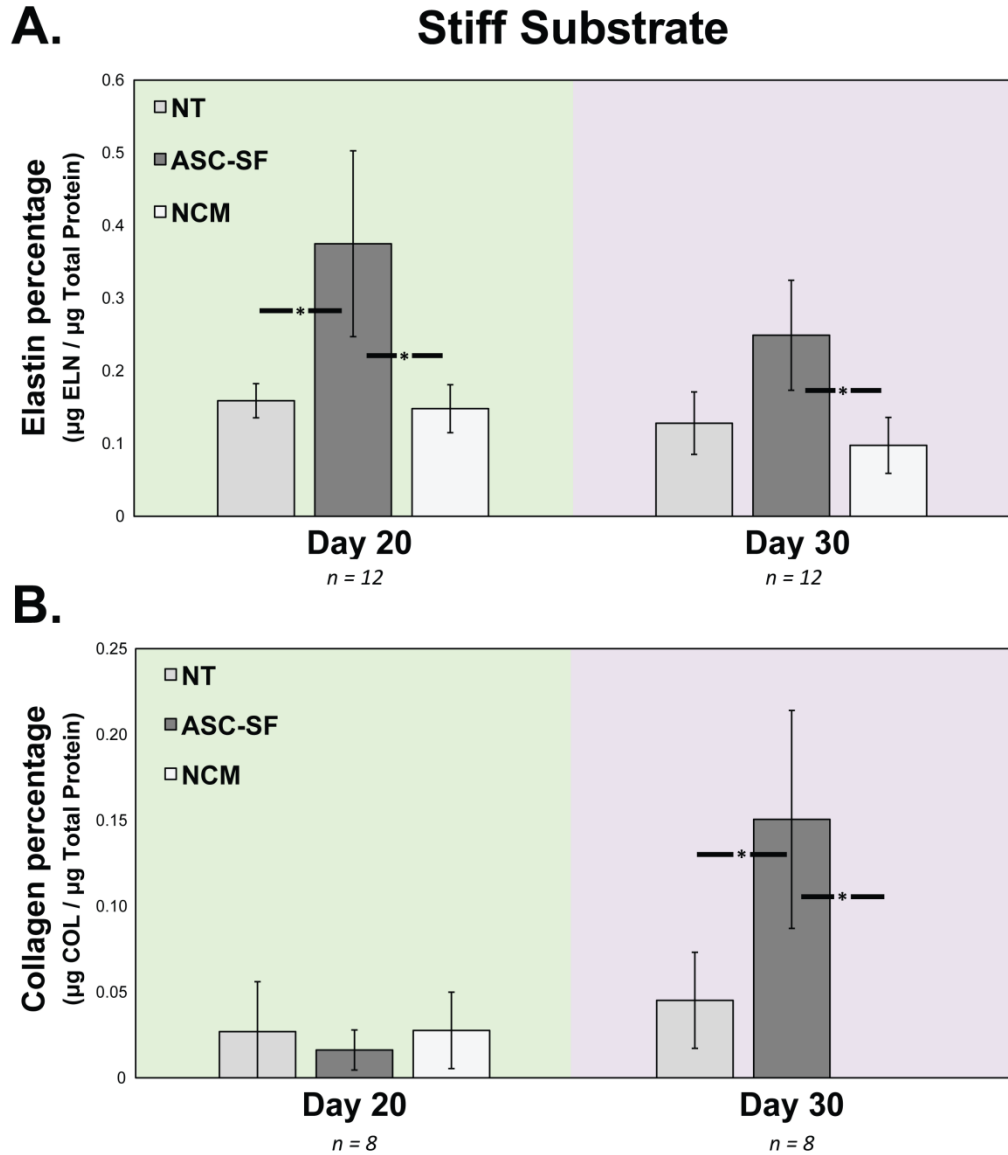


Figure 23: Insoluble elastin and collagen are enhanced by ASC-SF stimulation of SMC constructs plated on stiff substrates.

Stiff substrate fibrin gel SMC construct analysis of (A) insoluble elastin percentage and (B) collagen percentage of total protein, comparing control NT and NCM treatments with ASC-SF stimulation. Day 30 collagen percentage for NCM-treated constructs was consistently below detection threshold.

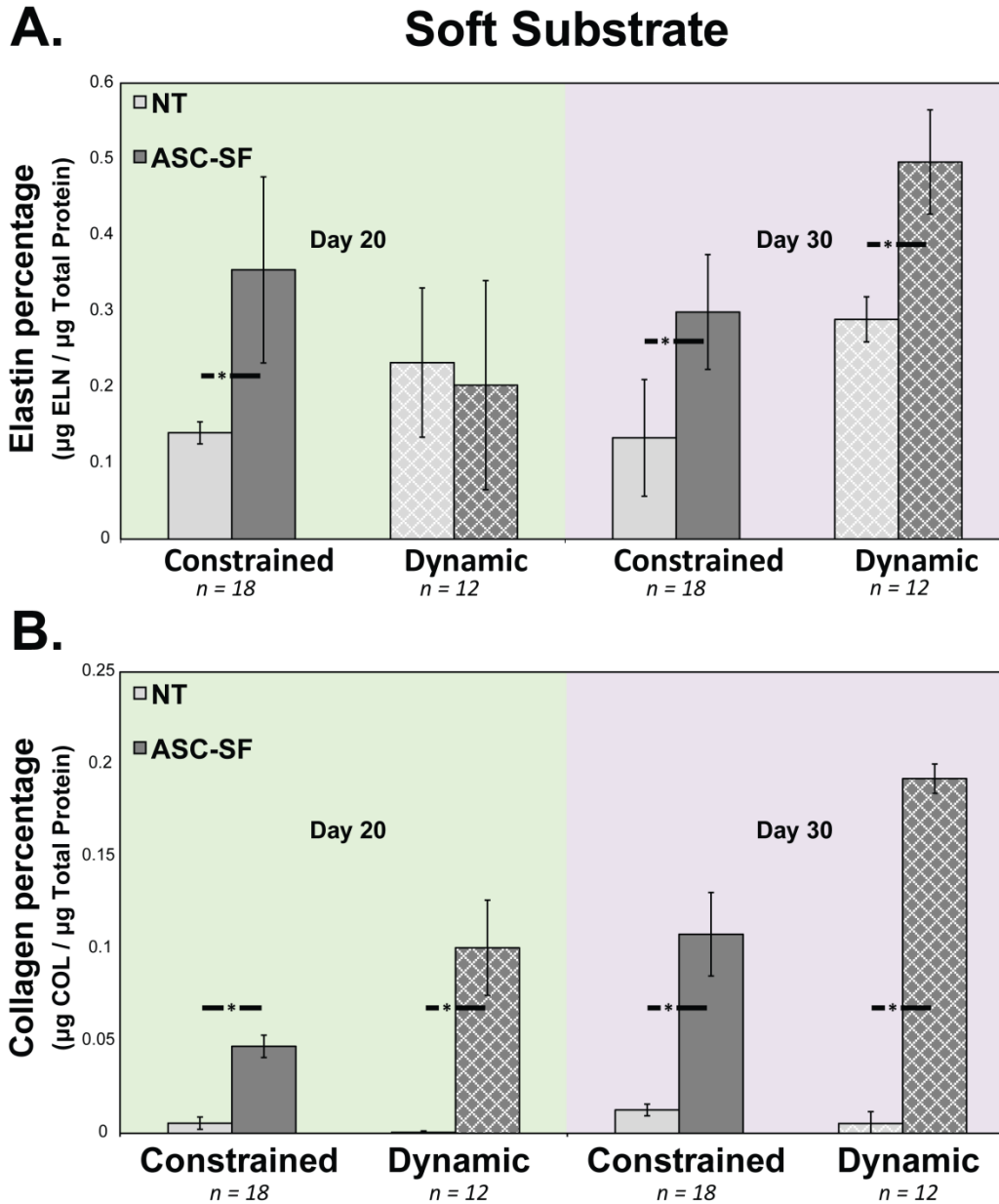


Figure 24: Insoluble elastin and collagen are enhanced by ASC-SF stimulation of soft substrate SMC constructs, under Constrained and Dynamic loading conditions.

Soft substrate analysis of (A) insoluble elastin percentage and (B) collagen percentage of total protein, comparing NT control treatment to ASC-SF stimulation under constrained (solid bars) and dynamic (checkered bars) loading conditions.

2.3.15 High modulus is increased in ASC-SF stimulated soft substrate SMC constrained constructs after 30 days.

Blank gels displayed an almost linear response to extension (**Figure 25**). The NT gels displayed a more non-linear response and the ASC-SF gels display a j-curve type response to extension that is typically exhibited by soft connective tissue, owing to the presence of mechanically functional elastin and collagen. High and low modulus, defined as the slope of the given sample's mechanical response curve within the high stretch range (final third of the curve) and low stretch range (first third of the curve), were then quantified. After 30 days, ASC-SF induced a 151% increase in high elastic modulus (49.93 ± 8.829 kPA NT control vs 125.2 ± 54.24 kPA ASC-SF, $p = 0.00040$), while low elastic modulus remained statistically unchanged (12.87 ± 7.950 kPA NT control vs 12.90 ± 4.048 kPA ASC-SF) (**Figure 25C**). Blank gels displayed a significantly reduced low modulus (5.600 ± 1.335 kPA) and high modulus (8.011 ± 3.634 kPA). Ninhydrin assays on these tested samples detected a significant increase in insoluble elastin percentage of total protein ($0.088 \pm 0.028\%$ NT control vs $1.8 \pm 0.65\%$ ASC-SF, $p = 0.00074$) when stimulated by ASC-SF. Hydroxyproline assays detected a statistically significant increase in collagen percentage of total protein ($0.13 \pm 0.077\%$ NT control vs $0.30 \pm 0.076\%$ ASC-SF, $p = 0.0031$) when stimulated by ASC-SF.

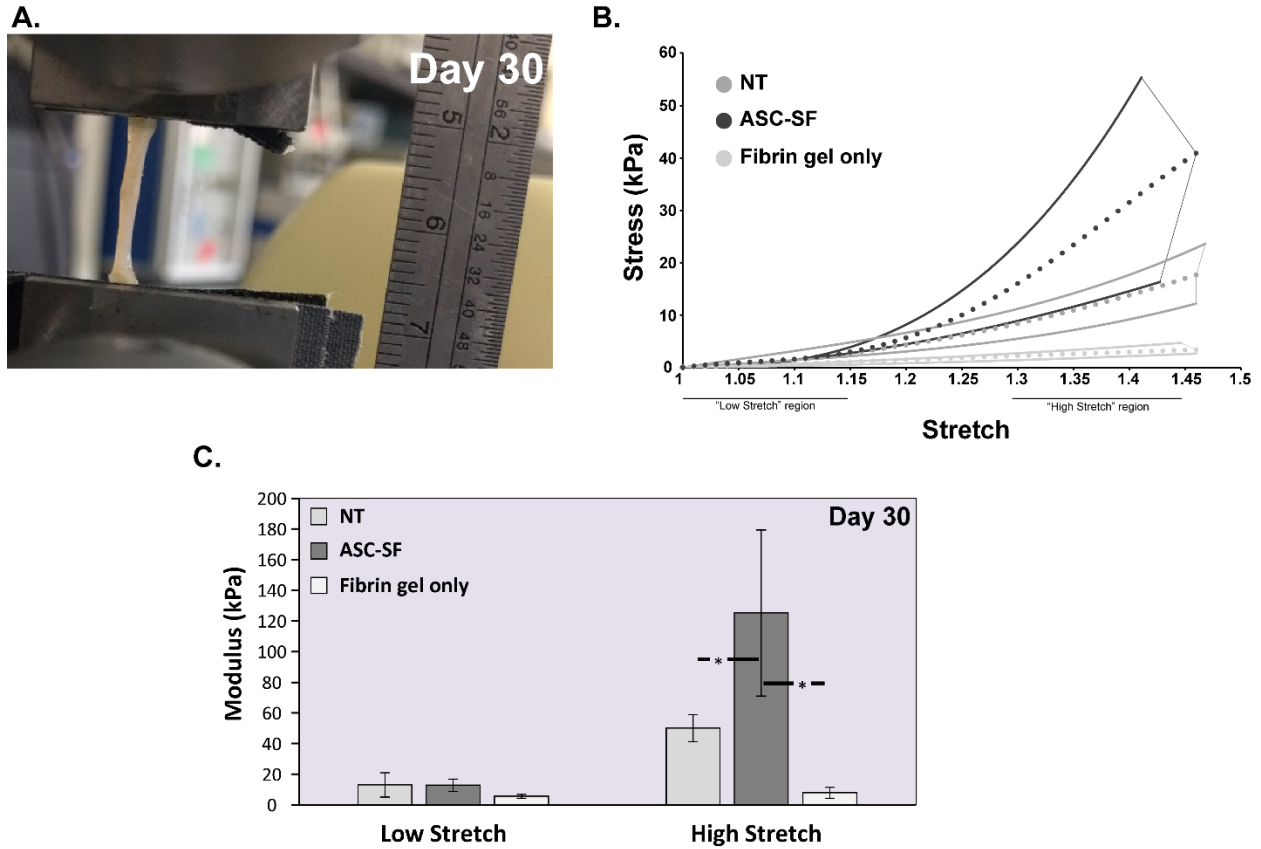


Figure 25: Mechanical properties of constrained, soft substrate ASC-SF stimulated SMC constructs.

(A) Image of tensile testing configuration (Instron #5543A, with sandpaper-lined pneumatic clamps) used to test 30-day NT and ASC-SF treated constrained fibrin gels, with ruler for scale. Full details of soft substrate construct harvesting and preparation is available in Figure 3. (B) Low and high modulus, defined as the slope of the mechanical response curve at low and high stretch, were analyzed on soft substrate-plated fibrin No Treatment (NT) and ASC-SF stimulated SMC constructs, alongside cell-free fibrin gel control constructs. Black dots indicate the fit lines (within the low and high stretch regions) used to calculate low and high elastic modulus. Envelopes around the fit lines indicate the most extreme testing curves, indicating a spread of the data between those bounds. (C) Comparison of elastic modulus at low stretch and high stretch regions for both 30-day NT and ASC-SF stimulated fibrin gel constructs, alongside cell-free fibrin gel constructs.

2.4 Discussion

The results of this study indicate that ASC-SF treatment induces SMC elastin stimulation within 3D fibrin gel constructs at each level of the elastogenesis cascade: tropoelastin and elastin organizational protein transcription (**Figure 17**), organized elastin fibril formation and networking (**Figure 21, Figure 22**), insoluble elastin protein deposition (**Figure 23, Figure 24**), and a mechanically-active extracellular matrix structure incorporating the deposition of collagen within 3D fibrin gel constructs (**Figure 25**). Both NCM and ASC-SF accelerates SMC migration and wound healing (**Figure 15**) as evidenced by the wound closure gap after 12 and 18 hours in culture when compared to standard culture media, with potential cell recruitment effects of either treatment effect (though no pro-migratory effect was uniquely a result of ASC-SF).

Tropoelastin, the core protein of elastic fibers, sees a nearly 5-fold transcription increase when adult SMCs are stimulated by either ASC-SF or NCM. However, production of tropoelastin without sufficient support from essential elastin chaperone matricellular proteins results in immature elastic fiber deposition (**Figure 1**). In AA, insufficient deposition of elastin chaperone proteins alongside tropoelastin and cross-linked collagen increases aortic stiffness and decreases compliance (caused by insufficient mature elastin), producing aortic conditions susceptible to rupture [77, 224]. In this study, ASC-SF stimulation has shown bioactivity that could address this issue, with significant transcriptional increases in fibulin-5 (which bundles tropoelastin coacervates), LOX (which cross-links tropoelastin via fibulin-4), and LOXL-1 (which cross-links tropoelastin via fibulin-5) (**Figure 17**). Microfibril protein fibrillin-1 is also increased with ASC-SF stimulation, potentially producing more deposition sites for elastin coacervates.

Elastic fiber analysis revealed that overall elastic fiber networking increases with ASC-SF stimulation, resulting from a combination of increasing intersection density and decreasing average fiber length (**Figure 21, Figure 22**). For example, in stiff substrate constructs, fiber intersection density increases significantly at both timepoints with the addition of ASC-SF, while fiber length initially spikes after 20 days and significantly decreases after 30 days in culture. This pattern suggests an initial formation of elastin coacervates and deposition onto microfibrils after 20 days, with inter-globule crosslinking only occurring after 30 days of constant ASC-SF stimulation. While stiff substrate insoluble elastin fraction was increased at both timepoints, collagen fraction only increased after 30 days, indicating the potential influence of substrate stiffness when evaluating SMCs even within 3D culture hydrogels.

Soft substrate constructs displayed key elastin deposition differences between constrained and dynamic cultures. Constrained soft substrate constructs saw increased insoluble elastin fraction and network formation after 20 days, while dynamic soft substrate constructs saw the same response only after 30 days.

These results suggest that dynamically-active constructs plated on flexible soft substrates, which are more accurate mimics of *in vivo* aortic conditions, may require an extended ASC-SF therapeutic window to produce chemically mature and mechanically active elastic fibers in patients with AA. This “delayed” elastogenic effect is of particular interest to bioengineers developing non-surgical therapeutic options tailored for small AA, with 30 days of the current ASC-SF delivery concentration every 48-72 hours as the baseline for generating mature elastin from SMCs.

ASC-SF treatment increases the high modulus, but not low modulus, of soft gels after 30 days of culture compared to the NT and fibrin-only controls (**Figure 25**). Elastin, a linearly

elastic material, is expected to influence the low modulus of the gels, as it provides elasticity in the low stretch region of the mechanical response curve to decrease the low modulus of native vessels [225-227]. Mechanical characterization in this study does not reveal a significant difference between the low modulus of the ASC-SF treated gels relative to the NT group, therefore suggesting that the elastin present in both sets of gels is statistically similar in mechanical function despite the former displaying relatively increased deposition and organization. **Figure 25** characterizes the elastic (non-time dependent) mechanical response of the gels; however, elastin also plays an important role in the viscous (time dependent) mechanical response [210]. It is therefore possible that despite displaying statistically similar low modulus, the ASC-SF treated group could display more physiologically relevant viscous mechanical properties (such as increased creep resistance) relative to NT controls. Future elastogenesis studies should therefore characterize viscous mechanical properties to further characterize the mechanical functionality of ASC-SF mediated elastin formation relative to NT control. Particular attention should be afforded to creep resistance, which would aid in resisting aneurysm growth over time.

Collagen deposition, mediated by ASC-SF (**Figure 23**, **Figure 24**), appears to significantly increase the high modulus of the gels (**Figure 25**). ASC-SF treatment also causes the gels to display a stretch-stiffening response that is characteristic of native arterial tissue and attributed to the de-crimping and elongation of collagen fibers [223, 226]. Collagen deposition is often defective in AA whereby fibers are not correctly oriented or crimped [228]. The collagen deposited in this study displays evidence of crimping as the mechanical response curves show a clear toe region and stretch-stiffening response. ASC-SF treatment therefore demonstrates the potential to not only trigger the deposition of mechanically active elastin, but also crimped

collagen fibers, both of which would contribute to halting AA growth, reducing rupture risk, and restoring homeostasis.

2.5 Conclusion

By coupling elastin extracellular matrix protein transcription with algorithm-based characterization of fiber network morphology, ECM protein quantification, and mechanical testing, the elastogenesis cascade analysis method outlined in this study illustrates the multiple levels of elastin production by SMCs after ASC-SF therapy. Future work would look to tailor this 3D construct platform to more accurately mimic aneurysmal aorta by seeding SMCs explanted from aneurysmal aortas, altering the stiffness of fibrin constructs, or modulating soft substrate stretch within the dynamic culture system.

Importantly, this study is a first step towards understanding the therapeutic effect of ASC-SF on aortic SMC elastogenesis. It also provides a baseline for ASC-SF delivery concentration, with extended release of ASC-SF as a goal for any future elastin-targeted therapeutic approach that utilizes ASC paracrine signaling pathways to smooth muscle cells.

2.6 Future Work

One major question unanswered by this study is the complete elastogenesis impact on soft substrate-plated, dynamically-loaded SMC constructs, as qPCR and elastin chaperone protein transcriptional analysis was not included in the initial experimental design. As a

significant elastin networking and insoluble elastin increases occurring between days 20 and 30 of dynamic culture, the leading hypothesis is the ‘delayed’ elastogenic effect is a result of cellular adaptation to a mechanically stimulated 3D microenvironment. Full analysis of elastin chaperone protein transcriptional changes between these points is needed to verify this hypothesis.

One limitation of elastic fiber analysis is reliance on a 2D projection of confocal fiber analysis in three dimensions, with each identified fiber “node” defined as the intersection of two identified fibers. However, these fibers could merely be crossing in different z-planes, necessitating a modification to the fiber analysis code that reconstructs a 3D elastic fiber microenvironment and analysis networking parameters in that context.

Additionally, dynamic culture conditions induced through the FlexCell system could be modulated to more accurately mimic diseased, rather than standard, aortic conditions. Here, we used a 1Hz frequency (simulating 60 beats per minute) and 10% displacement, both values based on a healthy vasculature. Reducing displacement, increasing frequency, and increasing the stiffness of the fibrin gel constructs through an increase in fibrinogen concentration could provide an *in vitro* method to mimic diseased aortic conditions. This modality might be a better *in vitro* model for cardiac fibrosis than aneurysm formation, and further study is warranted to establish a standard culture system to evaluate pro-elastogenic therapeutics.

This study also focused on initial proof-of-concept pro-elastogenic rat fetal lung fibroblasts, to establish fibrin gel constructs and elastogenesis cascade analysis tools, and on commercially-available healthy adult SMCs as an initial elastogenesis target for ASC-SF. The target SMCs will assuredly present with a significantly different phenotype within the medial layer of dilated, and altered elastogenesis effects in response to ASC-SF are to be expected. The

next step in the evaluation of ASC-SF as a pro-elastogenic therapy for small aneurysm is to integrate medial layer cells isolated from aortic layers in various states of dilation and disease, with initial studies available in **Chapter 3.0** and **Chapter 4.0** of this dissertation.

Analysis of other matricellular proteins, and their impact on both mature elastin formation and ECM mechanical response profile, can begin with the fibulin family. Fibulin-1 alongside aggrecan content within the aortic wall have recently shown key roles in age-related aortic stiffening [229], with significant deposits of aggrecan and versican accumulation found during proteomic analysis of human thoracic aortic aneurysm and dissection samples [230] due either increased synthesis or decreased proteolytic turnover. Given high stiffening conditions and predisposition towards dissection and aneurysm, fibulin-1, aggrecan, and versican present as a potential biomarker combination for aneurysmal risk evaluation. Based on the importance of the fibulins, a calcium-dependent elastin binding protein structure domain mimicking aspects of the fibulin family could be replicated to develop a therapeutic to aid in elastin assembly [69] or interrupt the pro-fibrotic feedback loop. Additionally, further multiphoton analysis on both elastic and collagen fiber deposition would provide an additional level of ECM analysis after ASC-SF stimulation within these fibrin constructs.

Our treatment regimen (30 days of ASC-SF delivered every 48-72 hours) must be optimized as clinical translation of this ASC-SF therapy progresses. A feasible delivery system would expand the potential target patient population for this elastin-targeted AA therapeutic. Extracellular vesicles packaging these secreted growth factors could modulate the SMC response [231] across a lengthened window, presenting with a mechanism to deliver either ASC-SF or a cocktail of potent pro-ECM factors. TGF- β [13], HGF, VEGF, IGF, PDGF, and pro-inflammatory factors within the interleukin family [232] all present with delivery opportunities

within the context of small AA [233]. Initial work to evaluate the pro-elastogenic effects of ASC-secreted exosomes and extracellular vesicles can be found in **Chapter 6.0**.

3.0 Specific Aim 2, Part 1: Elastogenesis Impact of Adipose-Derived Stromal Cell Secreted Factors on Adult Aneurysmal Smooth Muscle Cells

As shown in **Chapter 2.0**, adipose-derived stromal cell (**ASC**) secreted factors (**ASC-SF**) can upregulate four different points of the elastogenesis cascade in healthy adult aortic smooth muscle cells (**SMCs**): elastin chaperone matricellular protein transcription, elastin network formation, insoluble elastin (and total collagen) protein deposition, and a mechanically-active extracellular matrix (**ECM**) network within three-dimensional fibrin gel constructs. SMC phenotype in aneurysmal aortas, however, will be significantly different than the commercially-available SMCs studied in **Chapter 2.0**.

This chapter will focus on SMCs isolated from the medial layer of adult thoracic aortic aneurysm (**TAA**), generously provided by the Thoracic Aortic Disease Research laboratory at the University of Pittsburgh under the direction of Thomas Gleason, MD. The hypothesis of this chapter is that ASC-SF will increase specific steps of the elastogenesis cascade (chaperone protein transcription and insoluble elastin deposition) using TAA SMCs from patients with bicuspid aortic valve disease and Marfan syndrome.

3.1 Introduction

Marfan Syndrome (**MFS**), a disease impacting between 6.5 [24] to 10.2 [25] out of 100,000 individuals, results from a mutation in the gene coding for extracellular matrix (ECM) microfibril protein fibrillin-1 (*FBNI*), which serves as the main template for proper elastin

formation and cross-linking. The Ghent nosology, a set of defined clinical criteria to identify MFS, is reliant on presence of aortic dilation (particularly within the aortic root section) as a result of systemic elastin disruption. Early diagnosis and aortic treatment, both surgical and non-surgical, has been critical to increasing life expectancy of MFS patients, as mean death age has increased from 32 (± 16) in 1972 to 45 (± 17) in 1998 [22, 23] with a mean diagnosis age of 19 years old.

Bicuspid Aortic Valve (**BAV**) Disease is a commonly diagnosed cardiovascular disorder, with studies placing prevalence anywhere from 0.6% to 1.5% of the general population [30-32]. It involves the malformation of the tri-leaflet aortic valve, which regulates blood flow from the left ventricle through the aorta, and an often-accompanying dilation of the aortic root. BAV patients typically have only two separate leaflets, unequal in size, formed during valvulogenesis within the first eight weeks of fetal development [33]. BAV is commonly diagnosed among patients over 40 years old, with only ~2% diagnosed during childhood [34]. Incidence of adverse cardiovascular events among this population increased, such as calcification-related complications leading to leaflet or aortic stenosis [31], aortic incompetence due to myoxid degeneration of the valves [37], coarctation of the aorta aortic root dilation and ascending thoracic aortic aneurysm [35] or ascending thoracic aorta dissection [36].

TAA are present within MFS and BAV patients, as summarized in **Section 1.1.3**. TAAs necessitate surgical intervention once dilation has exceeded larger than 5.5cm in most adult patients [174]; for teenage MFS patients, this dilation threshold is typically 5cm [176, 177] and can be as low as 4cm (or growth rate-dependent) in younger pediatric patients [26]. Fragmentation of elastin, the ECM protein responsible for vascular recoil during blood flow,

often leads to a decrease in aneurysmal vasculature wall compliance resulting in concentrated sections of tissue particularly prone to rupture or dissection.

With aortic aneurysm rupture and dissection as the USA's 15th leading cause of death, with post-rupture mortality rates upwards of 80% [11], surgical repair and pre-emptive targeted therapies have been our primary research focus, as discussed in **Chapters 1.0 & 2.0**. Surgical repair is the primary interventional method for adult TAA at high risk of aneurysm rupture [181]. While early aortic aneurysm screening has reduced rupture rates over the last two decades [182], there is no standard intervention (beyond a “watchful waiting” imaging regimen every 6-to-12 months [234]) for patients with either TAA or AAA diameter below the aforementioned threshold for surgical intervention. Studies have shown that graft placement performed on sub-5cm dilated aneurysms provide no further benefit to long-term survival, necessitating the need for a non-surgical treatment for these patients with small aneurysm [174].

As discussed in prior chapters within this dissertation, the target of these small aortic aneurysm therapies should be effective mature elastin deposition, which consists of a multi-step elastogenesis cascade involving several families of matricellular proteins (**Figure 1**). A non-surgical therapeutic option must target dysregulated ECM. The development of an ASC-SF derived therapeutic for this function is a crucial part of that next step of treatment for small aortic aneurysm.

Previous studies have shown ASC delivery halts aneurysm progression, and **Chapter 2.0** of this work shows that ASC-SF induces increased insoluble elastin and related chaperone protein deposition in healthy adult SMCs. With signaling changes impacting ECM formation within MFS cells, the necessity is there to test the efficacy of exogenous TGF- β 1 and ASC-SF on SMCs sourced directly from diseased aortic tissue. Here, we work to test ASC-SF within our 3D

fibrin construct *in vitro* culture system using SMCs sourced from aortic walls of healthy patients, MFS patients, and BAV patients both with and without aortic aneurysm. Evaluation will be conducted using two components of the elastogenesis cascade described in **Section 2.1** (and **Figure 1**): (1) transcriptional analysis of elastin core protein tropoelastin, microfibril fibrillin-1, organizational proteins fibulin-4 and fibulin-5, crosslinking proteins LOX and LOXL-1, and elastin coacervate deposition protein LTBP-4; and (2) protein analysis of insoluble elastin and total protein deposition induced by exogenous factors.

3.2 Methods

3.2.1 Adult SMC cell culture conditions and patient information

SMCs isolated from explanted adult aortic medial layers were generously provided by the Thoracic Aortic Disease Research Lab (McGowan Institute for Regenerative Medicine, Pittsburgh PA 15219). All adult SMCs were cultured at 37°C and 5% CO₂, with growth media (#311K-500, Cell Applications Inc, San Diego, CA) changes every 48-72 hours. Cells used in experimental cultures were between passages 4 and 12.

Control cells were from patient 01-25 (**CTRL 01-25**), a 44-year-old Caucasian female heart transplant recipient, with collection performed on 6/25/2010. SMCs were isolated from the medial layer of the ascending aorta, had a “normal” diameter below 3.9cm.

MFS cells were from two different patients. **MFS 05-07** was from a 39-year-old Caucasian male, with tissue collected on 5/19/2011. SMCs were isolated from the medial layer of the ascending aorta, measuring 5.7cm in diameter. **MFS 05-04** was from a 22-year-old

Caucasian male, with tissue collected 1/5/2009. SMCs were isolated from the medial layer of the ascending aorta, measuring 4.5cm in diameter.

Bicuspid aortic valve (BAV) cells from a non-aneurysmal (NA) patient (**BAV-NA**), reference number 02-152, was obtained from a 61-year-old Caucasian male, with tissue collected on 10/31/2013. SMCs were isolated from the medial layer of the ascending aorta, measuring 3.5cm in diameter. BAV cells from an ascending thoracic aortic aneurysm (TAA) patient (**BAV-TAA**), reference number 03-2-77, were obtained from a 53-year-old male of Middle Eastern descent, with tissue collected on 12/3/2012. SMCs were isolated from the medial layer of ascending aorta, with maximum diameter at time of surgery measuring 5.0cm.

Tricuspid aortic valve (TAV) cells from a non-aneurysmal (NA) patient (**TAV-NA**), reference number 01-47, were collected from a 60-year-old Caucasian male on 11/9/2012 during a heart transplant. TAV-NA cells were banked as “control” cells by the Thoracic Aortic Disease Research Laboratory. SMCs were isolated from the ascending aorta medial layer, with maximum diameter below 4.2cm. TAV cells from an ascending thoracic aortic aneurysm (TAA) patient (**TAV-TAA**), reference 03-172, were isolated from a 68-year-old Caucasian female on 8/16/2017. SMCs were collected from the ascending aorta medial layer, with maximum diameter measuring 4.4cm.

3.2.2 Fibrin gel construct formation and exogenous stimulation conditions

Adult explanted aortic SMCs from all cells outlined in **Section 3.2.1** were seeded within fibrin gels, made by combining 4:1:1 ratios of fibrinogen, thrombin, and cells. Final concentrations for each fibrin gel construct used were 3.7mg/mL fibrinogen, 0.21U/mL thrombin, and 5×10^5 cells/mL, with fibrin gels formed within 7.94mm diameter circular

templates on 24-well tissue culture plastic plates. Constructs were cultured within 37°C, 5% CO₂ culture conditions.

Negative control exogenous stimulation group included No Treatment (**NT**) control, which consisted of SMC growth supplemented media with 10mM aminocaproic acid (**ACA**) to prevent cell-driven fibrinolytic degradation of fibrin gel constructs. Exogenous stimulation treatment groups included: (1) adipose-derived stromal cell secreted factors (**ASC-SF**), a 1:1 ratio mix of SMC growth supplemented media and ASC conditioned media collected every 24-72 hours; and (2) non-conditioned media (**NCM**), a 1:1 ratio mix of SMC growth supplemented media and fresh ASC culture media.

ASCs were collected from deidentified waste human adipose tissue collected during body sculpting surgeries of non-smoking, non-diabetic patients under 45 years old at UPMC Presbyterian Hospital, as described in **Section 2.2.4**. Standard ASC culture media consisted of 33% Dulbecco's Modified Eagles Medium (High Glucose, Gibco #12100046), 33% DMEM/F12 Medium (HEPES, Gibco #12400024), 7.5% fetal bovine serum (FBS, Premium Select Atlanta Biologics #S11550), 0.75% fungizone (Lonza BioWhittaker Antibiotics #BW17836E), 0.75% penicillin streptomycin (10,000 U/mL, ThermoFisher Scientific #15140122), 0.075 µM Dexamethasone (Sigma-Aldrich #D4902), and 25% Preadipocyte Growth Medium (PromoCell #C-39425). ASC conditioned media was collected from 40 to 70% confluence, and immediately frozen at -80°C.

3.2.3 qPCR transcription analysis of SMC-deposited tropoelastin and elastin chaperone proteins

Fibrin gel constructs were peeled from the tissue culture plastic plate and frozen in RNase-free tubes at -80°C. Frozen gel constructs were pulverized using a probe sonicator, with RNA collection (illustra RNAspin Mini Kit, GE Healthcare Life Sciences #25050070) and RNA concentration quantification (BioTek Take3) performed subsequently. After pre-heating template (65°C, 5 minutes), SuperScript IV First-Strand Synthesis System (Invitrogen #18091050) kit was used to synthesize first-strand cDNA (23°C/10 minutes, 55°C/10 minutes, 80°C/10 minutes). RT-qPCR was performed using KiCqStart SYBR Green ReadyMix with ROX (Sigma-Aldrich # KCQS02), and forward/reverse primers listed in **Table 2**. Post-amplification melt curves validated proper amplification.

3.2.4 Ninhydrin protein assay for insoluble elastin and hydroxyproline protein assay for total collagen

Frozen fibrin gel constructs were thawed immediately before base hydrolysis (0.1M NaOH, 1 hour, 98°C) for fibrin gel digestion and solubilization of non-elastin protein. Centrifugation (1500RPM, 5 minutes) was used to separate insoluble elastin protein from soluble non-elastin protein [216], with two subsequent wash and centrifugation steps to ensure full non-elastin protein separation. Acid hydrolysis (6N HCl, 24 hours, 110°C) solubilized all proteins, and assay quantification performed on soluble and insoluble fractions quantified insoluble elastin (via ninhydrin reaction) and collagen (via hydroxyproline) protein deposition within each fibrin gel construct, normalized to total deposited protein. Ninhydrin content was detectable using an

absorbance reading (at 570nm) after 1-hour incubation with a stannous chloride-based solution within a 56°C water bath. Hydroxyproline content used chloramine-T and dimethylaminobenzaldehyde-based reactions within a 37°C oven, and absorbance reading for quantification (570nm).

3.2.5 Statistical Analysis

Means comparisons were conducted using individual t-tests or one-way ANOVA with Tukey post-hoc tests, as appropriate. Significance threshold of $\alpha = 0.05$ was set for all presented data, with experimental sample size of tested constructs listed on each figure. IBM SPSS was used for all statistical analysis. All displayed data values written after “±” are Standard Deviation values.

3.3 Results

3.3.1 Elastogenesis is muted in MFS 05-07 SMCs after 30 days of TGF- β 1 stimulation, while collagen deposition is slightly increased.

After stimulation of seeded fibrin gels with 1ng/mL TGF- β 1, elastin deposition is statistically similar for CTRL 01-25 constructs (**Figure 26A**) after both 20 days ($0.155 \pm 0.0949\%$ NT $n=9$ vs $0.137 \pm 0.0769\%$ TGF- β 1 $n=6$) and 30 days ($0.829 \pm 0.188\%$ NT $n=6$ vs $0.137 \pm 0.0769\%$ TGF- β 1 $n=6$) in culture; however, a time-dependent increase in elastin deposition is seen across both treatment groups.

TGF- β 1 stimulation of MFS 05-07 constructs resulted in a statistically similar amount of insoluble elastin deposition after 20 days ($0.137\pm 0.194\%$ NT $n=3$ vs $0.117\pm 0.194\%$ TGF- β 1 $n=3$), but a significant muting effect after 30 days ($0.554\pm 0.280\%$ NT $n=3$ vs $0.0123\pm 0.0171\%$ TGF- β 1 $n=4$) (**Figure 26A**). TGF- β 1 stimulation of MFS 05-04 constructs resulted in a statistically similar amount of insoluble elastin deposition after both 20 days ($0.201\pm 0.0790\%$ NT $n=7$ vs $0.338\pm 0.102\%$ TGF- β 1 $n=3$) and 30 days ($0.541\pm 0.137\%$ NT $n=7$ vs $0.363\pm 0.230\%$ TGF- β 1 $n=3$) (**Figure 27A**, TGF- β 1 in red bars).

Collagen deposition following TGF- β 1 stimulation was statistically similar for CTRL 01-25 constructs (**Figure 26B**) after both 20 days ($0.122\pm 0.0387\%$ NT $n=9$ vs $0.145\pm 0.0266\%$ TGF- β 1 $n=6$) and 30 days ($0.145\pm 0.0385\%$ NT $n=14$ vs $0.165\pm 0.0242\%$ TGF- β 1 $n=6$) in culture. MFS 05-07 constructs collagen deposition statistically increased after 30 days in culture ($0.0971\pm 0.00481\%$ NT $n=3$ vs $0.134\pm 0.0286\%$ TGF- β 1 $n=3$) and saw a time-dependent decrease between 20 days ($0.180\pm 0.0249\%$ NT $n=3$ vs $0.216\pm 0.0620\%$ TGF- β 1 $n=3$) and 30 days of TGF- β 1 stimulation.

The TGF- β 1 induced increase in collagen deposition after 30 days in culture repeated with MFS 05-04 SMC constructs ($0.231\pm 0.0878\%$ NT $n=11$ vs $0.699\pm 0.0878\%$ TGF- β 1 $n=4$) (**Figure 27B**, TGF- β 1 in red bars). MFS 05-04 collagen deposition after 20 days of TGF- β 1 stimulation remained statistically similar ($0.157\pm 0.0707\%$ NT $n=7$ vs $0.206\pm 0.0261\%$ TGF- β 1 $n=3$).

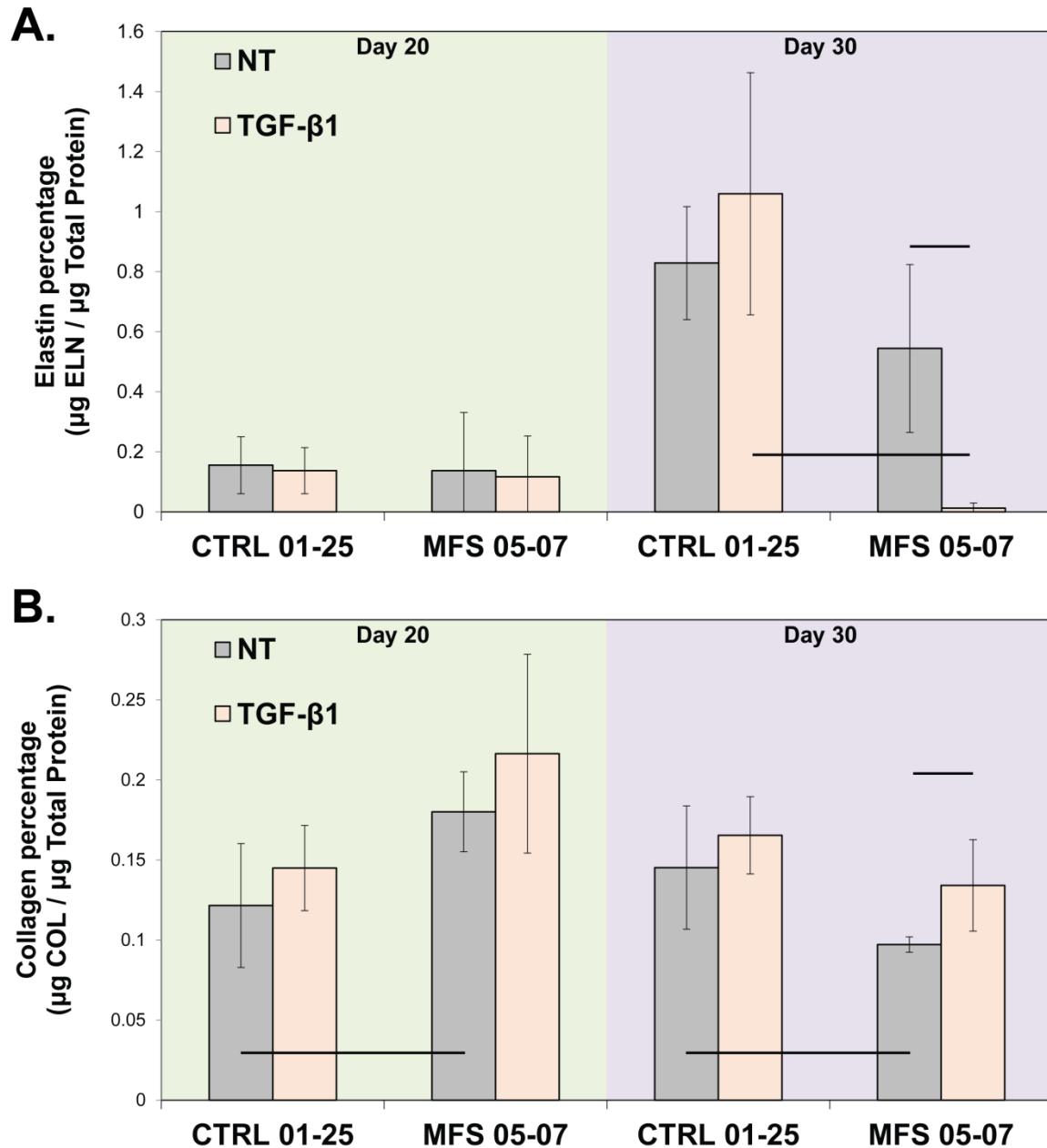


Figure 26: Insoluble elastin and total collagen deposition of TGF-β1 stimulated CTRL 01-25 and MFS 05-07 constructs, after 20 and 30 days.

A) Insoluble elastin fraction of total protein after 20 days (green) and 30 days (purple) of NT control and TGF-β1 stimulation, as determined by ninhydrin assay.

B) Total collagen fraction of total protein after 20 days (green) and 30 days (purple) of NT control and TGF-β1 stimulation, as determined by hydroxyproline assay. $\alpha = 0.05$.

3.3.2 MFS 05-04 SMC elastogenesis is muted after 20 days of ASC-SF stimulation but statistically increased after 30 days of NCM stimulation, while collagen deposition is statistically unchanged with ASC-SF and NCM stimulation.

Insoluble elastin deposition is statistically increased in ASC-SF stimulated CTRL 01-25 constructs (**Figure 27A**, dark grey bars) after 30 days in culture ($0.829 \pm 0.188\%$ NT $n=6$ vs $1.61 \pm 0.112\%$ ASC-SF $n=6$). 20-day CTRL 01-25 ASC-SF stimulated elastin deposition was unchanged ($0.155 \pm 0.0949\%$ NT $n=9$ vs $0.148 \pm 0.0885\%$ ASC-SF $n=4$). NCM stimulation, however, resulted in statistically increased insoluble elastin deposition after 30 days ($1.31 \pm 0.174\%$ NCM $n=4$) (**Figure 27A**, blue bars).

MFS 05-04 SMC insoluble elastin deposition was muted after ASC-SF stimulation for 20 days ($0.201 \pm 0.0790\%$ NT $n=7$ vs $0.0093 \pm 0.0095\%$ ASC-SF $n=4$), and statistically decreased after 30 days ($0.541 \pm 0.137\%$ NT $n=7$ vs $0.317 \pm 0.0436\%$ ASC-SF $n=4$) (**Figure 27A**, dark grey bars). NCM stimulation for 30 days, however, resulted in a statistically increased level of insoluble elastin deposition ($0.958 \pm 0.0255\%$ NCM $n=4$) (**Figure 27A**, blue bars).

Total collagen deposition was statistically increased in CTRL 01-25 constructs stimulated for 30 days in ASC-SF ($0.426 \pm 0.227\%$ $n=8$) (**Figure 27B**, dark grey bars) and NCM ($0.274 \pm 0.0421\%$ NCM $n=8$) (**Figure 27B**, blue bars) when compared to NT control ($0.145 \pm 0.0385\%$ NT $n=14$). Statistically similar collagen was deposited by 20-day ASC-SF stimulation ($0.122 \pm 0.0387\%$ NT $n=9$, vs $0.142 \pm 0.0702\%$ ASC-SF $n=4$).

ASC-SF stimulation left MFS 05-04 collagen deposition unchanged after stimulation for both 20 days ($0.157 \pm 0.0707\%$ NT $n=7$ vs $0.211 \pm 0.137\%$ ASC-SF $n=4$) and 30 days ($0.231 \pm 0.0878\%$ NT $n=11$ vs $0.103 \pm 0.0511\%$ ASC-SF $n=8$). 30 days of NCM stimulation also produced statistically similar collagen levels ($0.199 \pm 0.0176\%$ NCM $n=8$).

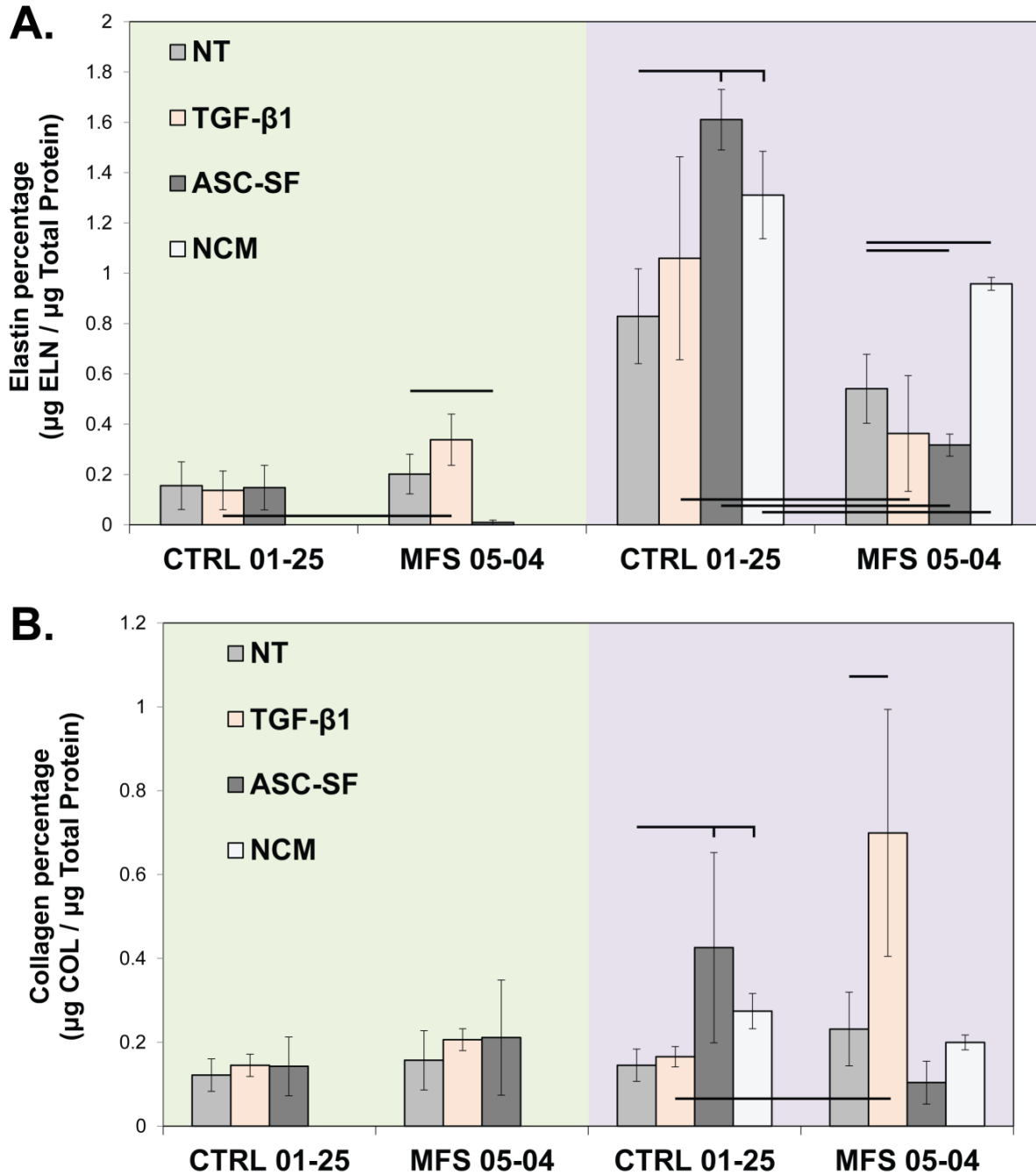


Figure 27: Insoluble elastin and total collagen deposition of CTRL 01-25 and MFS 05-07 constructs, after 20 and 30 days of TGF-β1 or ASC-SF exogenous stimulation.

A) Insoluble elastin fraction of total protein after 20 days (green) and 30 days (purple) of NT control, TGF-β1, ASC-SF, and NCM control stimulation, as determined by ninhydrin assay.

B) Total collagen fraction of total protein after 20 days (green) and 30 days (purple) of NT control, TGF-β1, ASC-SF, and NCM control stimulation, as determined by hydroxyproline assay. NCM was not run for 20 days. $\alpha = 0.05$.

3.3.3 TAV-TAA SMC elastogenesis is increased after TGF- β 1 stimulation, but collagen is reduced.

Insoluble elastin deposition by TAV-NA SMCs is muted after 30 days of TGF- β 1 stimulation ($0.285 \pm 0.275\%$ NT vs TGF- β 1 below detectable threshold for all samples). TAV-TAA SMCs saw a 466% increase in insoluble elastin deposition when stimulated for 30 days with TGF- β 1 ($0.0211 \pm 0.0365\%$ NT, vs $0.119 \pm 0.0389\%$ TGF- β 1) (**Figure 28A**).

Total collagen deposition, however, is reduced by 30 days of TGF- β 1 in both TAV-NA SMC constructs ($0.141 \pm 0.0204\%$ NT, vs $0.0703 \pm 0.0320\%$ TGF- β 1) and TAV-TAA SMC constructs ($0.0597 \pm 0.0264\%$ NT, vs $0.0142 \pm 0.0116\%$ TGF- β 1) (**Figure 28B**). Corresponding TAV-TAA SMCs produce significantly less total collagen than their TAV-NA SMC counterparts. TAV cells were not evaluated with ASC-SF for this study, as TAV-NA was determined to be phenotypically similar to the CTRL line.

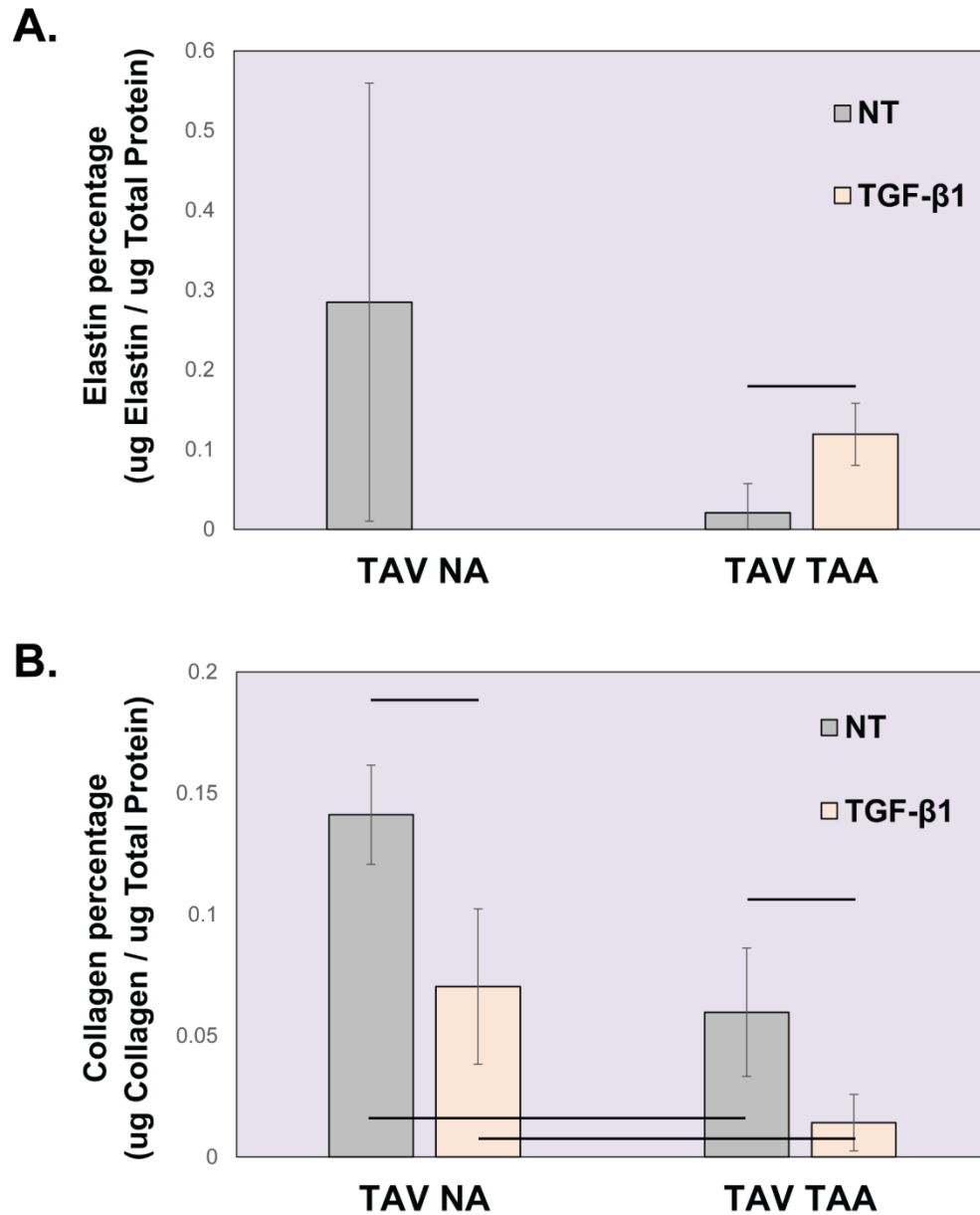


Figure 28: Tricuspid aortic valve (TAV) non-aneurysmal (NA) and ascending thoracic aortic aneurysmal (TAA) SMC insoluble elastin and total collagen deposition after 30 days of TGF- β1 stimulation.

A) Insoluble elastin fraction of total protein after 30 days of NT control and TGF- β1 stimulation (1ng/mL) of TAV-NA and TAV-TAA fibrin gel constructs, as determined by ninhydrin assay. TAV-NA TGF- β1 was below detectable threshold for all samples. $n=3$, $\alpha = 0.05$.

B) Total collagen fraction of total protein after 30 days of NT control or TGF- β1 stimulation (1ng/mL) of TAV-NA and TAV-TAA fibrin gel constructs, as determined by hydroxyproline assay. $n=3$, $\alpha = 0.05$.

3.3.4 BAV-NA fibrillin-1 transcription is significantly increased after 30 days of ASC-SF stimulation, while both LOX and LTBP-4 are muted with ASC-SF.

Initial qPCR analysis on a limited selection of elastin chaperone proteins revealed changes in BAV-NA protein transcription (**Figure 29**). Microfibril fibrillin-1 was significantly increased after 30 days of ASC-SF treatment (4.943 ± 2.157 fold change) when compared to NT control (1 ± 0.0303), while NCM muted fibrillin-1 transcription (0.0020 ± 0.0008).

Tropoelastin was not significantly changed with ASC-SF stimulation (0.5527 ± 0.3225) when compared to NT control (1 ± 0.1732), but is significantly increased with NCM (2.756 ± 0.3276).

Cross-linking LOX is not significantly different with ASC-SF stimulation (0.5166 ± 0.2424) when compared to NT control (1 ± 0.0394), while NCM mutes LOX deposition entirely (three samples all below detection threshold). Deposition protein LTBP-4 is significantly reduced with ASC-SF (0.0989 ± 0.0328) and muted after NCM (three samples all below detection threshold) stimulation, when compared to NT control (1 ± 0.3576).

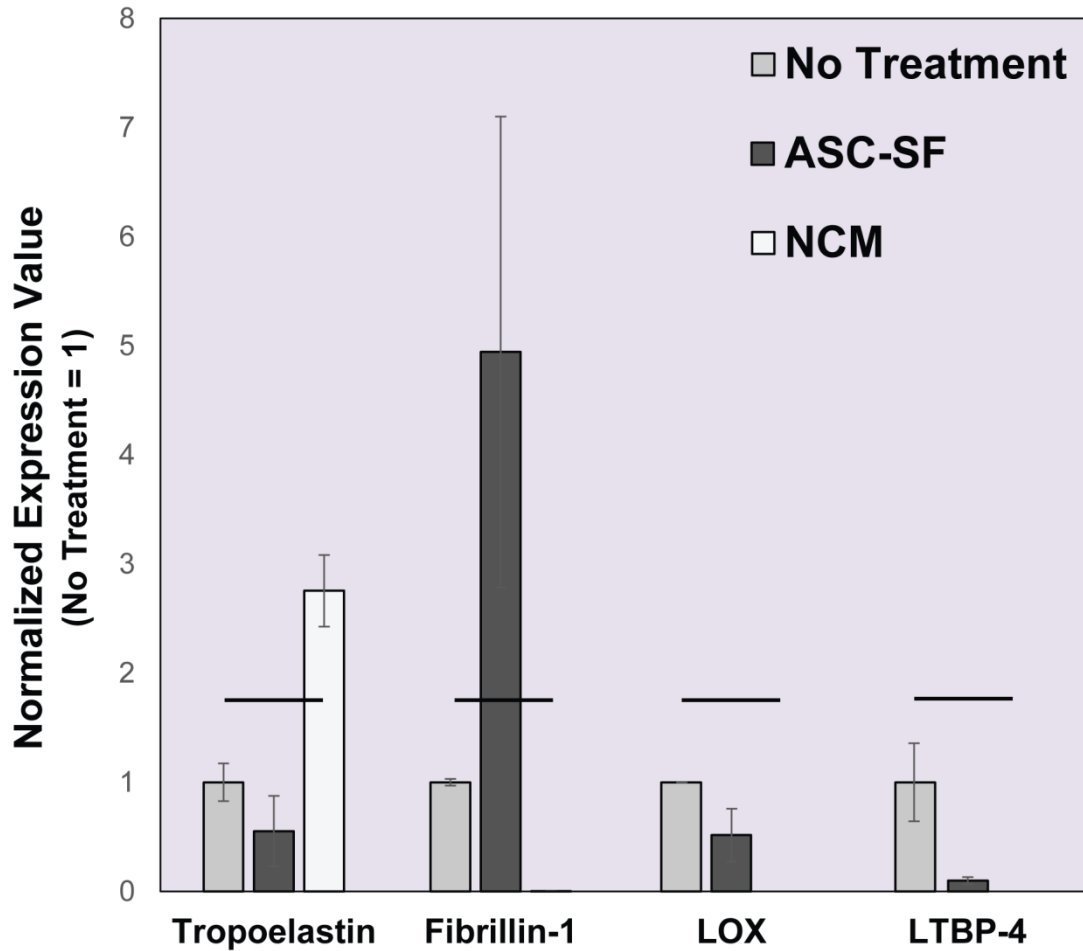


Figure 29: Preliminary data on BAV-NA transcriptional changes in tropoelastin and elastin chaperone matrix proteins after 30 days of ASC-SF stimulation.

RT-qPCR revealed an ASC-SF mediated increase in BAV-NA transcription of microfibril fibrillin-1, with no significant difference seen in tropoelastin or cross-linking protein LOX, while deposition protein LTBP-4 was significantly reduced with ASC-SF. NCM induced a significant increase in tropoelastin deposition, but muted fibrillin-1, LOX, and LTBP-4.

$n = 3, \alpha = 0.5.$

3.3.5 BAV-TAA transcription of fibrillin-1 is increased after 30 days of ASC-SF, while NCM increases LTBP-4 deposition.

Initial qPCR analysis on a limited selection of elastin chaperone proteins revealed changes in BAV-TAA protein transcription (**Figure 30**). ASC-SF stimulation increases deposition of microfibril fibrillin-1 (1.753 ± 0.0367) when compared to NT control (1 ± 0.0031), with no effect seen with NCM (1.152 ± 0.0023).

Tropoelastin deposition is increased after either ASC-SF (1.803 ± 0.4508) or NCM stimulation (7.398 ± 0.9742) when compared to NT control (1 ± 0.1750). A similar dramatic increase is seen in LTBP-4 transcription after NCM stimulation (5.778 ± 2.675) when compared to NT control (1 ± 0.0143), with no effect seen ASC-SF stimulation (1.046 ± 0.2623).

Elastin organizational protein fibulin-5 transcription is decreased after either ASC-SF (0.2408 ± 0.0662) or NCM (0.3405 ± 0.1793) stimulation, when compared to NT control (1 ± 0.0359).

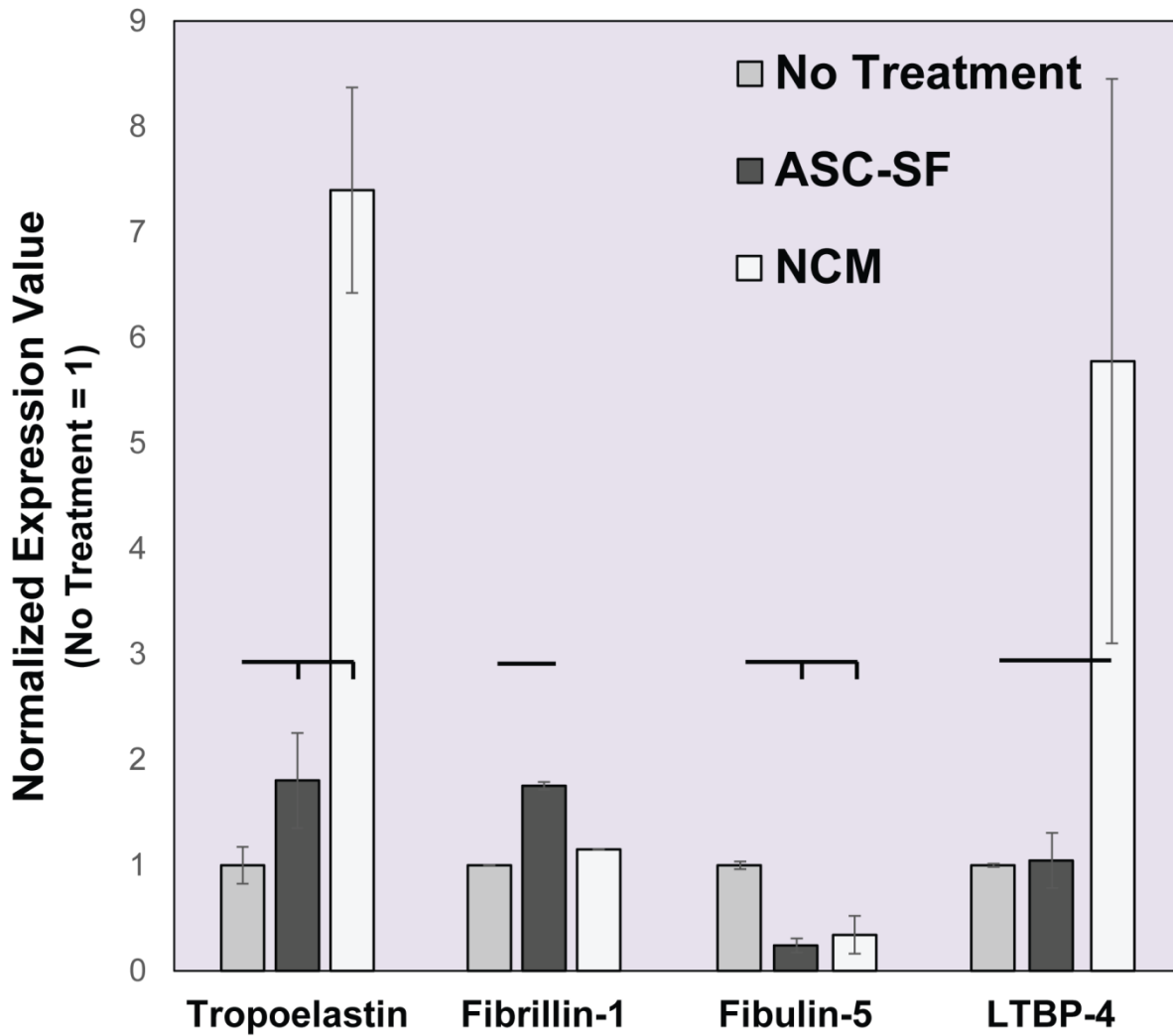


Figure 30: Preliminary data on BAV-TAA transcriptional changes in tropoelastin and elastin chaperone matricellular proteins after 30 days of ASC-SF stimulation.

RT-qPCR revealed tropoelastin deposition increases after either ASC-SF or NCM stimulation, while both ASC-SF and NCM significantly reduced fibulin-5 deposition. ASC-SF significantly increased fibrillin-1 transcription with no NCM effect seen. while NCM significantly increased LTBP-4 transcription with no ASC-SF effect seen.

$n = 3, \alpha = 0.5.$

3.3.6 BAV SMCs from both non-aneurysmal (NA) and aneurysmal (TAA) aortas produce increased insoluble elastin when stimulated with ASC-SF and NCM, but only non-aneurysmal SMC collagen fraction is increased.

After 30 days of stimulation within fibrin gel constructs, BAV-NA insoluble elastin deposition was increased by 102% with ASC-SF stimulation ($0.158 \pm 0.0564\%$ insoluble elastin of total protein) and 175% with NCM stimulation ($0.216 \pm 0.00280\%$) when compared to NT control ($0.0784 \pm 0.0129\%$) (**Figure 31A**). BAV-TAA insoluble elastin is also increased after 30 days of stimulation, 183% increase with ASC-SF ($0.164 \pm 0.0429\%$) and 195% with NCM ($0.171 \pm 0.0685\%$) when compared to NT control ($0.0579 \pm 0.0100\%$) (**Figure 31A**).

Total collagen deposition (**Figure 31B**) in 30-day BAV-NA fibrin gel constructs was increased 154% after ASC-SF stimulation ($0.601 \pm 0.228\%$ total collagen of total protein) and 100% after NCM stimulation ($0.473 \pm 0.0356\%$) when compared to NT control ($0.236 \pm 0.0953\%$). BAV-TAA collagen deposition was unchanged with 30 days of NT ($0.552 \pm 0.0196\%$), ASC-SF ($0.449 \pm 0.0811\%$), or NCM stimulation ($0.576 \pm 0.130\%$).

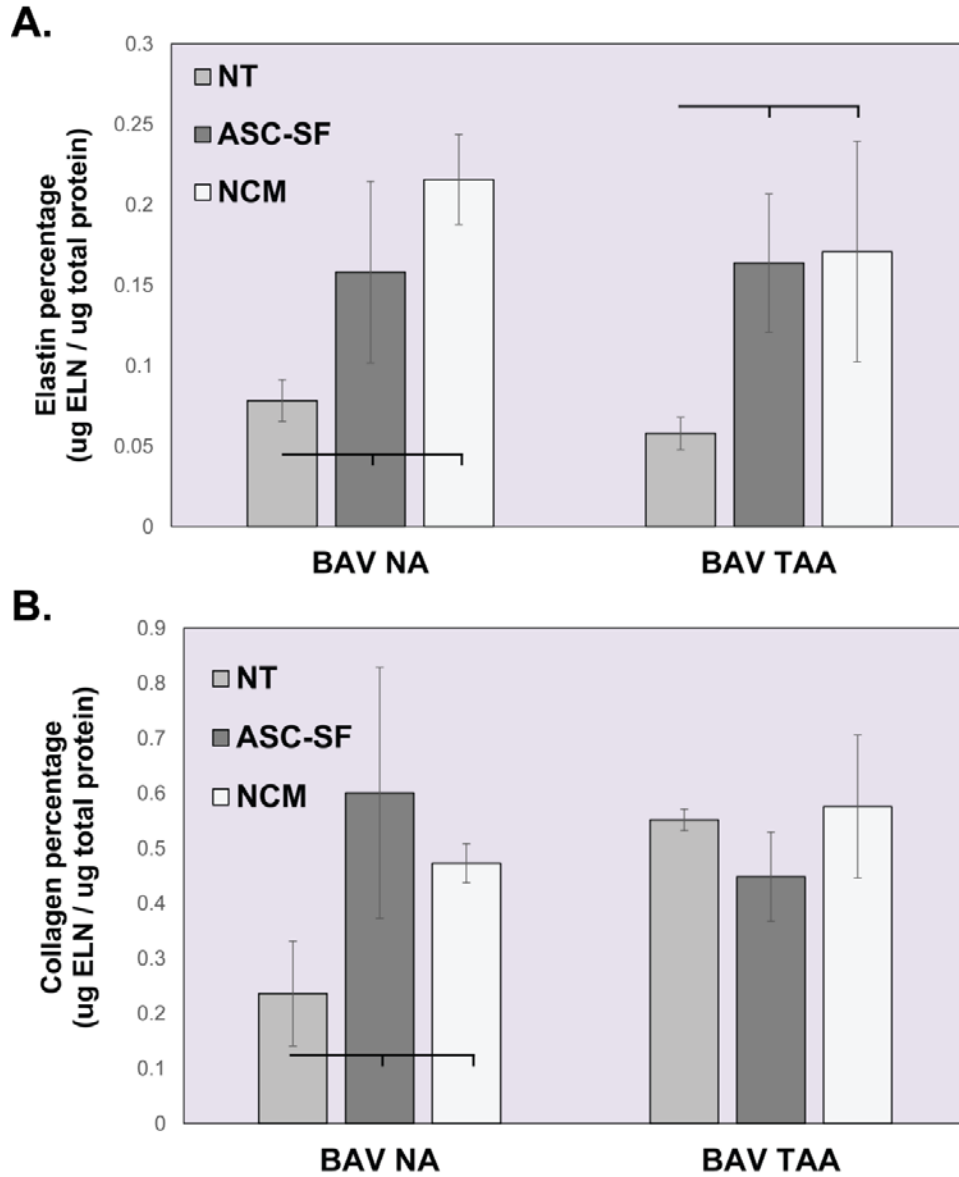


Figure 31: Bicuspid aortic valve (BAV) non-aneurysmal (NA) and ascending thoracic aortic aneurysmal (TAA) SMC insoluble elastin and total collagen deposition after 30 days of ASC-SF and NCM stimulation

- A) Insoluble elastin fraction of total protein after 30 days of NT control, ASC-SF, and NCM stimulation of BAV-NA and BAV-TAA fibrin gel constructs, as determined by ninhydrin assay. $n=4$, $\alpha = 0.05$.
- B) Total collagen fraction of total protein after 30 days of NT control, ASC-SF, and NCM stimulation of BAV-NA and BAV-TAA fibrin gel constructs, as determined by hydroxyproline assay. $n=4$, $\alpha = 0.05$.

3.4 Discussion

ASC-SF is a potent inducer of both insoluble elastin and collagen deposition within the CTRL01-25 line, sourced from the medial layer of a non-aneurysmal adult ascending aorta. This induction of both insoluble elastin and total collagen deposition after 30 days in culture (**Figure 27**) mirrors what was seen using ATCC-purchased adult aortic SMCs stimulated with ASC-SF (**Figure 23**), an indication that ASC-SF ECM effects are similar across multiple “healthy” SMC lines (including both CTRL and TAV-NA cells) and served as a patient-derived repeated study for our ASC-SF studies.

We also observed that TGF- β 1 stimulation had no effect on the CTRL01-25 line (**Figure 27**) which matches the results seen with ATCC-purchased SMCs (**Figure 14**), and saw TGF- β 1 muting of elastogenesis and total collagen deposition in the TAV-NA line (**Figure 28**). TGF- β 1 only induced an increase within late-culture MFS 05-04 total collagen (**Figure 27B**) and 30-day elastogenesis within TAV-TAA constructs (**Figure 28A**). The TAV-TAA results came alongside a muting of total collagen, however, resulting in a less-mature overall ECM profile. Any ECM targeted therapeutic must include multiple factors, or a single factor with a much more targeted signaling pathway effect than the broad Smad-pathway implications of TGF- β 1 stimulation.

In early cultures, the MFS 05-04 line had an elastogenesis muting effect when stimulated with ASC-SF for 20 days (**Figure 27A**), which reverts to baseline control levels after 30 days in culture. NCM, however, shows a more consistent increase in MFS 05-04 insoluble elastin deposition after 30 days. Though NCM-induced elastogenesis effects are not observed within ATCC-purchased “healthy” SMCs, the nutrient-rich culture media might serve as a useful and less resource-intensive alternative for ECM deposition when working with MFS-derived SMCs or working to develop a successful ECM therapeutic for MFS ATAA. NCM also increases both

insoluble elastin and total collagen deposition within CTRL 01-25 SMCs after 30 days in culture (**Figure 27**) and within both BAV-NA and BAV-TAA constructs (**Figure 31**), underscoring the potential of NCM as a media alternative for fibrin-based ECM-targeted bioreactors.

The inability for ASC-SF to induce elastogenesis by MFS 05-04 SMCs requires further study, with TGF- β signaling pathway dysregulation as a key starting point for any subsequent studies [235]. Fibrillin-1 mutations alter ECM signaling, and induce a cellular feedback response that increase the amount of extracellular TGF- β available [236]. LTBP complexes form to regulate the availability of this latent TGF- β (forming “large latent complexes” of stored TGF- β), which is released as ECM remodeling is needed. In MFS, however, the large latent complex is unable to sequester to microfibrils (as a result of fibrillin-1 malformation), resulting in elevated free TGF- β and a significant upregulation in Smad pathway phosphorylation [83]. ECM effects of this upregulation are not limited to the generation of collagen and elastin, however; matrix metalloproteases (MMPs) that degrade collagen, elastin, and chaperone proteins (including LTBPs that sequester TGF- β) are produced and cause malformation in the deposited local ECM complex [237]. LTBP degradation also disrupts the cellular mechanosensory feedback cycle responsible for fine-tuning local matrix stiffness and elasticity, leading to potential downstream muting of ECM matricellular protein production [238]. Thus, ASC-SF activation of downstream TGF- β pathway factors could be implicated within this disrupted feedback cycle, resulting in either increased matrix-degrading MMP deposition or decreased ECM protein deposition. While ASC-SF works as an ECM regenerative treatment for both healthy purchased SMCs and healthy primary isolated SMCs, it might not be an advisable broad-streamed strategy when dealing with disease states that involve abnormal signaling pathways, such as MFS and TGF- β .

A similar muting effect is seen within TGF- β 1 treatment of TAV-NA and TAV-TAA SMCs (**Figure 28**), reducing both elastin and collagen deposition with TAV-NA and muting TAV-TAA collagen after 30 days of stimulation.

While these adult BAV-NA and BAV-TAA produce more insoluble elastin with NCM treatment similarly to adult MFS SMCs, BAV-NA and BAV-TAA elastogenesis is also enhanced with 30-days of ASC-SF stimulation. While total collagen content is upregulated in BAV-NA SMCs with both ASC-SF and NCM, only baseline levels are seen within BAV-TAA constructs (**Figure 31**). The ASC-SF induced upregulation in insoluble elastin mimics the effects seen within both CTRL 01-25 and ATCC-purchased SMCs, but further study is needed to elucidate the reasoning for NCM possessing as similar upregulation effect.

As we are aiming to restore the elastin-to-collagen balance within these tissues, increasing insoluble elastin while maintaining collagen levels in BAV-TAA constructs is our desired result. Neither ASC-SF nor NCM treatment results in the aforementioned collagen muting seen within TGF- β 1 treated constructs, leaving ASC-SF as a viable therapy for aortic dilation within BAV patients.

3.5 Conclusion

This study found that exogenous factors can be used to regulate elastin and collagen deposition by medial aortic cells, but great care must be taken to balance the deposited elastin-to-collagen ratio (to minimize fibrosis) and the downstream signaling effects within each patient's disease condition. Factors contained within both ASC-SF and NCM can independently activate

deposition of one ECM component while silencing another, which means applications for diseased cells needs to be much more regulated than studies with CTRL and healthy lines.

BAV more closely mimics healthy SMC reactions to ASC-SF, when compared to MFS SMCs. This could be due to a more normalized ECM deposition signaling pathway, a further indication that ASC-SF might not be ideal as a readily available therapy for signaling pathway impacting disorders.

Improving BAV elastin-to-collagen ratio could extend to related fibrosis effects, with ASC-SF showing potential with this BAV-TAA cell line as well as “healthy” SMCs from both purchased and explanted non-aneurysmal aortas. NCM also has this potential, leading to its possible application as a culture medium for tissue engineered vascular constructs for BAV and TAV patients with thoracic aneurysm.

3.6 Future Work

As summarized, further studies need to be made to assess protein transcription within stimulated MFS constructs, to see impact of TGF- β /ASC-SF/NCM on elastin chaperone proteins. Disruptions in the TGF- β feedback cycle, and thus the ECM deposition loop to fine-tune local matrix stiffness, could be exacerbated by ASC-SF, with a concentration of factors reduced (or not present) within NCM to induce the muting effect seen here. A comparison could also be made between standard culture media and NCM when culturing MFS cells within a fibrin-based bioreactor to assess ECM deposition, making NCM a viable (and relatively inexpensive) alternative when compared to single-factor stimulation treatments to induce remodeling. Bioreactor studies would have to extend to a similar timeline as these stiff substrate experiments,

with 20-day treatment cycles (and media changes, at minimum, twice a week) to induce proper ECM deposition and accurately model *in vivo* MFS tissue. qPCR and Western Blot analysis could also be conducted on TGF- β , ASC-SF, and NCM MFS SMCs to assess phenotype changes induced by the exogenous treatments, which might play a role in the muting elastogenesis cascade effects induced by the factors within ASC-SF.

This work also points to NCM as a low-cost alternative to induce ECM deposition within BAV cells, particularly within the context of non-surgical therapies and integration within fibrin-based tissue engineered vascular grafts. Future work should examine the effects of NCM on existing cells seeded within bioreactor culturing methods, and compare it to single-factor stimulation. Additional supplements to NCM can be made to enhance SMC phenotype modulation and recruitment, anti-thrombolytic activity, and induction of mature ECM deposition. Examples include factors such as CCL2-supplemented NCM as non-surgical aneurysmal therapeutics, as media used to culture fibrin-based vascular grafts for TAA, and as integrated components within delivered grafts for these patients. Additionally, further analysis on additional elastin chaperone protein transcription by BAV-NA and BAV-TAA cells is needed to get a complete understanding of BAV response to exogenous therapeutic conditions.

4.0 Specific Aim 2, Part 2: Elastogenesis Impact of Adipose-Derived Stromal Cell Secreted Factors on Pediatric Aneurysmal Smooth Muscle Cells

Aortic aneurysms are dilations of the aorta, the large blood vessel responsible for transporting oxygenated blood from the heart to the extremities, usually caused by a disruption in vascular wall protein elastin. Surgical aortic intervention is often determined by aortic diameter (expansion from the healthy 2cm to over 5.5 in adults, and over 4cm for teens) or growth rate (over 0.5cm/year for pediatric patients). Non-surgical options available for pediatric aneurysms below these thresholds are limited to beta-blockers and angiotensin-converting enzyme inhibitors, both of which have unintended systemic effects. There is no standard, targeted intervention for pediatric patients with small, potentially lethal aortic aneurysms.

This chapter aims toward the development of a non-surgical treatment for aortic aneurysm in these young patients, by assessing the viability of adipose stromal cell secreted factors (ASC-SF) to target elastin deposition and the elastogenesis cascade from smooth muscle cells explanted from dilated pediatric aortas following surgery. This chapter also outlines the beginning of a pediatric aortic cell bank, in collaboration with Dr. Victor Morell and the Department of Cardiothoracic Surgery at the UPMC Children's Hospital of Pittsburgh. Smooth muscle cells and fibroblasts were isolated from discarded aortic tissue following graft replacement surgery, and placed in long-term storage available for collaborative projects designed to study these pediatric populations.

4.1 Introduction

Pediatric patients suffering from aortic aneurysms with origins both genetic (Marfan syndrome, **MFS**, and Loeys-Dietz syndrome, **LDS**, combined incidence of ~10 out of every 100,000 individuals) and non-genetic (bicuspid aortic valve, **BAV**, and tetralogy of Fallot, combined incidence of ~1 out of every 100 individuals) require multiple surgical interventions before adulthood. Aortic dilation, bordering on aneurysmal, is present among 80% of children diagnosed with MFS [29], and aneurysms were presented in 40% of Ehlers Danlos syndrome patients (**EDS**, another inherited connective tissue disorder, with patients often presenting multiple aneurysms) [239]. Most critically, the mean age of death for LDS patients is 26.1 years old, with sudden aortic complications as the primary cause of death [26].

Endovascular aneurysm repair is the primary surgical interventional method for both adult and pediatric aortic aneurysm patients at high risk of aneurysm rupture [181], repair consists of catheterization to place an endovascular graft. EDS patients post-endovascular surgery had a mortality rate of 24% [239]. While early aortic aneurysm screening has reduced rupture rates over the last two decades [182], there is no standard intervention for pediatric patients with aortic diameter below the aforementioned dilation threshold. Studies have shown that graft placement performed on sub-5cm dilated aneurysms provide no further benefit to long-term survival, necessitating the need for a non-surgical treatment [174].

This is particularly true for pediatric MFS, EDS, or LDS patients, as most clinicians favor non-surgical aneurysm treatments for patients under 21 years old, delaying the necessity for pediatric aneurysm surgical intervention as long as possible [183]. Recurring aneurysmal complications in LDS patients, in particular, is another major area of need for studies to

maximize time between repeated surgical interventions [26] as 33% of patients require additional surgeries.

Currently, non-surgical therapeutic options for small pediatric aneurysm are limited to beta-blockers and angiotensin converting enzyme inhibitors to slow aortic growth, both of which are non-specific and have unintended systemic effects. There is no standard, targeted intervention for pediatric patients with small, potentially lethal aortic aneurysms, and a combination therapy directed at improved elastin formation has not been explored. Low elastin content in ascending thoracic aortic aneurysms and lowered elastin concentration in infrarenal abdominal aortic aneurysms [80] have pointed to the secretion, coacervation and cross-linking of elastin as a worthwhile aneurysmal therapeutic target. This chapter focuses on the need for an elastin-targeted therapeutic option targeted for pediatric aortic aneurysms.

Previous work by our lab has shown that adipose-derived stromal cell (ASC) delivery to a growing elastase-induced mouse abdominal aortic aneurysm halts aneurysmal growth, prevents further elastin degradation, and possibly stimulates new elastin synthesis, as evidenced by *in vivo* maintenance of elastic lamellae [198]. In other work related to producing a small-diameter tissue engineered vascular graft, our group has also demonstrated that MSCs allow patency and ECM remodeling of an elastomeric tubular scaffold within interpositional abdominal aortic implants [199, 200].

In vitro work summarized in **Chapters 2.0 & 3.0** of this dissertation has shown that ASC secreted factors (ASC-SF) enhance elastic fiber production by smooth muscle cells (SMCs) from healthy, adult aortas. ASC-SF therapy for healthy aortic SMCs is designed to be the foundation of a non-surgical therapy designed to reorganize and fortify elastic fibers within pediatric dilated aortic walls, by packaging and delivering growth factors secreted by ASCs

directly to the aneurysm. However, assembly of elastic fibers involves a cadre of ECM accessory proteins that are needed for proper elastin processing and assembly, and these proteins have not been monitored in the regenerative context.

This work, extending on the tissue transfer infrastructure established with Dr. Victor Morell's Department of Cardiothoracic Surgery and the Division of Pediatric Pathology at the Children's Hospital of Pittsburgh at UPMC, utilized a fibrin-based three-dimensional *in vitro* culture system for explanted diseased pediatric SMCs, and will analyze two steps of the elastogenesis cascade by ASC-SF stimulated pediatric SMCs: (1) transcriptional analysis of elastin core protein tropoelastin, microfibril fibrillin-1, organizational proteins fibulin-4 and fibulin-5, crosslinking proteins LOX and LOXL-1, and elastin coacervate deposition protein LTBP-4; and (2) protein analysis of insoluble elastin and total protein deposition induced by exogenous factors.

The central hypothesis is that packaging growth factors secreted by mesenchymal stem cells and delivering these factors directly to pediatric aortic aneurysms will reorganize and fortify previously damaged elastic fibers within aortic aneurysm walls, establishing a viable non-surgical therapeutic option to delay the need for pediatric aorta surgery.

4.2 Methods

4.2.1 Inclusion criteria for explanted pediatric dilated aortic tissue

The current inclusion criteria were established under the guidance of the Vascular Bioengineering Laboratory, Vascular ECM Dynamics Laboratory, and Dr. Victor Morell and the Department of Cardiothoracic Surgery at the UPMC Children's Hospital of Pittsburgh. Discarded aortic tissue is collected from the Children's Hospital Division of Pediatric Pathology, from pediatric patients (under 21 years old) scheduled for aortic surgery with dilation of the abdominal or thoracic aorta, dilation of the aortic root, aortic insufficiency, or a family history (or verified case) of connective tissue disorders (MFS, Williams syndrome, LDS, cardiac-valvular EDS, Cutis Laxa, bicuspid aortic valve). After deidentification by the Division of Pediatric Pathology, discarded waste aortic tissue is stored in RPMI 1640 medium (ThermoFisher Scientific, # 11875093) and transported on ice to the Vascular Bioengineering Laboratory.

Cells collected and patient information for all collection attempts are listed in **Table 3**. Labeling convention includes prefix MOR (for Morell), followed by a 1 for medial layer or 2 for adventitial layer, followed by the patient number in chronological collection order.

Three cell lines were chosen for *in vitro* fibrin gel construct elastogenesis evaluation, following exogenous ASC-SF and NCM stimulation. **MOR 1-01** were SMCs from the medial layer of a 2-year-old dilated aortic root explanted following a Ross Procedure, with patient co-morbidities including aortic valve stenosis and insufficiency. **MOR 1-04** were SMCs from the aortic medial layer of an 11-year-old patient with ascending thoracic aortic aneurysm (ATAA), with co-morbidities of pulmonary arteriovenous malformation, aortic root dilation, and a

maternal history of ATAA and aortic root dilation. **MOR 1-07** were SMCs from the aortic root medial layer of a 15-year-old patient following a valve-sparing root replacement and root dilation, with co-morbidities autosomal dominant polycystic kidney disease and hypertension.

Table 3: Database of the newly established pediatric aortic cell bank stored at the Vascular Bioengineering Laboratory/Vascular ECM Dynamics Laboratory, sourced from UPMC Children’s Hospital of Pittsburgh

Cell line label	Date collected	Tissue Layer	Patient Information	# of cell aliquots
MOR 00	3/9/2017	Entire sample (very small)	3 years old; Tricuspid atresia, truncus arteriosus, severe aortic insufficiency, DiGeorge Syndrome, no connective tissue disorder	None viable, sample too small
MOR 1-01	4/17/2017	Medial	2 years old; Aortic valve stenosis, aortic valve insufficiency, aortic root dilation, Ross procedure	21x aliquots, 1M cells each
MOR 1-02	4/7/2017	Medial	32 years old; Bicuspid aortic valve, Ross procedure	7x aliquots, 1M cells each
MOR 2-02	4/7/2017	Adventitial		2x aliquots, 1M cells each
MOR 1-03	5/8/2017;	Subaortic membrane	18 years old; trisomy 21, s/p repair of atrioventricular septal defect and previous resection of subaortic membrane	5x aliquots, 1M cells each
MOR 1-04	8/29/2017	Medial	11 years old; Valve-sparing aortic root replacement; aortic root dilation, ascending aorta aneurysm, pulmonary arteriovenous malformation, suspected connective tissue disorder, as many maternal family members with aortic root dilation/aneurysm	6x aliquots, 1.5M cells each
MOR 2-04	8/29/2017	Adventitial		6x aliquots, 1.5M cells each
MOR 1-05	8/31/2017	Entire sample (very small)	7 months old; Aortic valvotomy and resection of supra-avalvular aortic stenosis.	3x aliquots, 1.5M cells each
MOR 1-06	9/1/2017	Medial	15 years old; Valve-sparing aortic root replacement; repaired atrial septal defect, ventricular septal defect, and coarctation of aorta. Now aortic root dilation, <i>misdiagnosed</i> bicuspid aortic valve without stenosis or insufficiency, no known connective tissue disease.	6x aliquots, 1.5M cells each
MOR 2-06	9/1/2017	Adventitial		6x aliquots, 1.5M cells each

Table 3 (continued)

MOR 1-07	1/22/2018	Medial	15 years old; Valve-sparing aortic root replacement; aortic root dilation of unknown etiology, autosomal dominant polycystic kidney disease, hypertension	10x aliquots, 1.5M cells each
MOR 2-07	1/22/2018	Adventitial		9x aliquots, 1.5M cells each
MOR 1-08	4/2/2018	Medial	21 years old; Marfan syndrome diagnosed at age 9, valve sparing aortic root replacement. Completed NIH randomized trial of Losartan and Atenolol.	5x aliquots, 1.5M cells each, <i>cells not viable</i>
MOR 2-08	4/2/2018	Adventitial		5x aliquots, 1.5M cells each
MOR 1-09	9/7/2018	Medial	17 years old; Bicuspid aortic valve, aortic stenosis, ventricular septal defect, coarctation of the aorta, moderate aortic insufficiency. Modified Ross procedure. At 4 months of age had surgical aortic valvuloplasty, closure of ventricular septal defect, subclavian flap repair of coarctation of the aorta	<i>None viable</i>
MOR 2-09	9/7/2018	Adventitial		<i>None viable</i>
MOR 1-10	2/8/2019	Medial	27 years old; Valve-sparing aortic root replacement, after progressive aortic root dilation. History of coarctation of the aorta, repaired at 11 years of age.	7x aliquots, 1M cells each
MOR 2-10	2/8/2019	Adventitial		5x aliquots, 1M cells each

4.2.2 Isolation, culture, and storage of medial SMCs and adventitial fibroblasts from explanted pediatric aortic tissue

The intimal layer of tissue is scraped (to avoid endothelial cell contamination), with medial and adventitial layers peeled apart (**Figure 32**). Each tissue section is dissected into 1mm² sections and digested using 0.1% (w/v%) collagenase type IV and 0.05% (w/v%) elastase (Worthington Biochemical Corp, # LS004189 & # LS002294) in Dulbecco's Modified Eagle's Medium (DMEM, ThermoFisher Scientific, #11965). Medial layer cells were cultured using Smooth Muscle Growth Supplement (Cell Applications, # 311K-500), and adventitial cells were cultured using DMEM. All cultures are performed at 37°C and 5% CO₂. Cells are frozen using 90% fetal bovine serum and 10% dimethyl sulfoxide (Sigma Aldrich, # D2650).

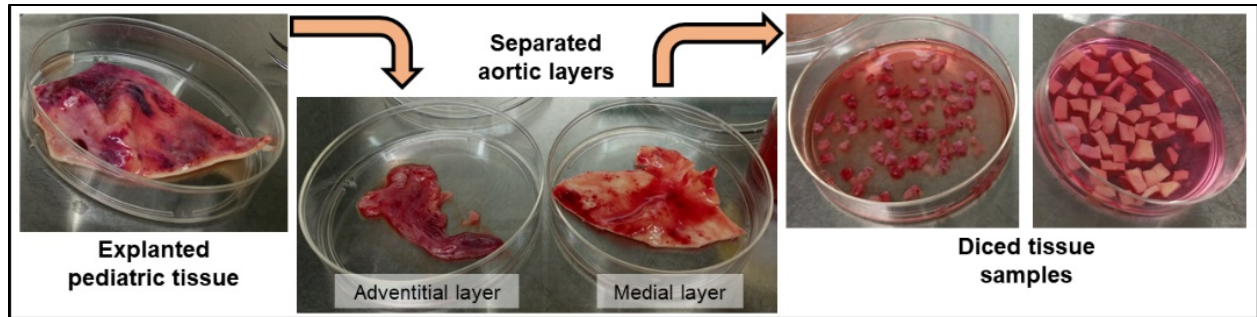


Figure 32: Cellular isolation technique from medial and adventitial layers of explanted pediatric aneurysmal tissue.

Explanted pediatric aortic sections as provided by Dr. Victor Morell's Cardiothoracic Surgery group and the Division of Pediatric Pathology at the UPMC Children's Hospital of Pittsburgh. Intimal layer is scraped off, and the remaining layers are peeled apart, with adventitial layer and medial layer placed into separate dishes. Each layer is diced into $\sim 1\text{cm}^2$ sections and digested in 0.1% collagenase type IV and 0.05% elastase, with cellular outgrowth cultured in standard conditions following tissue digestion.

4.2.3 Fibrin gel construct formation and exogenous stimulation conditions

Pediatric SMCs were seeded within fibrin gels (3.7mg/mL fibrinogen, 0.21U/mL thrombin, and 5×10^5 cells/mL), with fibrin gels formed within 8mm diameter circular templates on 24-well tissue culture plastic plates, as previously summarized in **Sections 2.2.3 & 3.2.2** . Each treatment will continue for 30 days of culture. Culture media was changed every 48-72 hours, with the following exogenous treatment conditions: No Treatment (**NT**) consisting of standard SMC culture media with 10mM fibrinolysis-inhibiting aminocaproic acid (**ACA**); ASC-SF, containing a 1:1 ratio of ASC conditioned media (as summarized in **Section 2.2.4**) and standard SMC culture media with 10mM ACA; and Non-Conditioned Media (**NCM**), consisting of a 1:1 ratio of fresh ASC culture media and standard SMC culture media with 10mM ACA.

4.2.4 qPCR analysis of elastin chaperone protein transcription

Following sonication of frozen fibrin gel constructs, RNA collection (illustra RNAspin Mini Kit, GE Healthcare Life Sciences #25050070) and RNA concentration quantification (BioTek Take3) was performed. After pre-heating template (65°C, 5 minutes), synthesis of first-strand cDNA used SuperScript IV First-Strand Synthesis System (Invitrogen #18091050) (23°C/10 minutes, 55°C/10 minutes, 80°C/10 minutes). RT-qPCR was performed using KiCqStart SYBR Green ReadyMix with ROX (Sigma-Aldrich # KCQS02), and forward/reverse primers listed in **Table 2**. Post-amplification melt curves validated proper amplification.

4.2.5 Ninhydrin and hydroxyproline protein analysis of insoluble protein and total collagen

Fibrin gel constructs, frozen at -80°C following culture without fixation, were thawed immediately before base hydrolysis (0.1M NaOH, 1 hour, 98°C) for fibrin gel digestion and solubilization of non-elastin protein, which was separated using subsequent centrifugation to separate insoluble elastin protein from soluble non-elastin protein [216]. Acid hydrolysis (6N HCl, 24 hours, 110°C) solubilized all proteins, and assay quantification on both soluble and insoluble fractions (ninhydrin-based for elastin, hydroxyproline-based for collagen) allow for protein deposition quantification within each 3D construct. Ninhydrin content was detectable using an absorbance reading (at 570nm) after 1-hour incubation with a stannous chloride-based solution within a 56°C water bath.

4.2.6 Statistical Analysis

Means comparisons were conducted using individual t-tests or one-way ANOVA with Tukey post-hoc tests, as appropriate. Significance threshold of $\alpha = 0.05$ was set for all presented data, with experimental sample size of tested constructs listed on each figure. IBM SPSS was used for all statistical analysis. All displayed data values written after “ \pm ” are Standard Deviation values.

4.3 Results

4.3.1 MOR 1-01 SMCs treated with ASC-SF increased transcription of tropoelastin, fibrillin-1, and LOX, and decreased transcription of fibulin-5, LOXL-1, and LTBP-4.

qPCR analysis of ASC-SF and NCM stimulated fibrin gel constructs seeded with MOR1-01 SMCs, from the medial layer of a 2-year-old dilated aortic root explanted following a Ross Procedure, revealed a transcriptional change in elastin chaperone protein patterns (**Figure 33**).

Constructs simulated for 30 days with ASC-SF saw significant increases in core elastin protein tropoelastin (4.485 ± 1.159 ASC-SF fold increase, vs 1 ± 0.1368 NT and 0.5500 ± 0.2031 NCM) and microfibril protein fibrillin-1 (20.46 ± 2.785 ASC-SF fold increase, vs 1 ± 0.0515 NT and 0.5461 ± 0.0558 NCM). Both ASC-SF and NCM increased crosslinking protein LOX transcription (2.018 ± 0.4014 ASC-SF and 1.936 ± 0.3678 NCM fold increase, vs 1 ± 0.1281 NT).

ASC-SF had a muting effect on elastin organizational protein fibulin-5 (0.0821 ± 0.1042 ASC-SF fold decrease, vs 1 ± 0.7069 NT and 0.9019 ± 0.5121 NCM), and LTBP-4 (ASC-SF relative expression was below detectable threshold on all samples, vs 1 ± 0.3122 NT and 0.4445 ± 0.8397 NCM). Both ASC-SF and NCM stimulation muted crosslinking protein LOXL-1 (0.1953 ± 0.0645 ASC-SF and 0.2864 ± 0.0645 NCM fold decrease, vs 1 ± 0.2176 NT). There was no significant change in elastin organizational protein fibulin-4 transcription with either ASC-SF or NCM (0.8122 ± 0.0317 ASC-SF and 0.8586 ± 0.3300 NCM relative expression, vs 1 ± 0.0933 NT).

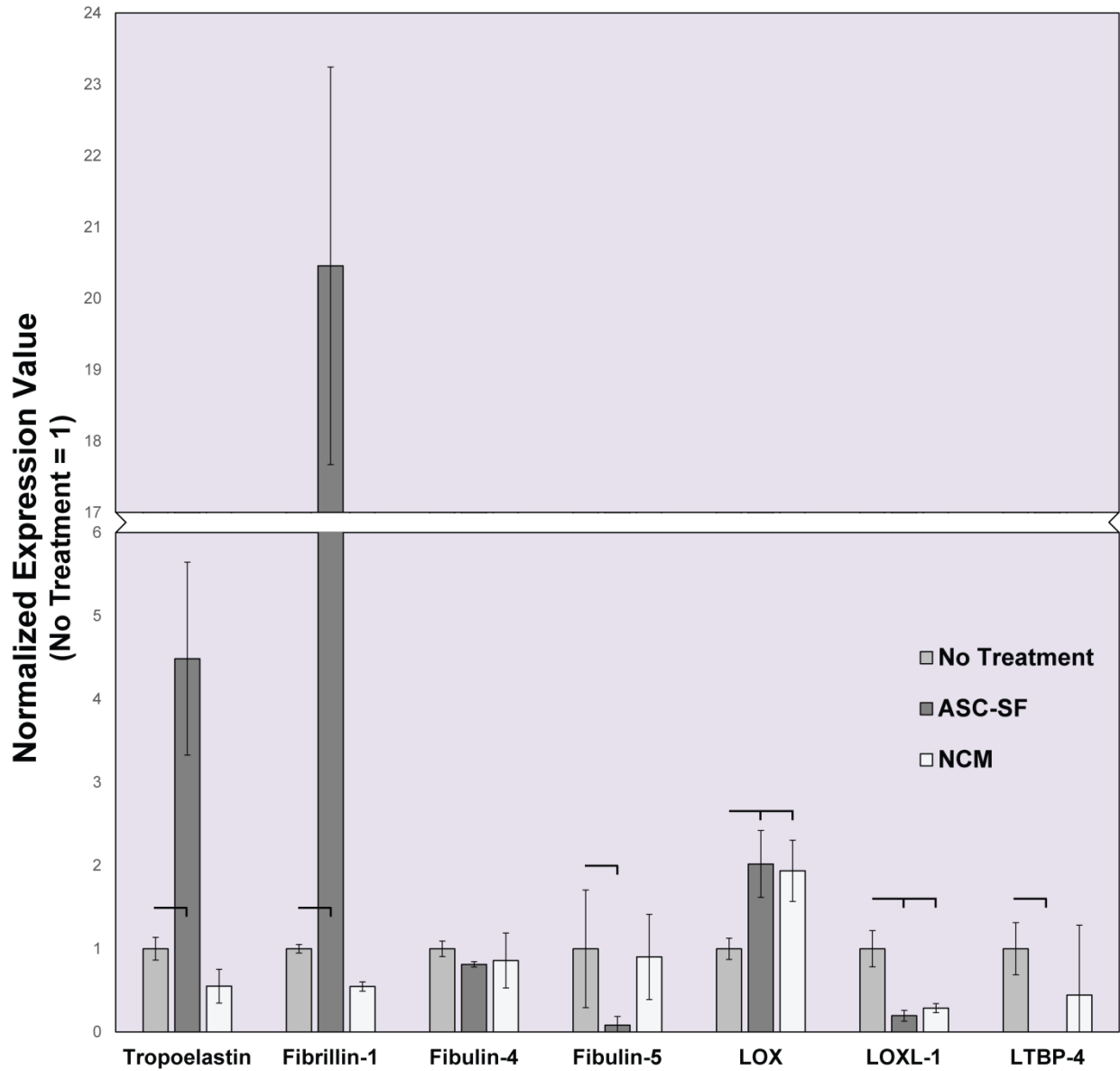


Figure 33: MOR1-01 SMC transcriptional analysis reveals an ASC-SF induced increase in tropoelastin, microfibril protein fibrillin-1, and crosslinking protein LOX, with a decrease in fibulin-5, LOXL-1, and LTBP-4.

n=4, α =0.05 for all.

4.3.2 MOR 1-01 SMCs saw increased insoluble elastin and muted collagen deposition after ASC-SF stimulation.

MOR 1-01, pediatric aortic root SMCs from a 2-year-old patient following dilation and a Ross Procedure, saw a significant 226% increase in insoluble elastin deposition after 30 days of ASC-SF stimulation ($0.190\pm 0.0718\%$ elastin of total protein), but no statistically significant difference after NCM stimulation due to high deviation ($0.132\pm 0.101\%$) when compared to NT control ($0.0584\pm 0.0516\%$) (**Figure 34A**).

MOR 1-01 total collagen deposition, however, was muted after 30 days of ASC-SF stimulation ($0.0205\pm 0.0101\%$ total collagen of total protein) and statistically similar after NCM stimulation ($0.206\pm 0.0587\%$) when compared to NT control ($0.317\pm 0.0985\%$) (**Figure 34B**).

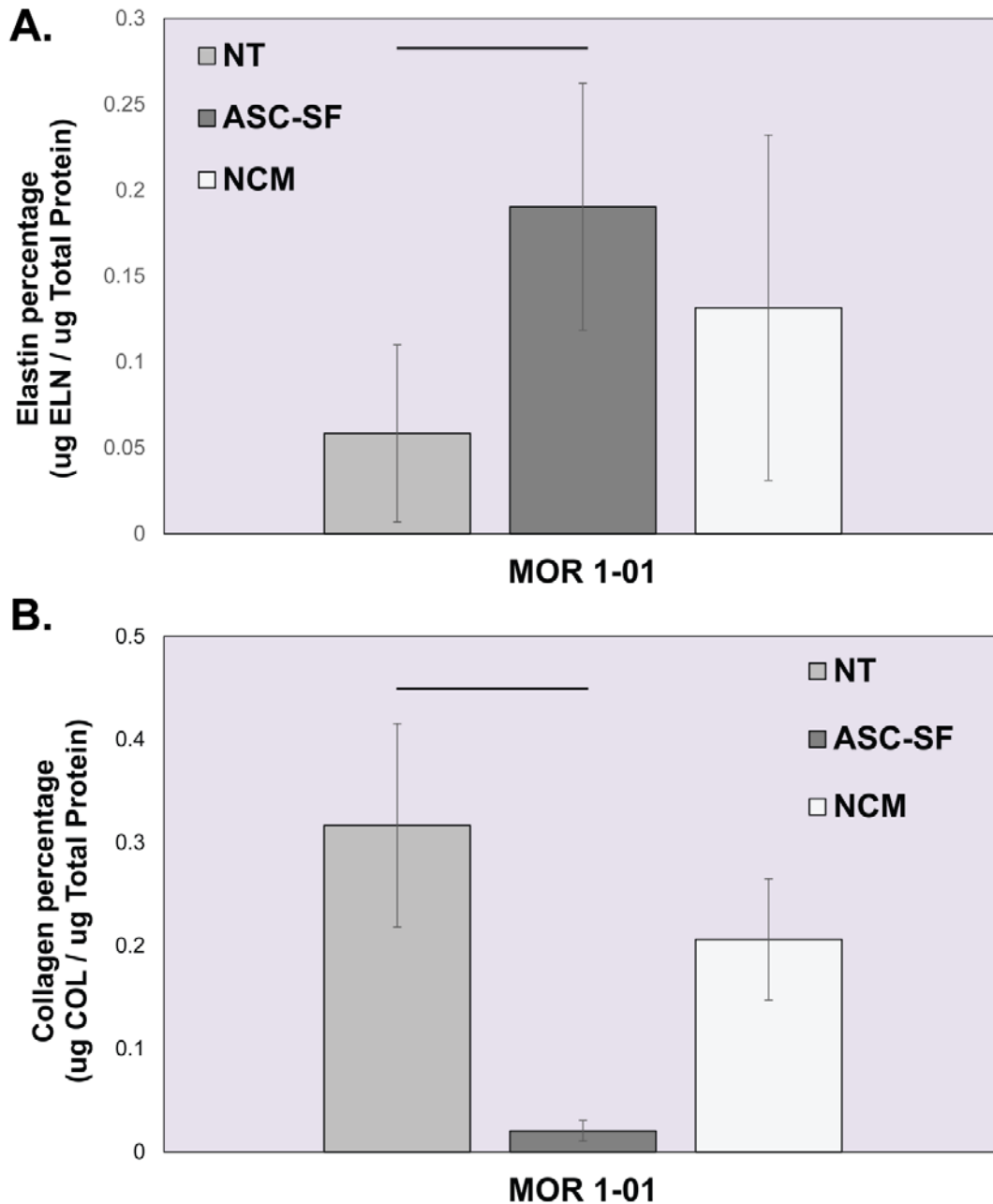


Figure 34: MOR 1-01 SMCs, from the medial layer of a 2-year-old dilated aortic root explanted following a Ross Procedure, deposit significantly increased insoluble elastin and decreased total collagen after 30 days of ASC-SF stimulation.

A) Insoluble elastin deposition by fibrin construct-embedded MOR 1-01 cells after 30 days of stimulation with NT control, ASC-SF, or NCM. $n=4$, $\alpha = 0.05$.

B) Total collagen deposition by fibrin construct-embedded MOR 1-01 cells after 30 days of stimulation with NT control, ASC-SF, or NCM. $n=4$, $\alpha = 0.05$.

4.3.3 MOR 1-04 qPCR

qPCR analysis of MOR1-04 SMCs, pediatric aortic medial layer SMCs from an 11-year-old patient with ascending TAA within fibrin gel constructs, stimulated with ASC-SF and NCM also revealed a transcriptional alteration in elastin chaperone protein patterns (**Figure 35**).

Both ASC-SF and NCM 30-day stimulation induced significant increases in elastin organizational protein fibulin-5 (3.428 ± 0.8009 ASC-SF and 5.046 ± 0.5803 NCM fold increase, vs 1 ± 0.1648 NT) and crosslinking protein LOX (2.003 ± 0.2007 ASC-SF and 2.045 ± 0.1241 NCM fold increase, vs 1 ± 0.0534 NT).

Core elastin protein tropoelastin transcription was not significantly changed with ASC-SF stimulation, but was significantly increased with NCM (1.344 ± 0.2553 ASC-SF and 1.584 ± 0.2054 NCM fold change, vs 1 ± 0.0615 NT). NCM also induced a significant transcriptional increase in microfibril fibrillin-1 (1.912 ± 0.6308 NCM fold increase, vs 1 ± 0.0532 NT and 1.236 ± 0.2310 ASC-SF).

LTBP-4, an elastin cocervate deposition protein, was significantly downregulated by both ASC-SF and NCM (0.1657 ± 0.0686 ASC-SF and 0.3733 ± 0.0504 NCM fold decrease, vs 1 ± 0.0113 NT).

No significant difference was seen with either ASC-SF o/r NCM in transcription of organizational protein fibulin-4 (0.8671 ± 0.2799 ASC-SF and 1.170 ± 0.1227 NCM fold change, vs 1 ± 0.1827 NT) or crosslinking protein LOXL-1 (1.000 ± 0.4439 ASC-SF and 1.120 ± 0.1005 NCM fold change, vs 1 ± 0.2527 NT).

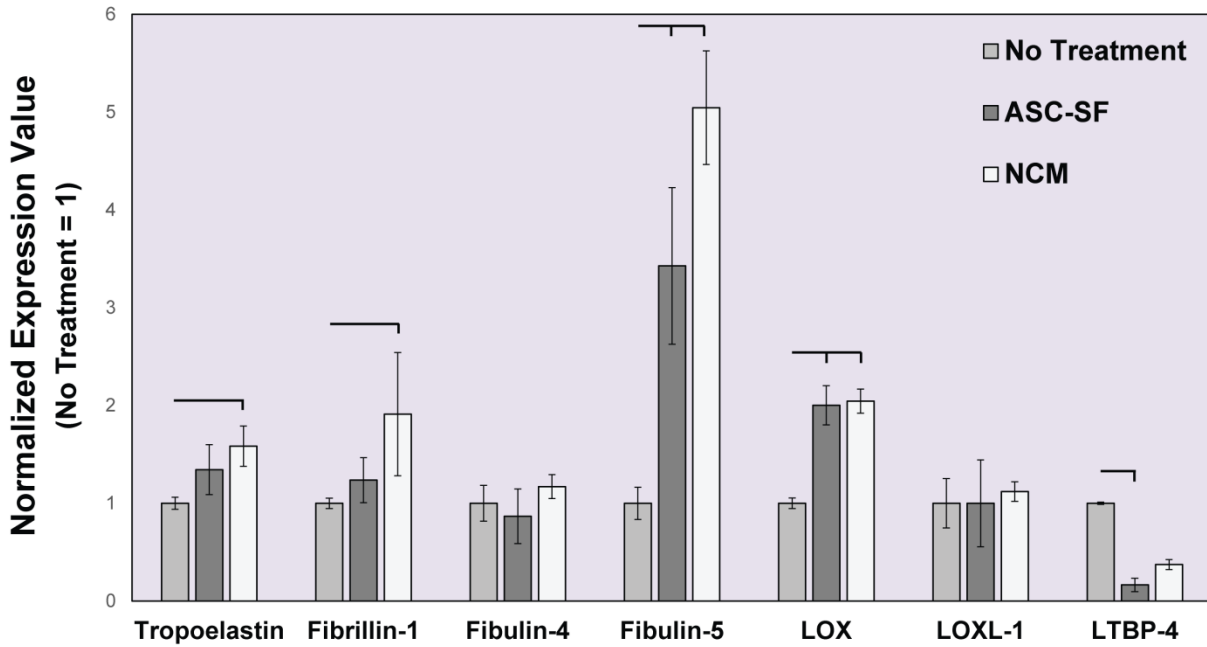


Figure 35: MOR1-04 SMC transcriptional analysis reveals ASC-SF and NCM induced increases in tropoelastin, elastin organizational protein fibulin-5, and crosslinking protein LOX, with a decrease in LTBP-4 and an NCM-only increase in microfibril protein fibrillin-1.

$n=4$, $\alpha=0.05$ for all.

4.3.4 MOR 1-04 SMCs produce increased insoluble elastin and total collagen percentage after 30 days of ASC-SF stimulation, and increased total collagen percentage after 30 days of NCM stimulation.

MOR 1-04, pediatric aortic medial layer SMCs from an 11-year-old patient with ascending TAA, saw a 156% significant increase in insoluble elastin deposition after 30 days of ASC-SF stimulation ($0.661 \pm 0.223\%$ elastin of total protein), but no significant difference after NCM stimulation for 30 days ($0.173 \pm 0.0651\%$) when compared to NT control ($0.158 \pm 0.147\%$) (**Figure 36A**).

MOR 1-04 total collagen deposition was also significantly increased, over six-fold, after 30 days of ASC-SF stimulation ($0.365 \pm 0.0349\%$ total collagen of total protein) and over twelve-fold after 30 days of NCM stimulation ($0.625 \pm 0.220\%$) when compared to NT control ($0.0474 \pm 0.0203\%$) (**Figure 36B**).

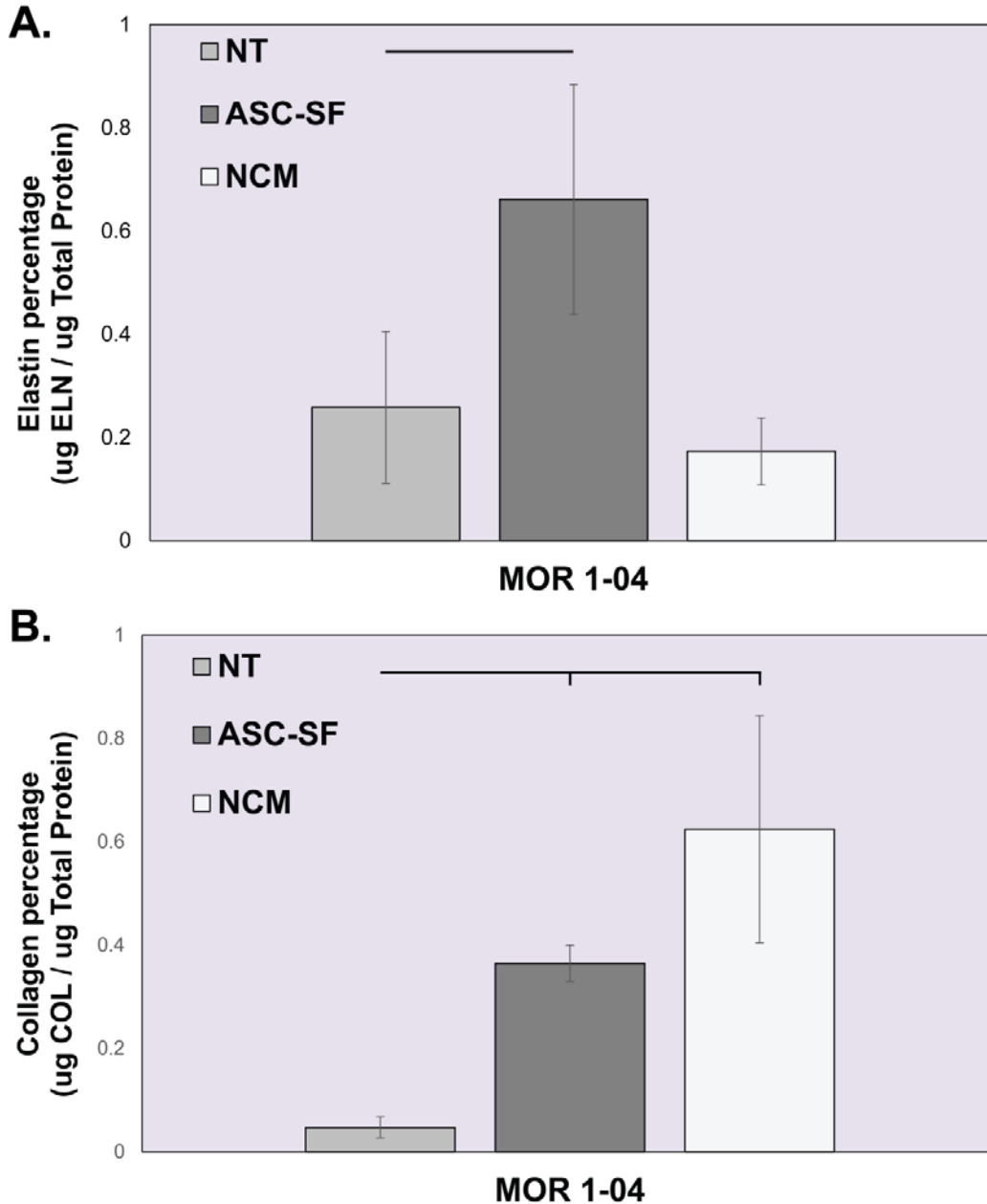


Figure 36: MOR 1-04 SMCs, from the aortic medial layer SMCs from an 11-year-old patient with ascending TAA, deposit significantly increased insoluble elastin after 30 days of ASC-SF stimulation, and significantly increased total collagen after 30 days of both ASC-SF and NCM stimulation.

A) Insoluble elastin deposition by fibrin construct-embedded MOR 1-04 cells after 30 days of stimulation with NT control, ASC-SF, or NCM. $n=4$, $\alpha = 0.05$.

B) Total collagen deposition by fibrin construct-embedded MOR 1-04 cells after 30 days of stimulation with NT control, ASC-SF, or NCM. $n=4$, $\alpha = 0.05$.

4.3.5 MOR 1-07 deposition of fibulin-5, LOX, and LOXL-1 was significantly increased with either ASC-SF or NCM stimulation, with no changes to tropoelastin deposition observed.

qPCR analysis (**Figure 37**) revealed MOR 1-07 SMC deposition of tropoelastin was unchanged after 30 days of ASC-SF (1.178 ± 0.5899 fold change) or NCM stimulation (1.221 ± 0.2513) when compared to NT control (1 ± 0.07135).

ASC-SF and NCM likewise induced no significant change in MOR 1-07 deposition of microfibril protein fibrillin-1 (0.5114 ± 0.1507 ASC-SF and 0.6663 ± 0.08434 NCM, vs 1 ± 0.05143 NT) or elastin organizational protein fibulin-4 (0.8350 ± 0.1107 ASC-SF and 0.9494 ± 0.1017 NCM, vs 1 ± 0.01663 NT).

Elastin organizational protein fibulin-5, however, was significantly increased with either ASC-SF or NCM stimulation (7.469 ± 1.264 ASC-SF and 12.21 ± 1.663 NCM, vs 1 ± 0.01172 NT).

Similarly, deposition of both elastin crosslinking proteins LOX (2.637 ± 0.3001 ASC-SF and 2.065 ± 0.2316 NCM, vs 1 ± 0.05739 NT) and LOXL-1 (2.790 ± 0.4885 ASC-SF and 2.348 ± 1.009 NCM, vs 1 ± 0.07885 NT) were significantly increased with either ASC-SF or NCM stimulation.

Elastin coacervate deposition protein LTBP-4 was statistically similar after ASC-SF stimulation (0.5895 ± 1.007) but was muted after NCM (0.2231 ± 0.1035) when compared to NT control (1 ± 0.09876).

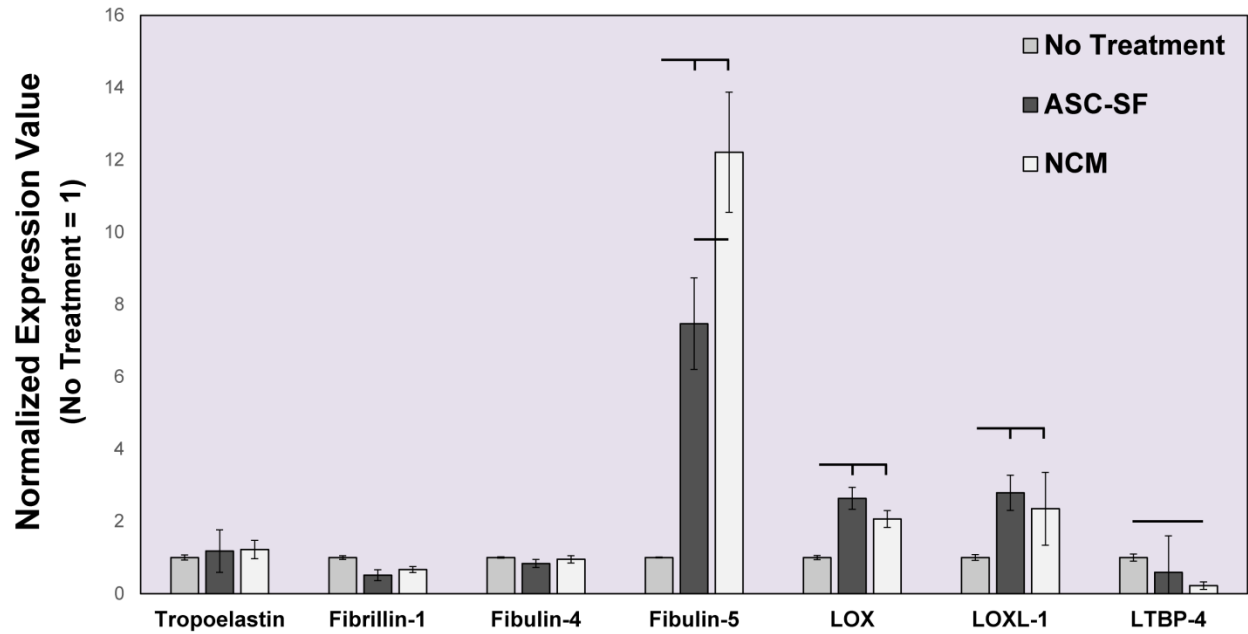


Figure 37: MOR1-07 SMC transcriptional analysis reveals 30 days of ASC-SF and NCM stimulation induced increased in fibulin-5, LOX, and LOXL-1, with NCM inducing a decrease in LTBP-4.

n=4, α =0.05 for all.

4.3.6 MOR 1-07 insoluble elastin deposition is induced after ASC-SF or NCM stimulation for 30 days, but total collagen is unchanged.

MOR 1-07, SMCs from the aortic root medial layer of a 15-year-old patient following a valve-sparing root replacement and root dilation, saw a 45.7% significant increase in insoluble elastin deposition after 30 days of ASC-SF stimulation ($0.372\pm 0.0129\%$ elastin of total protein) and a 38.1% increase after NCM stimulation ($0.353\pm 0.0675\%$) when compared to NT control ($0.255\pm 0.0083\%$) (**Figure 38A**).

MOR 1-04 total collagen deposition remained statistically unchanged after 30 days of either ASC-SF stimulation ($0.0972\pm 0.0148\%$ total collagen of total protein) or NCM stimulation ($0.101\pm 0.0158\%$) when compared to NT control ($0.108\pm 0.0241\%$) (**Figure 38B**).

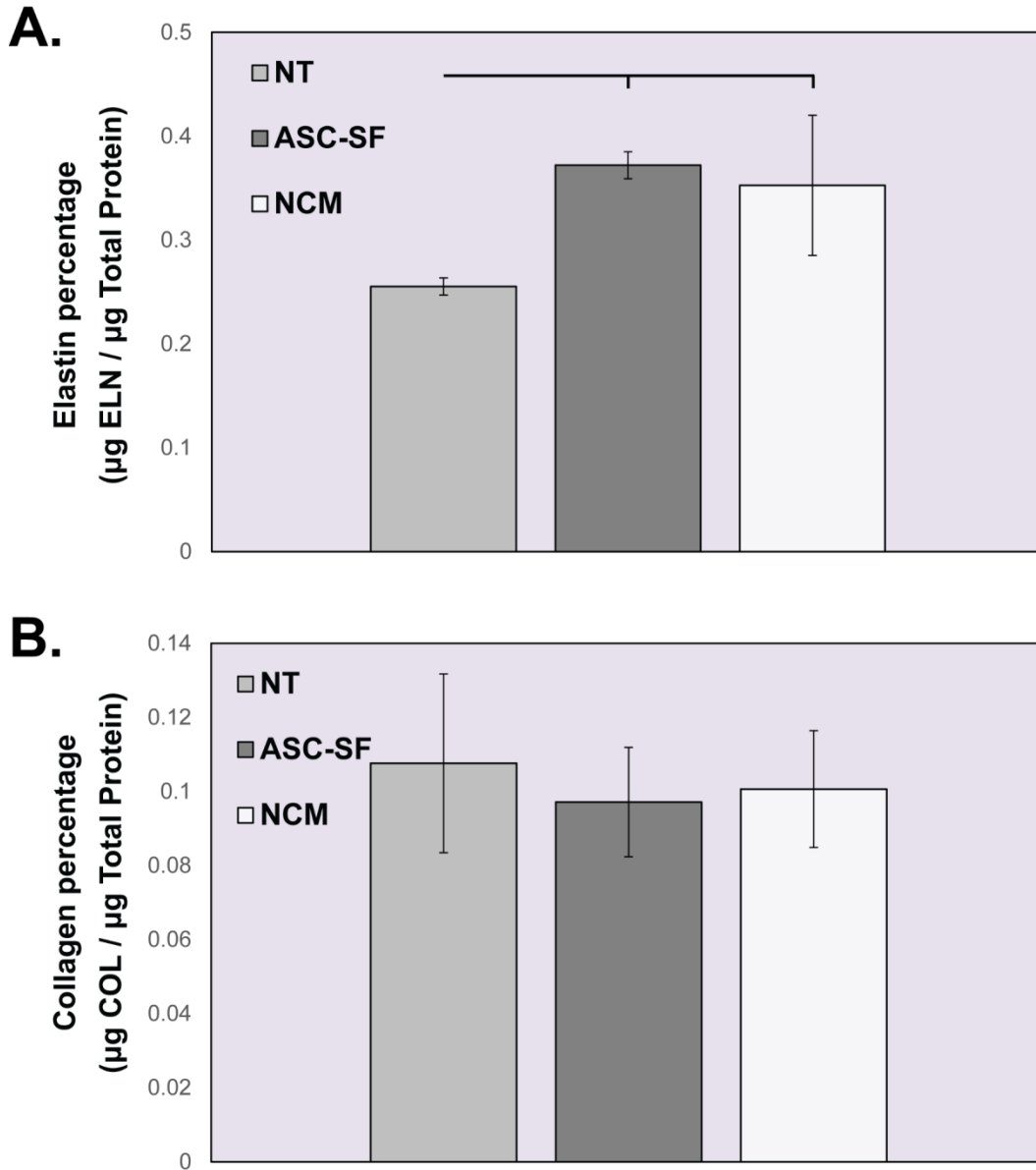


Figure 38: MOR 1-07 SMCs, from the aortic root medial layer of a 15-year-old patient following a valve-sparing root replacement and root dilation, deposit significantly increased insoluble elastin after 30 days of ASC-SF and NCM stimulation, but no change in total collagen.

A) Insoluble elastin deposition by fibrin construct-embedded MOR 1-07 cells after 30 days of stimulation with NT control, ASC-SF, or NCM. $n=4$, $\alpha = 0.05$.

B) Total collagen deposition by fibrin construct-embedded MOR 1-07 cells after 30 days of stimulation with NT control, ASC-SF, or NCM. $n=4$, $\alpha = 0.05$.

4.4 Discussion

Cellular cross-contamination while culturing different layers of tissue is common (medial layers typically contain SMCs, adventitial layers contain fibroblasts). Confirmation of each cell phenotype, using common SMC surface markers and immunocytochemistry techniques, is a clear way to verify cell populations.

ASC-SF stimulation of MOR1-01 SMCs, from medial layer of 2-year-old dilated aortic root tissue, has distinct effects when comparing the two “units” of tropoelastin coacervation (**Figure 1**): (1) tropoelastin, fibulin-4, and LOX; and (2) tropoelastin, fibulin-5, and LOXL-1. ASC-SF significantly increased core elastin protein tropoelastin, microfibril protein fibrillin-1, and crosslinking protein LOX (**Figure 33**). Fibulin-4, a LOX-linked elastin organizational protein, is not changed with ASC-SF or NCM. Meanwhile, components of the complementary elastin coacervate complex, fibulin-5 and LOXL-1, are significantly muted with ASC-SF stimulation. A downregulation of both fibulin-5 and LOXL-1 potentially limits ASC-SF mediated mature insoluble elastin deposition, distinctly impacting one of the two major elastin coacervation mechanisms.

NCM increased MOR1-01 SMC LOX deposition with no effect on tropoelastin, fibulin-4, or fibrillin-1, showing that a selection of components within ASC culture media has a stimulating effect for this single elastin chaperone protein. NCM also mutes LOXL-1 but has no significant effect on fibulin-5 deposition, underscoring that the mechanism for ECM pathway activation by these exogenous factors can individually act on each component of elastin coacervation complexes outlined above.

MOR1-01 insoluble elastin is significantly increased with 30 days of ASC-SF therapy (**Figure 34A**), potentially as a result of a combination of increased tropoelastin, fibrillin-1, and

LOX. Total collagen, however, is muted with ASC-SF stimulation (**Figure 34B**), showing that ASC-SF individually stimulates ECM pathways in this young pediatric SMC line.

MOR1-04, medial layer ascending thoracic aortic SMCs from a 11-year-old patient with severe ATAA, deposited significantly more tropoelastin, fibulin-5, and LOX when stimulated with either ASC-SF or NCM for 30 days. Only NCM increased fibrillin-1 deposition (**Figure 35**). With this similar pattern of elastin chaperone protein transcription, one would expect similar levels of mature elastin deposition between ASC-SF and NCM. However, only ASC-SF induced increased insoluble elastin deposition, with NCM producing a statistically similar level with the NT controls (**Figure 36A**). This disparity could be due to additional elastin chaperone protein activity outside our analysis (EMILIN-1, LTBP family members), or a level of activity and exposed binding sites of these deposited factors outside of our analysis. Substrate stiffness could also play a role in enhancing pro-elastogenesis effects of ASC-SF, with an additional factor present (or a degradation factor missing) when compared to the composition of factors within NCM.

Meanwhile, MOR1-04 total collagen production was increased in both ASC-SF and NCM stimulated constructs (**Figure 36B**). LOX works to crosslink and stabilize both collagen and elastin, and has shown effects in tendon collagen fibrillogenesis [240] and healing within atherosclerotic lesions [241] in addition to its dysfunction being linked within aortic aneurysm development [242]. While this is essential for proper collagen function, only ASC-SF combines increased organizational protein transcription, insoluble elastin deposition, and total collagen deposition, leading it to be the favorable treatment group to pursue for MOR04 and similar phenotype patients with ATAA.

Investigating MOR1-07, however, shows that total collagen levels remain unchanged and insoluble elastin levels are slightly upregulated with either ASC-SF or NCM stimulation (**Figure 38**) with increases in fibulin-5, LOX, and LOXL-1 induced in parallel (**Figure 37**) and tropoelastin levels left unchanged. An increase in tropoelastin coacervation (via fibulin-5) and crosslinking (via LOX and LOXL-1) could induce this greater level of mature elastin deposited, but the unchanged collagen response and overall decrease in both ECM protein fractions stand out with this SMC line.

4.5 Conclusion

Aortic aneurysm research directions within most cardiovascular research groups, including the Vascular Bioengineering Lab and the Vascular ECM Dynamics Lab, focus on engineered grafts and therapies for adult populations with aortic aneurysms, adult patients with genetic disorders, or adults with high blood pressure, diabetes, or smokers. Pediatric aortic disease progression is considerably different than adult aortic disease, and few labs combine expertise in ECM analysis and aortic aneurysm treatment with the access to pediatric tissue sources. As cell isolation methods become more efficient, reducing the amount of passages between tissue digestion and cell storage, research groups with proximity to a pediatric cardiothoracic surgery facility can work to improve the literature concerning *ex vivo* pediatric patient-derived cell culture analysis.

By studying elastogenesis of three different explanted pediatric dilated aortic SMCs, we have found that ASC-SF therapy can induce a relative increase of insoluble elastin deposition across all age groups (**Figure 34**, **Figure 36**, & **Figure 38**) due to increased tropoelastin and

elastin chaperone protein transcription (**Figure 33, Figure 35, & Figure 37**), but has shown to downregulate total collagen in the youngest patient SMC line.

We also worked to establish a tissue transfer and cell isolation and storage protocol to establish a biorepository of explanted aortic SMCs and fibroblasts from dilated pediatric aortas by combining the local expertise in pediatric cardiothoracic surgery, vascular engineering, and vascular cell biology. Funding to our team from the Pediatric Device Initiative (2016-2017), set up the initial infrastructure needed to combine efforts between the research groups at the Children's Hospital at UPMC and the University of Pittsburgh's Bioengineering Department. This included Institutional Review Board (IRB) approval (#PRO16080251), coordination of procedures with the Children's Hospital of UPMC Pathology department, and resources needed to expand our cryogenic storage capacity. To date, we have successfully stored SMCs from 10 patients undergoing surgical repair of the ascending aorta and/or aortic root at the Children's Hospital (**Table 3**)

This biorepository is the only local resource for a variety of investigations of benefit to this population of pediatric patients suffering from cardiovascular disease and can be applied in the future to research groups across campus.

4.6 Future Work

Ongoing work is being conducted to evaluate cellular phenotype of the medial layer cells used in this aim. Pediatric cells from each evaluated patient line (SMCs or fibroblasts from MOR 01, MOR 04, and MOR 07) were plated from liquid nitrogen storage into tissue culture treated flasks (T75 or T175) and passed once, cultured to ~90% confluency using standard culture

media, serum-deprived for 24-48 hours, and collected in RNA-Later for qPCR. SMC phenotype targets will include α -smooth muscle actin, calponin, and smooth muscle myosin heavy chain (or MYH11), but should be negative for discoidin domain receptor 2 (DDR2) and fibroblast surface protein. Fibroblast cell confirmation will include positive quantification for DDR2 and fibroblast-specific protein 1 and negative for MYH11.

Given that the average half-life of human mature elastin is around 74 years *in vivo* [243], the goal for ASC-SF pediatric SMC therapy was to induce long-term elastin deposition. In order to test this *in vitro*, a FlexCell dynamic culture system within 3D fibrin gel constructs must be used, and the final elastogenesis cascade output of mechanical activity (particularly creep resistance) is necessary for future studies.

LTBP-4 production is muted by both ASC-SF and NCM in both MOR1-01 (**Figure 33**) and MOR1-04 (**Figure 35**) SMCs, a trend seen in healthy adult SMCs as well (**Figure 17**). LTBP-4 plays a complementary role in tethering tropoelastin coacervates to fibrillin-1 microfibril complexes, providing an organized template for inter-coacervate crosslinking and functionality. Generating elastin for aortic mechanical functionality, within the context of both non-surgical regenerative aneurysmal therapeutics and within tissue engineered vascular graft remodeling, must include modification of ASC-SF that counters this LTBP-4 muting effect.

MOR1-07 and MOR2-07 also both deserve more study, as total ECM protein fraction is significantly reduced when compared to MOR1-01 and MOR1-04. This SMC line, MOR1-07, was sourced from a slightly older patient (15 years old) with unknown etiology of aortic root dilation and co-morbidity of autosomal dominant polycystic kidney disease. ECM deposition effects within both a slightly more degraded fibrin construct (by reducing fibrinolysis inhibitor ACA concentration) and increased cellular characterization could lead to an identification of the

cause of aortic root dilation, and a guide for ASC-SF or NCM based non-surgical therapeutic development.

5.0 Specific Aim 3, Part 1: Periadventitial Magnetic Localization of Mesenchymal Stem Cells to a Murine Abdominal Aortic Aneurysm

The goal of this chapter was to develop a technique and method for iron nanoparticle-loaded adipose-derived mesenchymal stem cell (MSC) delivery periadventitially to the aortic wall. The combination of a Tri-Syringe device, designed to form a fibrin-based ASC hydrogel, and external magnet was formulated through iterative *in vitro* pilot studies, and ultimately tested through an *in vivo* murine abdominal aortic aneurysm model developed by Dr. John Curci at Vanderbilt University. The hypothesis of this study was that the Tri-Syringe injection device would allow for simultaneous mixing of hydrogel components and therapeutic cells for immediate treatment delivery, and magnetic localization mechanism would target cells to the surface of specific tissues or organs through minimally invasive means, as the magnetic field draws therapeutic cells to targeted surface where they are fixed in place with a hydrogel.

5.1 Introduction

Rupture of an abdominal aortic aneurysm (AAA), a dangerous dilation of the abdominal aorta, is the 15th leading cause of death in the United States [17-19]. Diagnosed as a AAA once dilation exceeds 1.5x initial diameter (from 2cm to beyond 3cm in adults), patients typically undergo endovascular repair once their aneurysm grows beyond 5.5 cm in diameter [175]. Surgical repair below this diameter fails to improve survival rates, as risk of surgery outweighs risk of rupture [17] (see **Section 1.4**), and as AAAs below this diameter are only monitored

without any targeted treatment option, new non-surgical therapeutic methods to halt AAA dilation are necessary to overcome these shortcomings.

Stem cell-based therapeutic options have been explored within the context of cardiovascular repair through paracrine pro-angiogenic secreted factors [244], increased immunomodulatory properties [245, 246], and extracellular matrix microvascular patterning [247]. However, many of the targeted sites for delivery of cells to treat these diseases are internal and therefore difficult to reach. Currently available technologies for therapeutic cell delivery to diseased areas include biodegradable scaffolds [202, 248] or matrix-derived scaffolds [196, 249], hydrogels [250, 251], and stem-cell patches [252-254]. Direct injection with aid of magnetic nanoparticles has also been extensively studied, as reviewed in [255]. Despite studies identifying fibrin as a viable cellular delivery mechanism or tissue engineering biomaterial [256-262], none of these technologies can combine fibrin gel delivery and magnetic nanoparticle-aided localization to accurately deliver cells to internal locations and fix them in place at therapeutically-relevant locations.

Our group has previously demonstrated the effectiveness of periadventitally-delivered MSCs in halting aortic expansion within an elastase-induced murine AAA model [198]. Localized delivery method, via the surgical implantation of a subcutaneous port leading to a sponge sutured to the AAA at the time of elastase perfusion, relied solely on the implanted sponge to provide a “localization” effect to the anterior aortic surface. A method to effectively pull MSCs to the outer AAA surface has yet to be developed or tested in large animals. Therefore, the goal of this chapter was the design, *in vitro* evaluation, and *in vivo* delivery method to actively localize MSCs to the periadventitial AAA surface. The novel method

employed herein can be used to guide stem cell-based treatments for AAA, providing a minimally invasive and robust means of localized delivery of therapeutic cells.

5.2 Methods

5.2.1 Iron nanoparticle delivery optimization through fibrin gels

200nm iron nanoparticles (Chemicell, #4114) were passively loaded into aortic smooth muscle cells (SMCs) (ATCC #PCS-100-012, Manassas, Virginia, passage 8) by resuspending the stock 5.2g/mL nanoparticles to a 81.89mg/mL final concentration within SMC growth supplemented media (#311K-500, Cell Applications Inc, San Diego, CA). Iron nanoparticles and SMCs (abbrev. **FeSMCs**) were cultured at 37°C and 5% CO₂ for 36 hours before integration within fibrin gels. Negative control group included fresh SMCs (passage 8) without iron nanoparticle incubation.

0.4mL fibrin gels were formed within 24 well tissue culture treated wells, consisting of three components: fibrinogen, thrombin, and cells. Fibrinogen (3.7mg/mL) (Sigma Aldrich, #F8630) stock was suspended in a 20mM HEPES/0.9% saline solution. Thrombin solution was made using 0.208 units/mL bovine thrombin (Sigma Aldrich, #T7513) and 3mM calcium chloride, suspended in High Glucose DMEM + Glutamax media (Life Technologies, #10564). 1×10^5 iron nanoparticle loaded SMCs were integrated within each gel, resuspended in SMC growth supplemented media. A 4:1:1 volumetric ratio of fibrinogen:thrombin:cells was combined to form the fibrin gels within a 15mL conical tube, and transferred to the 24 well plate.

Immediately after fibrin construct seeding, six single neodymium permanent magnets (surface field of ~4,100 Gauss) were positioned outside of the plate, tangential to each column along the bottom row of the 24 well plate. Fibrin constructs and the magnetic row were allowed to culture for 30 minutes at 37°C and 5% CO₂, before SMC growth supplemented media addition (1mL per well) and subsequent 4-hour incubation.

MTT Assay (CellTiter 96 Non-Radioactive Cell Proliferation Assay, Promega #G4000) was used to visualize cell locations within each fibrin gel construct, with location comparisons made between FeSMC and SMC loaded constructs.

5.2.2 Tri-Syringe Delivery Device for FeMSC-loaded fibrin gels

A Tri-Syringe delivery device was designed using computer aided design and 3D printed using a stereolithography printer with a sterilizable dental photopolymer resin. The design was developed using 3D modeling software SolidWorks (Dassault Systèmes), and exported as a stereolithography (STL) file. STL file design is loaded into PreForm (Formlabs) for preparation and optimization before printing. Dental photopolymer resin cartridges (Formlabs, white #FLFLGR02, grey #FLGPGR03) was loaded into the Formlabs 2 SLA printer, and the Tri-Syringe device was printed on printed struts for support. The struts were removed after completion using wire cutters, and the Tri-Syringe was immersed in 99% isopropyl alcohol for 15 minutes to remove uncured resin. Finally, the printed Tri-Syringe was cured under a ultraviolet lamp for 1 hour before use.

The Tri-Syringe system combines three 1mL syringe chambers that combine when pushed together: (1) fibrinogen (3.7mg/mL in 20mM Hepes/0.9% saline); (2) thrombin (0.208units/mL with 3mM calcium chloride in High Glucose DMEM/Glutamax media); and (3)

cell solution. Previously isolated patient-derived adipose MSCs from non-diabetic, non-smoking patients under 45 years old were passively loaded with iron nanoparticles (abbrev. **FeMSCs**) as described in **Section 5.2.1** using MSC culture media, consisting of “ASC culture media”, consisting of 33% Dulbecco’s Modified Eagles Medium (High Glucose, Gibco #12100046), 33% DMEM/F12 Medium (HEPES, Gibco #12400024), 7.5% fetal bovine serum (FBS, Premium Select Atlanta Biologics #S11550), 0.75% fungizone (Lonza BioWhittaker Antibiotics #BW17836E), 0.75% penicillin streptomycin (10,000 U/mL, ThermoFisher Scientific #15140122), 0.075 μ M Dexamethasone (Sigma-Aldrich #D4902), and 25% Preadipocyte Growth Medium (PromoCell #C-39425).

The Tri-Syringe can be used in combination with a magnetic field to deliver iron nanoparticle-loaded cells to *in vitro* and *in vivo* locations, combining equal volumes for fibrin gel constructs over 0.5mL. Combined constructs can be successfully delivered through a needle as small as a 30-gauge sterile needle, without shearing the fibrin or the encased cells. Tri-Syringe was designed to inject through the predesigned port/catheter/sponge *in vivo* delivery port by the lab of Dr. John Curci at Vanderbilt University.

5.2.3 Iron nanoparticle-loaded MSC localization optimization following fibrin gel delivery to rat peritoneal cavity

FeMSC fibrin gel constructs were delivered via Tri-Syringe to the rat peritoneal cavity, to mimic distance and tissue interruption of the magnetic field in subsequent *in vivo* mouse aneurysm delivery and localization studies. 6mL fibrin constructs were made using 2mL fibrinogen (3.7mg/mL), 2mL thrombin (0.208 units/mL) with 3mM calcium chloride, and 2mL FeMSCs (5×10^5 per gel, resuspended in sterile HBSS). FeMSC fibrin gel constructs were

injected onto the anterior abdominal aorta section of a sacrificed rat (n = 6). The experimental group (n = 3) had a magnet placed underneath the rat for 30 minutes while the control group (n = 3) did not have a magnet. Constructs were allowed to solidify for 30 minutes at 37°C under magnetic experimental conditions, and for 2 hours at 37°C after the magnet was removed.

Abdominal aortic sections were harvested and fixed using 4% PFA (fixed overnight), with light microscopy and staining for DAPI and human nuclear antigen was used to determine cell location within the peritoneal cavity. Gel quantification (ImageJ) of inverse intensity values of the rectangular region of interest.

5.2.4 Optimization of Tri-Syringe fibrin gel delivery and iron nanoparticle-loaded MSC localization using explanted chicken wing radial artery

An explanted chicken wing brachial artery partially embedded in agar was used as a tissue mimetic to evaluate the impact of magnetic forces over an interrupted distance, as preparation for *in vivo* mouse aneurysm delivery and localization studies.

Fibrin gels were made by combining equal parts (0.2mL each) fibrinogen, thrombin, and cell solutions within the Tri-Syringe delivery device. Fibrinogen solution was made using 3.7 mg/mL bovine fibrinogen suspended in a 20mM Hepes/0.9% saline solution, thrombin solution was made using 0.208 units/mL bovine thrombin and 3mM calcium chloride in High Glucose DMEM + Glutamax media, and cell solution was made using 5×10^5 FeMSCs and 10mM aminocaproic acid suspended in Mouse MSC Growth Media.

Explanted chicken radial artery sections (approximately 6cm in length) was placed on top of agarose gel (n = 6) in a 10cm petri dish. 5% agarose gels were made using 3.75g agarose (Sigma, #A9539) and 75mL of sterile water, and poured within 10cm petri dishes at

approximately 5mm thickness per plate. Chicken wing radial artery sections were placed on warm agarose gels immediately after pouring, with over half of the artery exposed to simulate the exposed anterior peritoneal section of mouse aorta. Sponge/catheter ports, provided by the Curci group at Vanderbilt University, was sutured into place after over 6 hours of agarose gel curing.

The control group consisted of FeMSC fibrin gel constructs without a magnet (**Figure 45A**), while the experimental group consists of the FeMSC fibrin gel constructs with a magnet placed underneath the agarose gel for 30 minutes (**Figure 45B**). Cross-sections of each sponge/construct/artery/agar experimental plate and light microscopy was used to determine cellular location are relative to the radial artery and agarose gel, and whether FeMSCs can be drawn through the sponge towards the artery.

5.2.5 Tri-Syringe periadventitial delivery and magnet-guided localization of iron nanoparticle-loaded MSCs in an elastase-induced AAA mouse model

C57BL/6 Mouse Mesenchymal Stem Cells (**MSCs**) (Cyagen, #MUBMX-01001) were cultured using OreCell™ Mouse MSC Growth Medium (Cyagen, #MUXMX-90011) within a 37°C, 5% CO₂ sterile culture incubator. Mouse MSCs were passively loaded with 200nm iron nanoparticles (Chemicell, #4114) at a 0.4 mg/mL concentration in Mouse MSC Growth Medium for 12 hours. Cells were also passively loaded with CellTracker Red CMTPX Dye (Invitrogen, #C34552), at 23µM within Mouse MSC Growth Media, for 1 hour before fibrin gel delivery.

Our established murine model of elastase-induced AAA was chosen to perform *in vivo* testing of the magnetic delivery methodology. All murine subjects were housed in at Vanderbilt University, under the supervision of Dr. John Curci and Jamie Adcock. AAA was induced within

adult male C57BL/6 mice via elastase submersion, as described previously [198] (n=12). Briefly, a midline laparotomy was made to expose the peritoneum after sedation and sterile preparation. A subcutaneous microport (Instech) was connected to polyurethane catheter tubing (Braintree Scientific), sutured in the retroperitoneal space. The isolated infrarenal aorta was submerged for five minutes in a solution containing type I porcine pancreatic elastase (PPE, 0.16 U/mL; Sigma-Aldrich). Elastase submersion was used in lieu of elastase perfusion due to pressure-induced aortic diameter variability. A pressure-controlled elastase perfusion rig is currently in development to address this issue (Dr. Timothy Chung at the VBL). Following elastase submersion, an Invalon sponge (5mm x 8mm) was connected to the end of the catheter tubing, and sutured over the infrarenal aorta. Mice were allowed to completely recover before returning to standard housing, and maintained with standard food and water for 5 days.

Fibrin gels were made by combining equal parts (0.2mL each) fibrinogen, thrombin, and cell solutions within a custom-made syringe delivery device. Fibrinogen solution was made using 3.7 mg/mL bovine fibrinogen (Sigma Aldrich, #F8630) suspended in a 20mM Hepes/0.9% saline solution. Thrombin solution was made using 0.208 units/mL bovine thrombin (Sigma Aldrich, #T7513) and 3mM calcium chloride, suspended in High Glucose DMEM + Glutamax media (Life Technologies, #10564). Cell solution was made using 5×10^5 Mouse MSCs and 10mM aminocaproic acid, suspended in Mouse MSC Growth Media.

AAA was induced by elastase delivery to the abdominal aorta on day 0, a port system was implanted above the aorta, and the animal was closed and allowed to recover. At day 5, mice were anesthetized and placed on a custom designed surgical stage (**Figure 39**), with a magnet directed immediately below AAA site for experimental groups and without magnet as controls. MSCs (both iron-loaded and fluorescently tagged with a red marker) were injected into the port

using the fibrin gel mixing chamber (**Figure 40C & Figure 42**, displayed *in vitro*) so that the MSCs would become encapsulated around the nascent AAA.

Fibrin gel deliveries were made 5 days after AAA induction, using the custom tri-syringe device and a 18G laboratory needle to inject at the retroperitoneal microport. Gels were allowed to solidify for 30 minutes, as the mice were sedated on the surgical stage. Magnet placement was made for 6 mice, with the remaining 6 mice receiving fibrin gel delivery without magnet placement. A total of 12 mice were injected in this manner – 6 had a posterior magnet during delivery (experimental) while 6 did not (control). Two mice were harvested from each group at one of three timepoints: 1 hour, 3 days, and 7 days post-delivery. All experiments were performed at Vanderbilt University, in the laboratory of Dr. John Curci and Jamie Adcock.

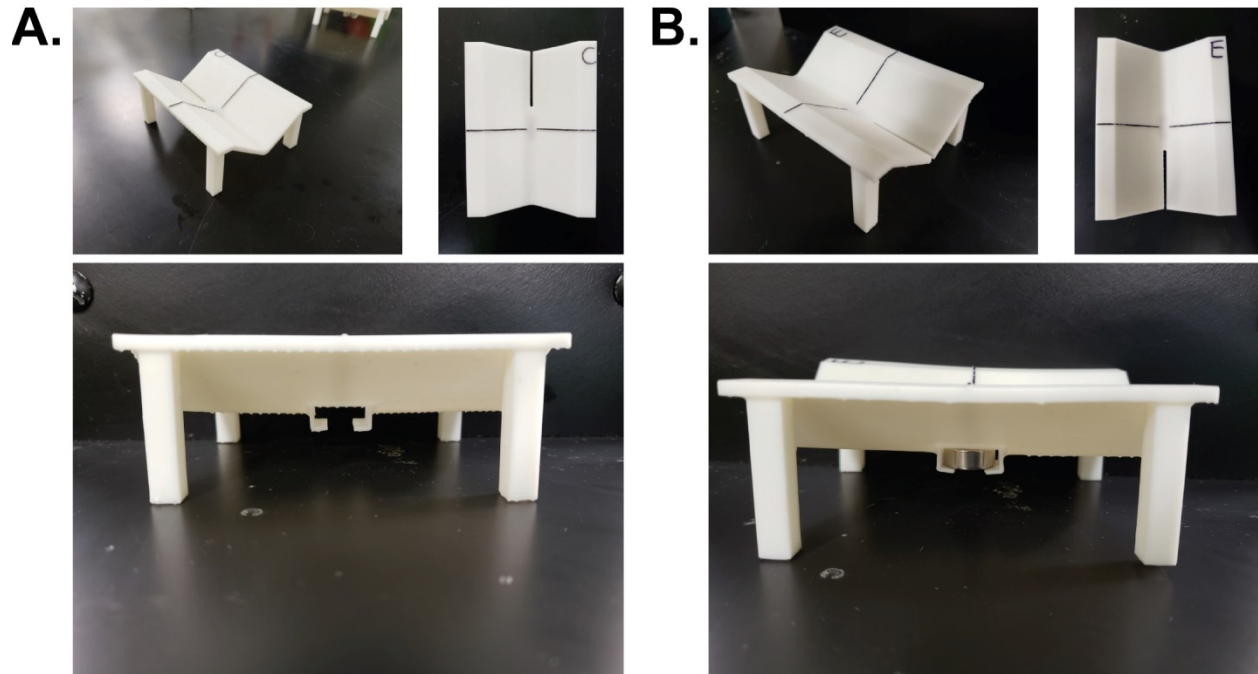


Figure 39: Surgical stage for FeMSC periadventitial delivery and localization during mouse surgeries, designed and printed for surgeries performed by Dr. John Curci's group at Vanderbilt University.

A) Control stage, with no magnet present underneath the mouse during FeMSC fibrin gel delivery.

B) Experimental stage, with a single neodymium permanent magnet (surface field of $\sim 4,100$ Gauss) sitting immediately below the elastase-induced murine AAA, positioned at the black intersecting marks on the stage surface during FeMSC fibrin gel delivery.

5.3 Results

Design and printing of the Tri-Syringe device was performed in collaboration with Dr. Timothy Chung and Yogev Baruch in the Vascular Bioengineering Laboratory, and all murine studies were performed at Vanderbilt University in collaboration with Dr. John Curci's group.

5.3.1 Fabrication of “Tri-Syringe” mixing chamber to deliver cell-seeded fibrin gel constructs

The Tri-Syringe delivery device went through several iterations, starting with an in-line design (**Figure 40A**) which combined equal volumes of the fibrinogen, thrombin, and FeMSC solutions into a mixing chamber, with delivery through a Luer-Lok needle. Despite the middle lane of the mixing chamber being shorter than either end lanes, the volumes were calibrated to mix equally and evenly. This in-line design was unwieldy during use, needed two hands to push the plunger evenly (otherwise the solutions would combine unequally), and syringe changes were difficult to easily and quickly perform.

The next design iteration adopted a triangular shape for the syringes and the plunger (**Figure 40B**), enabling easier use with one-hand which was essential for future *in vivo* applications. The mixing chamber was redesigned with three equal volume, equal length chambers leading to a Luer-Lok needle for delivery that minimized lost volume of combined fibrin gels. The final design (**Figure 40C**) added three guiding pins to the plunger and a tapered insertion design for the guiding pins on the syringe holder, ensuring that all three syringes are deployed with equal pressure regardless of where force is applied on the plunger.

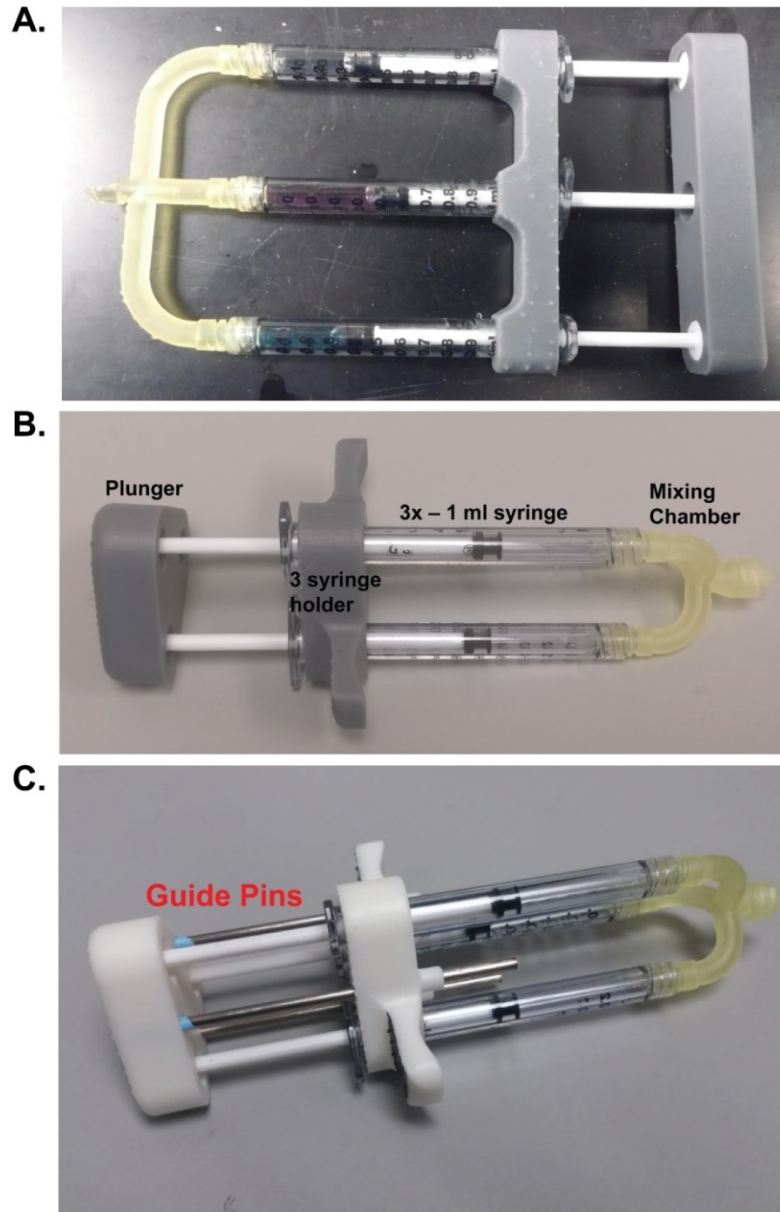


Figure 40: “Tri-Syringe” mixing device iterations to form and deliver cell-rich fibrin gel constructs.

- A) Initial in-line design, consisting of *three 1mL syringes* containing fibrinogen (clear solution top), thrombin/calcium chloride (pink solution, middle), and cell solutions (synthetically colored blue, bottom), a *syringe holder* to hold all three syringes in place, a *plunger* to simultaneously push each syringe, and a *mixing chamber* where the solutions combine and push into a Leur-Lok exit.
- B) Second triangular design of the Tri-Syringe, enabling easier single-hand use and syringe replacement, with a redesigned mixing chamber to reduce fibrin gel losses.
- C) Final Tri-Syringe design, with the addition of *guide pins* that ensured equal injection along all three syringes.

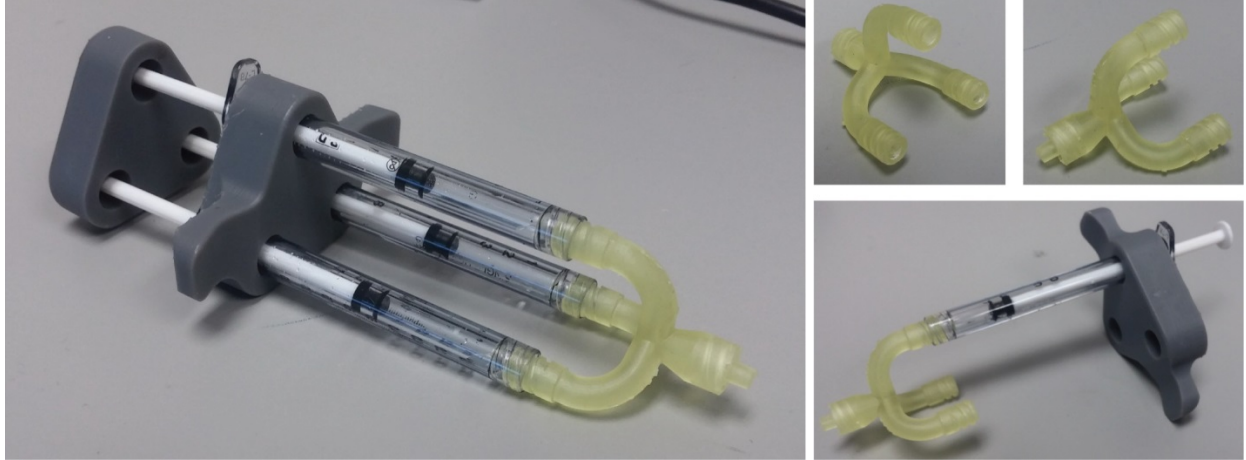


Figure 41: Additional views of the Tri-Syringe fibrin gel injection delivery device.

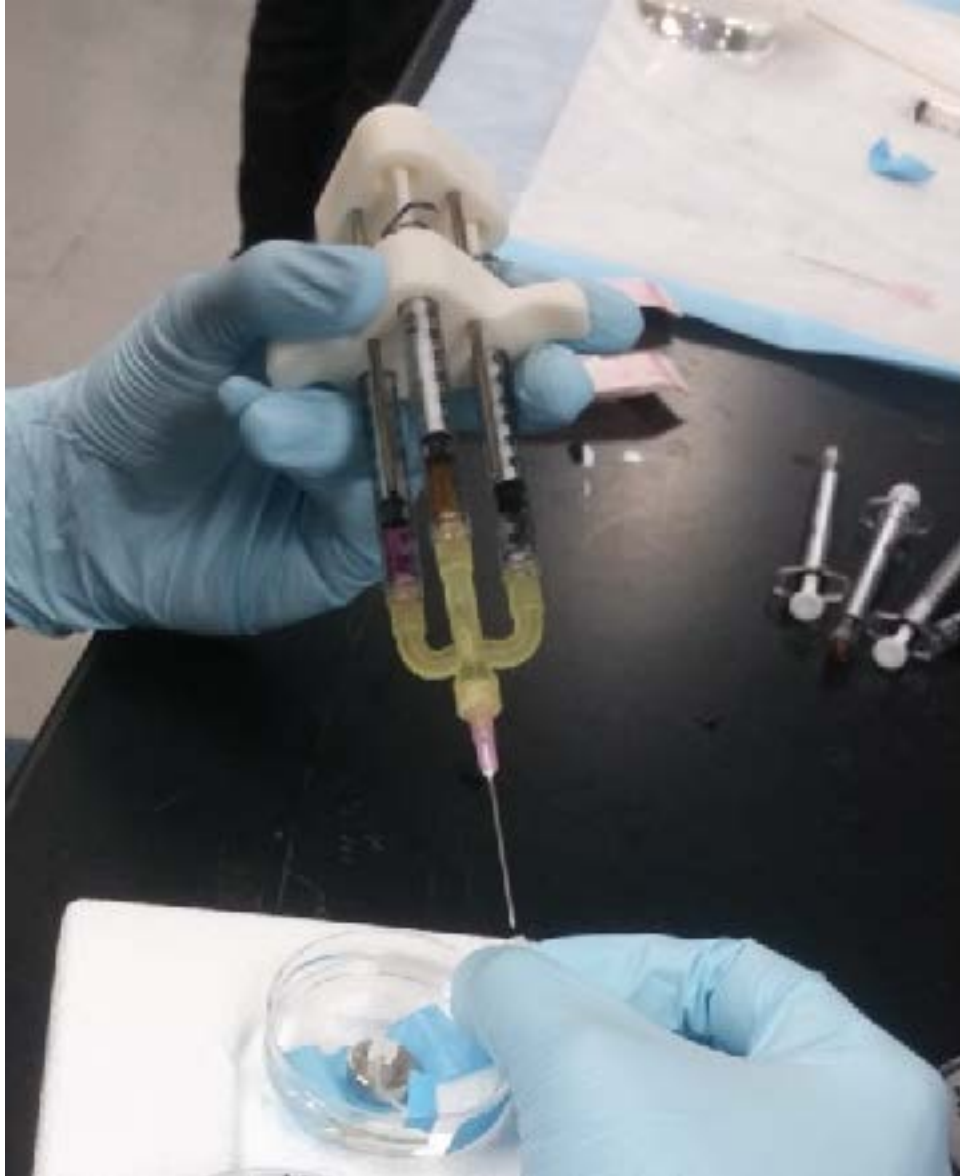


Figure 42: Tri-Syringe fibrin gel injection device in use during *in vitro* FeMSC localization studies, with syringes for fibrinogen (clear solution, right), FeMSCs (brown solution, middle), and thrombin (pink solution, left) being combined and injected through an 18-gauge needle into the port/catheter/sponge device designed by Dr. John Curci's group at Vanderbilt University.

5.3.2 *In vitro* magnet-guided migration of iron nanoparticle-loaded MSCs within fibrin gels.

After applying the MTT assay, it was evident that loaded cells localized towards the magnet (**Figure 43**). Furthermore, *in vitro* experiments applying MSCs and fibrin gel to the anterior of a rat aorta (with and without a dorsal magnet) tested whether the cells were being localized to the region of interest while allowing for the fibrin gel to polymerize above the cells. When a magnetic field was present, the nanoparticle loaded MSCs were drawn to the surface of the well closest to the magnet as the fibrin gel polymerized surrounding the cells (**Figure 43A**).

At short distances, the experimental group (FeMSCs, fibrin, and magnet) demonstrated that the cells were localized onto the anterior surface of the aorta while being encapsulated by fibrin gel (**Figure 43A**). The control group (unmodified MSCs, fibrin, and magnet) revealed a homogeneous distribution of cells within the fibrin gel (**Figure 43C**). Extending the distance to the next row of wells, however, negated the effects of the magnet on both Experimental (**Figure 43B**) and Control (**Figure 43D**) groups.

Analysis was performed using the “Intensity Map” function on ImageJ (open source), drawing a rectangle down the middle of each well, resulting in a corresponding localization map of darker pixels (**Figure 43**, right panel).

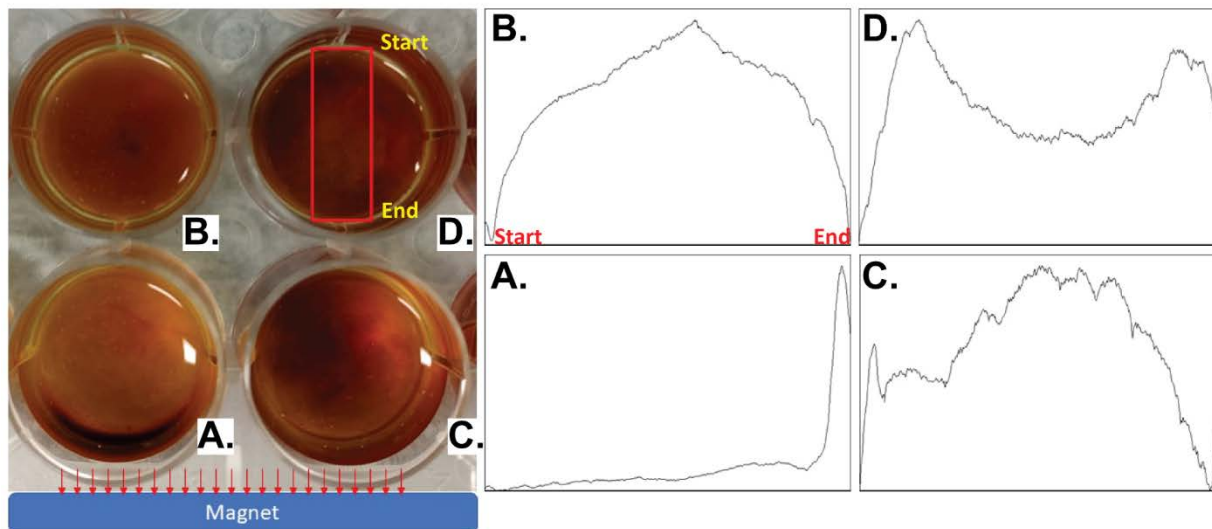


Figure 43: Quantitative analysis of cell location via MTT assay, with and without the presence of a magnetic field and at different distances.

A) Left panel: Fibrin-embedded FeMSCs in the first row of a 24 well plate, with a magnet placed on the plate's outer edge. Right panel: Corresponding intensity map of cell distribution.

B) Left panel: Fibrin-embedded FeMSCs in the second row, as magnet placement remained constant. Right panel: Corresponding intensity map of cell distribution.

C) Left panel: Fibrin-embedded unmodified MSCs (without iron nanoparticles) in the first row of a 24 well plate, with a magnet placed on the plate's outer edge. Right panel: Corresponding intensity map of cell distribution.

D) Left panel: Fibrin-embedded unmodified MSCs (without iron nanoparticles) in the second row, as magnet placement remained constant. Right panel: Corresponding intensity map of cell distribution.

5.3.3 FeMSCs localize to the aortic surface when delivered via Tri-Syringe to a rat peritoneal cavity within a fibrin gel in the presence of an external magnet

FeMSC delivery to the open peritoneal cavity of a rat, with a dorsally-present permanent magnet, leads to an even distribution of FeMSCs localized to the exposed aortic surface (**Figure 44A & Figure 44C**). FeMSCs are only present along the exposed ventral half of the abdominal aorta, and the fibrin gel (with 3mM calcium chloride concentration to increase speed of gelation) maintains the monolayer of localized FeMSCs at the aortic surface.

Quantification of FeMSC location, using a monochrome rendering and a manual selection of the solid fibrin gel cross-section (**Figure 44C & Figure 44D**) indicated that experimental group exhibited a higher peak response near the aortic surface (**Figure 44E**), while control is more evenly distributed (**Figure 44F**).

Sections of the aorta and surrounding tissue were also imaged after being stained with DAPI and HNA. It was seen (both qualitatively and quantitatively) that the FeMSCs are on top of the anterior portion of the aorta with encased in fibrin gel while the fibrin gel in the control group has homogenously distributed cells.

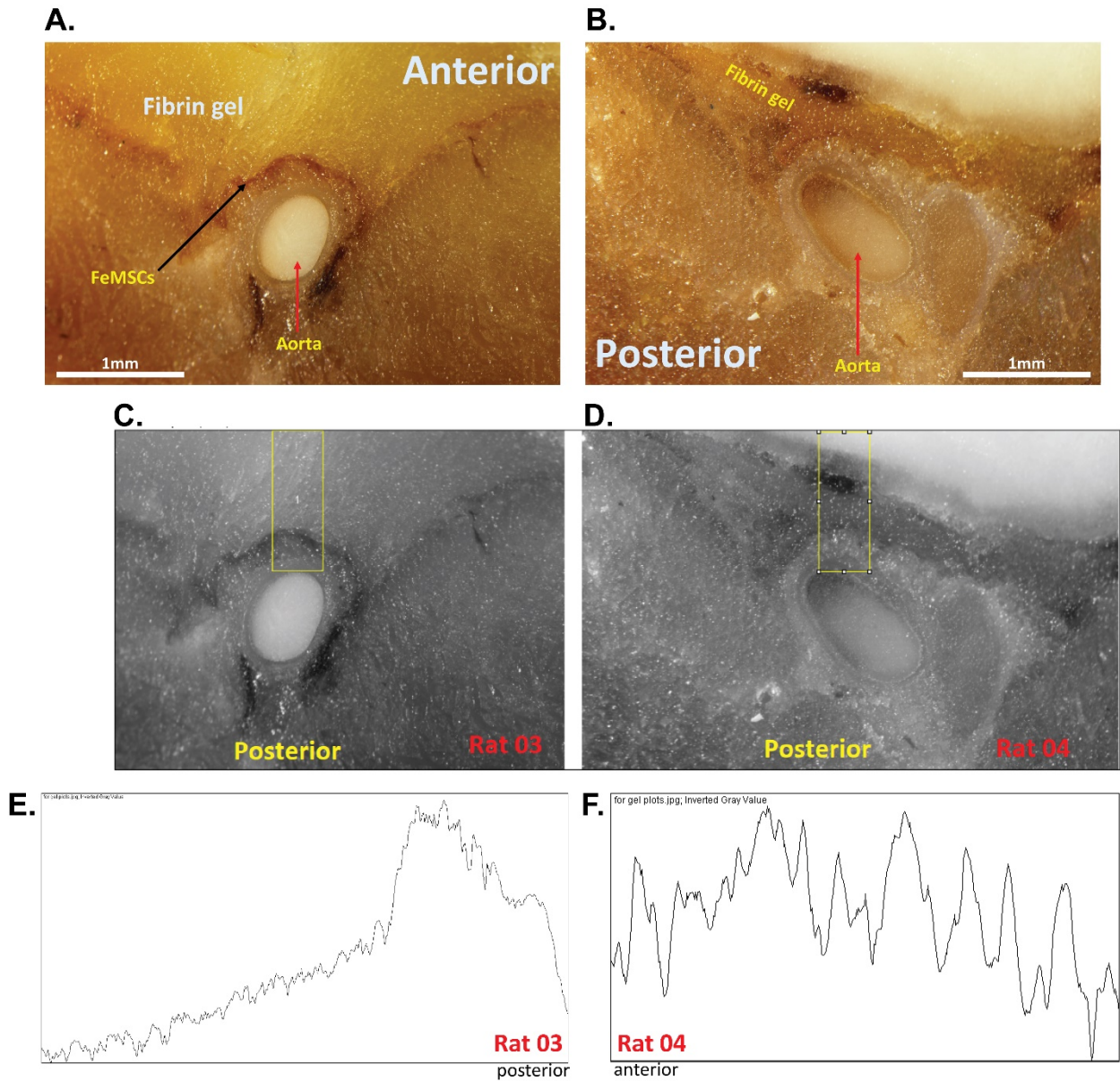


Figure 44: Magnet-driven localization and quantification of FeMSC-rich fibrin gel constructs within a rat peritoneal cavity.

(A)-(C) & (B)-(D) Light microscope images and their counterpart black-and-white renderings of FeMSCs delivered within a fibrin gel construct via Tri-Syringe, within the peritoneal space of a rat. Dark band of FeMSCs underneath fibrin gel in the presence of a magnetic field (A, C) and without a magnetic field (B,D), under 3x magnification. (E) & (F) Distribution profiles, as determined via ImageJ, of delivered FeMSCs as determined within the yellow selection box present in (C) and (D).

5.3.4 Agar-embedded chicken brachial artery *in vitro* model of catheter-delivered Fe-MSC fibrin gel constructs to a surgical sponge shows distance bounds of magnet-guided migration.

A simplified FeMSC *in vitro* localization experimental setup was designed, using a 5% agarose gel with an explanted chicken wing brachial artery partially exposed to an open surface, and Dr. John Curci's sponge/catheter/port delivery device sutured in place (**Figure 45**). A customized stage to hold the magnet flush underneath the petri dish, directly below the embedded artery, was used to simulate experimental groups with the magnet present during delivery.

Light microscopy of explanted agarose/artery cross-sections (**Figure 46**) show that FeMSCs are evenly distributed and contained throughout the sponge without the presence of a permanent magnet (**Figure 46A**). Delivery in the presence of a magnet, however, pulls the FeMSCs to the exposed brachial arterial surface (**Figure 46B**), mirroring the effect seen without the sponge after direct injection into an open rat peritoneal cavity (without localized catheter-guided delivery) (**Figure 44A**). Interestingly, while fibrin gel-embedded FeMSCs are contained in the sponge without a magnet, the presence of a magnet pulls the FeMSCs out and results in a complete coating at the open surface closest to the magnet.

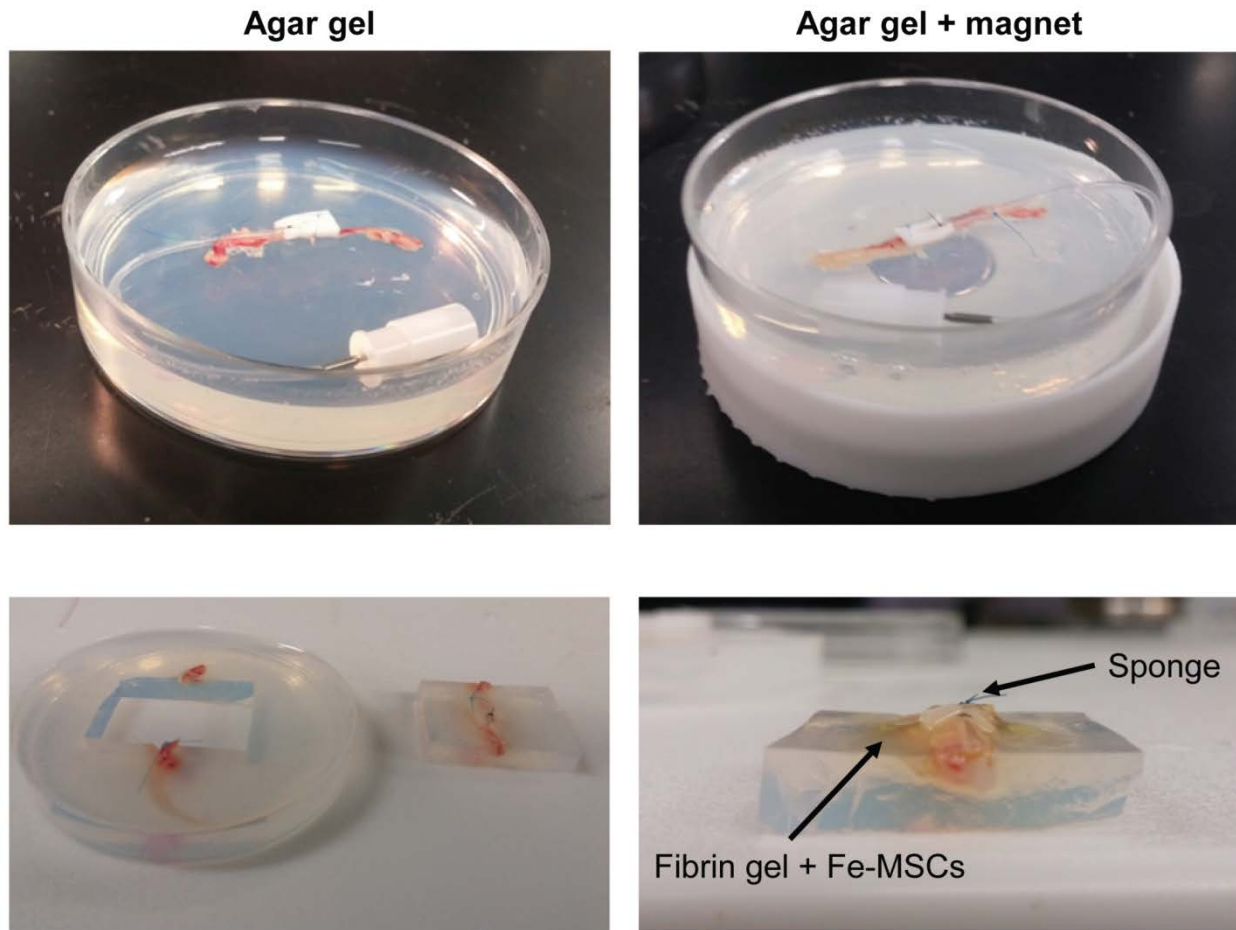


Figure 45: Agarose-embedded chicken wing brachial artery *in vitro* model for FeMSC delivery through port/catheter/sponge device, within a 10cm petri dish.

Left panel: Control group, delivery of fibrin-embedded FeMSCs to explanted chicken wing artery and agarose gel to a sutured sponge with no magnet underneath. Bottom image shows agarose gel and artery removed from petri dish.

Right: Experimental group, with artery and agarose setup and a single neodymium permanent magnets (surface field of ~4,100 Gauss) sitting immediately below the sponge and artery site within a 3D-printed magnet holder (white) to hold the magnet flush to the bottom surface of the petri dish. Bottom image shows a cross-section of agarose gel and embedded artery, sutured sponge, and delivered FeMSC/fibrin gel for FeMSC location analysis.

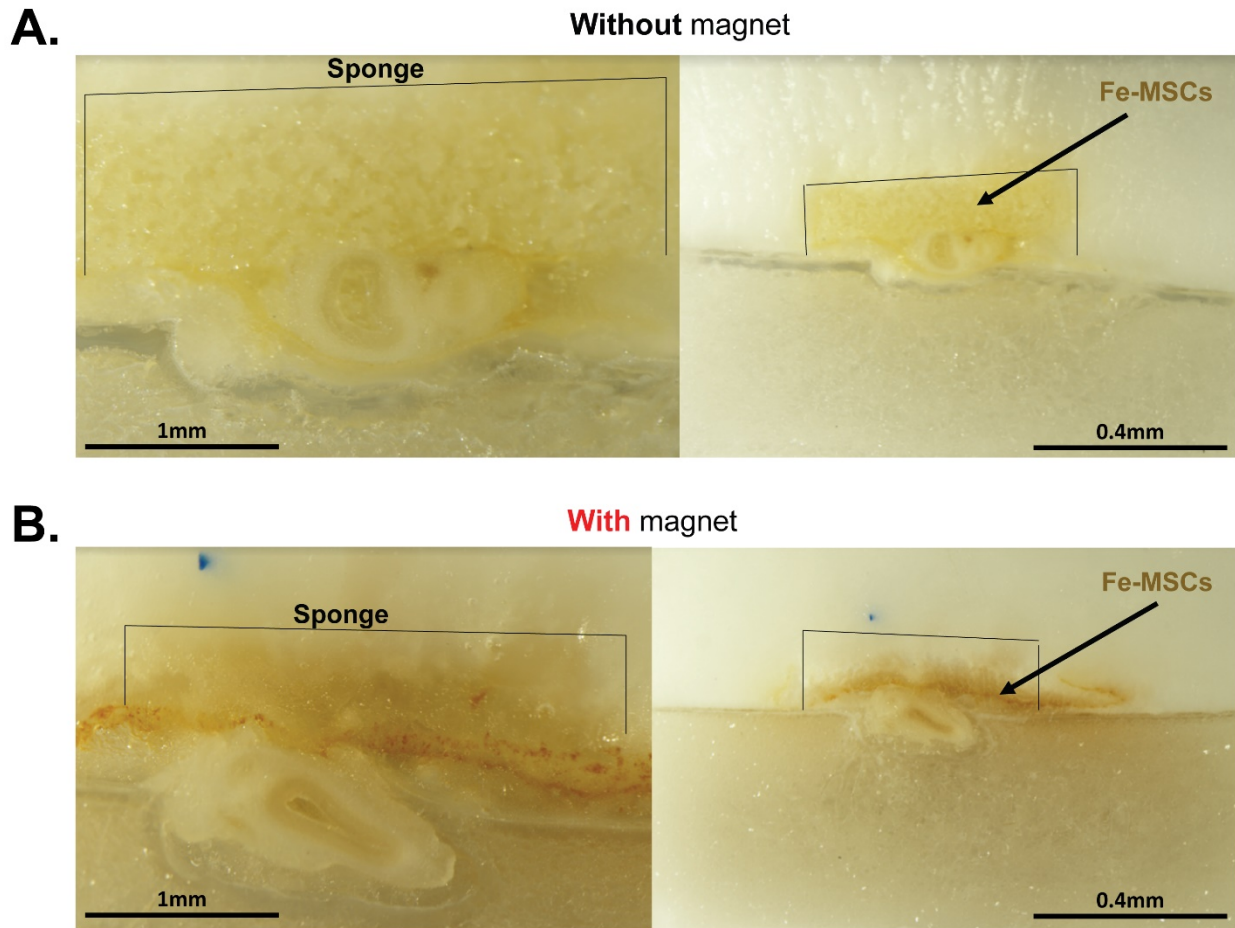


Figure 46: Light microscopy of delivered FeMSCs within agarose and artery setup.

- A) Control group, distribution of FeMSCs (dark brown) in the sponge, without a magnet present. Sponge is outlined, and chicken wing brachial artery is embedded directly below sponge, within a 5% agarose gel.
- B) Experimental group, FeMSCs distributed in a sponge with a single neodymium permanent magnets (surface field of ~4,100 Gauss) sitting immediately below the sponge and artery site at the time of FeMSC delivery. Chicken wing brachial artery embedded directly below sponge, within a 5% agarose gel.

5.3.5 Delivery of Fe-MSC seeded fibrin gels to growing elastase-induced mouse aneurysm shows external magnet guidance and cell retention both 1 hour and 3 days after delivery.

After port/catheter/sponge delivery through the Tri-Syringe device to the site of a murine elastase-induced AAA, preliminary results suggest that the cells in the control group remained in the sponge and were not drawn towards the magnet that was placed posteriorly 1 hour after delivery (**Figure 47**, top panel, left image), as indicated by the presence of CellTracker-dyed FeMSCs throughout the sponge. The experimental group with the magnetic field showed slight quantitative evidence of FeMSCs localized closer to the surface of the aorta both 1 hour and 3 days after delivery (**Figure 47**: , bottom panel). FeMSC CellTracker signal was strong surrounding the aorta 3 days after delivery in the experimental group, while after 3 days in the control group it seemed like a small fraction of cells migrated to surround the aorta from the sponge (**Figure 47**, top panel, right image). Validation of these results will require more experimental trials.

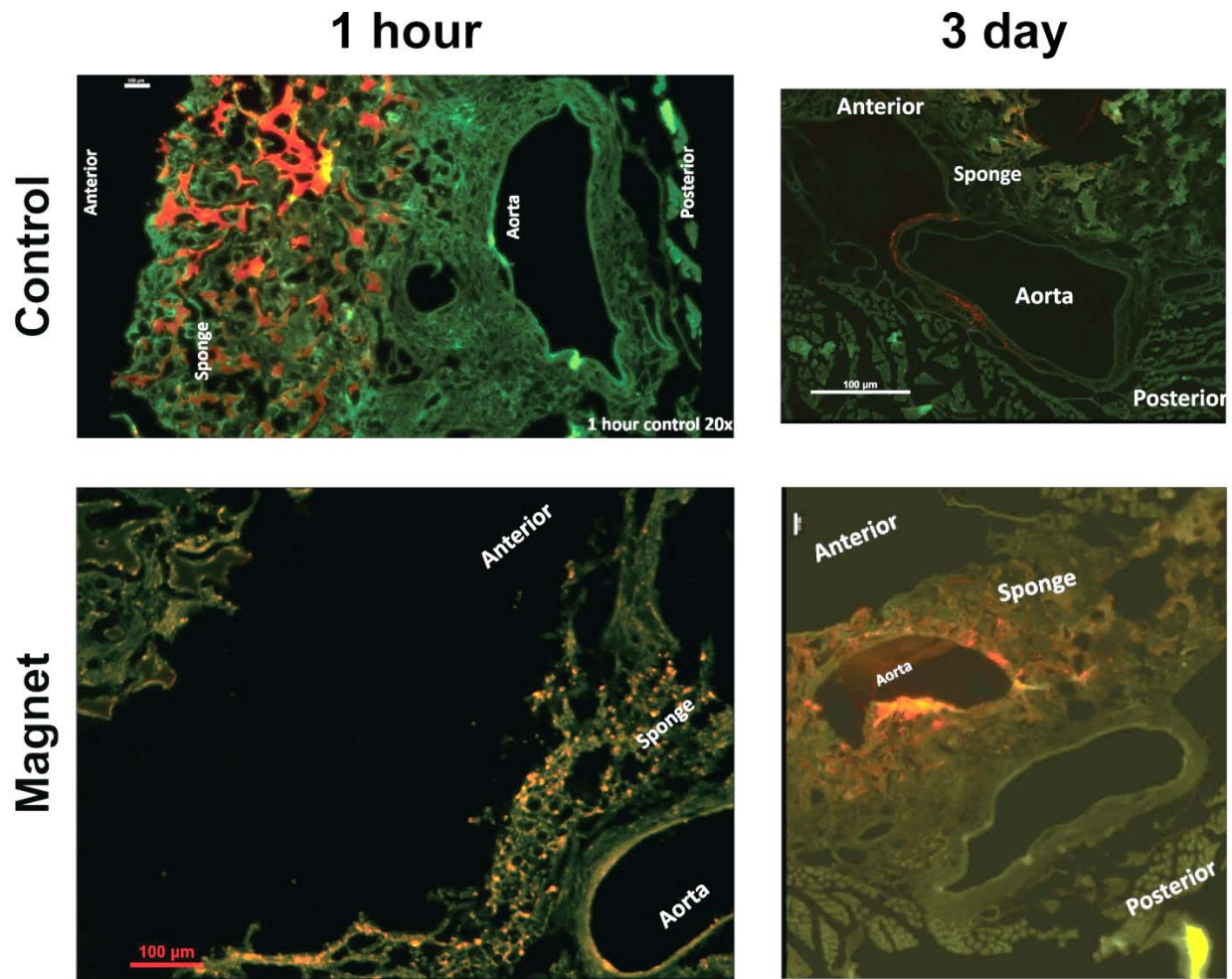


Figure 47: Periadventitial delivery and magnet-driven localization of FeMSCs (red) to an elastase-induced murine abdominal aortic aneurysm (autofluorescence in green).

Top panel: Control section of mouse, AAA, and sponge saturated with fibrin-embedded FeMSCs delivered without any magnet presence, after 1 hour (left) or 3 days (right) of before sacrifice.

Bottom panel: Experimental mouse, AAA, and sponge with Tri-Syringe delivered fibrin-embedded FeMSCs with a single neodymium permanent magnets (surface field of ~4,100 Gauss) sitting posterior to the delivery site for 30 minutes, after 1 hour (left) or 3 days (right) of before sacrifice.

5.4 Discussion

Our fibrin gel FeMSC delivery device, the Tri-Syringe, consists of three individually fabricated solutions (fibrinogen, thrombin, and a therapeutic cell of interest) delivered through a Luer-Lok needle to result in a deliverable cell-embedded fibrin hydrogel for *in vivo* studies. The revised Tri-Syringe design (**Figure 40C**) enables for even distribution of fibrin gel components, minimized volumetric loss (around 0.1mL total), ability to be used with one hand while securing the subject (in this case, the dorsally-available port in Dr. Curci's mouse surgical model), and the updated formula for the fibrin gel that varies from the rest of this dissertation is tailored for quick gelation while still allowing for magnetic-guided localization to the aortic surface (**Figure 47**).

The designed stage (**Figure 39**) provides a mechanism to hold a permanent magnet in place as the iron nanoparticle-loaded delivery cargo of choice (in our case, MSCs) were injected using the Tri-Syringe device. The stage design included a slit to allow for easy injection once the AAA was positioned immediately above the magnet, and was raised enough to allow for a degrees of freedom for the Tri-Syringe to inject at all angles.

The combination of FeMSCs and fibrin hydrogel injection mechanism allowed for a permanent magnet to localize the cargo to our specific area of interest, both *in vitro* (**Figure 43**, **Figure 45**, **Figure 46**) and *in vivo* (**Figure 44**, **Figure 47**). The fibrin gel sets to fix cargo in place, maximizing therapeutic function to a localized area of interest (in our case, potentially maximizing therapeutic effect of MSCs to the periadventitial surface of a AAA). These *in vitro* preliminary studies were also constructed to determine whether FeMSCs were able to overcome gravity by placing a magnetic field on the side of a well plate (**Figure 43**), showing that the magnetic strength was strong enough to localize against gravity. The agarose/chicken brachial artery *in vitro* setup (**Figure 45**) was intended to test the ability of the Tri-Syringe to push a

solidifying fibrin gel construct through the catheter and to the aneurysmal site, and to show that FeMSCs could be successfully localized through a surgical sponge before subsequent murine studies.

Preliminary murine model outlined in this chapter show this approach as a viable *in vivo* method to study periadventitially-delivered AAA therapeutics, ensuring that the cargo (whether whole-cell or cell-free) magnetically localizes to the aorta, held in place within a biocompatible fibrin hydrogel. The Tri-Syringe enabled mechanism of *in vivo* FeMSC delivery produced a similar effect to previous studies where gels were mixed outside of the animal, but was substantially easier to perform on the surgical tabletop. Dr. Curci's surgical model using a dorsally available port, silicone catheter, and sponge sutured to AAA site also enables aneurysmal studies on a growing AAA, without necessitating multiple surgeries. This presents with a distinct advantage over therapeutic evaluations immediately after elastase induction of AAA, or of the complication rate resulting from multiple surgeries.

5.5 Conclusion

Delivery of therapeutic cargo, a whole-cell therapeutic approach in the case of this chapter, to the adventitial surface of a growing AAA presents with a distinct advantage over many small aneurysm therapeutic approaches being currently pursued. Luminal delivery is impeded by the frequent presence of an intraluminal thrombus, impedes vasa vasorum function, and risks destabilizing the thinning aortic wall, making periadventitial therapeutic delivery preferable. Localization by an external magnet presents with no danger to the subject, and combining this magnetic localization technique with a fibrin hydrogel to fix therapeutic cells in

place maximizes potential therapeutic effects of the delivered cargo. Additionally, development of the Tri-Syringe device provides a level of control for fibrin gel formation previously unavailable.

5.6 Future Work

Additional *in vivo* localization studies using live murine animals are necessary to assess cargo retention and migration, with mouse studies available through further collaboration with Dr. Curci's group at Vanderbilt or with rat studies available through the Vascular Bioengineering Laboratory at the University of Pittsburgh. The only aspect studied here was the delivery and localization of FeMSCs to the aortic surface; further studies should include the therapeutic effects of FeMSC delivery, both with and without the presence of a localizing magnet. This includes AAA rupture and thrombosis rates (if present), AAA diameter at varying timepoints within two weeks of FeMSC injection, and *ex vivo* staining to assess elastic fiber integrity (Verhoeff-van Gieson), collagen fiber integrity (picrosirius red), and the presence of extracellular matrix protein within explanted AAA sections (ninhydrin and hydroxyproline assays). Additionally, MSC effect on vaso vasorum functionality could be studied following periadventitial MSC (or cell-free cargo) delivery.

A syringe pump is currently in development by Dr. Timothy Chung at the Vascular Bioengineering Lab, designed to control pressure induced by perfusion of elastase to generate mouse AAA models. Inconsistency of aortic diameter following standard elastase perfusion or submersion is commonly observed during murine studies, and future experiments using this syringe pump could remove that variation.

Cell-free delivery cargo, including iron nanoparticle-loaded microparticles containing proteins, exosomes, and free growth factors or peptides could be delivered through the Tri-Syringe device, with the end goal of achieving a therapeutic effect on AAA (ideally, an elastin-targeted therapeutic effect) without the need for live cell injections. As a follow-up for this dissertation work, periaortic delivery and magnetic localization of ASC-SF loaded microparticles (or ASC secreted extracellular vesicles) would be a natural next step.

6.0 Specific Aim 3, Part 2: Elastogenesis Impact of Adipose-Derived Stromal Cell Secreted Extracellular Vesicles on Healthy Adult Smooth Muscle Cells

Clinical translation strategies of adipose derived stromal cell (ASC) secreted factor (ASC-SF) paracrine therapy for small aortic aneurysm will consist of two primary steps: 1) concentrating potent factors within a smaller volume to enable delivery within multiple applications; and 2) ensuring shelf-life of secreted factor components to maximize pro-elastogenic effects induced after delivery. Isolation and elastogenesis evaluation of ASC-secreted extracellular vesicles and exosomes is a key step for both translational outcomes, and would produce a versatile pro-elastogenic therapy for future use by the Vascular Bioengineering Laboratory and Vascular Extracellular Matrix (ECM) Dynamics Laboratory for both regenerative medicine and tissue engineered vascular graft applications.

6.1 Introduction

Adipose-derived stromal cells (ASCs) used as an extracellular matrix (ECM)-targeting therapeutic for small aortic aneurysm has been studied and summarized previously within this dissertation (see **Section 1.4.2** , **Section 1.5**, **Section 2.1**, and **Section 5.1**), with ASC-seeding providing a intercellular signal or depositing a matrix scaffold for vascular applications. While it was initially theorized that ASC subpopulations delivered within these engineering solutions differentiated into functional vascular cells [203], subsequent studies have suggested that ASC secreted factors (ASC-SF) act in a paracrine manner on neighboring vascular host smooth

muscle cells (SMCs) and endothelial cells, specifically pointing to the importance of urokinase-type plasminogen activator [205] and monocyte chemoattractant protein-1 [206] in inflammatory remodeling. ASC-SF are rich in pro-angiogenic [207] and pro-inflammatory growth factors [208] vascular endothelial growth factor (**VEGF**), hepatocyte growth factor (**HGF**), IL-1 β , IL-6, IL-8, and TNF- α , which all play important roles in aneurysmal SMC ECM deposition [193, 209]. Within a murine MFS model, IL-6 induced MMP-9 activity and resultant elastin and collagen degradation, acting as a key regulatory mechanism for aortic dilation [263]. IL-8 has shown high colocalization with lymphocyte infiltration within abdominal AA wall [264], and TNF- α association with fibronectin helps to reverse lymphocyte chemotaxis [265].

Paracrine signaling has been hypothesized as the primary mechanism of action for stromal cell-induced vascular remodeling, as cell seeded vascular grafts retain the donor cells for less than seven days, but remain functional by stimulating immune recruitment and remodeling [206]. Maintaining this paracrine response in a clinically-translatable manner is essential to developing an off-the-shelf non-surgical small AA therapeutic treatment, and this can be achieved through utilization of exosomes and extracellular vesicle (EV)-mediated transfer of ASC secreted factor components.

ASC-derived EVs are secreted in large quantities compared to other cell types [266], providing protection to its cargo of factors from enzymatic degradation [267], and aiding in cellular endocytosis through favorable surface marker interactions to uptake of encapsulated factors [268]. Additionally, EVs aid in the transport of mRNA and miRNA [269, 270], another potent signaling mechanism to regulate cell phenotype, angiogenesis, mature ECM deposition, and immunomodulatory response [270, 271].

Evaluation of ASC-EVs to induce ECM deposition and AA-relevant remodeling would aid in the clinical translation capabilities of ASC secreted factor therapy, and provide potentially increased potency and tailored cargo for customized non-surgical elastin-targeted therapeutics. This study built on the elastogenesis cascade analysis tools established in **Chapter 2.0**, and works to evaluate the elastogenic effects of three additional exogenous treatment groups on healthy adult commercially-purchased ATCC SMCs: a standard EV concentration seen within established ASC-SF therapy (abbreviated **1x EV**), three-fold EV treatment concentration seen within ASC-SF (**3x EV**), and EV-depleted ASC-SF as a treatment group examining debris-free secreted factors (**dEV**).

6.2 Methods

6.2.1 ASC isolation and culture

ASCs were obtained from deidentified waste human adipose tissue collected during body sculpting surgeries of non-smoking, non-diabetic patients under 45 years old at UPMC Presbyterian Hospital (**Figure 2C**). 100ml of human adipose tissue was mechanically minced and digested in collagenase (1mg/mL) and bovine serum albumin (35 mg/mL) (protease free heat shock, Equitech-Bio Inc #BAH65), followed by filtration and heating (one hour in a 37°C shaker bath) [201, 202]. After secondary filtration (0.5mm gauze, ThermoFisher Scientific #22-415-469) to remove large particles, samples were centrifuged at 1000rpm and 4°C for 10 minutes, with pellets resuspended in 10mL of ACK Lysing Buffer (ThermoFisher Scientific #A10492-01). The suspension was passed through a sieve (500µm, pluriSelect #43-50500-01) and

centrifuged again under the same conditions. This ASC pellet was resuspended in “ASC culture media”, consisting of 33% Dulbecco’s Modified Eagles Medium (High Glucose, Gibco #12100046), 33% DMEM/F12 Medium (HEPES, Gibco #12400024), 7.5% fetal bovine serum (FBS, Premium Select Atlanta Biologics #S11550), 0.75% fungizone (Lonza BioWhittaker Antibiotics #BW17836E), 0.75% penicillin streptomycin (10,000 U/mL, ThermoFisher Scientific #15140122), 0.075 μ M Dexamethasone (Sigma-Aldrich #D4902), and 25% Preadipocyte Growth Medium (PromoCell #C-39425). ASC conditioned media (ASC-CM) was collected every 24-72 hours between passage 0 and 1 while cells progressed from 40 to 70% confluence, and immediately frozen at -80°C.

6.2.2 Isolation of ASC secreted exosomes

Collected ASC-CM was initially centrifuged (250xg, 20 minutes at 4°C) to remove any suspended cells, and the supernatant was spun again (2,500xg, 20 minutes at 4°C) to remove any remaining cell debris. Supernatant was filtered through a 0.22 μ m filter (Millipore #SLGPM33RS) to remove any remaining aggregates. Filtrate was divided into six 35mL samples and transferred into six thin-walled ultracentrifuge tubes (Beckman #326823) and weighed to ensure each tube did not deviate by more than 0.1 grams. Subsequent weight adjustments were made using PBS to ensure ultracentrifuge balance.

Sterilized ultracentrifuge tube cases housed each thin-walled tube, and were placed within an SW-28 ultracentrifuge rotor. The rotor was secured within a Beckman L8-70M Ultracentrifuge, and spun at 100,000xg for 70 minutes at 4°C under a sealed vacuum.

Supernatant is removed and stored for exogenous SMC elastogenesis treatment study, labelled EV-depleted conditioned media (**dCM**).

Thin-walled tubes were inverted on a sterile mat for 3 minutes, with residual liquid aspirated, and 100 μ L of cold PBS was added to the pellet and remaining volume (approximately 500 μ L) and incubated at room temperature for 30 minutes. This resuspended EV isolate, 600 μ L in total of crude EVs suspended in PBS, was stored in a sterile Eppendorf tube at 4°C until use and was always used within 5 days of storage.

6.2.3 Transmission electron microscopy to visualize ASC secreted exosome morphology

TEM was performed using a JEM-1011 TEM (JOEL, MA, USA). Briefly, 5 μ L of fresh EV isolate was applied to a 3 mm carbon coated grid and excess liquid was wicked away using filter paper. A 1% uranyl acetate (UA) solution (5 μ L) was applied to the grid to stain lipids and therefore increase contrast of the EV membrane relative to the grid. The UA solution was wicked away using filter paper. The stained EVs on the carbon grids were imaged using the TEM at between 60 and 200x magnification.

6.2.4 Dynamic light scattering of ASC secreted exosomes

Dynamic light scattering (DLS) was performed using a Nano-ZS90 Zetasizer (Malvern Panalytical, UK). Briefly, 80 μ L of Fresh EV isolate was added to an ultra-micro 8.5mm cuvette (Brandtech Scientific, CT, USA). The cuvette was inserted into the zetasizer and allowed to equilibrate to 25°C for 60 seconds prior to particle measurement at an automatically determined

attenuation and duration. EVs were presumed to have the same refractive index and absorption as protein suspended in water. Data was processed using a protein analysis model.

6.2.5 Determination of total protein concentration contained within ASC secreted exosomes

Total protein content of the fresh EV isolate prior to and followed lysis was quantified using a micro bicinchoninic acid (BCA) protein assay (#23225, Thermo Scientific, USA). Briefly, 50µL of fresh EV isolate was diluted to 500µL in either PBS or sodium dodecyl sulfate (SDS, final concentration 2%). Samples were then vortexed for 30 seconds. SDS and vortexing was employed to lyse intact EVs and encourage them to release their encapsulated protein cargo. 150µL of EVs, suspended in either PBS or SDS, were added to the wells of a 96 well plate in triplicate. 150µL of working solution was then added to each well in order to initiate the colorimetric reaction. Two standard curves were also plated in triplicate for bovine serum albumin (BSA) suspended in either PBS or SDS at concentrations ranging from 0 to 200µg/ml). The plate was incubated at 37°C for 2 hours, cooled to room temperature and protein content was quantified using a microplate reader.

6.2.6 Healthy adult SMC culture

Human aortic SMCs (ATCC #PCS-100-012, Manassas, Virginia) were cultured at 37°C and 5% CO₂, with growth media (#311K-500, Cell Applications Inc, San Diego, CA) changes every 48-72 hours. Cells used in experimental cultures were between passages 4 and 12.

6.2.7 Fibrin gel construct formation and culture

SMC-seeded fibrin gel constructs [212, 213] were formed using 3.7mg/mL bovine fibrinogen type I (Sigma-Aldrich #8630), 0.21U/mL bovine thrombin (Sigma-Aldrich #T7513), and 5×10^5 SMCs/mL. ‘Stiff substrate’ 200 μ L fibrin gel constructs (**Figure 2A**) were seeded within heat-stamped circular molds made using 7.94mm (5/16”) diameter cork borers onto tissue-culture treated plastic. “Soft substrate” 600 μ L fibrin gel constructs (**Figure 2B**) were formed between nylon anchors of FlexCell Linear TissueTrain untreated plates (FlexCell Int’l Corp #T-5001U), with “constrained” constructs cultured without external mechanical stimuli. “Dynamic” soft substrate fibrin gel constructs were subjected to a 10% stretch at 1 Hertz cyclic uniaxial mechanical loading using a FlexCell FX-4000 strain unit, to mimic standard aortic cardiovascular conditions [214]. Aminocaproic acid (ACA) (Sigma-Aldrich #07260), a lysine-mimicking fibrinolysis inhibitor, was added at 12mM to inhibit cell-driven degradation of the fibrin gel constructs. Treatment changes (see: “Media treatment conditions”) were made every 48-72 hours, beginning 24 hours after initial gel polymerization and continuing through harvest at 20- or 30-days post-fabrication.

6.2.8 Exogenous stimulation treatment groups

No Treatment (NT) was standard SMC growth media, used to initially culture SMCs. Non-conditioned media (NCM) was made using a 1:1 ratio of the ‘ASC culture media’ and SMC growth media. ASC secreted factors (ASC-SF) were prepared by mixing freshly-thawed ASC conditioned media at a 1:1 ratio with SMC growth media. All fibrin gel culture and treatment

conditions were supplemented with 12mM ACA for fibrinolysis inhibition to preserving the 3D SMC constructs.

6.2.9 SMC proliferation analysis

An Alamar blue assay was used to quantify the effect of EVs on SMC proliferation. Briefly, 15k ATCC SMC suspended in 500 μ L of supplemented basal media were plated in each well of a 48 well plate. After 18 hours, the media on the cells was removed and a mixture of 300 μ L unsupplemented basal media and 30 μ L alamar blue reagent was added to each well. After 4 hours of incubation at 37°C, the mixture was removed and a baseline value for cell proliferation was measured using a plate reader. Treatments were added to each well of the plate (150 μ L treatment + 150 μ L unsupplemented basal media). The plate was incubated for 24 hours at 37°C after each treatment was removed and a mixture of 300 μ L unsupplemented basal media and 30 μ L alamar blue reagent was added to each well. After 4 hours of incubation at 37°C, the mixture was removed and a final value for cell proliferation was measured using a plate reader. SMC proliferation is presented as the absorbance of the final reading relative to the absorbance of the baseline reading.

6.2.10 SMC scratch assay migration analysis

SMCs were seeded within a 24 well tissue culture treated plate, at 5.5×10^4 cells per well, and cultured for 24-36 hours in standard culture media before being used in the scratch assay. Prior to scratch, culture media was removed, and cells were washed once in 0.5mL sterile 1xHBSS. CellTracker Red CMTPX Dye (#C34552, Invitrogen) was diluted to 10mM in DMSO,

diluted further to 20 μ M in unsupplemented SMC basal media (#311K-500, Cell Applications Inc), and added to each well after wash (150 μ L per well) for a 20-minute incubation at 37°C and 5% CO₂.

Following incubation, 350 μ L per well of SMC growth supplemented media was added slowly down the walls of each well, without removing CellTracker and disturbing the bed of SMCs. A scratch is then created by moving a sterile 1mL plastic pipette tip from the top to the bottom of each 24 well plate, without allowing the pipette tip to skip or scratch the tissue culture plate surface. CellTracker-rich media is then slowly removed via manual pipetting at the endpoint site of the scratch. Each well then received 250 μ L of unsupplemented SMC basal media, orthogonal to each scratch and slowly down the side of each well's wall. 250 μ L of each treatment group was then added, as summarized below.

Treatment groups included: (1) a No Treatment (NT) positive control of SMC growth supplemented media; (2) ASC-SF, by adding 250 μ L of freshly-thawed ASC conditioned media; (3) NCM; and (4) Unsupplemented SMC basal media.

The lid was placed onto the 24 well plate and taken to the Thoracic Aortic Disease Research Lab (McGowan Institute for Regenerative Medicine, Pittsburgh PA 15219) for imaging on a Nikon TE2000-E Inverted Fluorescence Eclipse Microscope with Intensilight System E, within a Tokai Hit Microscope Stage Top Incubator for Live Cell Imaging (37°C and 5% CO₂). Images were taken every 2 hours for a 36-hour incubation period, with scratch area evaluated using image processing package Fiji (ImageJ, open source). Wound closure percentage was defined as [(initial scratch area – timepoint scratch area) / initial scratch area].

6.2.11 qPCR analysis of tropoelastin and elastin chaperone transcription

Following sonication of frozen fibrin gel constructs, RNA collection (illustra RNAspin Mini Kit, GE Healthcare Life Sciences #25050070) and RNA concentration quantification (BioTek Take3) was performed. After pre-heating template (65°C, 5 minutes), synthesis of first-strand cDNA used SuperScript IV First-Strand Synthesis System (Invitrogen #18091050) (23°C/10 minutes, 55°C/10 minutes, 80°C/10 minutes). RT-qPCR was performed using KiCqStart SYBR Green ReadyMix with ROX (Sigma-Aldrich # KCQS02), and forward/reverse primers listed in **Table 2**. Post-amplification melt curves validated proper amplification.

6.2.12 Ninhydrin and hydroxyproline protein analysis of insoluble elastin and total collagen

Fibrin gel constructs, frozen at -80°C following culture without fixation, were thawed immediately before base hydrolysis (0.1M NaOH, 1 hour, 98°C) for fibrin gel digestion and solubilization of non-elastin protein, which was separated using subsequent centrifugation to separate insoluble elastin protein from soluble non-elastin protein [216]. Acid hydrolysis (6N HCl, 24 hours, 110°C) solubilized all proteins, and assay quantification on both soluble and insoluble fractions (ninhydrin-based for elastin, hydroxyproline-based for collagen) allow for protein deposition quantification within each 3D construct. Ninhydrin content was detectable using an absorbance reading (at 570nm) after 1-hour incubation with a stannous chloride-based solution within a 56°C water bath.

6.2.13 Mechanical testing of soft substrate SMC fibrin gel constructs

Tensile testing was performed as previously described in **Section 2.2.10** . Constructs were harvested, without fixation, by cutting the pair of nylon tabs within the Linear TissueTrain plates to keep each gel intact. Tensile testing was performed on all samples, with sample width-to-length ratios holding a mean of 0.216 ± 0.0741 and a range of 0.0263-0.409. 21 out of the 71 samples exceeding the recommended 0.25:1 geometrical guideline [217]; these samples were excluded for final calculations.

A uniaxial tensile testing device (Instron, #5543A, Norwood, MA) was used to assess the mechanical properties of the SMC fibrin gel constructs (as seen in **Figure 25**), with sandpaper-lined pneumatic clamps on the dried nylon tabs to improve grip fidelity [218, 219]. Samples were measured using photos obtained after 0.01N preloading to eliminate slack, as follows: thickness (1.25 ± 0.38 mm NT, 1.13 ± 0.25 mm NCM, 1.15 ± 0.20 mm dEV, 1.25 ± 0.25 mm ASC-SF, 1.10 ± 0.48 mm 1x EV, 1.16 ± 0.18 mm 3x EV), width (2.25 ± 0.58 mm NT, 2.14 ± 0.31 mm NCM, 1.93 ± 0.46 mm dEV, 2.39 ± 0.37 mm ASC-SF, 2.00 ± 0.42 mm 1x EV, 2.01 ± 0.49 mm 3x EV), and gauge length (12.89 ± 2.23 mm NT, 10.74 ± 2.44 mm NCM, 10.31 ± 2.90 mm dEV, 11.06 ± 1.97 mm ASC-SF, 7.86 ± 1.81 mm 1x EV, 10.40 ± 2.64 mm 3x EV) (as seen in **Figure 25A**) (FIJI, public domain).

Mechanical characterization under quasi-static loading utilized a constant 0.1 mm/second crosshead speed extension until failure of the fibrin constructs [220]. Force and displacement values were recorded throughout the test and converted to stress-stretch ratio plots, where – Stretch ratio: $\lambda = L/L_0$; Stress $\sigma = F/A_0$. These measurements were calculated from the sample gauge length in the loaded (L) and unloaded configuration (L_0), along with the force (F) and

original cross-sectional area (A_0) recorded during each mechanical test, using a previously described analysis method [221].

Low and high modulus, defined in in **Section 2.2.10** , are defined as the slope of the linear portion of the mechanical response curve in the low and high stretch regions [222, 223]. This translated to dividing the curves into three equal parts and treating the initial and final thirds of the curve as the low and high stretch regions respectively.

6.2.14 Statistical Analysis

Means comparisons were conducted using individual t-tests or one-way ANOVA with Tukey post-hoc tests, as appropriate. Significance threshold of $\alpha = 0.05$ was set for all presented data, with experimental sample size of tested constructs listed on each figure. IBM SPSS was used for all statistical analysis. All displayed data values written after “ \pm ” are Standard Deviation values.

6.3 Results

6.3.1 Visual characterization of ASC secreted EVs

TEM verified the presence of clusters of exosomes within the isolated EV fraction of ASC-SF, with the presence of dark shading among most of the sample images regardless of magnification (**Figure 48**). Exosomes resembled deflated spheres, clearly visible from side-facing (120x) and front-facing (200x) views.

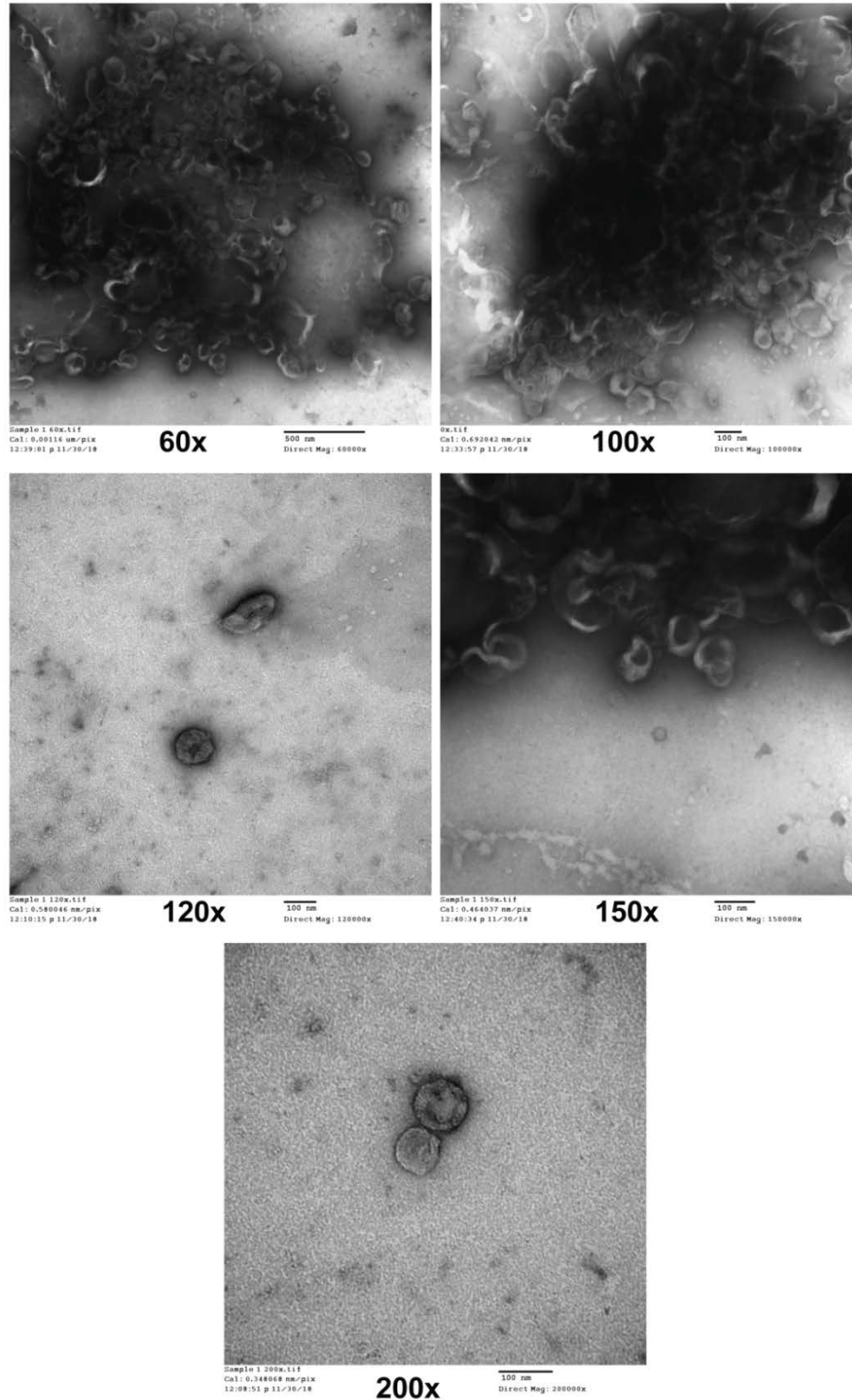


Figure 48: TEM images of ASC secreted EVs.

Visible at 60x, 100x, 120x, 150x, and 200x magnification resolutions, as labelled. Black shadowing is free protein present within the EV isolate resuspension.

6.3.2 Dynamic light scattering size characterization and BCA protein analysis of ASC-EVs

DLS analysis reveals the presence of two particle size populations within the EV isolate. **Figure 49A** displays the intensity-diameter distribution of particles measured during analysis as a percentage of total measured intensity. The initial peak represents particles with an average diameter of approximately 60nm and the second peak represents particles with an average diameter of approximately 300nm, indicative of exosomes and microvesicles respectively. **Figure 49B** displays the number-diameter distribution of particles measured during analysis as a percentage of the total number of particle measurements. The two peaks are reduced to a single peak at 60nm. The single peak in **Figure 49B** indicates that although the EV isolate contains two populations of particle size (exosomes and microvesicles), the exosomes occur far more frequently by number. The peak representing a population of microvesicles is visible in **Figure 49A** and not in **Figure 49B** as larger particles generate larger fluctuations in intensity during analysis.

BCA analysis (**Figure 49C**) reveals that the protein concentration of intact and lysed EV isolate is 887.9 ± 2.2 and $926.3 \pm 2.85 \mu\text{g/ml}$ respectively. This indicates that there is a release of $38.41 \mu\text{g/ml}$ or a 4.32% increase in total protein content following lysis of the EV isolate and supports the preceding TEM and DLS evidence that EVs are present in the EV isolate and they the EVs are encapsulating protein.

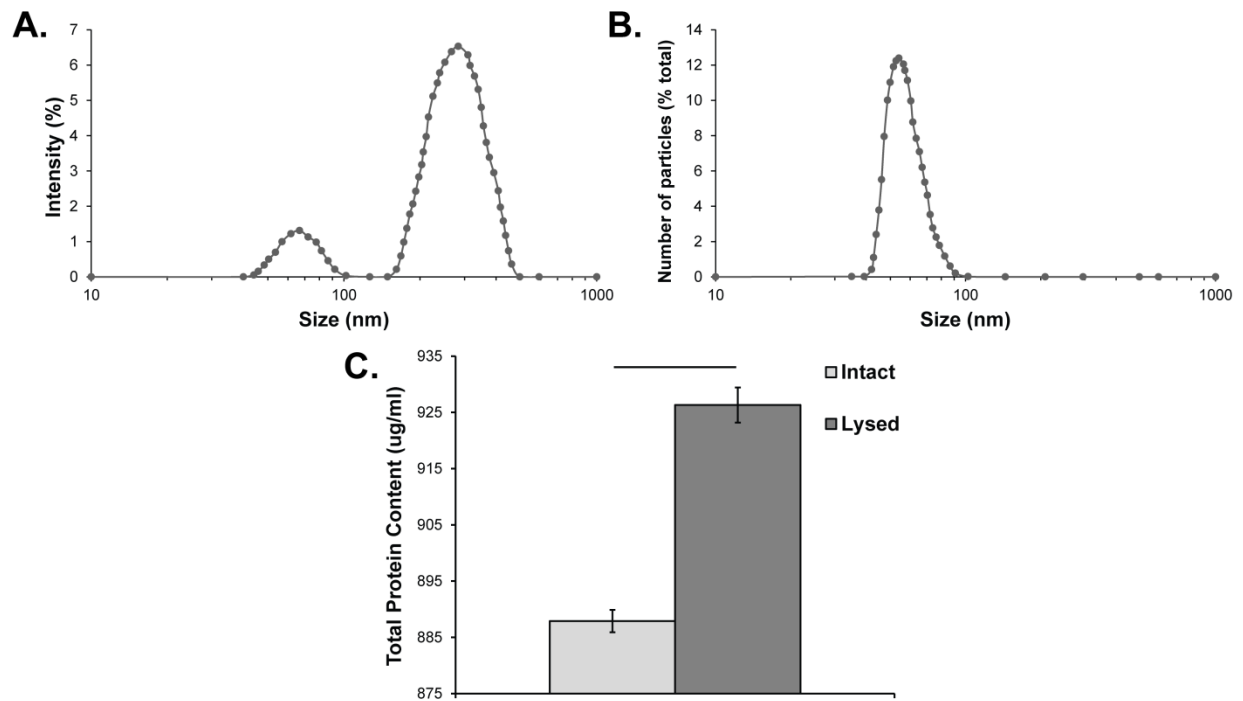


Figure 49: Dynamic light scattering (DLS) characterization of ASC-EVs, and BCA protein analysis of encapsulated protein.

A) Intensity-size characterization of ASC-secreted EVs shows an initial particle diameter population peak at approximately 60nm in diameter (representing exosomes), and a second peak at approximately 300nm (microvesicles).

B) Number of particulate distribution of ASC-EVs shows a single peak at 60nm, indicating a higher frequency of exosomes when compared to microvesicles within ASC-EV isolate.

C) BCA assay showing protein content within intact ASC-EVs and lysed ASC-EVs.

6.3.3 1x EV causes an increase in SMC proliferation, but significantly less than supplemented ASC culture media, full conditioned media, EV-depleted conditioned media, or non-conditioned media

Treating SMCs with 0.2x standard EV concentration (0.2x EV) induced no change on proliferation when compared to unsupplemented basal media (BM) control (0.9064 ± 0.0149 relative intensity units 0.2x EV, vs 0.8422 ± 0.0317 BM). Treatment with 1x EV concentration (1x EV) induced a 14% increase when compared to BM (0.9631 ± 0.0157 1xEV). Both EV-based treatments exhibited proliferation levels significantly lower than supplemented ASC basal media (SBM) positive control (1.187 ± 0.0161), and all groups were significantly increased when compared to PBS-treated negative control (0.7167 ± 0.0497) (**Figure 50A**).

Looking at variations on whole conditioned media, however, showed that non-conditioned media (NCM, 1.293 ± 0.0297), full ASC conditioned media (CM, 1.169 ± 0.0315), and EV-depleted conditioned media (dCM, 1.159 ± 0.0467) were all statistically similar to SBM positive control, and all significantly increased when compared to BM negative control (**Figure 50B**).

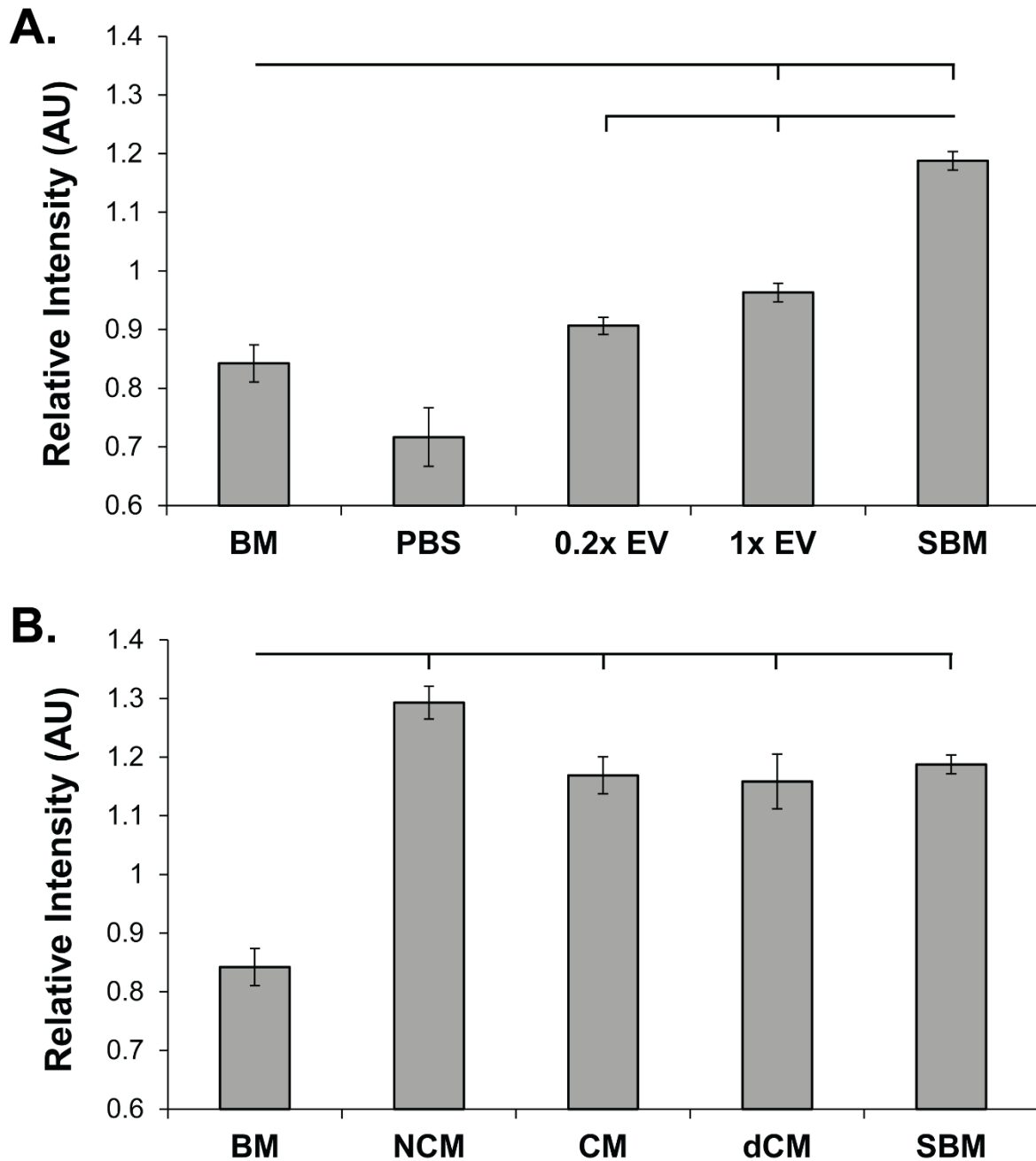


Figure 50: SMC proliferation, via Alamar Blue assay, when treated with ASC-secreted exosomes or full conditioned media.

A) SMC proliferation after treatment with 0.2x EV or 1x EV concentrations, when compared to unsupplemented basal media (BM) and PBS negative control, and supplemented basal media (SBM) positive control.

B) SMC proliferation after treatment with non-conditioned ASC media (NCM), ASC conditioned media (CM), or EV-depleted conditioned media (dCM), compared to BM negative control or SBM positive control. $n = 6$, $\alpha = 0.05$

6.3.4 While all treatment groups slightly accelerate SMC migration only non-conditioned ASC media induces full scratch wound closure

SMC migration after 0.2x EV ($36.95 \pm 2.510\%$ wound closure) and 1x EV ($45.12 \pm 3.776\%$) treatment were significantly increased over both negative control groups BM (22.75 ± 1.678) and PBS (25.32 ± 4.555) (**Figure 51A**). Positive control SBM wound healing migration ($100 \pm 0\%$) saw full wound closure on all repeated wells was significantly higher than both EV treatment groups.

SMC migration after CM treatment ($61.34 \pm 5.501\%$) and dCM treatment ($55.62 \pm 3.399\%$) were both significantly higher than BM negative control and EV-based treatment groups (**Figure 51B**). NCM was the only experimental treatment group that saw full closure ($100 \pm 0\%$) on all wound groups, statistically higher than all experimental and negative control groups and statistically similar to the SBM positive control.

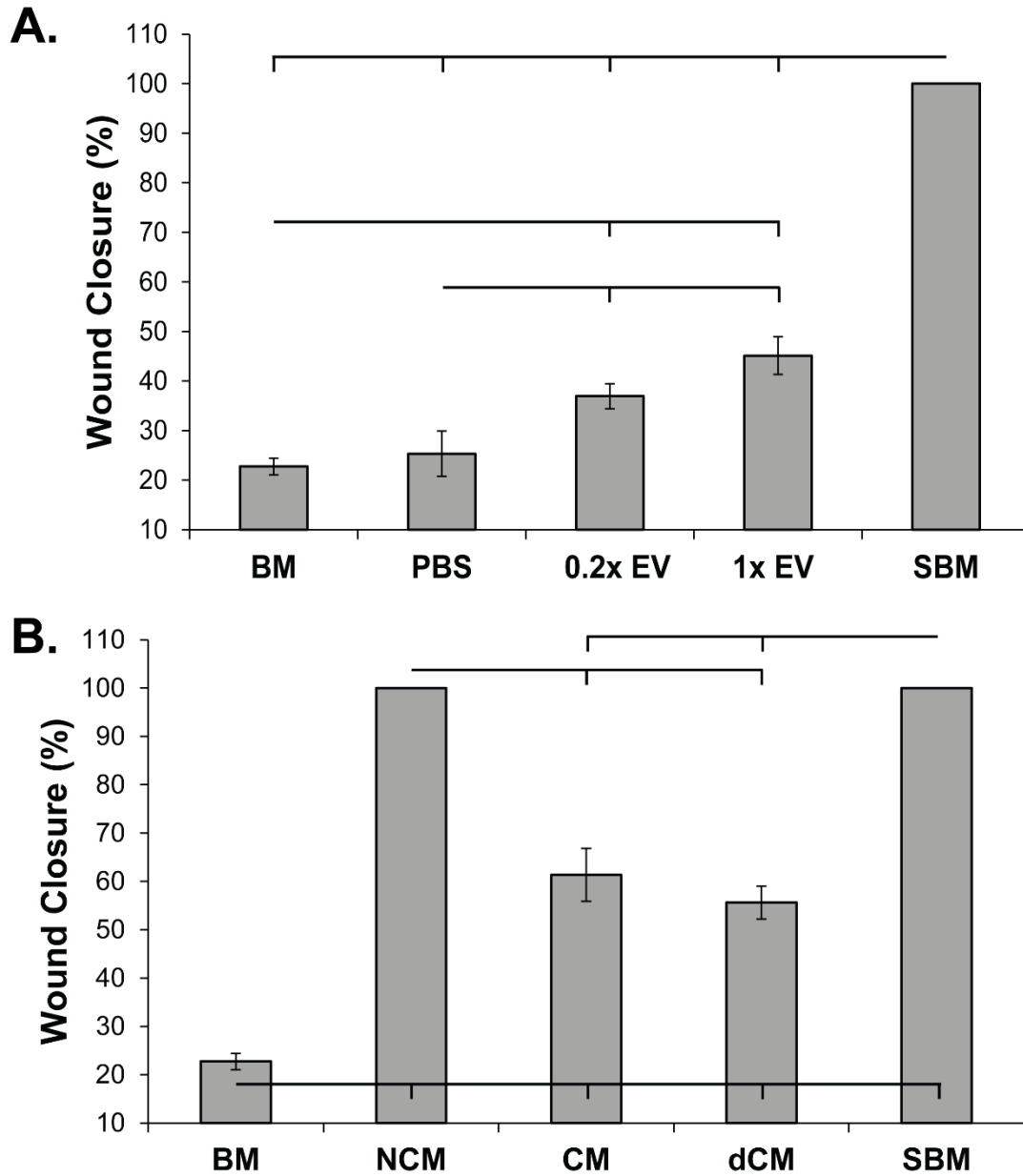


Figure 51: SMC migration, via scratch assay, when treated with ASC-sereted exosomes or full conditioned media.

A) SMC migration after treatment with 0.2x EV or 1x EV concentrations, when compared to unsupplemented basal media (BM) and PBS negative control, and supplemented basal media (SBM) positive control.

B) SMC migration after treatment with non-conditioned ASC media (NCM), ASC conditioned media (CM), or EV-depleted conditioned media (dCM), compared to BM negative control or SBM positive control. $n = 6$, $\alpha = 0.05$

6.3.5 ASC secreted EVs induce an SMC transcriptional increase in organizational proteins fibulin-4 and fibulin-5, and crosslinking protein LOX.

SMC transcription (**Figure 52**) of tropoelastin is significantly decreased when stimulated with either EV-depleted ASC-SF (dSF, 0.3981 ± 0.0390 fold change) or ASC-SF (0.4522 ± 0.0625) when compared to NT control (1 ± 0.0404), a different effect than seen in **Chapter 2.0**. No significant change in tropoelastin deposition was seen in after 30 days of stimulation with NCM (0.8071 ± 0.3740), 1x EV (0.8399 ± 0.4369), or 3x EV (0.9105 ± 0.2985).

Microfibril protein fibrillin-1 transcription was decreased with either NCM (0.8249 ± 0.0371 fold change) or ASC-SF (0.5936 ± 0.1149) treatment when compared to NT control (1 ± 0.0367). No significant difference was seen with dSF (1.139 ± 0.1924), 1x EV (0.7890 ± 0.1521), or 3x EV (1.151 ± 0.0513). 3x EV treatment, however, did induce significantly more fibrillin-1 deposition when compared to both ASC-SF and 1x EV treatment groups.

Elastin organizational protein fibulin-4 transcription was significantly upregulated after dSF (1.607 ± 0.0224), 1x EV (1.371 ± 0.2710), and 3x EV (1.734 ± 0.1987) treatments when compared to NT control (1 ± 0.0385). No significant change was seen with NCM (1.209 ± 0.3167) or ASC-SF (1.000 ± 0.0930). 3x EV induced significantly more fibulin-4 than ASC-SF.

Elastin organizational protein fibulin-5 transcription was significantly increased by all treatment groups when compared to NT control (1 ± 0.1269): NCM (2.636 ± 0.1599), dSF (2.486 ± 0.3724), ASC-SF (1.575 ± 0.1811), 1x EV (2.428 ± 0.2468), and 3x EV (2.447 ± 0.3182). Of those, only ASC-SF was statistically different, producing on average 37% less fibulin-5 than the other treatment groups.

Similarly, transcription of elastin crosslinking protein LOX was significantly increased by all treatment groups when compared to NT control (1 ± 0.0612): NCM (3.089 ± 0.2826), dSF

(2.217±0.2126), ASC-SF (1.351±0.1082), 1x EV (2.325±0.3348), and 3x EV (2.832±1.019). ASC-SF induced 48.3% less LOX, on average, than all other treatment groups.

Elastin crosslinking protein LOXL-1 transcription saw a wide variation after NT treatment (1±0.6322), resulting in a lack of statistically significant difference from other treatment groups. NCM (0.9458±0.2838) and ASC-SF (0.7828±0.0676) groups induced little change in LOXL-1 transcription, while dSF (2.139±0.5221) and 1x EV (1.694±0.1627) groups had higher average expression levels but were statistically similar to NT control. 3x EV expression levels had high deviation (1.273±0.8702), and were statistically similar to NT control.

LTBP-4, elastin coacervate localization protein, was significantly decreased with dSF (0.0417±0.0097), 1x EV (0.3347±0.3101), and 3x EV (0.3446±0.0579) treatments compared to NT control (1±0.0411). Expression levels were statistically similar with NCM (0.5264±0.4453) and ASC-SF (0.3739±0.4922) treatment.

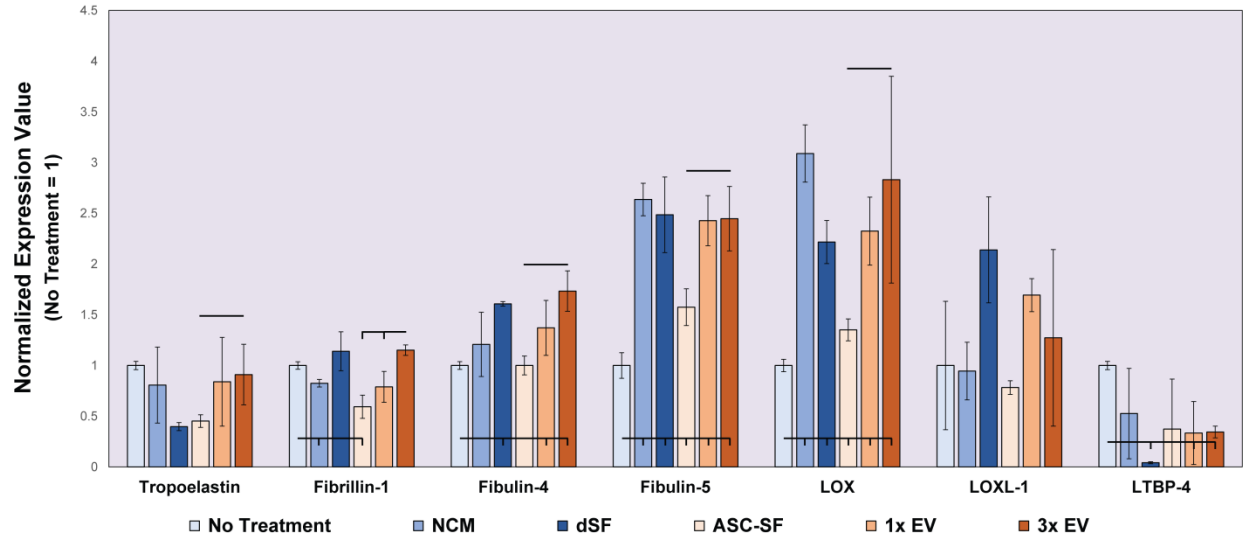


Figure 52: EV-induced SMC transcription analysis of elastin chaperone proteins reveals an increase in organizational proteins fibulin-4 and fibulin-5 and crosslinking protein LOX after treatment with 3x EV concentration.

$n = 4, \alpha = 0.05$ for all.

6.3.6 ASC secreted factors and EVs increase insoluble elastin deposition in stiff substrate

SMC constructs

Insoluble elastin percentage within SMC-embedded constructs (**Figure 53A**) is statistically similar when comparing 30 days of treatment with NT control ($0.0742 \pm 0.0691\%$ elastin of total protein), NCM ($0.0295 \pm 0.0367\%$), and dSF ($0.0440 \pm 0.0372\%$). Statistically significant increases in insoluble elastin deposition are induced after ASC-SF ($0.2698 \pm 0.1182\%$), 1x EV ($0.2521 \pm 0.1025\%$), and 3x EV ($0.2205 \pm 0.0960\%$) treatments. No statistical differences are seen between ASC-SF or either EV-based treatment group.

6.3.7 ASC secreted factors and EVs increase collagen protein deposition in stiff substrate

SMC constructs

Total collagen deposition within SMC-embedded fibrin gel constructs (**Figure 53B**) is statistically similar when comparing NT control ($0.0354 \pm 0.0462\%$ total collagen of total protein) to NCM ($0.1323 \pm 0.0631\%$) and dSF ($0.0950 \pm 0.0310\%$) treatments. A significant increase in total collagen deposition is induced by ASC-SF ($0.1618 \pm 0.0283\%$), 1x EV ($0.2303 \pm 0.0886\%$), and 3x EV ($0.3068 \pm 0.0280\%$) 30-day treatments. Additionally, 3x EV treatment induces significantly more total collagen deposition when compared to ASC-SF.

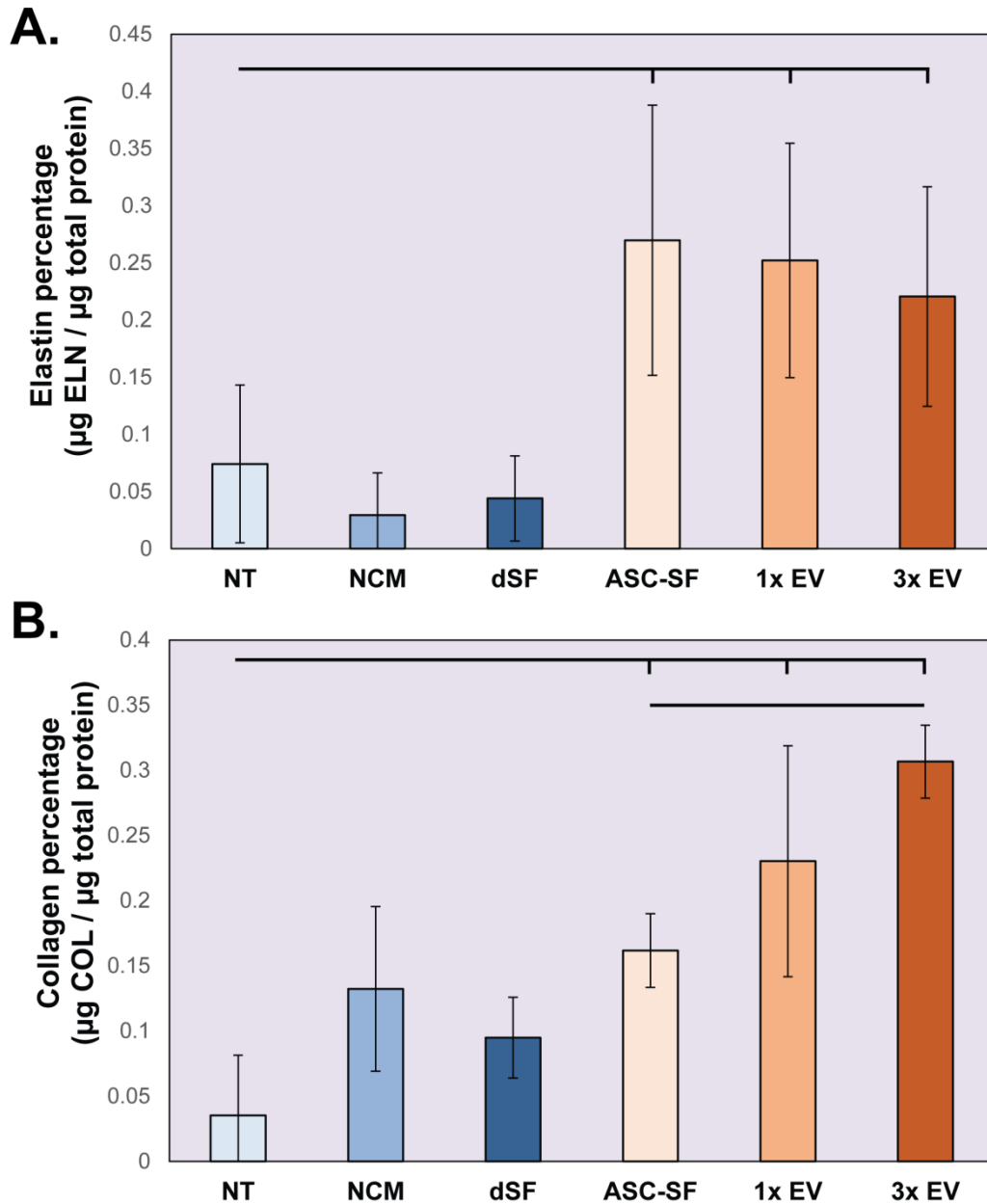


Figure 53: SMC insoluble elastin and collagen deposition is increased after both ASC secreted factor and ASC secreted EV treatment.

A) Insoluble elastin deposition by fibrin construct-embedded SMCs after 30 days of stimulation with No Treatment (NT) control, non-conditioned media (NCM), EV-depleted secreted factors (dSF), ASC secreted factors (ASC-SF), 1x extracellular vesicle treatment (1x EV), or 3x EV treatment. $n=4$, $\alpha = 0.05$.

B) Total collagen deposition by fibrin construct-embedded SMCs after 30 days of stimulation with NT, NCM, dSF, ASC-SF, 1x EV, or 3x EV. $n=4$, $\alpha = 0.05$.

6.3.8 Mechanical activity of SMC ECM following ASC secreted exosome stimulation

High and low modulus, defined as the slope of the given sample's mechanical response curve within the high stretch range (final third of the curve) and low stretch range (first third of the curve), were quantified on SMC constructs plated on soft substrate FlexCell Tissue Train plates.

Due to high variation in the 12 samples of each treatment group, no statistically significant difference was observed in either low or high elastic modulus (**Figure 54**) when compared to NT control (low modulus: 46.74 ± 26.09 kPa; high modulus: 51.99 ± 32.03 kPa). All low modulus values were statistically similar, with no overall trend observed between NCM (100.7 ± 75.60 kPa), dSF (87.19 ± 46.43 kPa), ASC-SF (77.10 ± 37.07 kPa), 1x EV (105.9 ± 82.80 kPa), or 3x EV (103.3 ± 81.04 kPa) treatments.

High modulus values did not produce statistically significant differences among treatment groups NCM (989.69 ± 40.54 kPa), dSF (126.1 ± 74 kPa), ASC-SF (118.6 ± 82.23 kPa), 1x EV (152.7 ± 155.1 kPa), or 3x EV (205.2 ± 243.0 kPa). 3x EV treatments displayed a higher mean and larger variation than all treatment groups and NT control.

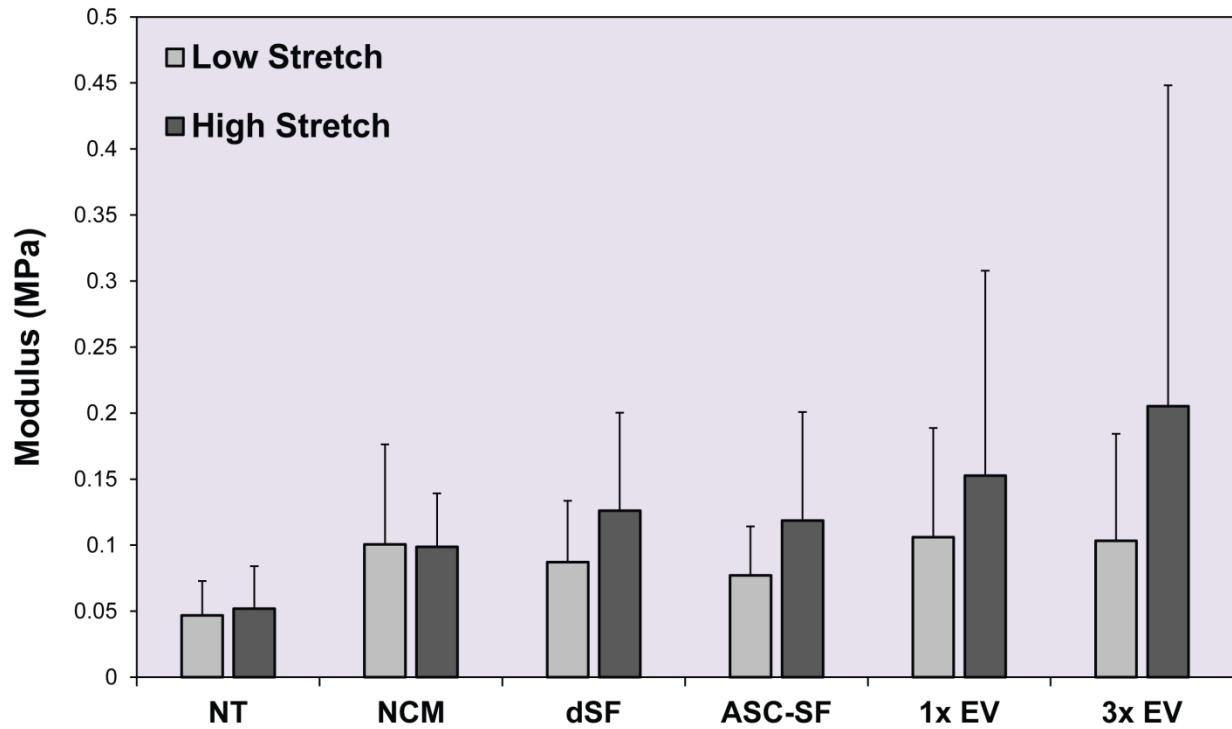


Figure 54: Low and high modulus of ASC secreted exosome-treated SMC fibrin gel constructs.

Comparison of elastic modulus at low stretch and high stretch regions for 30-day soft substrate fibrin gel constructs, stimulated with No Treatment (NT), Non-Conditioned Media (NCM), Exosome-Depleted ASC-SF (dSF), ASC-SF, standard exosome concentration (1x EV), and three-fold exosome concentration (3x EV). Low Stretch and High Stretch modulus was defined as the slope of the mechanical response curve at low and high stretch regions.

$n=12$, $\alpha = 0.05$.

6.3.9 ASC-SF and 1x EV treatments induce increased SMC insoluble elastin deposition, and increased total collagen is induced after ASC-SF, 1x EV, and 3x EV treatment on soft substrate tensile tested fibrin gel constructs

Ninhydrin assays on these tested samples detected a statistically similar level of insoluble elastin (**Figure 55A**) within both non-EV containing treatments when compared to NT control ($0.2087 \pm 0.1333\%$ elastin of total protein): NCM ($0.2025 \pm 0.0904\%$) and dSF (0.2449 ± 0.2322). Statistically increased insoluble elastin was induced by both ASC-SF ($0.9414 \pm 0.6799\%$, $p = 0.015$) and 1x EV ($0.8978 \pm 0.6217\%$, $p = 0.004$). 3x EV produced a statistically similar level of insoluble elastin ($0.6541 \pm 0.3751\%$, $p = 0.137$).

Hydroxyproline assays detected a statistically similar level of total collagen percentage of total protein (**Figure 55B**) within both non-EV containing treatments when compared to NT control ($0.1014 \pm 0.0835\%$ total collagen of total protein): NCM ($0.2064 \pm 0.0577\%$) and dSF ($0.2280 \pm 0.1390\%$). All three EV-containing treatment groups induced a higher level of total collagen deposition when compared to NT control: ASC-SF ($0.5521 \pm 0.1445\%$), 1x EV ($0.3549 \pm 0.0638\%$), and 3x EV ($0.3791 \pm 0.0625\%$).

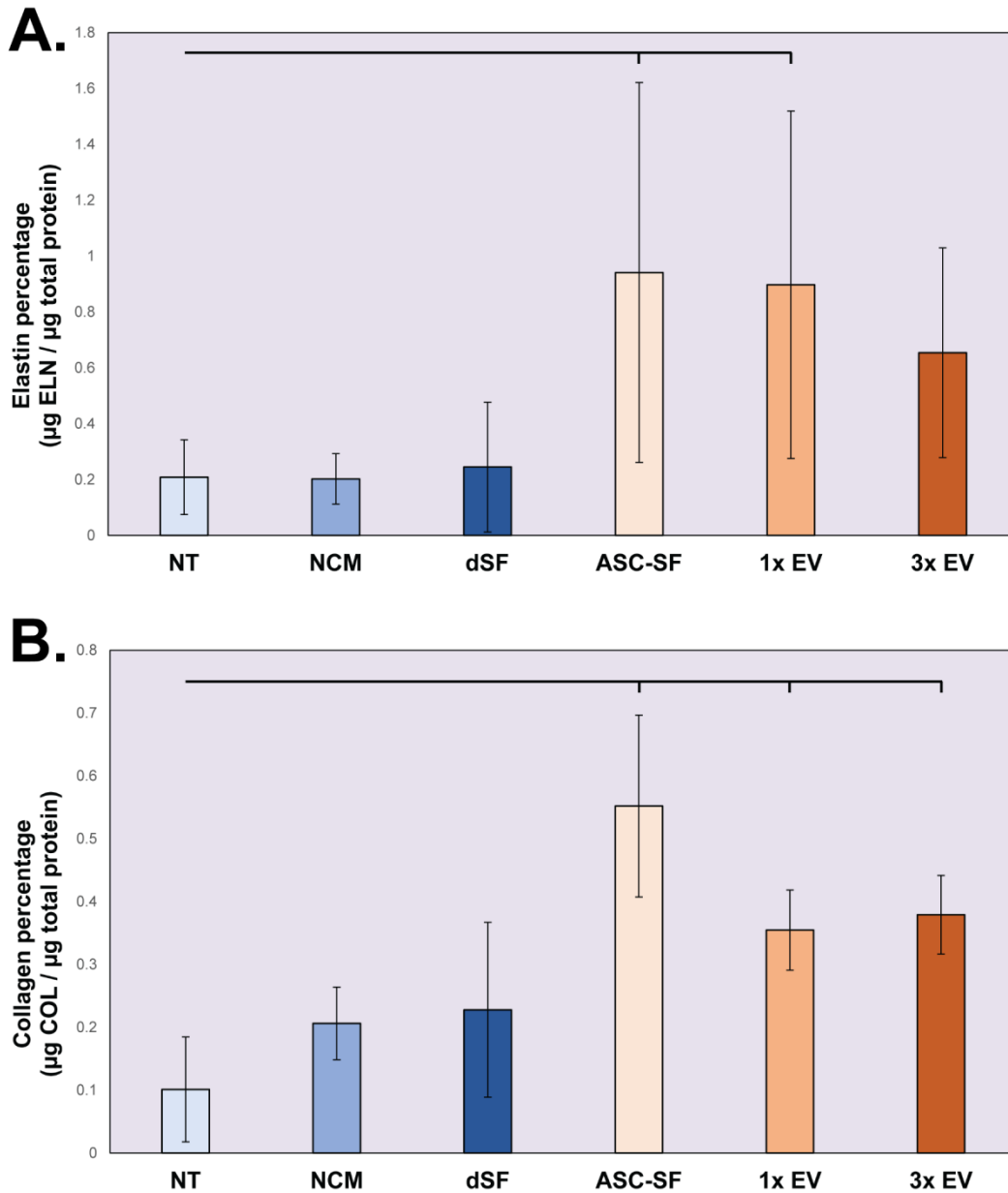


Figure 55: SMC insoluble elastin and collagen deposition on tensile-tested soft substrates are increased after 30 days of EV-containing treatment groups.

A) Insoluble elastin deposition by fibrin construct-embedded SMCs on soft substrates, after 30 days of stimulation with No Treatment (NT) control, non-conditioned media (NCM), EV-depleted secreted factors (dSF), ASC secreted factors (ASC-SF), 1x extracellular vesicle treatment (1x EV), or 3x EV treatment. $n=12$, $\alpha = 0.05$.

B) Total collagen deposition by fibrin construct-embedded SMCs after 30 days of stimulation with NT, NCM, dSF, ASC-SF, 1x EV, or 3x EV. $n=12$, $\alpha = 0.05$.

6.4 Discussion

The results of this study indicate that ASC-secreted EVs can be isolated (**Figure 48**) and contain encapsulated protein (**Figure 49C**), promote SMC migration (**Figure 51A**), and induce the SMC elastogenesis cascade through increased deposition of elastin chaperone proteins (**Figure 52**), and increase SMC insoluble elastin deposition (**Figure 53A, Figure 55A**) and total collagen deposition (**Figure 53B, Figure 55B**).

Isolation of EVs can be performed using centrifugation, immune capture methods, microfluidic size- or density- gradient manipulation sorting and filtration methods, or through precipitation kits that alter EV solubility. Isolation via ultracentrifugation, as done in this study, improves overall EV yield in comparison to filtration-based and immune-based methods, but is susceptible to protein contamination despite additional density-gradient centrifugation steps [272]. Indeed, though ASC-secreted EVs we successfully isolated via ultracentrifugation, the dark shadowing seen in **Figure 48** TEM images indicates the presence of free protein that persisted past each round of high-speed centrifugation. Protein assay levels seen in **Figure 49C** also confirm the presence of free protein, with significant protein content present before EV lysing was performed to release EV-encapsulated protein. Addition of sucrose-based density-gradient substrates still result in this free protein ‘contaminate’, with the possibility of substituting iodixanol for sucrose to utilize its isosmotic properties to improve EV yield while preserving vesicle size, shape, and functionality [273].

SMC migration (**Figure 51**) was reduced with the addition of EVs, as 1x EV and 3x EV treatments were formed by adding isolated EVs to the NCM media treatment. While NCM maintained full SMC wound healing as seen in basal media, the addition of EVs reduced SMC migration to levels seen with free protein-rich CM and dCM conditions. Comparisons between

both EV-rich treatments and EV-free NCM extended to elastogenesis effects, with NCM mimicking induction of elastin transcriptional proteins induced by EVs (**Figure 52**). Free protein presence, due to ‘contamination’ could cause this reduction in migration, which is present in the ultracentrifuge-based EV isolation procedure used in this study.

ASC-SF in this study produced a significantly different effect on SMC elastin chaperone transcription (**Figure 52**) than seen in **Chapter 2.0** of this dissertation (**Figure 17**). Mechanical activity was also reduced using this study’s ASC-SF (**Figure 54**) when compared to **Chapter 2.0** (**Figure 25**). Initially thought to be ASC phenotypic variation, as this study limited secreted factor collection to one patient while **Chapter 2.0** included ASCs from multiple patients, one significant difference between the two studies was EV-depletion of fetal bovine serum used within the “collection media” described in this study. EV depletion intended to isolate all effects seen to ASC-EVs, rather than EVs present within fetal bovine serum used to supplement the culture medium. **Chapter 2.0** used EV-rich serum to culture and collect, as isolating secreted EV effects were not intended as an endpoint of that study.

By comparing ASC-SF and 3x EV treatments, we were able to isolate the effect of increasing EV concentration while limiting free protein levels. 3x EV treatments produced a statistically similar level of insoluble elastin (**Figure 53A**) and a significant increase in total collagen (**Figure 53B**) when compared to ASC-SF, despite increasing transcriptional levels of tropoelastin microfibril fibrillin-1, organizational fibulin-4 and fibulin-5, and crosslinking LOX (**Figure 52**). Insoluble elastin levels might have remained constant due to additional free elastin chaperone proteins present within ASC-SF that were not studied in this study (such as EMILIN-1). However, achieving a statistically similar level of ASC-SF induced elastogenesis by

combining isolated ASC-EVs shows that ECM deposition can be maintained (and, in the case of collagen, enhanced).

6.5 Conclusion

The primary goal of this study was to determine whether the pro-elastogenic effects induced by ASC-SF could be standardized through the isolation and delivery of only ASC-EVs. By successfully isolating patient-derived ASC-EVs, and inducing similar SMC pro-elastogenesis cascade effects seen using ASC-SF, we show that treatment standardization through delivery of only ASC-EVs remains a viable option for future aortic aneurysm regenerative medicine and tissue engineered vascular graft design. Reducing non-surgical small aneurysm treatment to delivery of EVs takes another step towards a cell-free therapeutic option. The stability of EV-encapsulated protein and DNA/miRNAs [274], when compared to free floating counterparts, also points towards a viable EV-based off-the-shelf small aneurysm therapeutic and improved vascular graft design.

6.6 Future Work

Mechanical analysis showed a wide variation of tensile properties in EV-treated constructs seeded on soft substrates (**Figure 54**), which was also seen in insoluble elastin analysis of the same constructs (**Figure 55A**). The higher variability, especially when compared to stiff substrate ECM protein analysis in **Figure 53**, suggest that the forces induced by the

varying substrates play an important role in SMC ECM deposition response even within a 3D fibrin construct. Additionally, the increased volume of treatment needed for soft substrate cultures (1mL for stiff substrates, 4mL for soft substrates) introduces a greater variability of delivered factors to each construct. A standardized method to mix treatments, or reconfiguring soft substrate cultures to use a treatment volume similar to stiff substrates could control this effect for future studies.

Additionally, the variation of EV content between patient-derived ASCs could induce a difference in pro-ECM deposition effects. By analyzing the elastogenic effects of commercially-purchased ASCs, such as those sold by Rooster Bio Inc (Frederick, MD; product #MSC-023), would help standardize EV content and greatly simplify EV generation. Using commercially-available ASCs for EV collection enables a scale-up option for increased *in vivo* studies (and long-term high-volume production of small aneurysm therapeutics).

EVs isolated from alternative cell sources could also prove beneficial within regenerative approaches to treat small aneurysm. Placental EVs derived from amniotic fluid have shown to contain pro-angiogenic regulatory factors [275], endometrial remodeling-inducing matrix metalloproteinases (CD147) and cytokines (interleukin family members) [276], and immunomodulatory and pro-angiogenic paracrine miRNAs [277]. Collaboration to acquire amniotic fluid-derived EVs could present with a potent alternative to adipose tissue.

7.0 Project Summary

Patients with small diameter abdominal aortic aneurysm, a life-threatening dilatation of the aorta induced by the degradation of extracellular matrix protein elastin, are left with “watchful waiting” (imaging every six-to-twelve months) as the standard-of-care. In this work, cellular biology and bioengineering approaches are combined to produce a wide-lens analysis of the elastogenesis cascade after adult aortic smooth muscle cells are stimulated by secreted factors from adipose-derived stromal cells. Our results potentially uncover an elastin-targeted treatment avenue for patients with small aortic aneurysms, acting as a supplement to the currently employed passive monitoring strategy. Additionally, the elastogenesis analysis workflow explored here could guide future mechanistic studies of elastin formation, which in turn could lead to new non-surgical treatment strategies.

7.1 Summary of Results

7.1.1 Specific Aim 1

The overarching goal of Specific Aim 1 was the establishment of a 3D *in vitro* SMC culture platform to enable accurate study of ECM deposition during long-term (20- to 30-day) cultures, establishment of a battery of elastogenesis cascade (**Figure 1**) analysis techniques to capture all facets of mature deposition (including elastin chaperone protein transcription, elastin network formation, insoluble elastin deposition, and mechanical characterization of the 3D

construct), and analysis of a variety of exogenous factors' ability to induce SMC mature elastin deposition. Fibrin gel constructs were successfully used to form two different 3D culture formats (**Figure 2**): (1) circular constrained constructs plated on a stiff substrate and (2) elongated constructs plated on flexible soft substrates able to be mechanically stimulated via cyclic uniaxial loading. Rat fetal lung fibroblasts were used to establish elastogenesis cascade analysis tools (**Figure 4, Figure 5, Figure 6, Figure 8**), and both TGF- β 1 and ASC-SF were used to stimulate embedded SMCs to deposit mature elastin (**Figure 14**). ASC-SF successfully induced deposition of tropoelastin and related elastin chaperone proteins (**Figure 17**), increased network formation (**Figure 21, Figure 22**), increased insoluble elastin and total collagen within the fibrin construct (**Figure 23, Figure 24**), and increased high elastic modulus of the constructs (**Figure 25**).

7.1.2 Specific Aim 2

The goal of Specific Aim 2 was to evaluate the impact of ASC-SF on select aspects of the elastogenesis cascade, using patient-derived cells from at-risk aneurysmal aortic medial layers.

Part 1 focused on adult-derived aneurysmal SMCs provided by the Thoracic Aortic Disease Research laboratory under the direction of Thomas Gleason MD, from Marfan syndrome thoracic aortic aneurysm, bicuspid aortic valve thoracic aortic aneurysm, and tricuspid aortic valve aortic aneurysm (alongside healthy control SMC lines). Two lines of Marfan syndrome showed an elastogenesis muting effect after treatment with either TGF- β 1 or ASC-SF stimulation (**Figure 26, Figure 27**). TGF- β 1 stimulation had a similar muting effect on tricuspid aortic valve SMCs (**Figure 28**). Bicuspid aortic valve aneurysmal SMCs showed increased insoluble elastin and total collagen deposition with either ASC-SF or Non-Conditioned Media

(NCM) stimulation, with NCM effects also holding for late culture Marfan SMCs (**Figure 29, Figure 30, Figure 31**).

Part 2 focused on the dilated aortic medial layer cells from pediatric cells, sourced from Victor Morell, MD and the Division of Cardiothoracic Surgery at the UPMC Children's Hospital of Pittsburgh. Tissue was successfully transferred from the Children's Hospital to the Vascular Bioengineering Laboratory, with cells successfully isolated from both medial and adventitial aortic layers using a modified tissue digestion and culture protocol (**Figure 32**). Cell lines were successfully cultured and stored from explanted dilated aortas from ten patients (**Table 3**), with three medial layer cell lines integrated within the 3D fibrin construct system, treated with ASC-SF for 30 days, and evaluated for elastogenesis response. While 2-year-old medial layer cells increased elastin chaperone protein transcription and insoluble elastin deposition, collagen response was muted with ASC-SF treatment (**Figure 33, Figure 34**). 11-year-old medial layer cells stimulated with ASC-SF saw increased elastin chaperone protein transcription and insoluble elastin deposition without muting collagen (**Figure 35, Figure 36**). 15-year-old medial layer cells produced less overall ECM and saw slight increases in transcriptional and insoluble elastin when stimulated with ASC-SF (**Figure 37, Figure 38**).

7.1.3 Specific Aim 3

The goal of Specific Aim 3 was to begin clinical translation steps for ASC and ASC-SF based therapeutic strategies for small aortic aneurysm.

Part 1 concerned the development of a modified delivery system for fibrin gel constructs containing therapeutic cargo of choice, and the evaluation of magnetic localization and subsequent securement using the fibrin hydrogel delivery mechanism. A successful Tri-Syringe

device (**Figure 40, Figure 41**) was iterated and used during an *in vivo* study to localize iron nanoparticle-loaded adipose-derived mesenchymal stem cells to the periaortic surface of an elastase-induced murine abdominal aortic aneurysm. Magnetic localization was successful *in vitro* regardless of magnetic direction and with the presence of a surgical sponge for fibrin delivery (**Figure 43, Figure 44, Figure 46**). Initial results suggest magnetic localization plays a role in *in vivo* localization to the murine abdominal aortic aneurysm (**Figure 47**), but further study is needed to determine if treatment efficacy is improved with this improved localization.

Part 2 concerned the simplification of ASC-SF therapy to exosomes and extracellular vesicles secreted by ASCs (ASC-EVs) (**Figure 48**), and the elastogenic potential of ASC-secreted exosomes on healthy adult aortic SMCs. ASC-EVs induced an increase in elastin chaperone protein transcription (**Figure 52**) and insoluble elastin fraction (**Figure 53, Figure 55**) on both stiff and soft substrates, but did not have a significant effect on the mechanical response of the construct (**Figure 54**).

7.2 Summary of Accomplishments

This dissertation work resulted in production of the following academic manuscripts:

1. Krawiec JT, Weinbaum JS, Liao HT, **Ramaswamy AK**, Pezzone DJ, Josowitz AD, D'Amore A, Rubin JP, Wagner WR, Vorp DA. In Vivo Functional Evaluation of Tissue-Engineered Vascular Grafts Fabricated Using Human Adipose-Derived Stem Cells from High Cardiovascular Risk Populations. *Tissue Engineering Part A*. May 2016, 22(9-10): 765-775. doi:10.1089/ten.tea.2015.0379.

2. **Ramaswamy AK**, Vorp DA, Weinbaum. Functional Vascular Tissue Engineering Inspired by Matricellular Proteins. *Frontiers in Cardiovascular Medicine*. [in revision]
3. **Ramaswamy AK**, Sides RE, Cunnane EM, Lorentz KL, Reines LM, Vorp DA, Weinbaum JS. Adipose-derived stromal cell secreted factors induce elastogenesis within 3D aortic smooth muscle cell constructs. [under review]
4. **Ramaswamy AK** & Cunnane EM, et al. Elastogenesis effect of secreted exosomes on aortic smooth muscle cells: primary versus commercial adipose stromal cells. [in preparation]
5. Gupta P, Lorentz KL, Haskett DG, Cunnane EM, **Ramaswamy AK**, Weinbaum JS, Vorp DA, Mandal BB. Bioresorbable silk grafts for small diameter vascular tissue engineering applications: In vitro and In vivo functional analysis. [in preparation]
6. **Ramaswamy AK**, et al. Elastogenesis analysis of dilated medial aortic layer cells after long-term adipose-derived stromal cell secreted factor stimulation. [in preparation]
7. Cunnane EM, et al. Exosome-functionalized silk scaffolds for tissue engineered vascular applications. [in preparation]

The following patent application was filed as a result of the work in **Chapter 5.0**:

1. Vorp DA, **Ramaswamy AK**, Weinbaum JS, Blose KJ, Chung TK, Kickliter T, Baruch Y. Magnetic Delivery System and Hydrogel Fixative for Therapeutic Cells. US Patent Application No. 62/747,767. Oct 19, 2018.

The following research grants and fellowships were earned by the author or by mentored students during the completion of this dissertation:

1. **NIH T32 HL094295.** “Impact of Adipose-Derived Mesenchymal Stem Cell Conditioned Media on Aortic Smooth Muscle Cell Elastin Deposition”, 9/2014 – 8/2015. [Training fellowship to Aneesh Ramaswamy]
2. **McCune Foundation Pediatric Device Initiative grant.** “Improved Elastogenesis for Pediatric Patients with Genetic Defects of the Aorta”, 8/2016 – 6/2017. PIs: Dr. David Vorp & Dr. Victor Morell.
3. **Leonard H. Berenfield Graduate Fellowship in Cardiovascular Engineering.** “Impact of Mesenchymal Stem Cell Secreted Factors on the Secretion and Organization of Elastic Fibers within Pediatric Thoracic Aortic Aneurysms”, 9/2016 – 8/2017. PIs: Dr. David Vorp & Dr. Justin Weinbaum. [Predoctoral fellowship to Aneesh Ramaswamy]
4. **Undergraduate Summer Research Internship Scholarship,** Swanson School of Engineering, University of Pittsburgh, 6/2017 – 8/2017. [Summer fellowship to Rachel Sides (mentored undergraduate student)]
5. **International Studies Fund,** University Center for International Studies, University of Pittsburgh, 6/2017 – 8/2017. PIs: Dr. David Vorp & Dr. Hiromi Yanagisawa (University of Tsukuba). [Summer fellowship to Rachel Sides (mentored undergraduate student)]

The following awards were earned during the completion of this dissertation:

1. **Outstanding Poster in Tissue Engineering.** Smooth Muscle Cell Elastin Generation Stimulated by Adipose-Derived Mesenchymal Stem Cells. McGowan Institute Scientific Retreat. Mar 9, 2015 (Farmington, PA).
2. **University of Pittsburgh co-representative.** American Association for the Advancement of Science (AAAS) Catalyzing Advocacy in Science and Engineering 2017 Workshop. Apr 2-5, 2017 (Washington DC).
3. **University of Pittsburgh co-representative.** American Institute for Medical and Biological Engineering (AIMBE) Public Policy Institute for Rising Leaders 2017. Oct 30-31, 2017 (Washington, DC).
4. **Graduate Student Honoree.** Understanding Science Funding, Advocacy, & Communication. Bioengineering Student Awards Seminar. Dec 7, 2017 (Pittsburgh, PA).
5. **2nd Place, American Society for Mechanical Engineering – Bioengineering Division PhD Level Student Paper Competition.** Improved Adult & Pediatric Aortic Elastogenesis Driven by Adipose-Derived Mesenchymal Stem Cell Secreted Factors. 8th World Congress of Biomechanics, July 10, 2018 (Dublin, Ireland).
6. **2nd place, 3 Minute Thesis Competition.** Elastogenesis for Aortic Aneurysms. Swanson School of Engineering, University of Pittsburgh. May 20, 2019 (Pittsburgh, PA).

7.3 Future Work

Future directions for each project within this dissertation work are summarized at the conclusion of each chapter. Future directions for Specific Aim 1 can be found in **Section 2.6**, for Specific Aim 2 Part 1 in **Section 3.6**, for Specific Aim 2 Part 2 in **Section 4.6**, for Specific Aim 3 Part 1 in **Section 5.6**, and for Specific Aim 2 Part 2 in **Section 6.6**.

Bibliography

- [1] S. Hinderer *et al.*, "In vitro elastogenesis: instructing human vascular smooth muscle cells to generate an elastic fiber-containing extracellular matrix scaffold," *Biomedical Materials*, vol. 10, no. 3, Jun 2015, Art. no. 034102.
- [2] C. L. Papke and H. Yanagisawa, "Fibulin-4 and fibulin-5 in elastogenesis and beyond: Insights from mouse and human studies," *Matrix Biology*, vol. 37, pp. 142-149, Jul 2014.
- [3] M. Hirai *et al.*, "Fibulin-5/DANCE has an elastogenic organizer activity that is abrogated by proteolytic cleavage in vivo," *Journal of Cell Biology*, Article vol. 176, no. 7, pp. 1061-1071, Mar 2007.
- [4] M. J. Underwood, G. El Khoury, D. Deronck, D. Glineur, and R. Dion, "The aortic root: structure, function, and surgical reconstruction," *Heart (British Cardiac Society)*, vol. 83, no. 4, pp. 376-380, 2000.
- [5] M. Drexler, R. Erbel, U. Müller, N. Wittlich, S. Mohr-Kahaly, and J. Meyer, "Measurement of intracardiac dimensions and structures in normal young adult subjects by transesophageal echocardiography," *The American Journal of Cardiology*, vol. 65, no. 22, pp. 1491-1496, 1990/06/15/ 1990.
- [6] J. Xu and G.-P. Shi, "Vascular wall extracellular matrix proteins and vascular diseases," *Biochimica et Biophysica Acta (BBA) - Molecular Basis of Disease*, vol. 1842, no. 11, pp. 2106-2119, 2014/11/01/ 2014.
- [7] J. E. Wagenseil and R. P. Mecham, "Vascular extracellular matrix and arterial mechanics," *Physiol Rev*, vol. 89, no. 3, pp. 957-89, Jul 2009.
- [8] E. Ladich, J. Butany, and R. Virmani, "Chapter 5 - Aneurysms of the Aorta: Ascending, Thoracic and Abdominal and Their Management," in *Cardiovascular Pathology (Fourth Edition)*, L. M. Buja and J. Butany, Eds. San Diego: Academic Press, 2016, pp. 169-211.
- [9] R. Bar-Shavit, A. Eldor, and I. Vlodaysky, "Binding of thrombin to subendothelial extracellular matrix. Protection and expression of functional properties," *The Journal of clinical investigation*, vol. 84, no. 4, pp. 1096-1104, 1989.
- [10] D. M. Milewicz *et al.*, "Genetic basis of thoracic aortic aneurysms and dissections: Focus on smooth muscle cell contractile dysfunction," *Annual Review of Genomics and Human Genetics*, vol. 9, pp. 283-302, 2008.

- [11] A. C. Zannettino *et al.*, "Multipotential human adipose-derived stromal stem cells exhibit a perivascular phenotype in vitro and in vivo," *J Cell Physiol*, vol. 214, no. 2, pp. 413-21, Feb 2008.
- [12] C. Fleming, E. P. Whitlock, T. L. Bell, and F. A. Lederle, "Screening for abdominal aortic aneurysm: A best-evidence systematic review for the US Preventive Services Task Force," *Annals of Internal Medicine*, vol. 142, no. 3, pp. 203-211, Feb 2005.
- [13] E. Gillis, L. Van Laer, and B. L. Loeys, "Genetics of Thoracic Aortic Aneurysm: At the Crossroad of Transforming Growth Factor- Signaling and Vascular Smooth Muscle Cell Contractility," *Circulation Research*, vol. 113, no. 3, pp. 327-340, Jul 2013.
- [14] K. C. Kent *et al.*, "Analysis of risk factors for abdominal aortic aneurysm in a cohort of more than 3 million individuals," *Journal of Vascular Surgery*, vol. 52, no. 3, pp. 539-548, Sep 2010.
- [15] K. C. Kent, "Abdominal Aortic Aneurysms," *New England Journal of Medicine*, vol. 371, no. 22, pp. 2101-2108, Nov 2014.
- [16] L. L. Hoornweg, M. N. Storm-Versloot, D. T. Ubbink, M. J. W. Koelemay, D. A. Legemate, and R. Balm, "Meta analysis on mortality of ruptured abdominal aortic aneurysms," *European Journal of Vascular and Endovascular Surgery*, vol. 35, no. 5, pp. 558-570, May 2008.
- [17] N. Kontopodis, D. Pantidis, A. Dedes, N. Daskalakis, and C. V. Ioannou, "The - Not So - Solid 5.5 cm Threshold for Abdominal Aortic Aneurysm Repair: Facts, Misinterpretations, and Future Directions," *Frontiers in Surgery*, vol. 3, Jan 2016, Art. no. Unsp 1.
- [18] W. H. Pearce, C. K. Zarins, J. M. Bacharach, and G. Writing, "Atherosclerotic Peripheral Vascular Disease Symposium II Controversies in Abdominal Aortic Aneurysm Repair," *Circulation*, vol. 118, no. 25, pp. 2860-2863, Dec 2008.
- [19] "Underlying Cause of Death 1999-2016 on CDC WONDER Online Database, released December 2017.," N. C. f. H. S. Centers for Disease Control and Prevention, Ed., ed. Vital Statistics Cooperative Program. , 2017.
- [20] L. Faivre *et al.*, "Clinical and Molecular Study of 320 Children With Marfan Syndrome and Related Type I Fibrillinopathies in a Series of 1009 Proband With Pathogenic *FBN1* Mutations," *Pediatrics*, vol. 123, no. 1, pp. 391-398, 2009.
- [21] B. L. Loeys *et al.*, "The revised Ghent nosology for the Marfan syndrome," *Journal of Medical Genetics*, vol. 47, no. 7, pp. 476-485, 2010.

- [22] R. W. Jeremy, H. Huang, J. Hwa, H. McCarron, C. F. Hughes, and J. G. Richards, "Relation Between Age, Arterial Distensibility, and Aortic Dilation in the Marfan-Syndrome," *American Journal of Cardiology*, vol. 74, no. 4, pp. 369-373, Aug 15 1994.
- [23] J. C. S. Dean, "Marfan syndrome: clinical diagnosis and management," *European Journal of Human Genetics*, vol. 15, no. 7, pp. 724-733, Jul 2007.
- [24] K. A. Groth *et al.*, "Prevalence, incidence, and age at diagnosis in Marfan Syndrome," *Orphanet Journal of Rare Diseases*, vol. 10, p. 153, 12/02 09/21/received 11/22/accepted 2015.
- [25] H.-H. Chiu, M.-H. Wu, H.-C. Chen, F.-Y. Kao, and S.-K. Huang, "Epidemiological Profile of Marfan Syndrome in a General Population: A National Database Study," *Mayo Clinic Proceedings*, vol. 89, no. 1, pp. 34-42, January 2014 2014.
- [26] G. MacCarrick *et al.*, "Loeys-Dietz syndrome: a primer for diagnosis and management," *Genet Med*, Special Article vol. 16, no. 8, pp. 576-587, 08//print 2014.
- [27] J. A. Williams *et al.*, "Early Surgical Experience With Loeys-Dietz: A New Syndrome of Aggressive Thoracic Aortic Aneurysm Disease," *The Annals of Thoracic Surgery*, vol. 83, no. 2, pp. S757-S763, 2// 2007.
- [28] J. J. Maleszewski, D. V. Miller, J. Lu, H. C. Dietz, and M. K. Halushka, "Histopathologic Findings in Ascending Aortas From Individuals With Loeys-Dietz Syndrome (LDS)," *American Journal of Surgical Pathology*, vol. 33, no. 2, pp. 194-201, Feb 2009.
- [29] C. Stheneur *et al.*, "Study of phenotype evolution during childhood in Marfan syndrome to improve clinical recognition," *Genet Med*, Original Research Article vol. 16, no. 3, pp. 246-250, 03//print 2014.
- [30] E. Tutar, F. Ekici, S. Atalay, and N. Nacar, "The prevalence of bicuspid aortic valve in newborns by echocardiographic screening," *American Heart Journal*, vol. 150, no. 3, pp. 513-515, 2005/09/01/ 2005.
- [31] I. Mordi and N. Tzemos, "Bicuspid Aortic Valve Disease: A Comprehensive Review," *Cardiology Research and Practice*, vol. 2012, p. 7, 2012, Art. no. 196037.
- [32] C. Ward, "Clinical significance of the bicuspid aortic valve," *Heart*, vol. 83, no. 1, pp. 81-85, 2000.

- [33] R. H. Anderson, S. Webb, N. A. Brown, W. Lamers, and A. Moorman, "Development of the heart: (3) Formation of the ventricular outflow tracts, arterial valves, and intrapericardial arterial trunks," *Heart*, vol. 89, no. 9, pp. 1110-1118, 2003.
- [34] R. O. Bonow *et al.*, "ACC/AHA 2006 Guidelines for the Management of Patients With Valvular Heart Disease," *Circulation*, vol. 114, no. 5, pp. e84-e231, 2006.
- [35] S. Nistri, M. D. Sorbo, M. Marin, M. Palisi, R. Scognamiglio, and G. Thiene, "Aortic root dilatation in young men with normally functioning bicuspid aortic valves," *Heart*, vol. 82, no. 1, pp. 19-22, 1999.
- [36] W. G. Guntheroth, "A Critical Review of the American College of Cardiology/American Heart Association Practice Guidelines on Bicuspid Aortic Valve With Dilated Ascending Aorta," *The American Journal of Cardiology*, vol. 102, no. 1, pp. 107-110, 2008/07/01/ 2008.
- [37] G. Yotsumoto *et al.*, "Congenital bicuspid aortic valve: analysis of 63 surgical cases," *The Journal of heart valve disease*, vol. 7, no. 5, pp. 500-503, 1998/09// 1998.
- [38] P. Stromme, P. G. Bjornstad, and K. Ramstad, "Prevalence estimation of Williams syndrome," *Journal of Child Neurology*, vol. 17, no. 4, pp. 269-271, Apr 2002.
- [39] R. T. Collins, "Cardiovascular Disease in Williams Syndrome," *Circulation*, vol. 127, no. 21, pp. 2125-2134, May 2013.
- [40] R. T. Collins, P. Kaplan, G. W. Somes, and J. J. Rome, "Long-Term Outcomes of Patients With Cardiovascular Abnormalities and Williams Syndrome," *American Journal of Cardiology*, vol. 105, no. 6, pp. 874-878, Mar 2010.
- [41] S. G. Wise and A. S. Weiss, "Tropoelastin," *The International Journal of Biochemistry & Cell Biology*, vol. 41, no. 3, pp. 494-497, 2009/03/01/ 2009.
- [42] B. A. Kozel *et al.*, "Williams syndrome predisposes to vascular stiffness modified by antihypertensive use and copy number changes in NCF1," *Hypertension*, vol. 63, no. 1, pp. 74-9, Jan 2014.
- [43] B. Callewaert *et al.*, "New insights into the pathogenesis of autosomal-dominant cutis laxa with report of five ELN mutations," *Hum Mutat*, vol. 32, no. 4, pp. 445-55, Apr 2011.
- [44] D. Y. Li *et al.*, "Novel arterial pathology in mice and humans hemizygous for elastin," *J Clin Invest*, vol. 102, no. 10, pp. 1783-7, Nov 15 1998.

- [45] C. Baldock *et al.*, "Shape of tropoelastin, the highly extensible protein that controls human tissue elasticity," *Proceedings of the National Academy of Sciences*, vol. 108, no. 11, pp. 4322-4327, 2011.
- [46] M. Zhang, R. A. Pierce, H. Wachi, R. P. Mecham, and W. C. Parks, "An open reading frame element mediates posttranscriptional regulation of tropoelastin and responsiveness to transforming growth factor beta1," *Mol Cell Biol*, vol. 19, no. 11, pp. 7314-26, Nov 1999.
- [47] J. S. Weinbaum *et al.*, "Deficiency in microfibril-associated glycoprotein-1 leads to complex phenotypes in multiple organ systems," *J Biol Chem*, vol. 283, no. 37, pp. 25533-43, Sep 12 2008.
- [48] A. Miyamoto, R. Lau, P. W. Hein, J. M. Shipley, and G. Weinmaster, "Microfibrillar proteins MAGP-1 and MAGP-2 induce Notch1 extracellular domain dissociation and receptor activation," *J Biol Chem*, vol. 281, no. 15, pp. 10089-97, Apr 14 2006.
- [49] T. Massam-Wu *et al.*, "Assembly of fibrillin microfibrils governs extracellular deposition of latent TGF beta," *J Cell Sci*, vol. 123, no. Pt 17, pp. 3006-18, Sep 1 2010.
- [50] A. Schiavinato *et al.*, "EMILIN-3, peculiar member of elastin microfibril interface-located protein (EMILIN) family, has distinct expression pattern, forms oligomeric assemblies, and serves as transforming growth factor beta (TGF-beta) antagonist," *J Biol Chem*, vol. 287, no. 14, pp. 11498-515, Mar 30 2012.
- [51] G. Litteri *et al.*, "Vascular Smooth Muscle Emilin-1 Is a Regulator of Arteriolar Myogenic Response and Blood Pressure," *Arteriosclerosis, Thrombosis, and Vascular Biology*, vol. 32, no. 9, pp. 2178-2184, 2012.
- [52] K. Noda *et al.*, "Latent TGF-beta binding protein 4 promotes elastic fiber assembly by interacting with fibulin-5," *Proceedings of the National Academy of Sciences of the United States of America*, vol. 110, no. 8, pp. 2852-2857, Feb 2013.
- [53] I. Bultmann-Mellin *et al.*, "Modeling autosomal recessive cutis laxa type 1C in mice reveals distinct functions for Ltbp-4 isoforms," *Disease Models & Mechanisms*, vol. 8, no. 4, pp. 403-415, Apr 2015.
- [54] I. B. Robertson, M. Horiguchi, L. Zilberberg, B. Dabovic, K. Hadjiolova, and D. B. Rifkin, "Latent TGF-beta-binding proteins," *Matrix Biology*, vol. 47, pp. 44-53, Sep 2015.

- [55] E. El-Hallous *et al.*, "Fibrillin-1 interactions with fibulins depend on the first hybrid domain and provide an adaptor function to tropoelastin," *Journal of Biological Chemistry*, vol. 282, no. 12, pp. 8935-8946, Mar 2007.
- [56] G. M. Northington, "Fibulin-5: two for the price of one maintaining pelvic support," *Journal of Clinical Investigation*, vol. 121, no. 5, pp. 1688-1691, May 2011.
- [57] J. Aziz *et al.*, "Molecular Mechanisms of Stress-Responsive Changes in Collagen and Elastin Networks in Skin," *Skin Pharmacology and Physiology*, vol. 29, no. 4, pp. 190-203, 2016.
- [58] C. M. Kelleher, S. E. McLean, and R. P. Mecham, "Vascular extracellular matrix and aortic development," *Developmental Vascular Biology*, vol. 62, pp. 153-188, 2004.
- [59] B. Saitow Cassandra, G. Wise Steven, S. Weiss Anthony, J. Castellot John, and L. Kaplan David, "Elastin biology and tissue engineering with adult cells," in *BioMolecular Concepts* vol. 4, ed, 2013, p. 173.
- [60] H. Zhang *et al.*, "Structure and expression of fibrillin-2, a novel microfibrillar component preferentially located in elastic matrices," *J Cell Biol*, vol. 124, no. 5, pp. 855-63, Mar 1994.
- [61] L. Carta *et al.*, "p38 MAPK is an early determinant of promiscuous Smad2/3 signaling in the aortas of fibrillin-1 (Fbn1)-null mice," *J Biol Chem*, vol. 284, no. 9, pp. 5630-6, Feb 27 2009.
- [62] L. Pereira *et al.*, "Targetting of the gene encoding fibrillin-1 recapitulates the vascular aspect of Marfan syndrome," *Nat Genet*, vol. 17, no. 2, pp. 218-22, Oct 1997.
- [63] L. Carta *et al.*, "Fibrillins 1 and 2 perform partially overlapping functions during aortic development," *J Biol Chem*, vol. 281, no. 12, pp. 8016-23, Mar 24 2006.
- [64] F. X. Sicot *et al.*, "Fibulin-2 is dispensable for mouse development and elastic fiber formation," *Mol Cell Biol*, vol. 28, no. 3, pp. 1061-7, Feb 2008.
- [65] Y. Yamauchi, E. Tsuruga, K. Nakashima, Y. Sawa, and H. Ishikawa, "Fibulin-4 and -5, but not Fibulin-2, are Associated with Tropoelastin Deposition in Elastin-Producing Cell Culture," *Acta Histochem Cytochem*, vol. 43, no. 6, pp. 131-8, Dec 29 2010.
- [66] S. de Vega, T. Iwamoto, and Y. Yamada, "Fibulins: multiple roles in matrix structures and tissue functions," *Cell Mol Life Sci*, vol. 66, no. 11-12, pp. 1890-902, Jun 2009.

- [67] S. L. Chapman *et al.*, "Fibulin-2 and fibulin-5 cooperatively function to form the internal elastic lamina and protect from vascular injury," *Arterioscler Thromb Vasc Biol*, vol. 30, no. 1, pp. 68-74, Jan 2010.
- [68] J. A. Spencer *et al.*, "Altered vascular remodeling in fibulin-5-deficient mice reveals a role of fibulin-5 in smooth muscle cell proliferation and migration," *Proc Natl Acad Sci U S A*, vol. 102, no. 8, pp. 2946-51, Feb 22 2005.
- [69] H. Yanagisawa *et al.*, "Fibulin-5 is an elastin-binding protein essential for elastic fibre development in vivo," *Nature*, vol. 415, no. 6868, pp. 168-71, Jan 10 2002.
- [70] J. H. Choi and M. Cho, "Calculations of intermode coupling constants and simulations of amide I, II, and III vibrational spectra of dipeptides," *Chemical Physics*, vol. 361, no. 3, pp. 168-175, Jul 15 2009.
- [71] M. Nakasaki *et al.*, "The matrix protein Fibulin-5 is at the interface of tissue stiffness and inflammation in fibrosis," *Nature Communications*, Article vol. 6, p. 8574, 10/15/online 2015.
- [72] B. Loeys *et al.*, "Homozygosity for a missense mutation in fibulin-5 (FBLN5) results in a severe form of cutis laxa," *Human Molecular Genetics*, vol. 11, no. 18, pp. 2113-2118, 2002.
- [73] M. E. Lindsay and H. C. Dietz, "The genetic basis of aortic aneurysm," *Cold Spring Harbor perspectives in medicine*, vol. 4, no. 9, pp. a015909-a015909, 2014.
- [74] M. Renard *et al.*, "Altered TGF beta signaling and cardiovascular manifestations in patients with autosomal recessive cutis laxa type I caused by fibulin-4 deficiency," *European Journal of Human Genetics*, vol. 18, no. 8, pp. 895-901, Aug 2010.
- [75] J. D. Humphrey and G. A. Holzapfel, "Mechanics, mechanobiology, and modeling of human abdominal aorta and aneurysms," *Journal of Biomechanics*, vol. 45, no. 5, pp. 805-814, Mar 2012.
- [76] D. A. Vorp, "Biomechanics of abdominal aortic aneurysm," *Journal of Biomechanics*, Review vol. 40, no. 9, pp. 1887-1902, 2007.
- [77] A. Tsamis, J. T. Krawiec, and D. A. Vorp, "Elastin and collagen fibre microstructure of the human aorta in ageing and disease: a review," *Journal of the Royal Society Interface*, vol. 10, no. 83, Jun 2013, Art. no. 20121004.

- [78] G. M. Longo, W. F. Xiong, T. C. Greiner, Y. Zhao, N. Fiotti, and B. T. Baxter, "Matrix metalloproteinases 2 and 9 work in concert to produce aortic aneurysms," *Journal of Clinical Investigation*, vol. 110, no. 5, Sep 2002.
- [79] K. Shimizu, R. N. Mitchell, and P. Libby, "Inflammation and cellular immune responses in abdominal aortic aneurysms," *Arteriosclerosis Thrombosis and Vascular Biology*, vol. 26, no. 5, pp. 987-994, May 2006.
- [80] G. Ailawadi, J. L. Eliason, and G. R. Upchurch, "Current concepts in the pathogenesis of abdominal aortic aneurysm," *Journal of Vascular Surgery*, vol. 38, no. 3, pp. 584-588, Sep 2003.
- [81] M. E. Lindsay and H. C. Dietz, "Lessons on the pathogenesis of aneurysm from heritable conditions," *Nature*, vol. 473, no. 7347, pp. 308-316, May 2011.
- [82] A. LopezCandales, D. R. Holmes, S. X. Liao, M. J. Scott, S. A. Wickline, and R. W. Thompson, "Decreased vascular smooth muscle cell density in medial degeneration of human abdominal aortic aneurysms," *American Journal of Pathology*, vol. 150, no. 3, pp. 993-1007, Mar 1997.
- [83] H. C. Dietz, B. Loeys, L. Carta, and F. Ramirez, "Recent progress towards a molecular understanding of Marfan syndrome," *American Journal of Medical Genetics Part C-Seminars in Medical Genetics*, vol. 139C, no. 1, pp. 4-9, Nov 2005.
- [84] B. L. Loeys *et al.*, "A syndrome of altered cardiovascular, craniofacial, neurocognitive and skeletal development caused by mutations in TGFBR1 or TGFBR2," *Nature Genetics*, vol. 37, p. 275, 01/30/online 2005.
- [85] K. J. Na and K.-H. Park, "Multiple aortic operations in loeys-dietz syndrome: report of 2 cases," *The Korean journal of thoracic and cardiovascular surgery*, vol. 47, no. 6, pp. 536-540, 2014.
- [86] C. Boileau *et al.*, "TGFB2 mutations cause familial thoracic aortic aneurysms and dissections associated with mild systemic features of Marfan syndrome," *Nature genetics*, vol. 44, no. 8, pp. 916-921, 2012.
- [87] I. M. B. H. van de Laar *et al.*, "Mutations in SMAD3 cause a syndromic form of aortic aneurysms and dissections with early-onset osteoarthritis," *Nature Genetics*, vol. 43, p. 121, 01/09/online 2011.
- [88] M. Cotrufo *et al.*, "Different patterns of extracellular matrix protein expression in the convexity and the concavity of the dilated aorta with bicuspid aortic valve: Preliminary

- results," *The Journal of Thoracic and Cardiovascular Surgery*, vol. 130, no. 2, pp. 504.e1-504.e9, 2005/08/01/ 2005.
- [89] G. Pepe *et al.*, "Identification of fibrillin 1 gene mutations in patients with bicuspid aortic valve (BAV) without Marfan syndrome," *BMC medical genetics*, vol. 15, pp. 23-23, 2014.
- [90] V. Garg *et al.*, "Mutations in NOTCH1 cause aortic valve disease," *Nature*, vol. 437, p. 270, 07/17/online 2005.
- [91] D.-C. Guo *et al.*, "Mutations in smooth muscle α -actin (ACTA2) lead to thoracic aortic aneurysms and dissections," *Nature Genetics*, vol. 39, p. 1488, 11/11/online 2007.
- [92] C. E. Gacchina, P. Deb, J. L. Barth, and A. Ramamurthi, "Elastogenic inductability of smooth muscle cells from a rat model of late stage abdominal aortic aneurysms," *Tissue engineering. Part A*, vol. 17, no. 13-14, pp. 1699-1711, 2011.
- [93] J. H. Eoh *et al.*, "Enhanced elastin synthesis and maturation in human vascular smooth muscle tissue derived from induced-pluripotent stem cells," *Acta Biomaterialia*, vol. 52, pp. 49-59, 2017/04/01/ 2017.
- [94] K. W. Lee, D. B. Stolz, and Y. D. Wang, "Substantial expression of mature elastin in arterial constructs," *Proceedings of the National Academy of Sciences of the United States of America*, vol. 108, no. 7, pp. 2705-2710, Feb 2011.
- [95] Z. Syedain *et al.*, "Tissue engineering of acellular vascular grafts capable of somatic growth in young lambs," *Nature Communications*, Article vol. 7, p. 12951, 09/27/online 2016.
- [96] N. Thuy-Uyen, A. B. Chris, and K. Vipuil, "Impact of elastin incorporation into electrochemically aligned collagen fibers on mechanical properties and smooth muscle cell phenotype," *Biomedical Materials*, vol. 11, no. 2, p. 025008, 2016.
- [97] T.-H. Chuang, C. Stabler, A. Simionescu, and D. T. Simionescu, "Polyphenol-stabilized tubular elastin scaffolds for tissue engineered vascular grafts," *Tissue engineering. Part A*, vol. 15, no. 10, pp. 2837-2851, 2009.
- [98] C. Thomas-Porch *et al.*, "Comparative proteomic analyses of human adipose extracellular matrices decellularized using alternative procedures," *Journal of Biomedical Materials Research Part A*, vol. 106, no. 9, pp. 2481-2493, 2018/09/01 2018.
- [99] B. Mahesh, G. S. Nanjundaswamy, D. Channe Gowda, and B. Siddaramaiah, "Synthesis of elastin-based polymer and evaluation of its intermolecular interactions with

- hydroxypropyl methylcellulose," *Journal of Applied Polymer Science*, vol. 134, no. 36, p. 45283, 2017.
- [100] S. D. Cushing *et al.*, "Minimally modified low density lipoprotein induces monocyte chemotactic protein 1 in human endothelial cells and smooth muscle cells," *Proceedings of the National Academy of Sciences*, vol. 87, no. 13, pp. 5134-5138, July 1, 1990 1990.
- [101] A. C. Doran, N. Meller, and C. A. McNamara, "Role of smooth muscle cells in the initiation and early progression of atherosclerosis," *Arteriosclerosis Thrombosis and Vascular Biology*, Review vol. 28, no. 5, pp. 812-819, May 2008.
- [102] K. J. Moore and I. Tabas, "Macrophages in the Pathogenesis of Atherosclerosis," *Cell*, Review vol. 145, no. 3, pp. 341-355, Apr 2011.
- [103] D. Gomez and G. K. Owens, "Smooth muscle cell phenotypic switching in atherosclerosis," *Cardiovascular Research*, Review vol. 95, no. 2, pp. 156-164, Jul 2012.
- [104] A. W. Orr, N. E. Hastings, B. R. Blackman, and B. R. Wamhoff, "Complex Regulation and Function of the Inflammatory Smooth Muscle Cell Phenotype in Atherosclerosis," *Journal of Vascular Research*, Review vol. 47, no. 2, pp. 168-180, 2010.
- [105] G. K. Owens, M. S. Kumar, and B. R. Wamhoff, "Molecular regulation of vascular smooth muscle cell differentiation in development and disease," *Physiological Reviews*, Review vol. 84, no. 3, pp. 767-801, Jul 2004.
- [106] E. W. Raines and R. Ross, "Smooth-Muscle Cells and the Pathogenesis of the Lesions of Atherosclerosis," *British Heart Journal*, Article vol. 69, no. 1, pp. S30-S37, Jan 1993.
- [107] Y. J. Geng, Q. Wu, M. Muszynski, G. K. Hansson, and P. Libby, "Apoptosis of vascular smooth muscle cells induced by in vitro stimulation with interferon-gamma, tumor necrosis factor-alpha, and interleukin-1 beta," *Arteriosclerosis Thrombosis and Vascular Biology*, Article vol. 16, no. 1, pp. 19-27, Jan 1996.
- [108] G. K. Owens, "Role of mechanical strain in regulation of differentiation of vascular smooth muscle cells," *Circulation Research*, Editorial Material vol. 79, no. 5, pp. 1054-1055, Nov 1996.
- [109] C. H. Li and Q. B. Xu, "Mechanical stress-initiated signal transduction in vascular smooth muscle cells in vitro and in vivo," *Cellular Signalling*, Review vol. 19, no. 5, pp. 881-891, May 2007.

- [110] F. D. Kolodgie *et al.*, "The thin-cap fibroatheroma: a type of vulnerable plaque - The major precursor lesion to acute coronary syndromes," *Current Opinion in Cardiology*, Review vol. 16, no. 5, pp. 285-292, Sep 2001.
- [111] M. Nakano, J. Stephen, M. A. Kramer, E. Ladich, F. Kolodgie, and R. Virmani, "Insights into the Natural History of Atherosclerosis Progression," in *Atherosclerosis: Clinical Perspectives Through Imaging*, A. J. Taylor and T. C. Villines, Eds.: Springer London, 2013, pp. 3-12.
- [112] S. Choi *et al.*, "TNF- α elicits phenotypic and functional alterations of vascular smooth muscle cells by miR-155-5p-dependent down-regulation of cGMP-dependent kinase 1," *Journal of Biological Chemistry*, vol. 293, no. 38, pp. 14812-14822, September 21, 2018 2018.
- [113] Z. Q. Yan and G. K. Hansson, "Overexpression of inducible nitric oxide synthase by neointimal smooth muscle cells," *Circulation Research*, Article vol. 82, no. 1, pp. 21-29, Jan 1998.
- [114] G. H. Jia, A. Aggarwal, S. H. Tyndall, and D. K. Agrawal, "Tumor necrosis factor- α regulates p27(kip) expression and apoptosis in smooth muscle cells of human carotid plaques via forkhead transcription factor O1," *Experimental and Molecular Pathology*, Article vol. 90, no. 1, pp. 1-8, Feb 2011.
- [115] E. W. Remus *et al.*, "miR181a protects against angiotensin II-induced osteopontin expression in vascular smooth muscle cells," *Atherosclerosis*, vol. 228, no. 1, pp. 168-174, May 2013.
- [116] M. I. Patel, J. Melrose, P. Ghosh, and M. Appleberg, "Increased synthesis of matrix metalloproteinases by aortic smooth muscle cells is implicated in the etiopathogenesis of abdominal aortic aneurysms," *Journal of Vascular Surgery*, vol. 24, no. 1, pp. 82-92, 1996.
- [117] N. Airhart *et al.*, "Smooth muscle cells from abdominal aortic aneurysms are unique and can independently and synergistically degrade insoluble elastin," *Journal of Vascular Surgery*, vol. 60, no. 4, pp. 1033-1042.e5, 2014.
- [118] G. Ailawadi *et al.*, "Smooth muscle phenotypic modulation is an early event in aortic aneurysms," *Journal of Thoracic and Cardiovascular Surgery*, vol. 138, no. 6, pp. 1392-1399, Dec 2009.
- [119] M. Ramella *et al.*, "Relevance of inflammation and matrix remodeling in abdominal aortic aneurysm (AAA) and popliteal artery aneurysm (PAA) progression," *American journal of translational research*, vol. 10, no. 10, pp. 3265-3275, 2018.

- [120] H. Li *et al.*, "Modulation of Immune-Inflammatory Responses in Abdominal Aortic Aneurysm: Emerging Molecular Targets," *Journal of immunology research*, vol. 2018, pp. 7213760-7213760, 2018.
- [121] M. A. Dale, M. K. Ruhlman, and B. T. Baxter, "Inflammatory cell phenotypes in AAAs: their role and potential as targets for therapy," *Arteriosclerosis, thrombosis, and vascular biology*, vol. 35, no. 8, pp. 1746-1755, 2015.
- [122] A. Kapustin *et al.*, "Fibulin-5 binds urokinase-type plasminogen activator and mediates urokinase-stimulated beta1-integrin-dependent cell migration," *Biochem J*, vol. 443, no. 2, pp. 491-503, Apr 15 2012.
- [123] A. R. Albig and W. P. Schiemann, "Fibulin-5 Antagonizes Vascular Endothelial Growth Factor (VEGF) Signaling and Angiogenic Sprouting by Endothelial Cells," *DNA and Cell Biology*, vol. 23, no. 6, pp. 367-379, 2004.
- [124] M.-S. Tsai *et al.*, "Galectin-1 Restricts Vascular Smooth Muscle Cell Motility Via Modulating Adhesion Force and Focal Adhesion Dynamics," *Scientific Reports*, vol. 8, no. 1, p. 11497, 2018/07/31 2018.
- [125] R. Haubner, W. Schmitt, G. Hölzemann, S. L. Goodman, A. Jonczyk, and H. Kessler, "Cyclic RGD Peptides Containing β -Turn Mimetics," *Journal of the American Chemical Society*, vol. 118, no. 34, pp. 7881-7891, 1996/01/01 1996.
- [126] S. Heydarkhan-Hagvall *et al.*, "The effect of vitronectin on the differentiation of embryonic stem cells in a 3D culture system," *Biomaterials*, Article vol. 33, no. 7, pp. 2032-2040, Mar 2012.
- [127] T. Taga *et al.*, "alpha v-Integrin antagonist EMD 121974 induces apoptosis in brain tumor cells growing on vitronectin and tenascin," *Int J Cancer*, vol. 98, no. 5, pp. 690-7, Apr 10 2002.
- [128] K. T. Preissner and U. Reuning, "Vitronectin in Vascular Context: Facets of a Multitalented Matricellular Protein," *Seminars in Thrombosis and Hemostasis*, Article vol. 37, no. 4, pp. 408-424, Jun 2011.
- [129] E. P. Moiseeva, Q. Javed, E. L. Spring, and D. P. de Bono, "Galectin 1 is involved in vascular smooth muscle cell proliferation," *Cardiovasc Res*, vol. 45, no. 2, pp. 493-502, Jan 14 2000.
- [130] I. M. Seropian *et al.*, "Galectin-1 Controls Cardiac Inflammation and Ventricular Remodeling during Acute Myocardial Infarction," *American Journal of Pathology*, Article vol. 182, no. 1, pp. 29-40, Jan 2013.

- [131] S. Hashmi and S. Al-Salam, "Galectin-1: a biomarker of surgical stress in murine model of cardiac surgery," *International journal of clinical and experimental pathology*, vol. 8, no. 6, pp. 7157-7164, 2015.
- [132] D. K. Ball, A. W. Rachfal, S. A. Kemper, and D. R. Brigstock, "The heparin-binding 10 kDa fragment of connective tissue growth factor (CTGF) containing module 4 alone stimulates cell adhesion," *J Endocrinol*, vol. 176, no. 2, pp. R1-7, Feb 2003.
- [133] A. C. Lake, A. Bialik, K. Walsh, and J. J. Castellot, Jr., "CCN5 is a growth arrest-specific gene that regulates smooth muscle cell proliferation and motility," *Am J Pathol*, vol. 162, no. 1, pp. 219-31, Jan 2003.
- [134] A. C. Lake and J. J. Castellot, Jr., "CCN5 modulates the antiproliferative effect of heparin and regulates cell motility in vascular smooth muscle cells," *Cell Commun Signal*, vol. 1, no. 1, p. 5, Nov 24 2003.
- [135] J. G. Castellot, Mark R Simon, Amy R, "Use of CCN5 for treatment of smooth muscle proliferation disorders," USA, 2007.
- [136] J. Sachdeva *et al.*, "Smooth muscle cell-specific Notch1 haploinsufficiency restricts the progression of abdominal aortic aneurysm by modulating CTGF expression," *PLOS ONE*, vol. 12, no. 5, p. e0178538, 2017.
- [137] H. Williams, C. A. Mill, B. A. Monk, S. Hulin-Curtis, J. L. Johnson, and S. J. George, "Wnt2 and WISP-1/CCN4 Induce Intimal Thickening via Promotion of Smooth Muscle Cell Migration," *Arterioscler Thromb Vasc Biol*, vol. 36, no. 7, pp. 1417-24, Jul 2016.
- [138] C. Mill *et al.*, "Wnt5a-Induced Wnt1-Inducible Secreted Protein-1 Suppresses Vascular Smooth Muscle Cell Apoptosis Induced by Oxidative Stress," *Arteriosclerosis, Thrombosis, and Vascular Biology*, vol. 34, no. 11, pp. 2449-2456, 2014.
- [139] C. Mill, J. Y. Jeremy, and S. J. George, "Wnt5A Signalling Promotes VSMC Survival via WISP-2: Consequences for VSMC Viability in Atherosclerotic Plaques," *Heart*, vol. 97, no. 20, pp. 1-2, Oct 2011.
- [140] K. Wallner, C. Li, M. C. Fishbein, P. K. Shah, and B. G. Sharifi, "Arterialization of human vein grafts is associated with tenascin-C expression," *J Am Coll Cardiol*, vol. 34, no. 3, pp. 871-5, Sep 1999.
- [141] T. Ishigaki, K. Imanaka-Yoshida, N. Shimojo, S. Matsushima, W. Taki, and T. Yoshida, "Tenascin-C enhances crosstalk signaling of integrin $\alpha\beta3$ /PDGFR- β complex by SRC

- recruitment promoting PDGF-induced proliferation and migration in smooth muscle cells," *Journal of Cellular Physiology*, vol. 226, no. 10, pp. 2617-2624, 2011.
- [142] T. Kimura *et al.*, "Tenascin-C is expressed in abdominal aortic aneurysm tissue with an active degradation process," *Pathology International*, vol. 61, no. 10, pp. 559-564, Oct 2011.
- [143] T. Kimura *et al.*, "Tenascin C protects aorta from acute dissection in mice," *Scientific Reports*, Article vol. 4, p. 4051, 02/11/online 2014.
- [144] B. Hinz, "The extracellular matrix and transforming growth factor-beta 1: Tale of a strained relationship," *Matrix Biology*, vol. 47, pp. 54-65, Sep 2015.
- [145] C. D. Hartman, B. C. Isenberg, S. G. Chua, and J. Y. Wong, "Vascular smooth muscle cell durotaxis depends on extracellular matrix composition," *Proceedings of the National Academy of Sciences*, p. 201611324, 2016.
- [146] W. Okech, K. M. Abberton, J. M. Kuebel, D. C. Hocking, and I. H. Sarelius, "Extracellular matrix fibronectin mediates an endothelial cell response to shear stress via the heparin-binding, matricryptic RWRPK sequence of FNIII1H," *American Journal of Physiology-Heart and Circulatory Physiology*, vol. 311, no. 4, pp. H1063-H1071, 2016.
- [147] S.-A. Xie *et al.*, "Matrix stiffness determines the phenotype of vascular smooth muscle cell in vitro and in vivo: Role of DNA methyltransferase 1," *Biomaterials*, vol. 155, pp. 203-216, 2018/02/01/ 2018.
- [148] T. Isaji *et al.*, "Improving the Outcome of Vein Grafts: Should Vascular Surgeons Turn Veins into Arteries?," *Ann Vasc Dis*, vol. 10, no. 1, pp. 8-16, Mar 24 2017.
- [149] J. S. Isenberg *et al.*, "Thrombospondin-1 limits ischemic tissue survival by inhibiting nitric oxide-mediated vascular smooth muscle relaxation," *Blood*, vol. 109, no. 5, pp. 1945-52, Mar 1 2007.
- [150] R. A. Majack, S. C. Cook, and P. Bornstein, "Control of smooth muscle cell growth by components of the extracellular matrix: autocrine role for thrombospondin," *Proc Natl Acad Sci U S A*, vol. 83, no. 23, pp. 9050-4, Dec 1986.
- [151] P. Ranjzad, H. K. Salem, and P. A. Kingston, "Adenovirus-mediated gene transfer of fibromodulin inhibits neointimal hyperplasia in an organ culture model of human saphenous vein graft disease," *Gene Ther*, vol. 16, no. 9, pp. 1154-62, Sep 2009.

- [152] K. Bergmann, A. Mańkowska-Cyl, M. Kretowicz, J. Manitius, and G. Sypniewska, "Fibulin-1 is associated with cardiovascular risk in non-obese, non-diabetic individuals," *Folia Medica Copernicana*, vol. 1, no. 1, pp. 18-22, 2013.
- [153] J. Huang *et al.*, "Fibulin-4 deficiency results in ascending aortic aneurysms: a potential link between abnormal smooth muscle cell phenotype and aneurysm progression," *Circulation research*, vol. 106, no. 3, pp. 583-592, 2010.
- [154] C. Zhang *et al.*, "Matricellular protein CCN3 mitigates abdominal aortic aneurysm," *The Journal of clinical investigation*, vol. 126, no. 4, pp. 1282-1299, 2016.
- [155] T. Shimoyama *et al.*, "CCN3 Inhibits Neointimal Hyperplasia Through Modulation of Smooth Muscle Cell Growth and Migration," *Arteriosclerosis Thrombosis and Vascular Biology*, Article vol. 30, no. 4, pp. 675-U80, Apr 2010.
- [156] B. L. Riser, J. L. Barnes, and J. Varani, "Balanced regulation of the CCN family of matricellular proteins: a novel approach to the prevention and treatment of fibrosis and cancer," *Journal of cell communication and signaling*, vol. 9, no. 4, pp. 327-339, 2015.
- [157] T. Ikeda, T. Shirasawa, Y. Esaki, S. Yoshiki, and K. Hirokawa, "Osteopontin Messenger-RNA is Expressed by Smooth Muscle-Derived Foam Cells in Human Atherosclerotic Lesions of the Aorta," *Journal of Clinical Investigation*, vol. 92, no. 6, pp. 2814-2820, Dec 1993.
- [158] H. Gao, M. C. Steffen, and K. S. Ramos, "Osteopontin regulates alpha-smooth muscle actin and calponin in vascular smooth muscle cells," *Cell Biol Int*, vol. 36, no. 2, pp. 155-61, Feb 2012.
- [159] B. Chellan, J. Narayani, and P. S. Appukuttan, "Galectin-1, an endogenous lectin produced by arterial cells, binds lipoprotein(a) [Lp(a)] in situ: relevance to atherogenesis," *Exp Mol Pathol*, vol. 83, no. 3, pp. 399-404, Dec 2007.
- [160] M. Lovett, K. Lee, A. Edwards, and D. L. Kaplan, "Vascularization Strategies for Tissue Engineering," *Tissue Engineering Part B-Reviews*, Review vol. 15, no. 3, pp. 353-370, Sep 2009.
- [161] J. Zhou *et al.*, "Regulation of Vascular Smooth Muscle Cell Turnover by Endothelial Cell-Secreted MicroRNA-126: Role of Shear Stress," *Circulation research*, vol. 113, no. 1, pp. 40-51, 2013 Jun 21 (Epub 2013 Apr 2013).
- [162] K. K. Hirschi, S. A. Rohovsky, L. H. Beck, S. R. Smith, and P. A. D'Amore, "Endothelial cells modulate the proliferation of mural cell precursors via platelet-derived growth

- factor-BB and heterotypic cell contact," *Circulation Research*, Article vol. 84, no. 3, pp. 298-305, Feb 1999.
- [163] M.-C. Tsai *et al.*, "Shear Stress Induces Synthetic-to-Contractile Phenotypic Modulation in Smooth Muscle Cells via Peroxisome Proliferator-Activated Receptor α/δ Activations by Prostacyclin Released by Sheared Endothelial Cells," *Circulation Research*, vol. 105, no. 5, pp. 471-480, 2009/08/28 2009.
- [164] E. Hergenreider *et al.*, "Atheroprotective communication between endothelial cells and smooth muscle cells through miRNAs," *Nature Cell Biology*, Article vol. 14, p. 249, 02/12/online 2012.
- [165] J. L. Brugnano, "Characterization and intracellular delivery of MK2-inhibitor peptides for inflammatory applications," 2012.
- [166] Y. X. Liu, S. Rayatpisheh, S. Y. Chew, and M. B. Chan-Park, "Impact of Endothelial Cells on 3D Cultured Smooth Muscle Cells in a Biomimetic Hydrogel," *Acs Applied Materials & Interfaces*, Article vol. 4, no. 3, pp. 1378-1387, Mar 2012.
- [167] T. Wang, Z. Xu, W. Jiang, and A. Ma, "Cell-to-cell contact induces mesenchymal stem cell to differentiate into cardiomyocyte and smooth muscle cell," *International Journal of Cardiology*, vol. 109, no. 1, pp. 74-81, 2006/04/28/ 2006.
- [168] L. Cho-Hao and L. Brenda, "Endothelial Cells Direct Mesenchymal Stem Cells Toward a Smooth Muscle Cell Fate," *Stem Cells and Development*, vol. 23, no. 21, pp. 2581-2590, 2014.
- [169] S. G. Ball, A. C. Shuttleworth, and C. M. Kielty, "Direct cell contact influences bone marrow mesenchymal stem cell fate," *International Journal of Biochemistry & Cell Biology*, Article vol. 36, no. 4, pp. 714-727, Apr 2004.
- [170] K. C. Vallabhaneni, H. Haller, and I. Dumler, "Vascular Smooth Muscle Cells Initiate Proliferation of Mesenchymal Stem Cells by Mitochondrial Transfer via Tunneling Nanotubes," *Stem Cells and Development*, vol. 21, no. 17, pp. 3104-3113, 2012.
- [171] T. P. Lozito, C. K. Kuo, J. M. Taboas, and R. S. Tuan, "Human mesenchymal stem cells express vascular cell phenotypes upon interaction with endothelial cell matrix," *Journal of Cellular Biochemistry*, vol. 107, no. 4, pp. 714-722, 2009.
- [172] A. D. van der Meer, V. V. Orlova, P. ten Dijke, A. van den Berg, and C. L. Mummery, "Three-dimensional co-cultures of human endothelial cells and embryonic stem cell-derived pericytes inside a microfluidic device," *Lab on a Chip*, 10.1039/C3LC50435B vol. 13, no. 18, pp. 3562-3568, 2013.

- [173] X. Tian *et al.*, "Adipose Stem Cells Promote Smooth Muscle Cells to Secrete Elastin in Rat Abdominal Aortic Aneurysm," *Plos One*, vol. 9, no. 9, Sep 22 2014, Art. no. e108105.
- [174] R. M. Greenhalgh *et al.*, "Early elective open surgical repair of small abdominal aortic aneurysms is not recommended: Results of the UK Small Aneurysm Trial," *European Journal of Vascular and Endovascular Surgery*, vol. 16, no. 6, pp. 462-464, Dec 1998.
- [175] L. A. Pape *et al.*, "Aortic diameter \geq 5.5 cm is not a good predictor of type A aortic dissection - Observations from the international registry of acute aortic dissection (IRAD)," *Circulation*, vol. 116, no. 10, pp. 1120-1127, Sep 4 2007.
- [176] J. A. Elefteriades, "Natural history of thoracic aortic aneurysms: indications for surgery, and surgical versus nonsurgical risks," *Ann Thorac Surg*, vol. 74, no. 5, pp. S1877-80; discussion S1892-8, Nov 2002.
- [177] G. Johansson, U. Markstrom, and J. Swedenborg, "Ruptured Thoracic Aortic Aneurysms - A Study of Incidence and Mortality Rates," *Journal of Vascular Surgery*, vol. 21, no. 6, pp. 985-988, Jun 1995.
- [178] B. T. Baxter, M. C. Terrin, and R. L. Dalman, "Medical management of small abdominal aortic aneurysms," *Circulation*, Article vol. 117, no. 14, pp. 1883-1889, Apr 2008.
- [179] A. S. Chun, J. A. Elefteriades, and S. K. Mukherjee, "Do β -Blockers Really Work for Prevention of Aortic Aneurysms?: Time for Reassessment," *AORTA*, vol. 1, no. 1, pp. 45-51, 06/01
01/09/received
03/08/accepted 2013.
- [180] S. Kaushal, C. L. Backer, S. Patel, J. G. Gossett, and C. Mavroudis, "Midterm Outcomes in Supravalvular Aortic Stenosis Demonstrate the Superiority of Multisinus Aortoplasty," *Annals of Thoracic Surgery*, vol. 89, no. 5, pp. 1371-1377, May 2010.
- [181] A. Dua *et al.*, "The effect of Surgical Care Improvement Project measures on national trends on surgical site infections in open vascular procedures," *Journal of Vascular Surgery*, vol. 60, no. 6, pp. 1635-1639, Dec 2014.
- [182] R. S. Von Allmen and J. T. Powell, "The management of ruptured abdominal aortic aneurysms: screening for abdominal aortic aneurysm and incidence of rupture," *J Cardiovasc Surg (Torino)*, vol. 53, no. 1, pp. 69-76, Feb 2012.
- [183] M. G. Keane and R. E. Pyeritz, "Medical management of Marfan syndrome," *Circulation*, vol. 117, no. 21, pp. 2802-2813, May 2008.

- [184] S. C. Nicholls, J. B. Gardner, M. H. Meissner, and K. H. Johansen, "Rupture in small abdominal aortic aneurysms," *Journal of Vascular Surgery*, vol. 28, no. 5, pp. 884-888, Nov 1998.
- [185] E. L. Eisenstein, L. Davidson-Ray, R. Edwards, K. J. Anstrom, and K. Ouriel, "Economic analysis of endovascular repair versus surveillance for patients with small abdominal aortic aneurysms," *Journal of vascular surgery*, vol. 58, no. 2, pp. 302-310, 2013/08// 2013.
- [186] M. J. Sweeting, S. G. Thompson, L. C. Brown, R. M. Greenhalgh, and J. T. Powell, "Use of angiotensin converting enzyme inhibitors is associated with increased growth rate of abdominal aortic aneurysms," *Journal of Vascular Surgery*, vol. 52, no. 1, pp. 1-4, Jul 2010.
- [187] A. C. Braverman, "Medical management of thoracic aortic aneurysm disease," *Journal of Thoracic and Cardiovascular Surgery*, vol. 145, no. 3, pp. S2-S6, Mar 2013.
- [188] K. McGee, E. Bollache, A. J. Barker, J. C. Carr, M. Markl, and P. Kansal, "Impact of Beta-blocker, ACE Inhibitor, and ARB therapy on thoracic aorta wall shear stress in bicuspid aortic valve patients," *Journal of Cardiovascular Magnetic Resonance*, vol. 18, no. Suppl 1, p. P345, 01/27 2016.
- [189] H. Abdul-Hussien, R. Hanemaaijer, J. H. Verheijen, J. H. van Bockel, R. H. Geelkerken, and J. H. N. Lindeman, "Doxycycline therapy for abdominal aneurysm: Improved proteolytic balance through reduced neutrophil content," *Journal of Vascular Surgery*, vol. 49, no. 3, pp. 741-749, 2009/03/01/ 2009.
- [190] C. Meijer, T. Stijnen, M. M. Wasser, and et al., "Doxycycline for stabilization of abdominal aortic aneurysms: A randomized trial," *Annals of Internal Medicine*, vol. 159, no. 12, pp. 815-823, 2013.
- [191] J. A. Curci, D. Petrincec, S. Liao, L. M. Golub, and R. W. Thompson, "Pharmacologic suppression of experimental abdominal aortic aneurysms: A comparison of doxycycline and four chemically modified tetracyclines," *Journal of Vascular Surgery*, vol. 28, no. 6, pp. 1082-1093, 1998.
- [192] L. Y. Lin and L. M. Du, "The role of secreted factors in stem cells-mediated immune regulation," *Cellular Immunology*, vol. 326, pp. 24-32, Apr 2018.
- [193] G. Swaminathan, V. S. Gadepalli, I. Stoilov, R. P. Mecham, R. R. Rao, and A. Ramamurthi, "Pro-elastogenic effects of bonemarrowmesenchymal stem cell-derived smooth muscle cells on cultured aneurysmal smooth muscle cells," *Journal of Tissue Engineering and Regenerative Medicine*, vol. 11, no. 3, pp. 679-693, Mar 2017.

- [194] G. Swaminathan, I. Stoilov, T. Broekelmann, R. Mecham, and A. Ramamurthi, "Phenotype-based selection of bone marrow mesenchymal stem cell-derived smooth muscle cells for elastic matrix regenerative repair in abdominal aortic aneurysms," *Journal of Tissue Engineering and Regenerative Medicine*, vol. 12, no. 1, pp. E60-E70, Jan 2018.
- [195] J. Xie *et al.*, "Human Adipose-Derived Stem Cells Suppress Elastase-Induced Murine Abdominal Aortic Inflammation and Aneurysm Expansion Through Paracrine Factors," *Cell transplantation*, vol. 26, no. 2, pp. 173-189, 2017.
- [196] J. P. Chow, D. T. Simionescu, A. L. Carter, and A. Simionescu, "Immunomodulatory effects of adipose tissue-derived stem cells on elastin scaffold remodeling in diabetes," *Tissue Engineering and Regenerative Medicine*, journal article vol. 13, no. 6, pp. 701-712, December 01 2016.
- [197] J. T. Krawiec *et al.*, "A Cautionary Tale for Autologous Vascular Tissue Engineering: Impact of Human Demographics on the Ability of Adipose-Derived Mesenchymal Stem Cells to Recruit and Differentiate into Smooth Muscle Cells," *Tissue Engineering Part a*, vol. 21, no. 3-4, pp. 426-437, FEB 1 2015 2015.
- [198] K. J. Blose, T. L. Ennis, B. Arif, J. S. Weinbaum, J. A. Curci, and D. A. Vorp, "Periadventitial adipose-derived stem cell treatment halts elastase-induced abdominal aortic aneurysm progression," *Regenerative Medicine*, vol. 9, no. 6, pp. 733-741, 2014 2014.
- [199] W. He *et al.*, "Pericyte-based human tissue engineered vascular grafts," *Biomaterials*, Article vol. 31, no. 32, pp. 8235-8244, NOV 2010 2010.
- [200] J. T. Krawiec *et al.*, "In Vivo Functional Evaluation of Tissue-Engineered Vascular Grafts Fabricated Using Human Adipose-Derived Stem Cells from High Cardiovascular Risk Populations," *Tissue Eng Part A*, vol. 22, no. 9-10, pp. 765-75, May 2016.
- [201] D. G. Haskett *et al.*, "An exploratory study on the preparation and evaluation of a "same-day" adipose stem cell-based tissue-engineered vascular graft," *The Journal of thoracic and cardiovascular surgery*, 2018/07// 2018.
- [202] J. T. Krawiec *et al.*, "Evaluation of the stromal vascular fraction of adipose tissue as the basis for a stem cell-based tissue-engineered vascular graft," *Journal of Vascular Surgery*, vol. 66, no. 3, pp. 883-+, Sep 2017.
- [203] P. C. Baer, "Adipose-derived mesenchymal stromal/stem cells: An update on their phenotype in vivo and in vitro," *World journal of stem cells*, vol. 6, no. 3, pp. 256-265, 2014.

- [204] S. M. Melief, J. J. Zwaginga, W. E. Fibbe, and H. Roelofs, "Adipose Tissue-Derived Multipotent Stromal Cells Have a Higher Immunomodulatory Capacity Than Their Bone Marrow-Derived Counterparts," *Stem Cells Translational Medicine*, vol. 2, no. 6, pp. 455-463, Jun 2013.
- [205] J. T. Krawiec *et al.*, "A Cautionary Tale for Autologous Vascular Tissue Engineering: Impact of Human Demographics on the Ability of Adipose-Derived Mesenchymal Stem Cells to Recruit and Differentiate Into Smooth Muscle Cells," *Tissue Engineering Part A*, 2014.
- [206] J. D. Roh *et al.*, "Tissue-engineered vascular grafts transform into mature blood vessels via an inflammation-mediated process of vascular remodeling," *Proc Natl Acad Sci U S A*, vol. 107, no. 10, pp. 4669-74, Mar 9 2010.
- [207] A. I. Hoch, B. Y. Binder, D. C. Genetos, and J. K. Leach, "Differentiation-Dependent Secretion of Proangiogenic Factors by Mesenchymal Stem Cells," *Plos One*, vol. 7, no. 4, Apr 2012, Art. no. e35579.
- [208] G. E. Kilroy *et al.*, "Cytokine profile of human adipose-derived stem cells: Expression of angiogenic, hematopoietic, and pro-inflammatory factors," *Journal of Cellular Physiology*, vol. 212, no. 3, pp. 702-709, Sep 2007.
- [209] S. S. Wang, M. Q. Tong, S. W. Hu, and X. M. Chen, "The Bioactive Substance Secreted by MSC Retards Mouse Aortic Vascular Smooth Muscle Cells Calcification," *Biomed Research International*, 2018, Art. no. 6053567.
- [210] A. J. Ryan and F. J. O'Brien, "Insoluble elastin reduces collagen scaffold stiffness, improves viscoelastic properties, and induces a contractile phenotype in smooth muscle cells," *Biomaterials*, vol. 73, pp. 296-307, Dec 2015.
- [211] J. L. Long and R. T. Tranquillo, "Elastic fiber production in cardiovascular tissue-equivalents," *Matrix Biology*, vol. 22, no. 4, pp. 339-350, Jun 2003.
- [212] J. L. Long and R. T. Tranquillo, "Elastic fiber production in cardiovascular tissue-equivalents," *Matrix Biol*, vol. 22, no. 4, pp. 339-50, Jun 2003.
- [213] J. S. Weinbaum, J. Qi, and R. T. Tranquillo, "Monitoring collagen transcription by vascular smooth muscle cells in fibrin-based tissue constructs," *Tissue Eng Part C Methods*, vol. 16, no. 3, pp. 459-67, Jun 2010.
- [214] J. S. Weinbaum, J. B. Schmidt, and R. T. Tranquillo, "Combating Adaptation to Cyclic Stretching by Prolonging Activation of Extracellular Signal-Regulated Kinase," *Cellular and Molecular Bioengineering*, vol. 6, no. 3, pp. 279-286, Sep 2013.

- [215] R. G. Koch *et al.*, "A custom image-based analysis tool for quantifying elastin and collagen micro-architecture in the wall of the human aorta from multi-photon microscopy," *Journal of Biomechanics*, vol. 47, no. 5, pp. 935-943, Mar 21 2014.
- [216] K. A. Ahmann, J. S. Weinbaum, S. L. Johnson, and R. T. Tranquillo, "Fibrin degradation enhances vascular smooth muscle cell proliferation and matrix deposition in fibrin-based tissue constructs fabricated in vitro," *Tissue Eng Part A*, vol. 16, no. 10, pp. 3261-70, Oct 2010.
- [217] J. J. Mulvihill and M. T. Walsh, "On the mechanical behaviour of carotid artery plaques: the influence of curve-fitting experimental data on numerical model results," *Biomechanics and Modeling in Mechanobiology*, vol. 12, no. 5, pp. 975-985, Oct 2013.
- [218] K. J. Blose, J. E. Pichamuthu, J. S. Weinbaum, and D. A. Vorp, "Design and validation of a vacuum assisted anchorage for the uniaxial tensile testing of soft materials," *Soft Materials*, vol. 14, no. 2, pp. 72-77, 2016.
- [219] A. Tsamis *et al.*, "Fiber micro-architecture in the longitudinal-radial and circumferential-radial planes of ascending thoracic aortic aneurysm media," *J Biomech*, vol. 46, no. 16, pp. 2787-94, Nov 15 2013.
- [220] G. A. Holzapfel, G. Sommer, and P. Regitnig, "Anisotropic Mechanical Properties of Tissue Components in Human Atherosclerotic Plaques," *Journal of Biomechanical Engineering*, vol. 126, no. 5, p. 657, 2004.
- [221] M. T. Walsh, E. M. Cunnane, J. J. Mulvihill, A. C. Akyildiz, F. J. H. Gijssen, and G. A. Holzapfel, "Uniaxial tensile testing approaches for characterisation of atherosclerotic plaques," *Journal of Biomechanics*, vol. 47, no. 4, pp. 793-804, Mar 2014.
- [222] E. M. Cunnane, J. J. E. Mulvihill, H. E. Barrett, M. M. Hennessy, E. G. Kavanagh, and M. T. Walsh, "Mechanical properties and composition of carotid and femoral atherosclerotic plaques: A comparative study," *Journal of Biomechanics*, vol. 49, no. 15, pp. 3697-3704, Nov 2016.
- [223] G. A. Holzapfel, "Determination of material models for arterial walls from uniaxial extension tests and histological structure," *Journal of Theoretical Biology*, vol. 238, no. 2, pp. 290-302, Jan 2006.
- [224] J. E. Wagenseil and R. P. Mecham, "Elastin in Large Artery Stiffness and Hypertension," *Journal of Cardiovascular Translational Research*, vol. 5, no. 3, pp. 264-273, Jun 2012.

- [225] M. J. Collins, J. F. Eberth, E. Wilson, and J. D. Humphrey, "Acute mechanical effects of elastase on the infrarenal mouse aorta: Implications for models of aneurysms," *Journal of Biomechanics*, vol. 45, no. 4, pp. 660-665, Feb 2012.
- [226] G. Holzapfel, *Biomechanics of Soft Tissue*. 2001, pp. 1049-1063.
- [227] A. Hemmasizadeh *et al.*, "Correlations between transmural mechanical and morphological properties in porcine thoracic descending aorta," *Journal of the Mechanical Behavior of Biomedical Materials*, vol. 47, pp. 12-20, Jul 2015.
- [228] S. Menashi, J. S. Campa, R. M. Greenhalgh, and J. T. Powell, "Collagen in Abdominal Aortic-Aneurysm - Typing, Content, and Degradation," *Journal of Vascular Surgery*, vol. 6, no. 6, pp. 578-582, Dec 1987.
- [229] Yasmin *et al.*, "The matrix proteins aggrecan and fibulin-1 play a key role in determining aortic stiffness," *Scientific Reports*, vol. 8, no. 1, p. 8550, 2018/06/04 2018.
- [230] F. S. Cikach *et al.*, "Massive aggrecan and versican accumulation in thoracic aortic aneurysm and dissection," *JCI insight*, vol. 3, no. 5, p. e97167, 2018.
- [231] E. M. Cunnane, J. S. Weinbaum, F. J. O'Brien, and D. A. Vorp, "Future Perspectives on the Role of Stem Cells and Extracellular Vesicles in Vascular Tissue Regeneration," *Frontiers in Cardiovascular Medicine*, Review vol. 5, p. 12, Jul 2018, Art. no. 86.
- [232] H. R. Hofer and R. S. Tuan, "Secreted trophic factors of mesenchymal stem cells support neurovascular and musculoskeletal therapies," *Stem Cell Research & Therapy*, vol. 7, Sep 2016, Art. no. 131.
- [233] A. Klink *et al.*, "Diagnostic and therapeutic strategies for small abdominal aortic aneurysms," *Nature reviews. Cardiology*, Review vol. 8, no. 6, pp. 338-47, Jun 2011.
- [234] R. A. P. Scott, P. V. Tisi, H. A. Ashton, and D. R. Allen, "Abdominal aortic aneurysm rupture rates: A 7-year follow-up of the entire abdominal aortic aneurysm population detected by screening," *Journal of Vascular Surgery*, vol. 28, no. 1, pp. 124-128, Jul 1998.
- [235] Yuan, Ma, Zhang, and Jing, "Transforming growth factor-beta signaling pathway in Marfan's syndrome: a preliminary histopathological study," *Vasa*, vol. 40, no. 5, pp. 369-374, 2011.
- [236] S. S. Chaudhry, S. A. Cain, A. Morgan, S. L. Dallas, C. A. Shuttleworth, and C. M. Kielty, "Fibrillin-1 regulates the bioavailability of TGFbeta1," *J Cell Biol*, vol. 176, no. 3, pp. 355-67, Jan 29 2007.

- [237] P. Booms *et al.*, "RGD-containing fibrillin-1 fragments upregulate matrix metalloproteinase expression in cell culture: A potential factor in the pathogenesis of the Marfan syndrome," *Human Genetics*, journal article vol. 116, no. 1, pp. 51-61, January 01 2005.
- [238] K. Benke *et al.*, "The role of transforming growth factor-beta in Marfan syndrome," *Cardiology Journal*, vol. 20, no. 3, pp. 227-234, May 2013.
- [239] D. Bergqvist, M. Bjorck, and A. Wanhainen, "Treatment of Vascular Ehlers-Danlos Syndrome A Systematic Review," *Annals of Surgery*, vol. 258, no. 2, pp. 257-261, Aug 2013.
- [240] A. Herchenhan *et al.*, "Lysyl Oxidase activity is required for ordered collagen fibrillogenesis by tendon cells," *Journal of Biological Chemistry*, May 15, 2015 2015.
- [241] O. A. Ovchinnikova *et al.*, "The collagen cross-linking enzyme lysyl oxidase is associated with the healing of human atherosclerotic lesions," *Journal of Internal Medicine*, vol. 276, no. 5, pp. 525-536, 2014.
- [242] J. M. Maki *et al.*, "Inactivation of the lysyl oxidase gene *Lox* leads to aortic aneurysms, cardiovascular dysfunction, and perinatal death in mice," *Circulation*, vol. 106, no. 19, Nov 5 2002.
- [243] S. D. Shapiro, S. K. Endicott, M. A. Province, J. A. Pierce, and E. J. Campbell, "Marked longevity of human lung parenchymal elastic fibers deduced from prevalence of D-aspartate and nuclear weapons-related radiocarbon," *The Journal of clinical investigation*, vol. 87, no. 5, pp. 1828-1834, 1991.
- [244] X. Lin, M. Robinson, T. Petrie, V. Spandler, W. D. Boyd, and C. S. Sondergaard, "Small intestinal submucosa-derived extracellular matrix bioscaffold significantly enhances angiogenic factor secretion from human mesenchymal stromal cells," *Stem Cell Research & Therapy*, journal article vol. 6, no. 1, p. 164, September 07 2015.
- [245] B. Follin, M. Juhl, S. Cohen, A. E. Pedersen, J. Kastrup, and A. Ekblond, "Increased Paracrine Immunomodulatory Potential of Mesenchymal Stromal Cells in Three-Dimensional Culture," *Tissue Engineering Part B: Reviews*, vol. 22, no. 4, pp. 322-329, 2016.
- [246] A. Yamawaki-Ogata, R. Hashizume, X.-M. Fu, A. Usui, and Y. Narita, "Mesenchymal stem cells for treatment of aortic aneurysms," *World journal of stem cells*, vol. 6, no. 3, pp. 278-287, 2014.

- [247] M. A. Roberts *et al.*, "Stromal Cells in Dense Collagen Promote Cardiomyocyte and Microvascular Patterning in Engineered Human Heart Tissue," *Tissue engineering. Part A*, vol. 22, no. 7-8, pp. 633-644, 2016.
- [248] R. D. Abbott *et al.*, "The Use of Silk as a Scaffold for Mature, Sustainable Unilocular Adipose 3D Tissue Engineered Systems," *Adv Healthc Mater*, May 19 2016.
- [249] V. Guneta, Q. L. Loh, and C. Choong, "Cell-secreted extracellular matrix formation and differentiation of adipose-derived stem cells in 3D alginate scaffolds with tunable properties," *Journal of Biomedical Materials Research Part A*, vol. 104, no. 5, pp. 1090-1101, 2016.
- [250] M. C. Ciuffreda *et al.*, "Synthetic extracellular matrix mimic hydrogel improves efficacy of mesenchymal stromal cell therapy for ischemic cardiomyopathy," *Acta Biomaterialia*, vol. 70, pp. 71-83, 2018/04/01/ 2018.
- [251] H. Itosaka *et al.*, "Fibrin matrix provides a suitable scaffold for bone marrow stromal cells transplanted into injured spinal cord: A novel material for CNS tissue engineering," *Neuropathology*, Oct 20 2008.
- [252] D. Bejleri *et al.*, "A Bioprinted Cardiac Patch Composed of Cardiac-Specific Extracellular Matrix and Progenitor Cells for Heart Repair," *Advanced Healthcare Materials*, vol. 7, no. 23, p. 1800672, 2018/12/01 2018.
- [253] M. T. Valarmathi, J. W. Fuseler, J. D. Potts, J. M. Davis, and R. L. Price, "Functional Tissue Engineering: A Prevascularized Cardiac Muscle Construct for Validating Human Mesenchymal Stem Cells Engraftment Potential In Vitro," *Tissue engineering. Part A*, vol. 24, no. 1-2, pp. 157-185, 2018.
- [254] L.-P. Gao, M.-J. Du, J.-J. Lv, S. Schmall, R.-T. Huang, and J. Li, "Use of human aortic extracellular matrix as a scaffold for construction of a patient-specific tissue engineered vascular patch," *Biomedical Materials*, vol. 12, no. 6, p. 065006, 2017.
- [255] L. Labusca, D. D. Herea, and K. Mashayekhi, "Stem cells as delivery vehicles for regenerative medicine—challenges and perspectives," *World journal of stem cells*, vol. 10, no. 5, pp. 43-56, 2018.
- [256] C. M. Brougham, T. J. Levingstone, S. Jockenhoevel, T. C. Flanagan, and F. J. O'Brien, "Incorporation of fibrin into a collagen–glycosaminoglycan matrix results in a scaffold with improved mechanical properties and enhanced capacity to resist cell-mediated contraction," *Acta Biomaterialia*, vol. 26, pp. 205-214, 2015/10/15/ 2015.

- [257] S. Jockenhoevel *et al.*, "Fibrin gel -- advantages of a new scaffold in cardiovascular tissue engineering," *Eur J Cardiothorac Surg*, vol. 19, no. 4, pp. 424-30, Apr 2001.
- [258] Q. Ye *et al.*, "Fibrin gel as a three dimensional matrix in cardiovascular tissue engineering," *Eur J Cardiothorac Surg*, vol. 17, no. 5, pp. 587-91, May 2000.
- [259] D. Pelaez, C. Y. Huang, and H. S. Cheung, "Cyclic Compression Maintains Viability and Induces Chondrogenesis of Human Mesenchymal Stem Cells in Fibrin Gel Scaffolds," *Stem Cells Dev*, Apr 9 2008.
- [260] R. Moreira *et al.*, "Tissue-Engineered Fibrin-Based Heart Valve with Bio-Inspired Textile Reinforcement," *Advanced Healthcare Materials*, vol. 5, no. 16, pp. 2113-2121, 2016.
- [261] C. Krug *et al.*, "Fibrin glue displays promising in vitro characteristics as a potential carrier of adipose progenitor cells for tissue regeneration," *Journal of Tissue Engineering and Regenerative Medicine*, vol. 0, no. ja, 2018/12/04 2018.
- [262] M. R. J., F.-K. Masako, B. Mark, Z. Yufeng, H. Maria, and C. Joseph, "Platelet-Rich Fibrin and Soft Tissue Wound Healing: A Systematic Review," *Tissue Engineering Part B: Reviews*, vol. 23, no. 1, pp. 83-99, 2017.
- [263] X. Ju *et al.*, "IL-6 Regulates Extracellular Matrix Remodeling Associated With Aortic Dilation in a Fibrillin-1 Hypomorphic mgR/mgR Mouse Model of Severe Marfan Syndrome," *Journal of the American Heart Association*, vol. 3, no. 1, p. e000476, 2014.
- [264] R. K. Middleton, M. J. Bown, G. M. Lloyd, J. L. Jones, N. J. London, and R. D. Sayers, "Characterisation of Interleukin-8 and Monocyte Chemoattractant Protein-1 Expression within the Abdominal Aortic Aneurysm and their Association with Mural Inflammation," *European Journal of Vascular and Endovascular Surgery*, vol. 37, no. 1, pp. 46-55, 2009.
- [265] S. Franitza *et al.*, "TNF- α Associated with Extracellular Matrix Fibronectin Provides a Stop Signal for Chemotactically Migrating T Cells," *The Journal of Immunology*, vol. 165, no. 5, pp. 2738-2747, 2000.
- [266] R. W. Y. Yeo *et al.*, "Mesenchymal stem cell: An efficient mass producer of exosomes for drug delivery," *Advanced Drug Delivery Reviews*, vol. 65, no. 3, pp. 336-341, 2013/03/01/ 2013.
- [267] L. Biancone, S. Bruno, M. C. Deregibus, C. Tetta, and G. Camussi, "Therapeutic potential of mesenchymal stem cell-derived microvesicles," *Nephrology Dialysis Transplantation*, vol. 27, no. 8, pp. 3037-3042, 2012.

- [268] S. A. A. Kooijmans, P. Vader, S. M. van Dommelen, W. W. van Solinge, and R. M. Schiffelers, "Exosome mimetics: a novel class of drug delivery systems," *International Journal of Nanomedicine*, vol. 7, pp. 1525-1541, 2012.
- [269] L. Huleihel *et al.*, "Matrix-bound nanovesicles within ECM bioscaffolds," *Science Advances*, vol. 2, no. 6, p. e1600502, 2016.
- [270] D. M. Pegtel *et al.*, "Functional delivery of viral miRNAs via exosomes," *Proceedings of the National Academy of Sciences*, vol. 107, no. 14, pp. 6328-6333, 2010.
- [271] B. McNeill, A. Ostojic, K. J. Rayner, M. Ruel, and E. J. Suuronen, "Collagen biomaterial stimulates the production of extracellular vesicles containing microRNA-21 and enhances the proangiogenic function of CD34+ cells," *The FASEB Journal*, vol. 0, no. 0, p. fj.201801332R, 2018.
- [272] P. Li, M. Kaslan, S. H. Lee, J. Yao, and Z. Gao, "Progress in Exosome Isolation Techniques," *Theranostics*, vol. 7, no. 3, pp. 789-804, 2017.
- [273] J. Van Deun *et al.*, "The impact of disparate isolation methods for extracellular vesicles on downstream RNA profiling," *Journal of extracellular vesicles*, vol. 3, p. 10.3402/jev.v3.24858, 2014.
- [274] Y. Jin *et al.*, "DNA in serum extracellular vesicles is stable under different storage conditions," *BMC cancer*, vol. 16, no. 1, pp. 753-753, 2016.
- [275] M. Tong and L. W. Chamley, "Placental extracellular vesicles and feto-maternal communication," *Cold Spring Harbor perspectives in medicine*, vol. 5, no. 3, pp. a023028-a023028, 2015.
- [276] D. Tannetta, R. Dragovic, Z. Alyahyaei, and J. Southcombe, "Extracellular vesicles and reproduction-promotion of successful pregnancy," *Cellular & molecular immunology*, vol. 11, no. 6, pp. 548-563, 2014.
- [277] C. Balbi *et al.*, "First Characterization of Human Amniotic Fluid Stem Cell Extracellular Vesicles as a Powerful Paracrine Tool Endowed with Regenerative Potential," *STEM CELLS Translational Medicine*, vol. 6, no. 5, pp. 1340-1355, 2017.